Environmentally Responsible Use of Nanomaterials for the Photocatalytic Reduction of Nitrate in Water

by

Kyle Doudrick

A Dissertation Presented in Partial Fulfillment
of the Requirements for the Degree
Doctor of Philosophy

Approved April 2013 by the
Graduate Supervisory Committee:

Paul Westerhoff, Chair
Rolf Halden
Kiril Hristovski

ARIZONA STATE UNIVERSITY

May 2013

ABSTRACT

Nitrate is the most prevalent water pollutant limiting the use of groundwater as a potable water source. The overarching goal of this dissertation was to leverage advances in nanotechnology to improve nitrate photocatalysis and transition treatment to the full-scale. The research objectives were to (1) examine commercial and synthesized photocatalysts, (2) determine the effect of water quality parameters (e.g., pH), (3) conduct responsible engineering by ensuring detection methods were in place for novel materials, and (4) develop a conceptual framework for designing nitrate-specific photocatalysts.

The key issues for implementing photocatalysis for nitrate drinking water treatment were efficient nitrate removal at neutral pH and by-product selectivity toward nitrogen gases, rather than by-products that pose a human health concern (e.g., nitrite). Photocatalytic nitrate reduction was found to follow a series of proton-coupled electron transfers. The nitrate reduction rate was limited by the electron-hole recombination rate, and the addition of an electron donor (e.g., formate) was necessary to reduce the recombination rate and achieve efficient nitrate removal. Nano-sized photocatalysts with high surface areas mitigated the negative effects of competing aqueous anions. The key water quality parameter impacting by-product selectivity was pH. For pH < 4, the by-product selectivity was mostly N-gas with some NH_4^+, but this shifted to NO_2^- above pH = 4, which suggests the need for proton localization to move beyond NO_2^-. Co-catalysts that form a Schottky barrier, allowing for localization of electrons, were best for nitrate reduction. Silver was optimal in heterogeneous systems because of its ability to improve nitrate reduction activity and N-gas by-product selectivity, and graphene was optimal in

two-electrode systems because of its ability to shuttle electrons to the working electrode. "Environmentally responsible use of nanomaterials" is to ensure that detection methods are in place for the nanomaterials tested. While methods exist for the metals and metal oxides examined, there are currently none for carbon nanotubes (CNTs) and graphene. Acknowledging that risk assessment encompasses dose-response and exposure, new analytical methods were developed for extracting and detecting CNTs and graphene in complex organic environmental (e.g., urban air) and biological matrices (e.g. rat lungs).

ACKNOWLEDGMENTS

There are a number of people and organizations that made this dissertation work possible. I think it goes without saying that the Doctoral advisor plays a major role in a Ph.D. student's academic career and the path they take in life. A good advisor will go beyond the standard requirements by helping you gain a research identity, figure out where you fit in the field, and obtain the confidence you need to move beyond graduate school. This is why the first person I must thank is my advisor and committee chair, Dr. Paul Westerhoff. On paper, I was not necessarily a no-brainer for the Ph.D. program, but Paul was able to see the passion and promise I had for a research career, and this support continued throughout my time at ASU. Even during his administrative stints, he continued to be a pro-active advisor, continuing to help me obtain funding and always keeping an open door. No matter the circumstances, he always made time available for me, a resource that is the most difficult to find, yet the most helpful for a Ph.D. student.

I also want to extend my gratitude to my other committee members, Drs. Kiril Hristovski and Rolf Halden, both who were excellent mentors to me long before being asked to serve on my committee. When I came to ASU, I had no experience in the lab, and Kiril had the task of turning a modeler into an efficient lab researcher. Beyond excellent training, he helped to shape my research interests and was the first to get me interested in synthesizing materials. As I progressed, our meetings turned from training into in-depth and exciting discussions about making innovative materials. I had the pleasure of taking multiple courses from Rolf, writing a proposal with him, and working on an NIH project with him. Throughout these, Rolf provided me with great insight about performing research on a high level, keys to writing a successful proposal, and why it is

important to be meticulous researcher. He and I always saw things in the same light and his understanding and guidance helped me greatly during my Ph.D.

There is no doubt in my mind that this journey would not have been near as rewarding if not for the fellowship I received from the Science Foundation Arizona to support my first two years at ASU. This fellowship allowed me to explore my curiosities about synthesizing nanomaterials and solving challenging environmental problems. These curiosities eventually led me to my dissertation topic and I was lucky enough to get continued support related to my dissertation work. I am very grateful for this support provided by the National Institute of Health, the Semiconductor Research Corporation, and the National Science Foundation. These allowed me to broaden my skillset and develop an identity for myself as an independent researcher.

Through all the support and guidance provided to me by my mentors, maintaining my sanity and happiness could only be accomplished by the wonderful support of my family, friends, and colleagues. I want to thank Dr. Pierre Herckes for his support, Dr. Matt Fraser for letting me make his lab my own, Dr. Andrea Clements for her friendship and constant training on the TOT, Dr. David Ladner for his ability to listen and give sound advice, my colleagues including Troy Benn, Ayla Kiser, Dave Hanigan, Ting Yang, Du Erdeng, Oihane Monzon, Sungyun Lee, Michelle Barry, Jacelyn Rice, Tom Bruton, Mac Gifford, Karthik Konduri, Peter Goguen, Tyler Harris, and many others. I also want to thank Alex Mangonon, Amada Hernandez, Natalie Geiger, and Nadratun Chowdhury for letting me use them to improve my mentoring skills.

Although they were not down in the trenches with me, my family provided an indescribable support and I thank my mother Julie, my father Richard, my brother Jeff, and Sue Ellen for their love and listening to my boring research stories.

TABLE OF CONTENTS

Page

LIST OF TABLES xiii

LIST OF FIGURES xiv

CHAPTER

1 INTRODUCTION 1

Dissertation Overview 2

2 BACKGROUND 5

2.1 Nitrate Pollution 5

Current Nitrate Treatment Technologies in Drinking Water 8

2.2 Photocatalytic Reduction of Nitrate 12

Importance of Developing Photocatalysts for Water Treatment 12

Photocatalyst Dissertation Terminology 12

A Short History of Photocatalysis for Environmental Applications 20

Titanium Dioxide as a Photocatalyst 21

Photocatalysis Charge Transfer with Application to TiO_2 21

Photocatalytic Reduction Reactions 23

Photocatalytic Reduction of Nitrate 25

3 NITRATE REDUCTION IN WATER USING COMMERCIAL TITANIUM DIOXIDE PHOTOCATALYSTS (P25, P90, AND HOMBIKAT UV100)* 34

3.1 Introduction 35

CHAPTER Page

3.2 Experimental Approach 40

Material Description 38

Photocatalytic Experiments 39

Analytical Methods for Nitrogen Species 41

Photocatalyst Material Characterization 41

Photoreactor Light Intensity 42

3.3 Results 44

Photocatalyst Material Characterization 44

Photocatalytic Nitrate Reduction in a Model Water 50

Photocatalytic Nitrate Reduction in Groundwater 54

Effect of Photocatalyst Surface Area 54

Kinetics and Quantum Yield of Photocatalytic Nitrate Reduction 56

Discussion 59

3.4 Summary 63

4 PHOTOCATALYTIC NITRATE REDUCTION IN WATER: MANAGING THE HOLE SCAVENGER AND REACTION BY-PRODUCT SELECTIVITY* 66

4.1. Introduction 67

4.2. Experimental methods 70

P90/Ag synthesis 70

Photocatalyst characterization 71

Photocatalytic experiments 72

CHAPTER Page

Analytical methods 74

Lamp irradiance measurements 75

4.3. Results and discussion 76

Photocatalyst characterization 76

Photocatalytic removal of nitrate and formate 77

Effect of photocatalyst dosage and silver loading 79

Effect of system pH on rate and selectivity 81

Effect of varying nitrate and formic acid concentrations 84

Controlling hole scavenger removal 87

Proposed mechanisms of formic acid 88

4.4 Implications for drinking water treatment 90

4.5 Supplemental Information 92

Photocatalyst mechanisms 92

Photocatalyst characterization 93

Photocatalytic removal 94

5 PHOTOCATALYTIC REDUCTION OF NITRATE USING TITANIUM DIOXIDE FOR REGENERATION OF ION EXCHANGE BRINE 98

5.1 Introduction 99

5.2 Materials and methods 103

Materials 103

Photocatalytic experiments 104

CHAPTER Page

IX system 106

Analytical methods 106

5.3 Results and discussion 107

Nitrate reduction in synthetic NaCl brines 107

Nitrate reduction in a real IX brine 110

Managing FA during IX resin regeneration 114

5.4 Conclusions 117

5.5 Supplemental Information 119

6 EXPLORATION OF CO-CATALYSTS FOR THE PHOTOCATALYTIC REDUCTION OF NITRATE OVER TITANIUM DIOXIDE 123

6.1 Introduction 123

6.2 Experimental Methods 128

Materials 128

Synthesis of Metal-Loaded Titanium Dioxide 128

Synthesis of TiO_2/CNT Composites 129

Synthesis of TiO_2/GNP and TiO_2/GO Composites 130

Thin Film Preparation 130

Micrograph Images 130

Photocatalytic Experiments 131

Photocurrent Experiments 131

6.3 Results 132

CHAPTER Page

Metal Co-Catalysts 132

Carbonaceous Co-Catalysts 133

6.4 Conclusions 137

7 DETECTION OF CARBON NANOTUBES AND GRAPHENE IN ENVIRONMENTAL MATRICES USING PROGRAMMED THERMAL ANALYSIS 139

7.1 Introduction 140

7.2 Experimental Details 143

CNT Sources and Sample Preparation 143

Environmental and Biological Matrices 145

Extraction of CNTs from Cyanobacteria 145

Analytical Methods 146

7.3 Results and Discussion 149

CNT Thermal Stability and Method Optimization 149

“Weak” and “Strong” Classification Using Raman Spectroscopy 154

Thermal Behavior of Environmental and Biological Matrices 155

Demonstration of CNT Detection in Environmental Matrices 159

7.4 Applicability and Future Development Needs 161

7.5 Supplemental Information 163

Carbon Nanotube Details 163

Analytical Method Details 165

CHAPTER Page

CNT Thermal Behavior 170

Raman Spectroscopy 171

Detection of Graphene 178

8 EXTRACTION OF CARBON NANOTUBES FROM COMPLEX ORGANIC MATRICES WITH APPLICATION TO RAT LUNG TISSUE 180

8.1 Introduction 181

8.2 Experimental Methods 183

Materials 183

Preparation of CNT Suspensions 184

Digestion of CNTs and Rat Lung Tissue 184

Programmed Thermal Analysis 185

Raman Spectroscopy 186

8.3 Results and Discussion 186

CNT Thermal Analysis 186

Raman Spectroscopy of CNTs 192

Rat lung tissue digestion 193

Demonstration of Final Digestion Method: Recovery of S-CNTs from Rat Lung Tissue 195

8.4 Summary and Conclusion 197

8.5 Supporting Info 198

CHAPTER Page

9 SYNTHESIS CHAPTER: A FRAMEWORK FOR ENGINEERING PHOTOCATALYSTS FOR NITRATE TREATMENT 200

Introduction 200

Choosing the Photocatalyst 204

Heterojunction Photocatalyst 209

Choosing the Co-Catalyst 210

Water as a Hole Scavenger 210

Engineering a Nitrate Reducing, Water Oxidizing Photoelectrochemical System 212

10 SUMMARY, CONCLUSIONS, AND FUTURE RECOMMENDATIONS 215

10.1 Summary 215

Dissertation Objectives 215

Observations 216

10.2 Conclusions 221

10.3 Future Recommendations 222

REFERENCES 223

LIST OF TABLES

TABLE Page

2.1. Current nitrate treatment technologies and their advantages and disadvantages 11

2.2. Comparison of Different Photocatalysts for Reduction of Nitrate 30

3.1. Groundwater Constituents and Their Concentrations 39

3.2. Photocatalyst Characterization Results 45

3.3. k and ξ_{poly} Values for P25 and P90 58

SI-4.1. Experimental matrix with first order rate constants for nitrate and formate 97

5.1. Characteristics of real IX brine 104

SI-5.1. Changes in FNR (formate to nitrate molar ratio) and pH for experiments with different IFNRs (initial formate to nitrate molar ratios). 122

7.1. Properties of CNTs used in this study 144

SI-7.1. Quantification methods for carbon nanotubes. 175

SI-7.2. CNT I_D/I_G ratios and the temperature at 50% CNT mass loss under oxidizing conditions. 177

9.1. Summary of materials tested for photocatalytic nitrate reduction using water as a hole scavenger. 212

LIST OF FIGURES

FIGURE Page

2.1. Average groundwater nitrate concentrations for the Phoenix metropolitan area (1996-1998). 7

2.2. Simplified Band Diagram of a Solid Semiconductor 13

2.3. Photoelectrochemical Cell 16

2.4. Photocatalyst (TiO_2) Particle Loaded with Pt (Cathode) and RuO_2 (Anode) 17

2.5. Semiconductor Heterostructures 18

3.1. XRD patterns for commercial TiO_2 photocatalysts 45

3.2. TEM images of commercial TiO_2 photocatalysts: (a) UV100 particles, (b) UV100 layered TiO_2 structure, (c) precursor of the UV100 layered structure in Figure 3.2b with a schematic of the multi-walled particle, (d) P90, and (e) P25. Scale bar = 50 nm for (a, b, c) and scale bar = 20 nm for (d, e). 47

3.3. UV-VIS absorbance spectrum for commercial TiO_2 photocatalysts and the nitrate anion (at the experimental molarity of 7.14 mM). 48

3.4. Average zeta potential for commercial titanium dioxide photocatalysts. Error bars represent 95% confidence intervals. 49

3.5. Nitrate fraction remaining as a function of photon concentration using an initial nitrate concentration of 100 mg-N/l and 40 mM formic acid 51

FIGURE Page

3.6. Percent nitrate removal after maximum irradiance (6.46 x 10^{22} photons/L). MW = model water, GW = groundwater, and 1 or 0.1 g/L represents the photocatalyst loading (40 mM formic acid and 100 mg-N/L nitrate initially). Removal of nitrate by UV100 (1 g/L) was 8% in model water. 52

3.7. Relationship between percent nitrate removal and the total surface area of P25 and P90 photocatalysts in solution. Inset: The percent difference between the percent nitrate removals for model water and groundwater as a function of total catalyst surface area. 55

3.8. Pseudo first-order kinetics of nitrate removal as a function of photon concentration using P90 in the presence of formic acid. 57

3.9. Standard reduction potentials (NHE) for nitrogen compounds in aqueous solution in relation to the band positions of anatase TiO_2. CB and VB represent the conduction and valence bands, respectively. The standard potentials of the nitrogen compounds were calculated for pH 7 (Pourbaix & De Zoubov, 1966). The band positions of TiO_2 at pH 7 were calculated for colloidal TiO_2 (Michael Gratzel, 1989). 62

4.1. TEM images of (a) P90 and (b) P90/Ag(5%). Black particles in (b) are silver nanoparticles; some are highlighted with circles (~2–3 nm). 76

FIGURE Page

4.2. Concentrations of nitrogen compounds and formate as functions of photon fluence for the baseline experiment (7.14 mM NO_3^-, 40 mM HCOOH, 1 g/L P90/Ag(1%), pH = 2.5). 78

4.3. NH_4^+ selectivity and the maximum NO_2^- concentration as a function of (a) photocatalyst concentration (P90/Ag) in the reactor and (b) the percent mass of silver loaded onto P90. The silver loading in (a) is kept constant at 1%, and the photocatalyst concentration in (b) is constant at 1 g/L. Initial concentrations for nitrate (100 mg-N/L) and formic acid (40 mM, pH = 2.5) were constant. Photon fluence = 29×10^{18} photons/cm^2 81

4.4. Nitrite and ammonium selectivity at different initial pH after 39 x 10^{18} photons/cm^2 (56 min) of irradiation and ~100% nitrate removal. Initial concentrations were 100 mg-N/L nitrate, 40 mM formate, and 1 g/L P90/Ag (1%). 84

4.5. The pseudo-first-order rate constant, k, at pH = 2.5–2.7 for nitrate and formate as a function of (a) FNR at a constant initial nitrate concentration, 7.14 mM, and (b) nitrate and formate concentration at a constant FNR, 5.6. (c) Relationship between moles of formate removed and moles of nitrate removed for all of these experiments performed at pH = 2.5. 86

SI-4.1. XPS spectrum of P90/Ag(2%). The dotted line represents the "Bulk Ag $3d_{5/2}$" peak position for silver. 93

FIGURE Page

SI-4.2. Kubelka-Munk absorbance as a function of photon wavelength for P90 and P90/Ag(1%). 93

SI-4.3. Zeta potential analysis for P90 and P90/Ag(1%). 94

SI-4.4. Pseudo-first-order kinetics for nitrate and formate as a function of photon fluence for the baseline experiment (7.14 mM NO_3^-, 40 mM HCOOH, 1 g/L P90/Ag(1%), pH = 2.5). 94

SI-4.5. The pseudo-first-order rate constant, k, for nitrate as a function of (a) photocatalyst concentration (P90/Ag(1%)) in the reactor and (b) the percent mass of silver loaded onto P90 (1 g/L). All samples had initial concentrations of 7.14 mM nitrate and 40 mM formic acid (pH = 2.5). 95

SI-4.6. Electrochemical potential of the one-electron nitrate couple and relevant reductants. 96

5.1. Nitrate removal in synthetic NaCl brines (0%, 3%, 6%, and 10% by weight) as a function of photon fluence absorbable by TiO_2 using (a) UV alone and (b) P90+FA+UV. The initial concentration of nitrate was ~500 mg-N/L for all samples. For P90+FA+UV samples, 1-g/L P90 and 200-mM formic acid were initially added to the solution. 109

FIGURE Page

5.2. Nitrate removal in a non-modified IX brine, synthetic brine (4.2% NaCl solution, 1740 mgN/L nitrate), and sulfate-removed IX brine as a function of photon fluence absorbable by TiO_2. The nitrate concentration in the IX brine was 1740 mgN/L. The concentration of P90 in solution was constant at 1 g/L. In all samples, 700 mM formic acid was added initially..... 112

5.3. Nitrate and formate removal as a function of photon fluence adsorbable by TiO_2 in sulfate-removed brine for varying initial formate to nitrate molar ratios (IFNRs). The concentration of P90 in solution was constant at 1 g/L. 114

5.4. Schematic of an ion exchange system integrated with photocatalytic nitrate reduction of IX brine for reuse. FA represents formic acid. 115

5.5. Breakthrough curves of nitrate and formate for fresh IX resin (a) and regenerated resin (b, c). The regenerant used before (b) was 6% NaCl containing 400-mM FA (500 mL), pH = 3.0; the regenerant used before (c) was 6% NaCl containing 400-mM FA (500 mL), pH=3.0, followed by 50 mL fresh 6% NaCl..... 117

SI-5.1. X-ray photoelectron spectrum of recycled P90 (TiO_2) after nitrate reduction in non-modified ion exchange brine. 119

SI-5.2. Nitrate removal in the real ion exchange brine with different sulfate concentrations varying at 50, 550, 1000, and 6000 mg/L as a function of photon fluence absorbable by TiO_2. The concentration of P90 in solution was constant at 1 g/L. Initially, 700-mM formic acid was added. 120

FIGURE Page

SI-5.3. Removal of nitrate, formate, and total dissolved nitrogen (TDN) as well as formation of nitrogen reduction by-products (NO_2^-, NH_4^+) as a function of photon fluence absorbable by TiO_2 in sulfate-removed brine. The concentration of P90 in solution was constant at 1 g/L. Initially, 700-mM formic acid was added. 121

6.1. Energy diagram of a typical n-type semiconductor. E_a is the electron affinity, E_G is the bandgap, Φ is the work function, and E_I is the ionization energy..... 124

6.2. Photocurrent measurement setup. 132

6.3. TEM image of P90 loaded with 1% Pt nanoparticles (examples circled in red). 133

6.4. TEM images of MWCNTs coated with TiO_2. 135

6.5. Current-potential diagram showing photocurrent for three graphene composites... 137

6.6. Image of TiO_2 sol/GNP(2%) coated FTO glass..... 137

7.1. Percent CNT mass remaining after heating to 870 °C under inert conditions for several CNTs..... 150

7.2. Percent CNT mass remaining after heating to 910 °C under oxidizing conditions. MW-F and MW-O were representative of all other raw CVD MWCNTs not shown. 153

7.3. I_D/I_G ratio as a function of oxidation temperature at 50% mass loss for all MWCNTs. 155

FIGURE Page

7.4. (a) Percent of NEC (NEC/TC × 100%) present in various laboratory, environmental, and biological matrices. (b) Percent NEC mass remaining from various matrices and percent mass remaining for three CNTs representing the lower (MW-F) and upper (MW-15) range of weak CNTs and strong (MW-Arc) CNTs. NEC mass is the percent remaining after treatment under inert conditions such that all volatile OC has been removed. 158

SI-7.1. Instrument schematic. 166

SI-7.2. Thermogram example (sucrose) showing how OC, PEC, and EC are traditionally defined using the NIOSH temperature program. A 100% He carrier gas is used for non-oxidizing conditions, and a 90% He/10% O_2 carrier gas is used for oxidizing conditions. 167

SI-7.3. Calibration curve for MW-F CNT stock solution (0.85 g/L) using a manual gas split. 169

SI-7.4. Thermograms of CNTs under non-oxidizing conditions using the NIOSH temperature program. 170

SI-7.5. Percent MW-O mass remaining after analysis under non-oxidizing conditions at various maximum temperatures. 170

SI-7.6. Mass loss curves of CNTs under oxidizing conditions. 171

FIGURE Page

SI-7.7. Raman spectroscopy of (a) MW-Arc and MW-P D-band and G-band peaks and (b) of the radial breathing mode for SWCNTs (SW) and MWCNTs (MW-P). SWCNTs (not shown) have a very similar D-band/G-band peak ratio as the MW-Arc. 172

SI-7.8. Raman spectroscopy of MW-Mitsui in a digest Cyanobacteria matrix loaded onto a quartz-fiber filter. Inset: Raman microscope image shows the CNT aggregate (indicated by arrow) used to gather the Raman spectrum. 173

SI-7.9. Thermograms of (a) urban air and (b) urban air spiked with 3 µg MW-Mitsui CNTs. The EC in (a) was determined by conventional air analysis using optical correction, and the CNTs in (b) by a manual split as discussed in this study... 174

SI-7.10. PTA analysis of GNP and GO – Fraction of graphene remaining as a function of oxidation time and temperature for (a) GNPs and (b) GO. 179

8.1. Digestion procedure for rat lung tissue and CNTs..... 185

8.2. Percent recovery for S-CNTs and W-CNTs following various digestion methods. 188

8.3. Peak fraction of the total CNT area for each temperature step and time required for 50% mass loss for a W-CNT under oxidizing conditions after treatment with various methods. Grey shaded area is the functionalized W-CNT (F-CNT) after treatment with Solvable. 190

FIGURE Page

8.4. Peak fraction of the total CNT area for each temperature step and time required for 50% mass loss for an S-CNT under oxidizing conditions after treatment with various methods. 191

8.5. I_D/I_G ratios obtained from Raman spectroscopy for CNTs after treatment with using various chemicals (60 °C for 24 hrs). 193

8.6. Rat lung tissue after various digestion methods and centrifugation. (a) Solvable, (b) ammonium hydroxide, (c) nitric acid, (d) sulfuric acid, (e) hydrochloric acid, (f) hydroflouric acid, (g) hydrogen peroxide, and (h) pro K. 195

8.6. Thermograms for a whole rat lung after treatment with (a) Solvable followed by (b) pro K. Data has been cropped to show only the temperatures that S-CNTs oxidize at (i.e., ~650-900 °C)..... 196

SI-8.1. PTA program for evaluating CNTs..... 198

SI-8.2. Image of functionalized W-CNT pellet after treatment with Solvable..... 198

SI-8.3. Thermograms for (a) S-CNTs and (b) W-CNTs after various treatments. 199

9.1. Band gaps of various metal oxides along with the reduction potentials for nitrate (to nitrite) and water (to oxygen). Data adapted from (Y. Xu & Schoonen, 2000). All numbers are subscripts..... 206

FIGURE Page

9.2. Band gaps of various metal sulfides along with the reduction potentials for nitrate (to nitrite) and water (to oxygen). Data adapted from (Y. Xu & Schoonen, 2000). All numbers are subscripts. 207

9.3. Conceptual design of a tandem photoelectrochemical system for nitrate reduction and water oxidation. E_F is the Fermi level. CB and VB are conduction band and valence band, respectively. 213

CHAPTER 1

INTRODUCTION

Population growth has a profound effect on our water quality. Not only does it further deplete our water sources, it ultimately leads to a larger influx of contaminants into surface and ground water, making it more difficult and expensive to use them for drinking water. As our potable supplies decrease, we will have to develop more sustainable and economic treatment technologies to keep up with the increased demand. With recent advances in material science and the introduction of nanotechnology, environmental engineers are poised to revolutionize the way we approach treatment issues.

Manipulation of materials at the nano-scale implements new physico-chemical properties that changes how materials behave compared to their macro counterparts. While this can be beneficial, it also introduces a new set of concerns about the risk of nanomaterial to human health and the environment. Often, materials scientists are only concerned with material design without much regard to how the material will be used or how it might impact the environment. As environmental engineers utilizing nanotechnology to develop new solutions for water treatment, we have a responsibility to evaluate the risks associated with the new materials we create. Within this dissertation, this is defined as responsible engineering.

Responsible engineering of new materials encompasses a number of risk assessment moieties including material characterization, dose-response, and exposure. The ability to identify the material in simple and complex matrices is essential to all parts

of risk assessment. Detection of nanomaterials is inherently difficult because the only thing that separates them from their macro counterparts is size, and defining this border is not simple. For some nanomaterials, this size difference also introduces unique properties that allow them to be identified (e.g., fluorescence of single-walled carbon nanotubes). In most cases though, such as that with metals, size is the only obvious property separating them from similar materials.

With the increase in population comes an increase in food demand. This results in an increased influx of nitrate-based fertilizers into our water sources, further limiting the availability of groundwater as a drinking water source. This dissertation aims to leverage recent advances in material science to implement photocatalysis as a sustainable solution for treatment of nitrate-laden water. To date, research on photocatalytic nitrate reduction has really been limited to material development and there has been no environmental engineering studies looking at the ability of photocatalysts to reduce nitrate under realistic or full-scale conditions. The results presented herein will help to set a precedent for engineering materials specifically for environmental applications.

Dissertation Overview

The overarching goal of this dissertation was to evaluate photocatalysis as a treatment option for nitrate in water. Both commercial and laboratory materials of nano- and macro-size were used and responsible engineering was invoked for the engineered nanomaterials. Background material is first presented to give the reader some relevant information about nitrate pollution, photocatalysis, and photocatalytic nitrate reduction

(Chapter 2). The main body of this dissertation is composed of a series of experiments isolated into main research objectives and is as follows:

1. Commercial TiO_2 photocatalysts were evaluated for nitrate reduction in a model water and a groundwater (Chapter 3).
2. The optimal commercial TiO_2 photocatalyst, P90, is improved through the use of a co-catalyst, silver. Macro-scale mechanisms of photocatalytic nitrate reduction relevant to operating conditions were investigated including photocatalyst concentration, silver loading, nitrate concentration, formate concentration, and pH (Chapter 4).
3. Commercial TiO_2 was evaluated as a photocatalytic treatment option for ion-exchange brines to extend the lifetime of brine regeneration systems (Chapter 5).
4. Various metal and carbonaceous nanoparticle co-catalysts for TiO_2 were screened for nitrate reduction to work toward improving nitrate removal activity and by-product selectivity toward N_2 (Chapter 6).
5. Of the nanomaterials utilized, carbon nanotubes and graphene were the only ones without an established detection method. To maintain responsible engineering, a new method was developed for detecting these nanomaterials in environmental matrices, with application to cyanobacteria and urban air for the carbon nanotubes (Chapter 7).
6. To improve upon the detection method for carbon nanotubes and assist with *in vivo* dose-response studies in rats, various extraction methods were evaluated for carbon nanotubes and applied to rat lungs (Chapter 8).

7. The results presented on photocatalytic reduction of nitrate were synthesized to create framework for engineering more efficient and nitrate-specific photocatalysts (Chapter 9).

Finally, a summary of the objectives and the outcomes of this dissertation, including conclusions and future recommendations are discussed (Chapter 10).

CHAPTER 2

BACKGROUND

2.1 Nitrate Pollution

Of the contaminants we are faced with today, nitrate (NO_3^-) is one the most prevalent in groundwater in North America (B. Nolan, 2004; B. T. Nolan & Hitt, 2006; Bernard T. Nolan, Hitt, & Ruddy, 2002; B. T. Nolan & Stoner, 2000). It is a naturally occurring inorganic ion, but anthropogenic sources have contributed to unbalancing the nitrogen cycle. Nitrate pollution stems from both agricultural (Rupert, 2008) and urban sources (Wakida & Lerner, 2005). The main source of anthropogenic nitrate is found in rural areas and originates from fertilizers, livestock, and septic systems. Only about 18% of the nitrogen in fertilizer (nitrates) is actually used by vegetation, leaving the remaining 82% in the soil (Carpenter et al., 1998). Because of the high water solubility of nitrate, the remaining mass can be transferred to surface waters from surface runoff or leached into the groundwater.

Excess nitrate that reaches surface waters contributes to eutrophication, which is detrimental to the aquatic ecosystem, depleting dissolved oxygen, killing fish, and creating a harmful environment for humans. One example of this is the Gulf of Mexico hypoxic “dead” zone (less than 2 ppm dissolved oxygen) located at the mouth of the Mississippi River. Nitrate has been shown to be the primary reason for this hypoxic zone (Scavia & Donnelly, 2007). The Gulf of Mexico zone is one of the largest known dead zones in the world covering approximately 7,000 square miles (Rabalais, Turner, & Scavia, 2002). It has a great societal and economic impact on the commercial and

recreational fisheries of the Gulf Coast, a $2.8 billion annual economy (Rabalais, Turner, & Wiseman, 2001).

Nitrate that leaches into the groundwater has the potential of polluting drinking water sources. People in rural areas are at the highest risk from excess fertilizer use, and almost 90% of the rural population uses groundwater for domestic purposes (Power & Schepers, 1989). A survey of 5,101 wells in the United States revealed that nitrate levels exceed the standard (10 mg/L as N) in approximately 8% wells (20% agricultural, 3% urban, 4% major aquifers), affecting over 24.6 million people (Burow, Nolan, Rupert, & Dubrovsky, 2010). Even with proper regulations in place and best management practices for fertilizers, nitrate concentrations in groundwater continue to increase (Rupert, 2008).

In Phoenix, AZ, where urban sprawl is abundant, nitrate poses a problem for water municipalities and private well owners that occupy land once used for agricultural purposes. Nitrate concentrations range from 2 to 40 mg-N/L, with the maximum average around 25 mg-N/L (Figure 2.1). The City of Glendale, which bears the weight of this legacy fertilizer pollution, currently treats for nitrate in order to meet the United States Environmental Protection Agency's (USEPA) drinking water requirements.

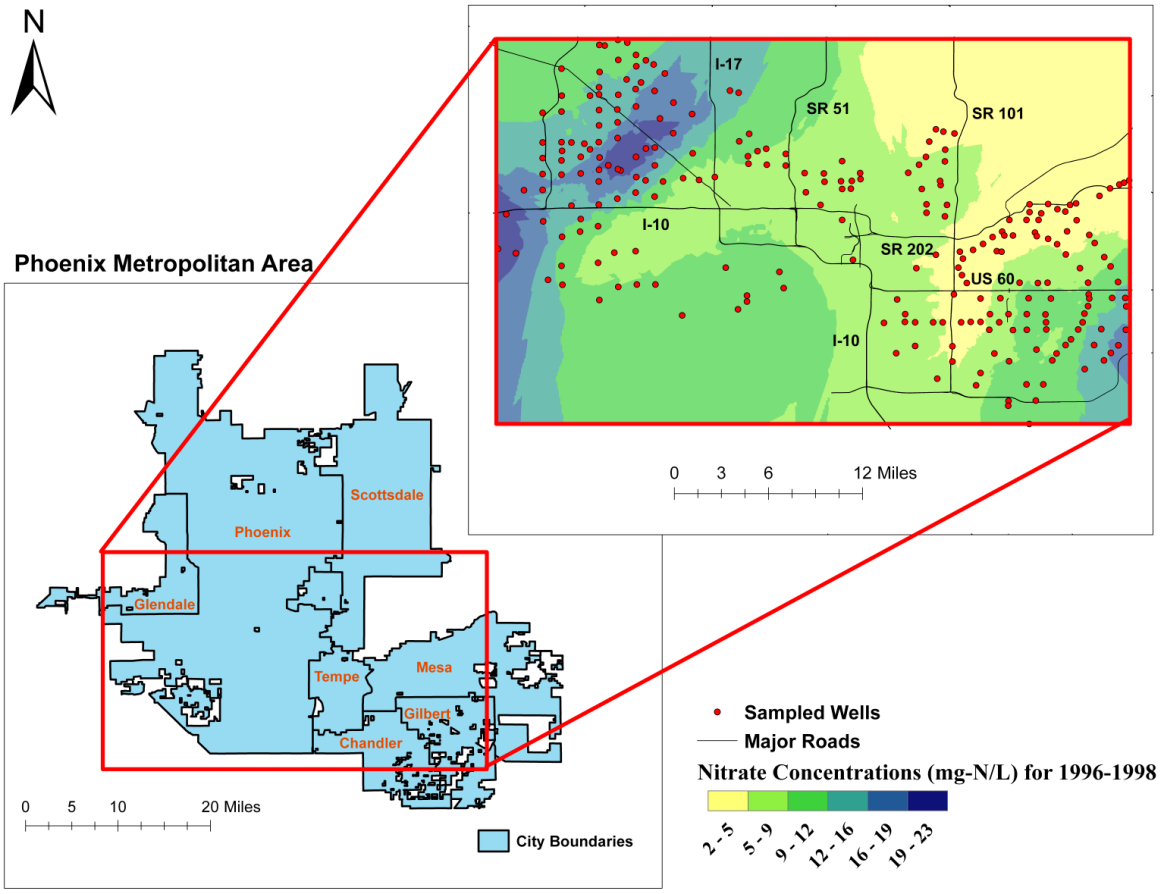


Figure 2.1. Average groundwater nitrate concentrations for the Phoenix metropolitan area (1996-1998).

Nitrate poses a risk to human health, and as such, it has been placed on the USEPA's Drinking Water Contaminant List, with maximum contaminant level of 10 mg/L as N. It is a known cause of methemoglobinemia, or "blue baby" syndrome, and could possibly be carcinogenic (National Research Council, 1995). Nitrate is relatively non-toxic to humans; however, it can be reduced by denitrifying bacteria in the upper gastro-intestinal tract to form nitrite, which is the underlying cause of methemoglobinemia. Nitrite absorbs into the bloodstream where it reacts with hemoglobin, oxidizing it to methemoglobin ($Fe^{2+} \rightarrow Fe^{3+}$), which cannot carry oxygen

thus causing cyanosis and anoxemia (Bruningfann & Kaneene, 1993). Adults are generally at low-risk for methemoglobinemia because they possess a key enzyme called NADH-cytochrome b_5 reductase, which reduces methemoglobin back to hemoglobin (Avery, 1999). However, infants are at a much higher risk to methemoglobinemia because the high pH of their gastro-intestinal tract promotes the growth of denitrifying bacteria, their hemoglobin is much more readily oxidized to methemoglobin, and they lack the important methemoglobin reductase (Atsdr, 2007; Avery, 1999). Nitrate has also been suggested to form compounds in the human body that are carcinogenic or endocrine disruptors (Guillette & Edwards, 2005; Hamlin, 2006; Hamlin et al., 2008)

Beyond human health and ecotoxicity implications, excess anthropogenic nitrate unbalances the natural nitrogen cycle. The National Academy of Engineers (NAE) considers management of the nitrogen cycle to be one of its Grand Challenges. Part of the nitrogen cycle is natural denitrification, which helps keep nitrogen in the environment balanced. Unfortunately, anthropogenic sources of nitrogen have unbalanced this system, and there is a need for engineered denitrification. The challenge will be figuring out how to reduce nitrate to innocuous forms rather than toxic by-products or greenhouse gases (e.g., ammonia and nitrous oxide, respectively).

Current Nitrate Treatment Technologies in Drinking Water

Table 2.1 shows the currently available nitrate treatment technologies, their current state with regards to full-scale implementation, the advantages, and the disadvantages. To date, the most efficient technologies for removing nitrate from drinking water are ion exchange and biological denitrification. Ion exchange is the most

used technology because it is simple to operate, efficient, and high concentrations of nitrate can be treated. However, this method produces a brine waste that still requires treatment, and competing anions can severely retard the efficiency. Biological denitrification is common for wastewater treatment, and it is starting to show some momentum for denitrification of drinking water sources (Gayle, Boardman, Sherrard, & Benoit, 1989; Hiscock, Lloyd, & Lerner, 1991; K.-C. Lee & Rittmann, 2002; Mateju, Cizinska, Krejci, & Janoch, 1992; McAdam & Judd, 2006b, 2008; Richard, 1989; M. I. M. Soares, 2000). It can treat large volumes of high concentration nitrate and it can reduce nitrate to non-toxic forms; however, biological denitrification is not without disadvantages. The process requires an electron donor and a carbon source, downstream treatment is usually required to remove contamination, the bio-membranes can be fouled, membrane fouling, and the startup time takes weeks so it is not suitable for intermittent operations (K.-C. Lee & Rittmann, 2002; McAdam & Judd, 2006b). Other treatment technologies for nitrate removal include **catalytic** (Barrabes & Sa, 2011; Barrabés et al., 2006; Chaplin et al., 2012; Daub, Wunder, & Dittmeyer, 2001; Devadas, Vasudevan, & Epron, 2011; Epron, Gauthard, & Barbier, 2002a, 2002b; W. Gao et al., 2003; Garron & Epron, 2005; Gauthard, Epron, & Barbier, 2003; Gašparovičová et al., 2007; Guo, Cheng, Hu, & Li, 2012; Guy, Xu, Yang, Werth, & Shapley, 2009; Horold, Vorlop, Tacke, & Sell, 1993; J. Y. Liu, Choe, Sasnow, Werth, & Strathmann, 2013; Nakamura, Yoshida, Mikami, & Okuhara, 2006; Palomares, Franch, & Corma, 2010; Palomares, Prato, Marquez, & Corma, 2003; Palomares, Prato, Rey, & Corma, 2004; Pintar, 2003; Prusse & Vorlop, 2001; Prüsse, Hähnlein, Daum, & Vorlop, 2000; Sa, Berger, et al., 2005; Sa, Gasparovicova, et al., 2005; Sakamoto, Kanno, Okuhara, & Kamiya, 2008; O. Soares,

Fan, Orfao, Lapkin, & Pereira, 2012; O. Soares, Orfao, & Pereira, 2008, 2010, 2011a, 2011b; Sun, Li, Gao, & Shang, 2012; Theologides, Savva, & Costa, 2011; Wada, Hirata, Hosokawa, Iwamoto, & Inoue, 2012; Wehbe, Guilhaume, Fiaty, Miachon, & Dalmon, 2010; Y. B. Xie, Cao, Li, Zhang, & Crittenden, 2011; Yi, Sakamoto, & Kamiya, 2009; F. X. Zhang et al., 2008), **electrochemical** (S. E. Bae & Gewirth, 2008; Benderskii, Krivenko, & Ponomarev, 1989; da Cunha, De Souza, & Nart, 2000; Dash & Chaudhari, 2005; Dortsiou, Katsounaros, Polatides, & Kyriacou, 2009; Duca, Kavvadia, et al., 2010; Duca, Khamseh, Lai, & Koper, 2010; Duca & Koper, 2012; Duca, van der Klugt, & Koper, 2012; Katsounaros et al., 2012; Katsounaros, Ipsakis, Polatides, & Kyriacou, 2006; Katsounaros & Kyriacou, 2008; Molodkina, Botryakova, Danilov, Souza-Garcia, & Feliu, 2012; Pletcher & Poorabedi, 1979; V. Rosca, Duca, de Groot, & Koper, 2009; Shimazu et al., 2007), **chemical** (Buresh & Moraghan, 1976; Chi, Zhang, Lu, Dong, & Yao, 2004; Fanning, 2000; Liou, Lo, Lin, Kuan, & Weng, 2005; Luk & Au-Yeung, 2002; Murphy, 1991; Ottley, Davison, & Edmunds, 1997; Ramavandi, Mortazavi, Moussavi, Khoshgard, & Jahangiri, 2011; Rodriguez-Maroto, Garcia-Herruzo, Garcia-Rubio, Gomez-Lahoz, & Vereda-Alonso, 2009; Westerhoff, 2003; Westerhoff & James, 2003; G. C. C. Yang & Lee, 2005; Young, Bungay, Brown, & Parsons, 1964), **reverse osmosis/electrodialysis** (Bohdziewicz, Bodzek, & Wasik, 1999; Cevaal, Suratt, & Burke, 1995; El Midaoui et al., 2002; Elmidaoui et al., 2001; Hell, Lahnsteiner, Frischherz, & Baumgartner, 1998; Howe & Gratzel, 1985; Indusekhar, Trivedi, & Shah, 1991; Kesore, Janowski, & Shaposhnik, 1997; Panyor & Fabiani, 1996; Rautenbach, Kopp, Vanopbergen, & Hellekes, 1987; Richards, Vuachere, & Schafer, 2010; Sata, Yamaguchi, & Matsusaki, 1995; Schoeman, 2009; Schoeman & Steyn, 2003), and

combinations of these (Kapoor, Inagaki, & Yoshida, 2005). Photocatalysis, the focus of this dissertation, is a relatively new technology for water treatment applications that emerged around thirty years ago (Hsiao, Lee, & Ollis, 1983).

Table 2.1. *Current nitrate treatment technologies and their advantages and disadvantage.*

Treatment Technology	Current Availability	Advantages	Disadvantages
Ion Exchange	Full-scale	Stable, fast removal, easily automated, cost-effective, low-maintenance, non-destructive	Requires treatment or disposal of brine waste, suitable only for small- and medium-scale operations, may produce toxic by-products, not good for waters with high total dissolved solids (i.e., groundwater only)
Blending	Full-scale	Easy, economic, non-destructive	Requires close non-nitrate source water
Membrane (e.g., reverse osmosis and electrodialysis)	Full-scale	Good for waters with high total dissolved solids content, no by-products, non-destructive	Expensive – energy intensive and large capital costs, inefficient nitrate removal, requires treatment or disposal of concentrate
Biological Denitrification	Full-scale	Produces a non-toxic by-product (i.e., N_2), suitable for large applications, can handle high concentrations, destructive method	Electron donor and carbon source required, requires downstream treatment (e.g., ozonation), high-maintenance, long start-up times, pH and temperature sensitive, membrane foulding
Electrochemical (e.g. SnO_2 electrode)	Full-scale	Selective toward non-toxic by-product (i.e., N_2), destructive method	Electrode fouling, operational difficulty, energy intensive
Catalytic (e.g., Pd)	Pilot-scale	Selective toward non-toxic by-product (i.e., N_2), efficient, destructive method	Catalyst fouling, expensive metals, reductant such as H_2
Chemical Denitrification (e.g., Al or Fe)	Bench-scale	High removal, zero-valent iron for in-situ treatment, efficient, destructive method	pH sensitive, no reuse of material
Photocatalysis (e.g., TiO_2)	Bench-scale	Selective toward non-toxic by-product (i.e., N_2), energy-efficient (through use of solar spectrum), destructive method	Electron-donor required (for current materials), *to be determined*

2.2 Photocatalytic Reduction of Nitrate

Importance of Developing Photocatalysts for Water Treatment

Advances in science and technology will be needed to meet the growing energy demand in the United States. More importantly will be the need for the advancement of cheap and clean energy to reduce our reliance on foreign oil and decrease greenhouse gas emissions. The United States Department of Energy (DOE) lists the generation of fuels from sunlight and the ability to create energy from carbon dioxide (i.e., clean energy) as two of the three strategic goals to secure a sustainable energy future for the United States (Energy, 2008). Currently, water treatment in the United States accounts for approximately 3% of the national energy consumption (USEPA, 2009). Development of photocatalyst technologies that are selective and visible-light active will have a large impact on the water-energy nexus. Photocatalytic technologies will reach a pinnacle when they can harness solar power to treat water and create a storable energy source from the treated by-products.

Photocatalyst Dissertation Terminology

The scope of this research encompasses a wide range of disciplines and many of the terms used henceforth are not familiar in the Environmental Engineering field. The following section gives an explanation of commonly used terms in photoelectrochemistry and solid-state physics.

Bands: Bands exist in solids and consist of a large number of overlapping orbitals with different energy levels based on the Pauli exclusion principle that overlapping orbitals

cannot occupy the same energy level. Bands are formed from the statistical or quantum distributions of energy levels in an atom, molecule, or solid. Figure 2.2 shows a simplified schematic of band structures of a semiconductor.

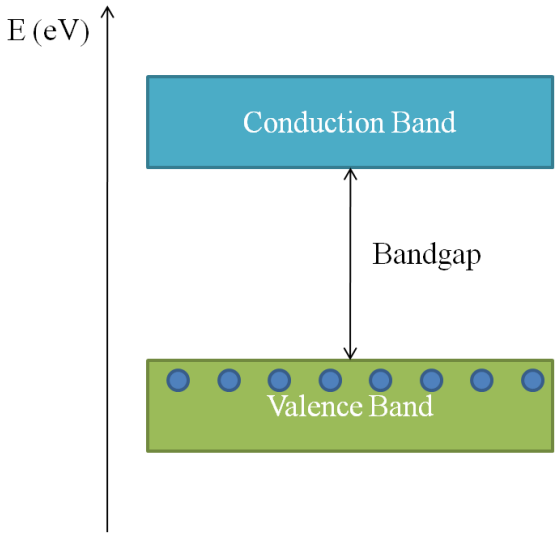


Figure 2.2. Simplified Band Diagram of a Solid Semiconductor

Conduction band: The upper band shown in Figure 2.2 is the conduction band (CB) and is synonymous with the lowest unoccupied molecular orbit (LUMO) of a molecule or the first excited state. For a semiconductor and under normal conditions, no electrons exist in the CB. Thermodynamically, it is a measure of the reduction potential of the semiconductor. The more negative the CB lies (NHE), the greater the reduction potential.

Valence band: The lower band shown in Figure 2.2 is the valence band (VB) is synonymous with the highest occupied molecular orbit in a molecule (HOMO). For a semiconductor and under normal conditions, electrons exist in the VB.

Thermodynamically, it is a measure of the oxidation potential of the semiconductor. The more positive the VB lies (NHE), the greater the oxidation potential.

Bandgap: The gap between the conduction band and valence band states is known as the bandgap, the area where no allowed electronic states exist (Figure 2.2). For metals, the bandgap is non-existent and the bands overlap (~0 eV), and for insulators, the bandgap is greater than about 5 eV (with some exceptions), and semiconductors fall between these. The zero bandgap of metals is what gives them their unique conductivity because electrons are able to move freely between bands. On the other hand, semiconductors need an external energy source (e.g., photons) to excite the electrons from the valence band to the conduction band.

Hole: A hole is the imaginary space charge in the valence band where an electron once resided. It is the absence of a negatively charged particle and it is considered a positively charged particle.

Fermi level: The Fermi level is the electrochemical potential or the chemical potential, μ, of electrons in the solid. It is dependent on the number of electrons and holes in energy levels of the solid.

Photo-excitation: The process of irradiating a semiconductor with a wavelength greater than the bandgap such that an electron in the valence band is excited to the conduction band, forming an electron-hole pair.

Exciton: Another name for the electron-hole pair that is created from excitation.

Recombination: A process where the electron and hole recombine in the valence band or other localized sites such as surface and bulk trap sites. The exciton can recombine within a matter of hundreds of nanoseconds if the electron or hole is not trapped or does not immediately participate in chemical reactions.

Work function: The energy required to remove an electron from a solid to a point immediately outside the solid (vacuum level).

Doping: The addition of charged carriers to a semiconductor to form majority and minority charged particles is called doping. For example, when Si (four valence electrons) is doped with phosphorus (5 valence electrons), four of the P atom's electrons bond with 4 of the Si atom's electrons, leaving one P atom electron free to move about the conduction band without leaving a hole in the valence band. This creates a majority of electrons, thus leaving the semiconductor negatively charged, also known as an n-type. Similarly, if Si is doped with B atoms (3 valence electrons), this leaves an excess of holes as the majority charge carrier, thus leaving the semiconductor positively charged, also known as a p-type. A p-type and an n-type semiconductor will have Fermi level shifted toward the valence band and conduction band, respectively. Doping can also be used to form traps in a semiconductor or photocatalyst. A trap is an allowed energy state within the forbidden energy state (e.g., bandgap) that will allow for tuning the chemical potential of the semiconductor. It can also act as a recombination site for the exciton. When doping

with metal cations, visible light efficiency can be improved given the lower energy states; however, they will be detrimental to the efficiency in UV light because of the increased number of locations for excitons to recombine (Litter, 1999).

Photoelectrochemical (PEC) cell: An electrochemical cell where the thermodynamic input is obtained from a photonic source. The anode and cathode are generally separated in an electrolyte solution and they are connected by a conductive wire to facilitate charge transfer. For an n-type electrode, the photoanode is the working electrode and the cathode serves as the counter electrode. In this particular case, the electrons flow from the working electrode to the counter electrode. A simplified illustration of a PEC cell is shown in Figure 2.3.

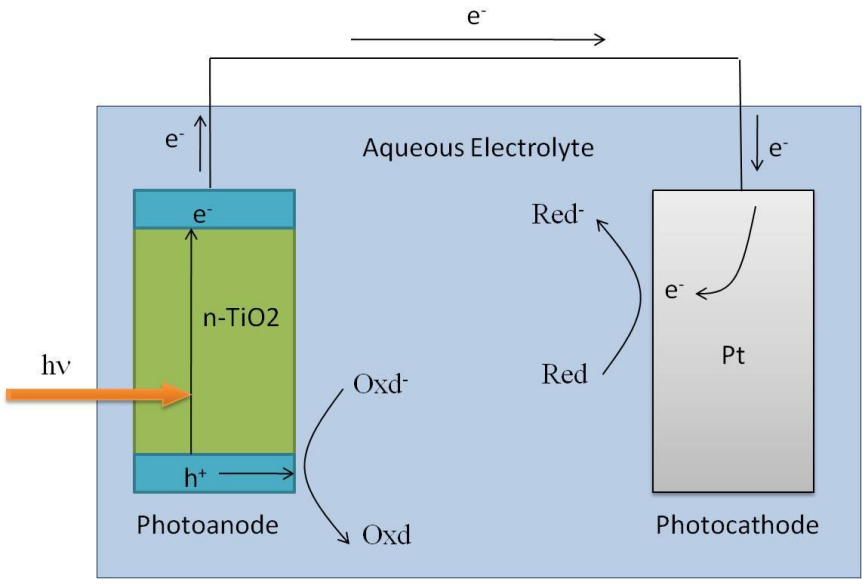


Figure 2.3. Photoelectrochemical Cell

Heterogeneous photocatalyst: As the name suggests, a photocatalyst is a light-activated catalyst, usually a semiconductor. Photocatalysis is based on semiconductor solid-state

and photoelectrochemical principles. Unlike an n-type PEC cell, where oxidation (at the anode) and reduction (at the cathode) reactions are physically separated, redox reactions on a heterogeneous photocatalyst occur simultaneously at the surface (Figure 2.4). In the case of Figure 2.4, Pt and RuO_2 have been loaded onto the surface of the TiO2 particle to act as an electron (anode) and hole (cathode) pooling site, respectively. When a semiconductor, such as TiO_2 or Si, absorbs a photon with an energy ($E = h\nu$) greater than or equal to the bandgap energy (E_{BG}) of the semiconductor, an electron is excited from the valence band into the conduction band.

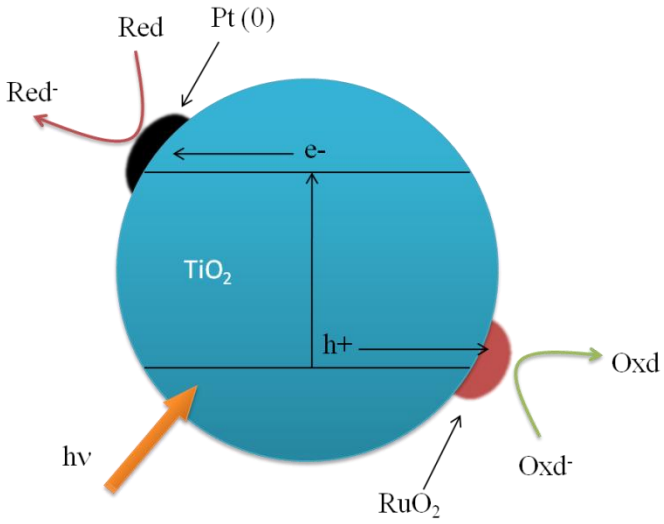


Figure 2.4. Photocatalyst (TiO_2) Particle Loaded with Pt (Cathode) and RuO_2 (Anode)

Hole scavenger: Also known as a sacrificial electron donor, it is a compound introduced into the sample matrix to act as a donor of electrons into the valence band to extend the lifetime of the electron.

Semiconductor homojunctions: A homojunction is created when two oppositely doped semiconductors of the same bandgap are joined at an interface known as the p-n junction

(e.g., n-type Si/p-type Si). After the junction is formed, the electrons from the p-type will flow toward the junction and holes from the n-type will flow toward the junction where they recombine. This leaves the p-type concentrated with holes in the bulk and electrons at the junction, the n-type concentrated with electrons in the bulk and holes at the junction, and the (p-n) junction a neutral, non-conductive zone.

Semiconductor heterojunctions: A heterojunction is created when two semiconductors (either p- or n-type) with different bandgaps are joined at an interface. There are three main types of heterojunctions that can be formed with respect to their band placement: straddled (Type I), staggered (Type II), and broken (Type III). These are illustrated in Figure 2.5. For optoelectronic applications such as photovoltaic cells and photocatalysts, Type II is the ideal case. Type I is generally used as a protective layer over a semiconductor that is susceptible to photocorrosion, such as ZnS, or to create p-type/n-type core/shells. Under normal conditions, the electrons will always move to higher potentials (down) and the holes to lower potentials (up).

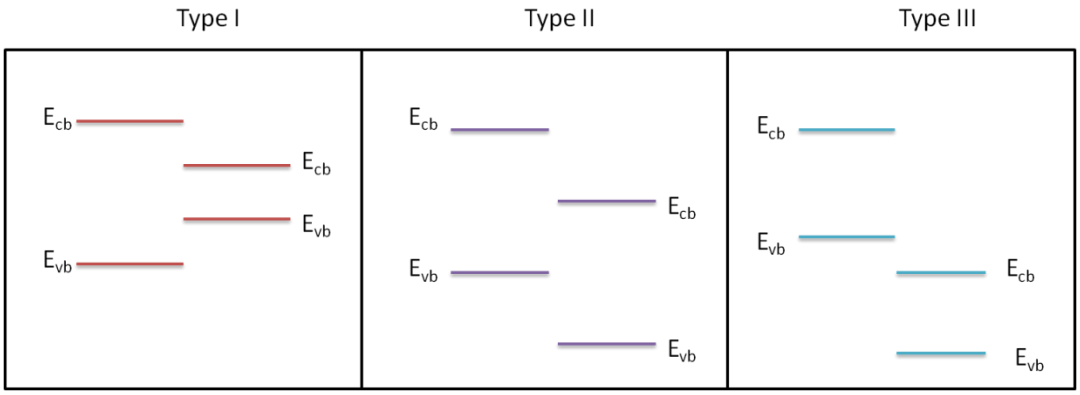


Figure 2.5. Semiconductor Heterostructures

When forming a junction between two solids, the Fermi level must be in thermal equilibrium. In other words, if a semiconductor possessing a work function (Φ_{S1}) comes into contact with a semiconductor having a working function (Φ_{S2}) less than Φ_{S1}, then electrons will flow from the smaller work function to the larger work function until the Fermi levels are equal. Thus the semiconductor with the smaller work function will become positively charged near the contact and negative into the bulk, whereas the semiconductor with the larger work function will do the opposite.

Schottky and ohmic contacts: A Schottky barrier is used to describe the potential interface between a metal and a semiconductor. It is the potential barrier seen by electrons trying to move toward the semiconductor. When a metal comes into contact with a semiconductor and the work function of the each is different, a Schottky potential barrier is formed. Under normal conditions, electrons will flow from the material with the lower work function to the higher work function. To move back across the interface the electron will need a potential greater than the Schottky barrier. For photocatalysts, this means that if the work function of the metal is higher than that of the semiconductor, then electrons will become trapped in the metal, thus acting as an electron scavenger or trap site. Compounds adsorbed to the metal can then react with the electrons. If the work functions of the two materials are similar, an ohmic contact is formed where electrons and holes are free to move across the junction. These types of composite semiconductors are very useful for charge separation and for loading photocatalysts with metals that have low hydrogen overpotentials in order to reduce water to H_2 (e.g., Pt).

Semiconductor-liquid interface: Similar to solid-solid junctions, when a bulk solid semiconductor comes into contact with a liquid, the Fermi level (i.e., chemical potential) of the solid must be in equilibrium with chemical potential of the liquid. This causes a bending of the bands up or down toward the liquid potential, depending on the location of the Fermi level. However, unlike bulk semiconductors which undergo band bending due to a potential difference, nano-sized semiconductors do not undergo band bending (or very little) because the distance between the bulk of the particle and the surface (i.e., particle radius) is large compared to the curvature of the bend (Hagfeldt & Gratzel, 1995).

A Short History of Photocatalysis for Environmental Applications

Semiconductor photocatalysts were first applied as photoelectrochemical cell systems for converting solar energy into chemical energy in the 1970s and 80s (A. Fujishima & Honda, 1972; Mills, Davies, & Worsley, 1993). Gratzel and co-workers were the first to make this technology efficient enough for full-scale use through his invention of a dye-synthesized titanium dioxide solar cell (M. Gratzel, 2001; Oregan & Gratzel, 1991). Formenti and co-workers were among the first to focus on the use of photocatalysts for environmental purposes (Formenti, Juillet, Meriaude.P, & Teichner, 1971; Formenti, Juillet, & Teichner, 1970; Formenti et al., 1972). These studies focused on paraffin oxidation in air and were very transcendent, showing the ability of photocatalysts to be used for decontamination. Some of the first and more well-known pioneering studies on photocatalytic treatment of compounds in water were done by Bard and co-workers (Frank & Bard, 1977), and Ollis and co-workers (Hsiao et al., 1983;

Pruden & Ollis, 1983). There are many thorough reviews available outlining the potential for heterogeneous photocatalysts for water treatment, and thus, this will not be discussed within this dissertation (Chong, Jin, Chow, & Saint, 2010; Herrmann, 1999; Hoffmann, Martin, Choi, & Bahnemann, 1995; Mills et al., 1993; Ollis, Pelizzetti, & Serpone, 1991; Ollis & Turchi, 1990; Robertson, Bahnemann, Robertson, & Wood, 2005; Huanjun Zhang, Chen, & Bahnemann, 2009).

Titanium Dioxide as a Photocatalyst

Since its conception in the water purification field, photocatalysis has expanded greatly, with most of the progress to date focused on the anatase phase of titanium dioxide (TiO_2) (Linsebigler, Lu, & Yates, 1995). TiO_2 has been used in many different applications including self-cleaning materials such as tiles, roofs, and clothing, and for the degradation of a myriad of organic and inorganic pollutants (Bhatkhande, Pangarkar, & Beenackers, 2002; Akira Fujishima & Zhang, 2006). It is a good model photocatalyst for environmental applications because it is relatively non-toxic, photostable, and inexpensive (Mills et al., 1993).

Photocatalysis Charge Transfer with Application to TiO_2

Photoexcited charge carrier kinetics govern the activity of the photocatalytic reaction. As such, minimizing the time it takes for the exciton to reach the photocatalyst surface is very important. The interfacial charge transfer is the rate at which an electron or hole migrates to the surface of the semiconductor and is then transferred to a species adsorbed to the surface, a catalyst loaded onto the surface, or constituents in the electric

double-layer. Laser flash photolysis or time-resolved spectroscopy has been used to show that the time of recombination is much faster than the rate of interfacial charge transfer (Hoffmann et al., 1995). The lifetime of the exciton can be extended by decreasing the rate of recombination or increasing the rate of interfacial charge transfer. For example, Bahnemann and co-workers (Bahnemann, Henglein, Lilie, & Spanhel, 1984) showed that the addition of platinum to the surface of the TiO_2 slowed the recombination rate by allowing the conduction band electrons (e^-_{cb}) to become irreversibly trapped in the metal catalyst. However, recent studies have shown the coinage metals (e.g., silver, copper) form true Schottky barriers, allowing for electron pooling, whereas other metals such as platinum and palladium form ohmic contacts with the photocatalyst (Takai & Kamat, 2011). Trapped electrons are available for reduction reactions at the surface of the metal catalyst or transfer to the double-layer. Transfer of the electron to a surface trap sites or other compounds on the surface, which then react with constituents of concern is considered an indirect transfer. A direct transfer is when the conduction band electron interacts directly with the adsorbed species on the surface of the TiO_2. Subsequently, holes will be available for oxidation reactions, whether it is from trapped holes (indirect) or from interfacial transfer (direct). Based on past studies on the mechanisms of semiconductor photocatalyst, additional materials should be added or coupled to the bare photocatalyst to inhibit recombination (e.g., Schottky barrier trap site).

The exciton transfer in a photocatalyst is diffusive and the theoretical transfer time for the exciton to reach the surface is given by Equation 2.1.

$$\tau = \frac{R^2}{\pi D}$$ (Robertson et al., 2005) (2.1)

Where, τ is the time for the charged carrier to reach the surface, R is the radius of the semiconductor particle, and D is the diffusion coefficient of excitons. Using a D = $5x10^{-3}$ cm^2/s and a radius of 2.5 nm, Bahnemann and co-workers (Robertson et al., 2005) determined a transit time of about 1.5 ps. Similarly, for P25 (radius ~ 11 nm), the transit time was calculated to be approximately 10 ps. These results highlight the importance of particle size for reduced recombination rates and increasing the photocatalytic activity.

Photocatalytic Reduction Reactions

Photocatalytic reactions can be tailored to suit either oxidation or reduction reactions. Most studies concerning photocatalysts to date have been focused on oxidation reactions (Chong et al., 2010; Hoffmann et al., 1995). The most likely reason for this is not that organic compounds are necessarily of more interest, but because the most stable photocatalysts (e.g., TiO_2) are metal oxides. Metal oxides have a strong oxidation potential (~3 V) as a result of valence bands formed by oxygen 2p orbitals, making them ideal for treating reduced pollutants. Consequently, the conduction band of metal oxides with band gaps approaching visible-light absorption (~ 3 eV) lie at or below the water reduction potential. As a result, the reduction potential for metal oxides is generally low (~ 0 V). Compounds, such as metal chalcogenides (e.g., ZnS) have more powerful reduction capabilities, as well as visible light activation, but they are susceptible to photocorrosion (i.e., self-oxidation) by the holes created in the valence band. Current

photocatalyst trends are now moving in the direction of engineering new semiconductor composites so that they have the ability for reduction and oxidation reactions, visible light activation, and photostability. These advanced photocatalysts can be classified as the third generation, and research is still heavily focused on material development with limited application. Even though most studies have been focused on oxidation of organics, there have been a number of studies looking at the reduction of carbon dioxide (CO_2) (Anpo, Yamashita, Ichihashi, Fujii, & Honda, 1997; Anpo et al., 1998; Cueto, Martinez, Zavala, & Sanchez, 2010; Dey, 2007; Guan, Kida, & Yoshida, 2003; Indrakanti, Kubicki, & Schobert, 2009; Inoue, Fujishima, Konishi, & Honda, 1979; Koci et al., 2010; Koci, Obalova, & Lacny, 2008; Koci et al., 2009; Nguyen & Wu, 2008a, 2008b; Nguyen, Wu, & Chiou, 2008; Ozcan, Yukruk, Akkaya, & Uner, 2007; Pan & Chen, 2007; Ren & Valsaraj, 2009; Roy, Varghese, Paulose, & Grimes, 2010; Sasirekha, Basha, & Shanthi, 2006; Torimoto, Liu, & Yoneyama, 1998; I. H. Tseng, Chang, & Wu, 2002; I. H. Tseng, Wu, & Chou, 2004; Woolerton et al., 2010; J. C. S. Wu, Wu, Chu, Huang, & Tsai, 2008; Yoneyama, 1997; Z. H. Zhao, Fan, Xie, & Wang, 2009) to useful fuels such as methane, the splitting of water to hydrogen and oxygen for fuel use (i.e., water reduction) (Bamwenda, Uesigi, Abe, Sayama, & Arakawa, 2001; Domen, Kudo, & Onishi, 1986; Domen, Naito, Onishi, & Tamaru, 1982; Hitoki, Ishikawa, et al., 2002; Hitoki, Takata, et al., 2002; Igarashi et al., 1995; Iwase, Kato, & Kudo, 2010; Kato, Asakura, & Kudo, 2003; Kato & Kudo, 1999; Kho et al., 2010; Kitano & Hara, 2010; A. Kudo, 2006, 2007; A. Kudo & Kato, 2000; A. Kudo, Kato, & Tsuji, 2004; A. Kudo & Miseki, 2009; Maeda, Higashi, Lu, Abe, & Domen, 2010; Maeda et al., 2006; Miseki, Kusama, Sugihara, & Sayama, 2010; Osterloh, 2008; Reisner, Powell, Cavazza,

Fontecilla-Camps, & Armstrong, 2009; Saadi, Bouguelia, & Trari, 2006; J. Sato et al., 2005; Sayama & Arakawa, 1993, 1994, 1996; Schrauzer & Guth, 1977; Tang, Durrant, & Klug, 2008; Yerga, Galvan, del Valle, de la Mano, & Fierro, 2009; A. P. Zhang & Zhang, 2010a, 2010b), the recovery of metal cations via reduction to zero-valent forms (Litter, 1999; Prairie, Evans, Stange, & Martinez, 1993; Rajeshwar, Chenthamarakshan, Ming, & Sun, 2002; Vinu & Madras, 2008; D. Zhao, Chen, Yu, Ma, & Zhao, 2009), and, similarly, the reduction of hexavalent chromium to a recoverable form (Hsu, Wang, & Tzou, 2007; Kajitvichyanukul, Ananpattarachai, & Pongpom, 2005; Mu, Long, Kang, & Mu, 2010; Testa, Grela, & Litter, 2001, 2004; N. Wang et al., 2010). The reduction of carbon dioxide and the splitting of water are exciting new areas of study with regards to sustainable energy. The former reduces a growing greenhouse gas while at the same time producing an energy source. Though, the process is very difficult in water because of the low solubility of CO_2. The latter takes the two most abundant substances on earth, light and water, and converts it to a source of storable clean energy, hydrogen. Both of these have the ability to be ground-breaking technologies for society if photocatalyst research can successfully engineer materials that have high efficiencies while using sunlight as the photonic source**.** For this study, understanding why different materials are better at water oxidation will be of great importance for treating oxidized pollutants because this can lead to the development of a photocatalyst that uses water as the hole scavenger.

Photocatalytic Reduction of Nitrate

Electrons and holes that do not recombine are available for chemical reactions, and they have a redox potential associated with the band energy positions of the

photocatalyst. For reduction reactions to occur, the conduction band potential must be more negative than the reduction potential of the desired species ($E_{CB} > E_{RED}$). Conversely, for the oxidation process to occur, the valence band must be more positive than the oxidation potential of the species ($E_{VB} > E_{OXD}$). In other words, the desired redox reaction potential must lie within the bandgap of the photocatalyst. The standard potentials of nitrate, nitrite, and ammonium in aqueous solution (pH = 7) all lay within the bandgap of TiO_2. Thus, TiO_2 photocatalyst can theoretically reduce nitrate to dinitrogen with a potential of at least 0.75 V at pH = 7. However, the potential to reduce nitrate to dinitrogen is a ten electron reduction process and is highly unlikely to occur, so these potentials should only be used to estimate the success of the reaction. Also, care must be taken if adjusting the material to visible-light wavelengths as dopant impurities might move the bands beyond the potentials of the pollutants.

Some of the first documented studies on the ability of nitrate to be photocatalytically reduced are from India by Rao and co-workers (Rao & Murty, 1936), Dhar and co-workers (Dhar, 1934; Dhar, Tandon, Biswas, & Bhateacharya, 1934), and Sarkaria and co-workers (Sarkaria, 1936). Their work was some of the first to study the interaction between light, semiconductors, and inorganic compounds, and yet, these studies are not well known. In 1936, Rao and co-workers (Rao & Murty, 1936) showed that in the presence of ultraviolet (UV) light, ferric oxide (Fe_2O_3) could catalyze both the reduction of nitrate and the oxidation of ammonia to nitrite simultaneously. Before that, Dhar and co-workers (Dhar, 1934; Dhar et al., 1934) showed that nitrite could be oxidized to nitrate in the presence of UV light and titanium dioxide (TiO_2), zinc oxide (ZnO) or Fe_2O_3 catalysts. Their results suggested that TiO_2 outperformed the other

catalysts for the oxidation and reduction reactions. These earlier studies were focused on nitrate fixation in soils, which contain the said catalysts. So, although photocatalytic redox reactions were observed, they were not focused on and thus there could have been cross-contamination from biological media in the soil. At the time, these researchers understood the idea of a catalyst, but were unaware of the mechanisms or benefits of semiconductor photochemistry.

Photocatalytic reduction of nitrate is a relatively new field of study. It was first examined in detail by Kudo and co-workers in 1987 (A. Kudo, Domen, Maruya, & Onishi, 1987b), in which metal (Pt, Pd, Ru) loaded TiO_2 [$Ti(SO_4)_2$ pyrolyzed] was irradiated with UV light. Results showed that TiO_2-Pt was the most effective photocatalyst for nitrate reduction. No removal was seen without a hole scavenger (methanol). Ammonium was formed as a by-product which was attributed to the low hydrogen (H_2) overpotential of Pt. This was confirmed by adding H_2 into the system, in which ammonia formation increased. Plain titanium dioxide had little removal with selectivity toward nitrite. Since then, many different types of semiconducting materials and composites have been tested for the photocatalytic nitrate reduction. To date, silver loaded TiO_2 (P25 and Hombikat) has shown to be the most promising photocatalyst with the use of an organic hole scavenger, formic acid (Sá, Agüera, Gross, & Anderson, 2009; F. X. Zhang et al., 2005). In 2002, Kato and co-workers (Kato & Kudo, 2002b) were able to reduce nitrate under UV irradiation with metal-loaded tantalates and using water as a hole scavenger. Although promising, the activity was low and there was no insight given about the mechanisms.

Various types of semiconductors have been studied for photocatalytic nitrate reduction including metal oxide semiconductors (Bems, Jentoft, & Schlogl, 1999; W. Gao et al., 2004; Kato & Kudo, 2002b; Ketir, Bouguelia, & Trari, 2009; Kominami et al., 2001a; Kominami et al., 2005b; A. Kudo et al., 1987b; Akihiko Kudo, Domen, Maruya, & Onishi, 1992; Y. Li & Wasgestian, 1998; L.-F. Liu, Zhang, Yang, Chen, & Yu, 2009; L. F. Liu, Dong, Yang, & Yu, 2008; Lozovskii, Stolyarova, Prikhod'ko, & Goncharuk, 2009; S. Park et al., 2007; Penpolcharoen, Amal, & Brungs, 2001; Ranjit, Varadarajan, & Viswanathan, 1995, 1996; Ranjit & Viswanathan, 1997b, 1997c; Rengaraj & Li, 2007b; Sychev, Lozovski, Prihod'ko, Erdmann, & Goncharuk, 2008; Sá et al., 2009; Sittinun Tawkaew, Yin, & Sato, 2001; F. X. Zhang et al., 2005), metal chalcogenide semiconductors (Hamanoi & Kudo, 2002; Korgel & Monbouquette, 1997; Ranjit, Krishnamoorthy, Varadarajan, & Viswanathan, 1995; Ranjit, Krishnamoorthy, & Viswanathan, 1994a; Sittinun Tawkaew, Fujishiro, Yin, & Sato, 2001), niobates (S. Tawkaew, Uchida, Fujishiro, & Sato, 2000; Sittinun Tawkaew, Yin, et al., 2001), titanates (Kato & Kudo, 2002b), and hollandites (Mori, Suzuki, Fujimoto, Watanabe, & Hasegawa, 1999a, 2000). Most of the recent work on nitrate photocatalytic reduction has focused on the metal oxide/metal composites, with TiO_2 being the most widely studied. No narrow bandgap semiconductor combinations from the III-V or the II-VI groups (e.g., GaAs) have been studied at for nitrate photoreduction. Table 2.2 shows a summary of materials that have been used for photocatalytic nitrate reduction. The calculated removal efficiency was normalized to time for comparison. However, a true comparison between materials cannot be made because each study used a different light source, reactor setup, nitrate concentration, pH, hole scavenger, and photocatalyst. The information is valuable

though to determine which materials are active for nitrate reduction and which hole scavengers are most efficient.

Table 2.2. *Comparison of Different Photocatalysts for Reduction of Nitrate*

Selected Catalyst	Hole Scavenger	Removal (%/hr)	Selectivity	Light Source	pH	Ref
Pd-TiO_2	Methanol	Negligible	NH_3 100%	UV (500 W Xe)	1	(A. Kudo et al., 1987b)
TiO_2, $SrTiO_3$, $K_4Nb_6O_{17}$, In_2O_3, and WO_3; some loaded with Pt, some with NiO	Methanol	Negligible	NH_3, NO_2, catalyst material dependent	UV (500 W Xe)	1	(Akihiko Kudo et al., 1992)
ZnS and Ru, Pt, Pd, or Rh (1%);	Sulphite/Sulphide	Negligible	NH_3*	UV (150 W Xe)	6	(Ranjit, Krishnamoorthy, & Viswanathan, 1994b)
TiO2-Ru (1%)	Water	Negligible	NH_3*	UV (150 W Xe)	7*	(Ranjit, Varadarajan, et al., 1995)
ZnO, ZrO2, Fe_2O_3, Fe_3O_4 (some w/Pt, Pd, Rh, or Ru)	Sulphite/sulphate 50 ppm	Negligible	NH_3*	UV (450 W Xe)	-	(Ranjit et al., 1996)
HTi_4O_9/CdS-Pt	Methanol	33%	55%-NO_2	UV (100 W HP Hg)	7*	(T. Sato, Sato, Fujishiro, Yoshioka, & Okuwaki, 1996)
HTi_4O_9/CdS-Pt	Methanol	2.75%		Vis (100 W HP Hg)	7*	(T. Sato et al., 1996)
TiO_2-Fe^{3+}, Cr^{3+}, Co^{2+}, Mg^{2+}	Water	Negligible	NH_3*	UV (450 W Xe)	7*	(Ranjit & Viswanathan, 1997a)
TiO_2-Fe^{3+} doped	Water	Negligible	NH_3*	UV (450 W Xe)	7*	(Ranjit & Viswanathan, 1997d)

TiO_2-Ru, Rh, Pt, Pd	Methanol, ethanol, EDTA	Negligible	NH_3*	UV (450 W Xe)	5-6	(Ranjit & Viswanathan, 1997c)
P25	Oxalic acid (5.2e-3 M)	16%	NH_3*	UV (150 W MP Hg)	2.3	(Y. Li & Wasgestian, 1998)
Hollandite, $K_xGa_xSn_{8-x}O_{16}$	Methanol (247 umol/L)	0.3%	50% N_2	UV (400 W Xe)	4	(Mori et al., 1999a)
Hollandite, $K_xGa_xSn_{8-x}O_{16}$	Methanol (247 umol/L)	0.3%	100% N_2	UV (400/500 W Xe)	3	(Mori et al., 2000)
P25-Ag, Cu, Pt, Pd, Co, Au, or Ni	Oxalic acid (200 umol)	29%	NH_3-100%	UV (400 W HP Hg)	2*	(Kominami et al., 2001a)
TiO_2 nano-sized Fe_2O_3 P25	Sucrose (1 mg-C/50 mL)	18%		UV (20 W Black light)	3.5	(Penpolcharoen et al., 2001; Sittinun Tawkaew, Fujishiro, et al., 2001)
TiO_2, TiO_2-Pt, $H_4Nb_6O_{17}$/Pt or TiO_2 or TiO_2-Pt	Methanol (10%)	20%	NH_3-80%, N_2-20%	UV (100 W HP Hg)	4	(Sittinun Tawkaew, Yin, et al., 2001)
$H_2Ti_4O_9$/CdS; $H_4Nb_6O_{17}$/CdS	Methanol (10%)	6%	$H_2Ti_4O_9$/CdS: N_2 66.67%, NO_2 33.3% AND for $H_4Nb_6O_{17}$/CdS: NH_3 28.3%, N_2 11.67%, NO_2 60%	VIS (100 W HP Hg)	7	(Sittinun Tawkaew, Fujishiro, et al., 2001)
ZnS-Ni (0.1% doped	Methanol (6.25%)	Negligible	NH_3, NO_2*	VIS (300 W Xe)	7*	(Hamanoi & Kudo, 2002)

TiO_2 (rutile), SiO_2 and $KTaO_3$, $BaTa_2O_6$, $K_3Ta_3Si_2O_{13}$, $NaTaO_3$, All with Ni (1% wt.)	Water	11%	N_2-44%, NH_3-39%	UV (450 W HP Hg)	7*	(Kato & Kudo, 2002b)
P25:Pd, Pt, Ni, Cu, Pd-Cu, Pt-Cu, and Ni-Cu (4% wt.)	Oxalic acid (0.005 M)	8.4%	NH_3 for best removal, N_2 for less removal	UV (125 W HP Hg)	2*	(W. Gao et al., 2004)
TiO_2-Cu/$MgTiO_3$ (4% Cu, Cu:Mg 3:1), Cu/TiO2 (4%), MgTiO3-TiO_2, P25	Sodium oxalate (0.005 M). Also tried ethanol and oxalic acid but were not as effective.	20%		UV (125 W HP Hg)	7*	(Jin et al., 2004)
P25/Cu, Pt, Pd, Au, Ag, Pd-Cu (0.5% wt.)	Oxalic acid or Sodium oxalate (200 umol)	4.67%	NH_3-100% with Cu, N_2-100% with Pd-Cu	UV (400 W HP Hg)	11	(Kominami et al., 2005b)
P25/Ag (1% wt.)	Formic acid (0.04 M). Also tried oxalic acid, sodium formate, sodium oxalate, methanol, acetic acid, sodium acetate.	197%	N_2-100%, 0.02 M formic acid gave 40% NO_2	UV (125 W HP Hg)	2.5	(F. X. Zhang et al., 2005)
P25	Formic acid (0.04 M)	30%	N_2-100%		2.5	(F. X. Zhang et al., 2005)
SCM ZnO	Methanol	8%	N_2*	UV (HP Hg)	8.3	(S. Park et al., 2007)
TiO_2-Bi^{3+} (1.5%wt; sol-gel)	Formic acid (1 mol NO_3^-:10 mol FA)	62%	NH_3-40%, N_2-60%*	UV	3.19	(Rengaraj & Li, 2007b)

P25, P25-Fe	Formic acid (0.05 M)	26%	N_2-100% (P25); N_2-72% (Fe/P25)	UV (20 W LP Hg)	2.5*	(L. Liu, Dong, & Yang)
TiO_2-Ag (1% wt.)	Formic acid (0.04 M)	2.5%	N_2-100%	UV (125 W HP Hg)	2.5*	(Sychev, Lozovski, Prihod'ko, et al., 2008)
$CuCrO_2$	Water	15%	NO_2*	VIS (Two-200W W Lamps)	7.6	(Ketir et al., 2009)
TiO_2-Ag (1% wt.)	Formic acid (0.04 M)	200%	N_2-100%*	UV (8 W LP Hg)	2.5*	(Lozovskii et al., 2009)
P25; Hombikat; With Cu, Ag, or Fe	Formic acid (0.04 M)	67%	N_2-96%	UV (110 W HP Hg)	2.5*	(Sá et al., 2009)
4.2% Pd–1.2% Cu/P25 P25	Formic Acid (0.02 M)	39%	N_2-100%	UV (Five-15 W HP Hg, 8.3 W/m2)	2.7	(Wehbe et al., 2009)
TiO_2-Pt, Cu, Pt-Cu	Benzene (10 mg/L)	17%	NO_2, NH_3	UV (250 W HP Hg)	5.8	(L. Y. Li et al., 2010)

*Indicates that the value was assumed or that no other value was given. For example, the study in line 3 only reported the formation of ammonia.

CHAPTER 3

NITRATE REDUCTION IN WATER USING COMMERCIAL TITANIUM DIOXIDE PHOTOCATALYSTS (P25, P90, AND HOMBIKAT UV100)*

*****Published: Doudrick, K.; Monzón, O.; Mangonon, A.; Hristovski, K.; Westerhoff, P. K., Nitrate Reduction in Water Using Commercial Titanium Dioxide Photocatalysts (P25, P90, and Hombikat UV100). *ASCE J. of Environ. Eng.*, 138(8), 852–861, 2012.

Abstract

Photocatalytic nitrate reduction was examined in a model water and in groundwater by utilizing three commercially available titanium dioxide photocatalysts (Evonik P25, Evonik P90, and Sachtleben Hombikat UV100). The photocatalysts were characterized using uniform methods (TEM, XRD, surface area, UV-VIS, surface charge) and their photocatalytic activity was differentiated using these results. Under all experimental conditions, P25 and P90 were superior to UV100, and P90 outperformed P25 with nitrate reductions as high as 77% at the maximum irradiance level used (6.46 x 10^{22} photons/L). The photocatalytic nitrate reduction activity was found to be dependent upon the rate of recombination, pH, and total photocatalyst surface area, with the recombination rate being the limiting variable. Nitrate reduction was more efficient in model water than in groundwater that contained constituents capable of occupying photocatalyst surface sorption sites or scavenging conduction band electrons. The greater efficiencies of P25 and P90 compared to UV100 were attributed primarily to the mixed-phase nature of the photocatalysts, which allow for better charge separation, and the greater activity of P90 over P25 was attributed to a larger surface area. The results should be helpful in the selection of these commercially available photocatalysts to treat a wide range of pollutants other than nitrate.

3.1 Introduction

Nitrate (NO_3^-) is one the most prevalent groundwater contaminants in North America (B. Nolan, 2004; B. T. Nolan & Hitt, 2006; B. T. Nolan et al., 2010; B. T. Nolan & Stoner, 2000). It poses a risk to human health, has a large impact on the natural nitrogen cycle and has an EPA maximum contaminant level (MCL) of 10 mg-N/L. Nitrate is a known cause of methemoglobinemia, or "blue baby" syndrome, and could be carcinogenic or an endocrine disruptor (Guillette & Edwards, 2005; Hamlin, 2006; Hamlin et al., 2008). Nitrate pollution stems from both agricultural (Rupert, 2008) and urban sources (Wakida & Lerner, 2005). A survey of nitrate concentrations in 5,101 wells in the United States revealed that 8% (20% agricultural, 3% urban, 4% major aquifers) exceeded the EPA MCL, affecting more than 24.6 million people (Burow et al., 2010). Even with proper regulations in place and best management practices for fertilizers, nitrate concentrations in groundwater continue to increase (Rupert, 2008).

Nitrate is a stable, highly soluble ion that is difficult to remove by traditional coagulation or adsorption processes because of its unique non-coordinating ligand chemistry. It belongs to a class of inorganic chemicals termed oxo-anions that includes arsenate, bromate, chlorate, perchlorate, selenate, tungstate, and vanadate, and more generally to a growing group of oxidized pollutants that occur in water supplies. Because some removal processes (e.g., ion exchange, membrane separation) produce concentrated waste streams, the risks from many oxidized pollutants are best mitigated through chemical or biological reduction to innocuous forms, such as the reduction of nitrate to dinitrogen gas (N_2). Biological nitrate reduction of wastewater, groundwater or concentrated waste streams produces non-aqueous nitrogen species (e.g., N_2, NO),

cellular biomass and soluble microbial products by utilizing organic compounds (e.g., ethanol) or hydrogen as electron donors (K.-C. Lee & Rittmann, 2002; McAdam & Judd, 2006b). Electro- or photo-catalytic nitrate reduction processes use an applied current or aqueous electrons produced from excitation of semiconductors, respectively, but the challenge with these processes has been to manage the yield of desirable non-aqueous species (e.g., N_2) relative to undesirable aqueous species (e.g., nitrite or ammonia), which themselves pose health or operational issues in drinking water.

Photocatalytic reduction of nitrate is a relatively new field of study that Kudo and co-workers first explored in detail (A. Kudo et al., 1987b). Briefly, photocatalysts can reduce nitrate when their electrons are excited to a free state using light energy (i.e., photons). Once freed, the electrons can be transferred to nitrate ions for reduction reactions. Concurrently, the excitation of the electron creates a hole in the photocatalyst, and to maintain electroneutrality the hole must be filled with an electron through the oxidation of other compounds. This is done by adding a hole scavenger (i.e., electron donor) to the system. If the electron recombines with the hole before a chemical reaction can take place, a process referred to as recombination, energy is wasted as heat. Various types of semiconductors have been examined for photocatalytic nitrate reduction, including metal oxides (Bems et al., 1999; W. Gao et al., 2004; Kato & Kudo, 2002a; Ketir et al., 2009; Kominami et al., 2001a; Kominami et al., 2005b; A. Kudo et al., 1987b; Akihiko Kudo et al., 1992; L. Y. Li et al., 2010; Y. Li & Wasgestian, 1998; L.-F. Liu et al., 2009; L. F. Liu et al., 2008; Lozovskii et al., 2009; S. Park et al., 2007; Penpolcharoen et al., 2001; Ranjit, Varadarajan, et al., 1995; Ranjit et al., 1996; Ranjit & Viswanathan, 1997a, 1997c; Rengaraj & Li, 2007b; Sychev, Lozovski, Prihod'ko,

Erdmann, & Goncharuk, 2008; Sa, Aguera, Gross, & Anderson, 2009; Sittinun Tawkaew, Yin, et al., 2001; F. X. Zhang et al., 2005), chalcogenides (Hamanoi & Kudo, 2002; Korgel & Monbouquette, 1997; Ranjit, Krishnamoorthy, et al., 1995; Ranjit et al., 1994a; Sittinun Tawkaew, Fujishiro, et al., 2001), niobates (S. Tawkaew et al., 2000; Sittinun Tawkaew, Yin, et al., 2001), titanates (Kato & Kudo, 2002a), and hollandites (Mori et al., 1999a, 2000). Semiconductors can be loaded with metal co-catalysts (e.g., Ag, Pt, Cu, Pd) in order to improve kinetics and by-product selectivity, but this increases the cost of the material and simulating the synthesis process can be difficult and time consuming.

Using commercial photocatalysts for laboratory studies and large scale water treatment applications is ideal because they are readily available and more economical than custom synthesized materials. Although commercial photocatalysts such as P25 and Hombikat UV100 (UV100) have been studied for nitrate reduction, they were used only in comparison to loading them with metal co-catalysts; their activity and mechanisms were not examined further (Kominami et al., 2001a; L. Liu et al.; Sa, Aguera, Gross, & Anderson, 2009; F. X. Zhang et al., 2005). P25 has long been used for degradation of many air and water pollutants because of its excellent photocatalytic activity (Ohtani, 2008). Although not as widely used as P25, UV100 has been applied as a photocatalyst for the oxidation of various organic and inorganic compounds (Ryu & Choi, 2008). The activity of P25 and UV100 is dependent upon the target substrate and the experimental conditions. For example, for P25 and UV100, Frimmel and co-workers (Doll & Frimmel, 2004, 2005) showed that adsorption capacity for the compound of concern determined which photocatalyst would have better activity. However, when P25 and UV100 had the same adsorption capacity for a compound, P25 dominated because of its ability to

separate charges and avoid recombination. When adsorption capacity was the limiting variable, UV100 dominated because of its large surface area. Therefore, including UV100 in this study will help to determine if the limiting variable for photocatalytic nitrate reduction is either the recombination rate or the surface area.

This paper compares the photocatalytic activity of three commercially available TiO_2 photocatalysts (P25, P90, and UV100) for nitrate reduction and characterizes the materials to determine the mechanisms influencing activity. Each photocatalyst was tested under identical conditions in order to eliminate the effect of experimental variables in order to use the recombination rate, zeta potential, crystallinity, and surface area to explain the differences in activity for three similar TiO_2 photocatalysts. Our study is the first to thoroughly characterize the newer P90 material and to evaluate its ability to reduce nitrate. The kinetics of nitrate reduction with and without organic hole scavengers are assessed for the different photocatalysts using a medium pressure ultraviolet (UV) lamp. Nitrate removal is compared using a model water and a local groundwater that contains a heterogeneous mixture of organic and inorganic constituents. Nitrate reduction results are scaled relevant to a quantum yield to make these results comparable to future studies that use different photocatalysts or lamp types.

3.2 Experimental Approach

Material Description

Three commercial TiO_2 photocatalysts, Evonik P25 (>99.5%), Evonik P90 (>99.5%), and Sachtleben Hombikat UV100 (99%), were obtained in powder form. P90 and P25 are synthesized using a similar method, high temperature flame hydrolysis of

$TiCl_4$ in the presence of oxygen and hydrogen; UV100 is synthesized by precipitation using a titanium sulfate precursor.

Sodium nitrate ($NaNO_3$, 99% EMD) was used as the nitrate source. Formic acid (HCOOH, 98% Fluka), oxalic acid ($H_2C_2O_2$, 99.5% EMD), and sodium formate (HCOONa, 99.3% Fisher) were used as hole scavengers. A model water was prepared using a Nanopure® (18.3 MΩ-cm) treatment system. Groundwater was taken from a local source in Mesa, AZ, and was analyzed for common water quality parameters. Table 3.1 shows the analyzed constituents and their concentrations.

Table 3.1. *Groundwater Constituents and Their Concentrations*

Constituent	**Anions, mg/L (mM)**
Carbonate	180 (3)
Sulfate	47 (0.50)
Chloride	200 (5.6)
Perchlorate	0.4 (0.004)
Arsenic	0.005 (6.7e-5)
Nitrate	1 (0.016)
Constituent	**Cations and COD, mg/L (mM)**
Lithium	0.24 (0.035)
Sodium	389 (17)
Potassium	10 (0.25)
Magnesium	13 (0.54)
Calcium	68 (1.7)
COD	31

Photocatalytic Experiments

Photocatalytic experiments were carried out in a photoreactor composed of two borosilicate bottles (1.8 L, transmittance $\lambda > 280$ nm) submerged in a cooling tank and irradiated by a UV lamp located 2 inches from each bottle; this setup is described in detail elsewhere (Westerhoff, Crittenden, Moon, & Minakata, 2010). The UV light source

consisted of a 450-W (Ace Glass power supply, 7830-60) medium-pressure mercury-vapor lamp (Ace Glass, 7825-34; Hanovia PC451.050) that was placed in a double-walled quartz immersion well (Ace Glass, 7854-25). Nitrate photolysis occurs mainly at $\lambda < 250$ nm resulting in nitrite formation (Mack & Bolton, 1999); therefore, nitrate photolysis in this system is not likely because the borosilicate reactors do not transmit below ~280 nm. System temperature was maintained at 25 °C using a chiller. For each run, catalyst was suspended under magnetic stirring in a solution of model water or groundwater containing nitrate (100 mg-N/L; 7.14 mM) and a hole scavenger (40 mM). The ratio of the initial hole scavenger concentration to the initial nitrate concentration was set at 5.6:1, which was previously shown to be the optimum ratio for TiO_2 at a nitrate concentration of 100 mg-N/L (F. X. Zhang et al., 2005). The pH was dependent on the choice of hole scavenger. For experiments requiring removal of oxygen, argon was bubbled before and during irradiation through a glass sparging tube. Prior to irradiation, each reactor bottle was stirred in the dark for 1 hr to determine the non-photocatalytic removal (i.e., adsorption). Control experiments were conducted in parallel and included: (1) nitrate, hole scavenger, irradiation, no photocatalyst, (2) nitrate, hole scavenger, photocatalyst, no irradiation, and (3) hole scavenger, photocatalyst, irradiation, no nitrate. During kinetic photocatalysis experiments, samples were collected over time, the photocatalyst removed from solution using filtration (0.45 μm nylon membrane), and the filtrate stored in amber glass vials in the dark at 3 °C until analysis, which occurred within 48 hrs.

Analytical Methods for Nitrogen Species

Samples were analyzed for nitrate, nitrite and ammonia. Nitrate and nitrite anions were measured using ion chromatography (Dionex DX-120; AS12A column) following EPA Standard Method 4110. All values were above the lowest standard used, and 5-point calibration curves included in each batch were linear with $R^2 > 0.995$. Quality control standards were included in each batch in one out of every 20 samples. Ammonia and total dissolved nitrogen (TDN) concentrations were determined using colorimetric methods (Hach DR2000 UV-VIS, Kit #TNT827, and Hach DR2000 UV-VIS, Kit #TNT830, respectively). Previous studies on the photocatalytic reduction of nitrate detected only, nitrite, ammonia, and dinitrogen as final by-products (W. Gao et al., 2004; Kato & Kudo, 2002a; Kominami et al., 2005b; SÃ¡ et al., 2009; Wehbe et al., 2009; F. X. Zhang et al., 2005). Therefore, the selectivity of gaseous nitrogen by-products (S(N Gas)) was approximated on the basis of a nitrogen mass balance of nitrate, nitrite, ammonia, and TDN (Eq. 3.1).

$$S\left(N_{gas}\right) = \frac{\left[NO_3^-\right]_0 - \left[NO_3^-\right]_t - \left[NH_4^+\right]_t - \left[NO_2^-\right]_t}{\left[NO_3^-\right]_0 - \left[NO_3^-\right]_t} \qquad (3.1)$$

Photocatalyst Material Characterization

Although P25 and UV100 have been characterized previously, the results are inconsistent, especially for UV100, for which a specific surface area (SSA) ranging from 280 to 400 m^2/g has been reported (Kirchnerova, Cohen, Guy, & Klvana, 2005).

Therefore, to equably compare P25, P90, and UV100, all materials were characterized in parallel using identical sample preparation and analysis procedures. The crystal structure was determined using powder X-ray diffraction (XRD) with a CuK_{α} source (Siemens D5000) and an aluminum holder. Each sample was scanned from $2\theta = 20°$ to 60° to detect the characteristic TiO_2 peaks. The XRD spectra were used to calculate the average crystallite size of each photocatalyst using Scherrer's equation (Patterson, 1939). Ultraviolet-visible light spectroscopy with diffuse reflectance (UV-VIS DR) was performed on a Perkin Elmer Lambda 650 using a Spectralon reflectance reference. The photocatalyst bandgap was estimated from the x-y tangential intersection at the onset of absorption. Electron micrograph images of the photocatalysts were obtained using a high-resolution scanning transmission electron microscope with energy dispersive X-ray capabilities (STEM Phillips CM-200). The surface charge of each photocatalyst was determined using the Phase Analysis Light Scattering technique (ZetaPALS, Brookhaven, NY) in 10 mM KNO_3 background electrolyte. Photocatalyst surface areas were obtained with the Branauer, Emmett and Teller (BET) model using a Tristar II 3020 automated gas adsorption analyzer (Micromeritics, USA).

Photoreactor Light Intensity

The light intensity of the photoreactor was determined using chemical actinometry based on the ferrioxalate method outlined previously (Hatchard & Parker, 1956). This method is accurate for UV and visible light wavelengths <500 nm. The major characteristic wavelengths emitted by the mercury lamp used in this study are 313 nm (7.5%), 366 nm (14.6%), 435.1 nm (11.5%), 546.1 nm (13.9%), and 578 nm (11.4%), as

denoted in the manufacturer specifications. Wavelengths less than 313 nm accounted for 24.2% of the total power output, and the remaining power is dedicated to near-infrared wavelengths. The water circulating around the lamp acted as an infrared light filter. The borosilicate glass bottles used as reaction chambers filtered out all light wavelengths less than approximately 280 nm. Therefore, because the bandgap of TiO_2 is approximately 387.5 nm, only the 313 nm and 366 nm major wavelengths were active for these experiments.

From actinometry, the light intensity for these experiments was determined to be 7.66×10^{-6} einsteins/L-s (7.66×10^{-6} moles of photons/L-s), which is valid for all wavelengths from approximately 280-500 nm for this experimental setup. Because this intensity measurement includes wavelengths greater than the required excitation energy for TiO_2 (3.2 eV, 387.5 nm), the intensity needed to be adjusted to include only the wavelengths of light emitted by the lamp that are capable of absorption by TiO_2, 280-387.5 nm (i.e., the power output ratio of wavelengths 313 nm and 366 nm to the total power output between 280 and 500 nm). This adjusted intensity was calculated to be 4.96×10^{-6} einsteins/L-s. Thus, although using actinometry for measuring the intensity of experiments involving both polychromatic lamps and photocatalysts can be difficult, the intensity was approximated by adjusting the actinometrical results with respect to the bandgap of the photocatalyst.

3.3 Results

Photocatalyst Material Characterization

Characterization of the photocatalysts is important because the parameters can be used to interpret the results and mechanisms underlying photocatalytic nitrate reduction. Photocatalyst characterization results are summarized in Table 3.2. XRD patterns for P25, P90, and UV100 are shown in Figure. 3.1. For P25 and P90, the XRD patterns are quite similar and indicate a mixed phase of anatase and rutile. In contrast, the UV100 spectrum exhibits broad peaks indicating a low degree of crystallinity, and it has a single-phase crystal structure consisting of only anatase. The main anatase peak for all samples is the (101) at $2\theta = 25.27°$, and the main rutile peak for P25 and P90 is the (110) at $2\theta = 27.41°$. The ratios of anatase to rutile for P25 and P90 were calculated as 88:12 and 86:14, respectively. The manufacturer states the ratio for P25 is 80:20, but this ratio varies in the literature because each batch is slightly different, and older batches are particularly different from newer commercialized batches. Evonik's improved manufacturing process can account for this inconsistency, as newer batches of P25 (90:10) are more active than older batches of P25 (80:20), which was attributed to more polyhedral particles in the newer batches (Balazs et al., 2008). The XRD spectra also indicate that the average anatase crystal size for P90 (12 nm) is smaller than that for P25 (16 nm); however, both photocatalysts have an average rutile crystal size of ~18 nm. In contrast, UV100 has a much smaller average anatase crystal size of approximately 6 nm.

Table 3.2. *Photocatalyst Characterization Results*

Sample ID	Surface area (m^2/g)	Crystal structure	Crystal size[1] (nm)	Isolectric point (pH_{IEP})
P25	51	88% anatase: 12% rutile	16 nm anatase 18 nm rutile	6.4
P90	104	86% anatase: 14% rutile	12 nm anatase 18 nm rutile	6.6
Hombikat UV100	403	100% anatase	6 nm anatase	5.3

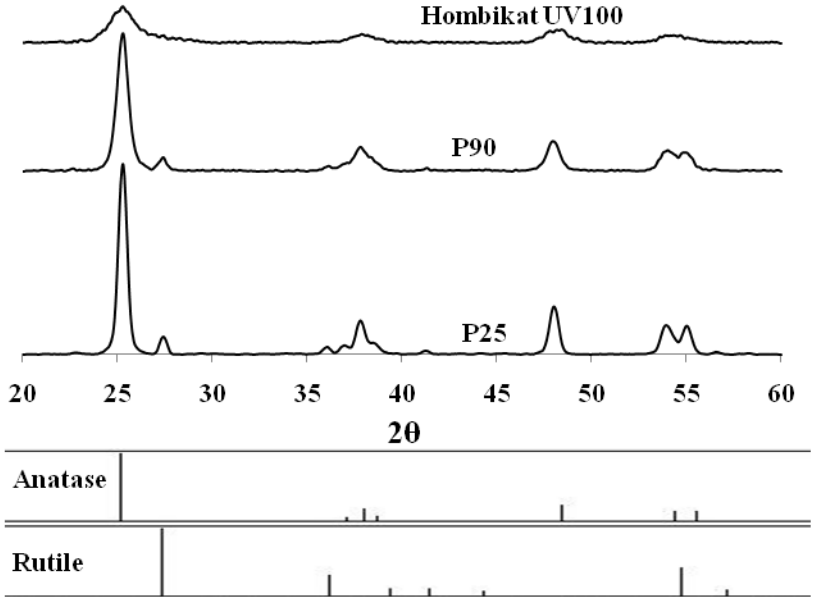


Figure. 3.1. XRD patterns for commercial TiO_2 photocatalysts

TEM images of the photocatalysts are shown in Figure. 3.2. Figures. 3.2(a,b,c) show that UV100 is a mixture of small TiO_2 particles (3.2a) and layered TiO_2 sheet-like structures (EDX confirmed) similar to titanates (Figure 3.2b). Figure 3.2c shows small TiO_2 tube- or multi-walled-like particles found in the sample, which are believed to be the precursors of the layered structures in Figure 3.2b. The structures in Figure 3.2b were

prevalent throughout the samples, extending to microns in length, and had the anatase crystalline structure according to the XRD spectra. On the basis of the literature available to the authors, these structures have not been reported previously for UV100 and may be able to help explain some of the photocatalytic results for UV100. Figures 3.2d and 3.2e show that both P90 and P25 are composed of discrete particles of varying size with a maximum particle size exceeding 30 nm.

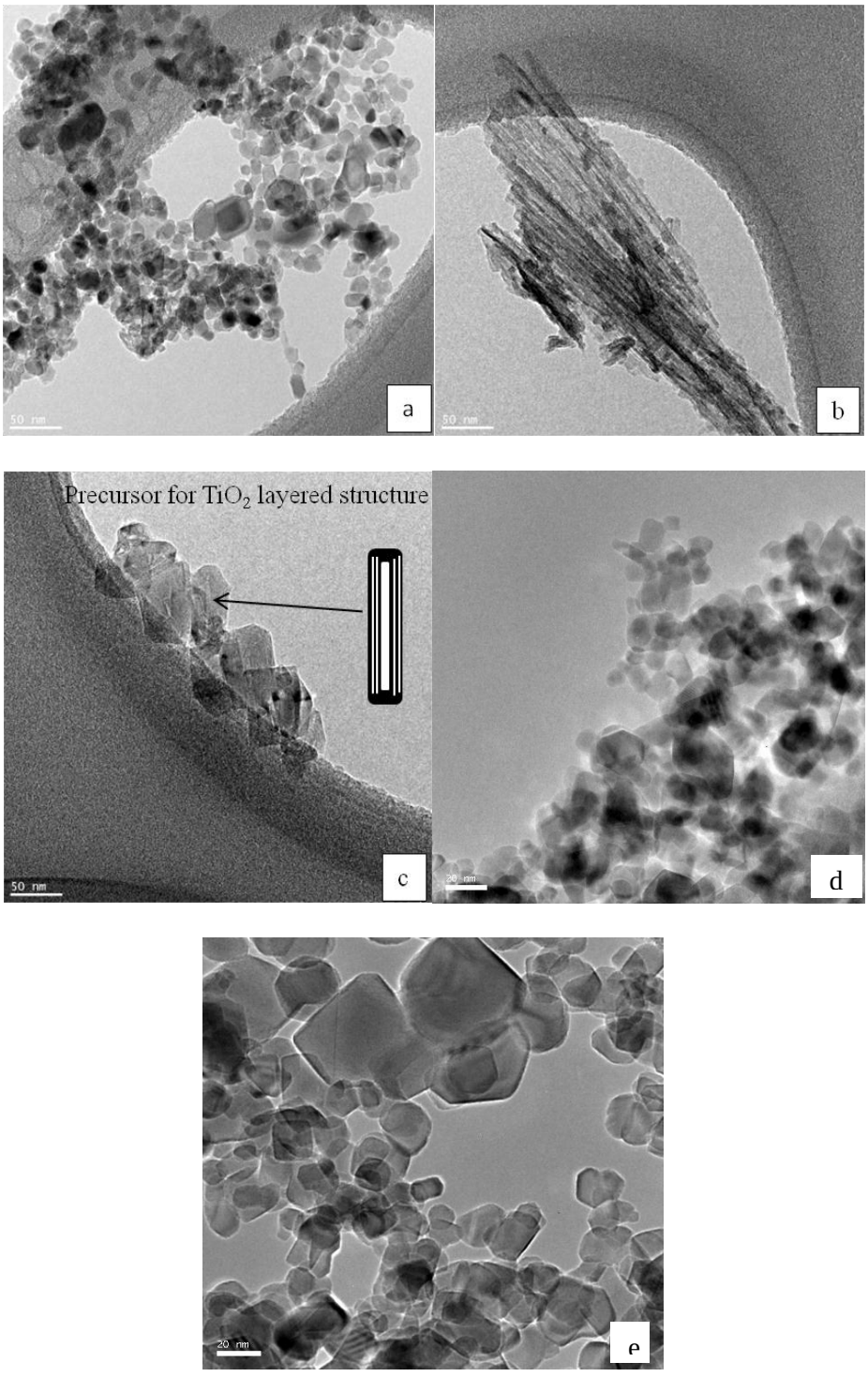


Figure 3.2. TEM images of commercial TiO_2 photocatalysts: (a) UV100 particles, (b) UV100 layered TiO_2 structure, (c) precursor of the UV100 layered structure in Figure 3.2b with a schematic of the multi-walled particle, (d) P90, and (e) P25. Scale bar = 50 nm for (a, b, c) and scale bar = 20 nm for (d, e).

The UV-VIS absorption spectra for P25, P90, UV100, and nitrate are shown in Figure 3.3. Each photocatalyst was similar, with greater absorbance in the UV-C range than in the UV-B and UV-A. On the basis of the absorption spectra, the bandgap for each catalyst was estimated to be 3.2 eV (387.5 nm), which is in good agreement with the bandgap of anatase (Linsebigler et al., 1995). Nitrate absorbs wavelengths primarily below approximately 250 nm with a minor absorption peak (<1% of total) around 305 nm. The majority of nitrate absorption wavelengths are blocked by the borosilicate glass, with the exception of the minor peak. Nitrite (not shown) also has a small absorption peak around 354 nm. Furthermore, the TiO_2 suspension absorbs most of the light below 387.5 nm, thus blocking light that can be absorbed by nitrate and nitrite ions. Therefore, no direct photolysis of nitrate or nitrite should occur and results should be purely photocatalytic.

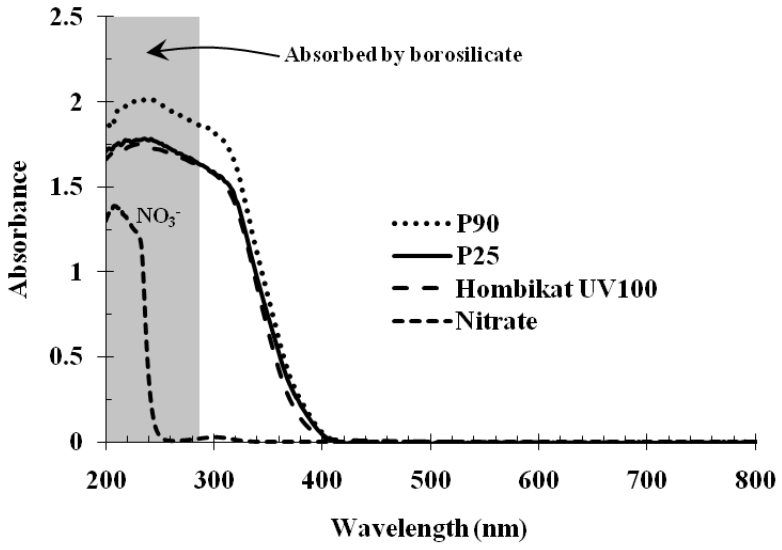


Figure 3.3. UV-VIS absorbance spectrum for commercial TiO_2 photocatalysts and the nitrate anion (at the experimental molarity of 7.14 mM).

Surface area measurements indicated that P90 (104 m^2/g) has approximately twice the surface area as P25 (51 m^2/g). In contrast, UV100 has a much larger surface area of approximately 403 m^2/g, which is due to its smaller particle size and layered structure, as shown in Figures 3.2a and 3.2b, respectively.

Figure 3.4 shows average zeta potential measurements for UV100, P25, and P90 with 95% confidence intervals. The average isoelectric point (IEP) of UV100, P25, and P90 was approximately 5.3, 6.4, and 6.6, respectively).

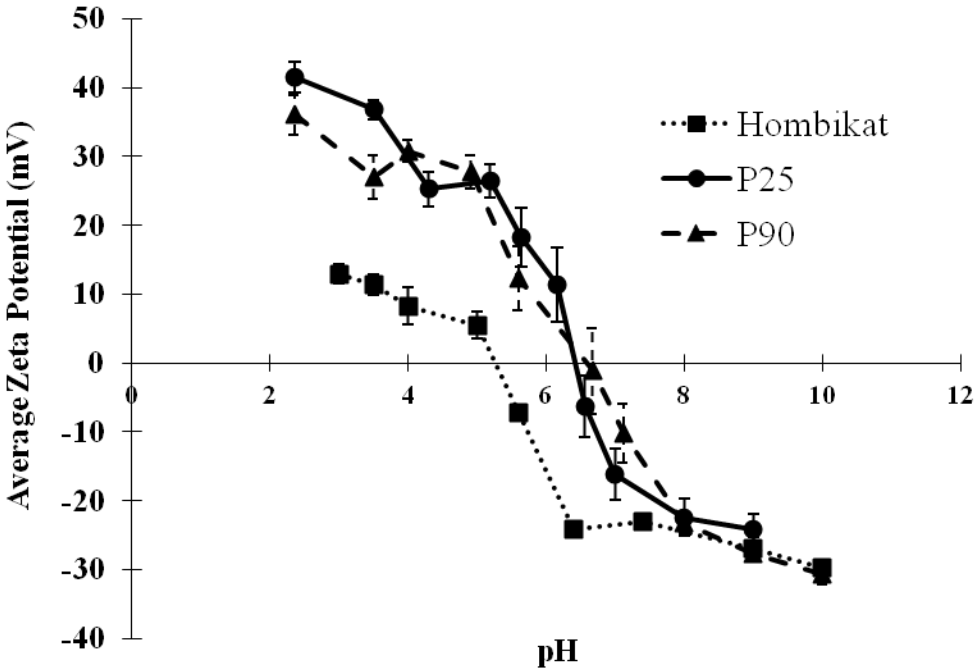


Figure 3.4. Average zeta potential for commercial titanium dioxide photocatalysts. Error bars represent 95% confidence intervals.

Characterization has shown that even though each photocatalyst is TiO_2, their material properties differ, and these may have an effect on their activity for nitrate reduction. As expected, results showed that P25 and P90 are essentially the same, but

with P90 having a smaller crystal size and thus a larger surface area. This allows for an easy method to determine if surface area is a limiting property independent of the surface chemistry, light source, pH, and other experimental conditions.

Photocatalytic Nitrate Reduction in a Model Water

Photocatalytic nitrate reduction was first examined in a model water to eliminate the effects of any interfering compounds. In the absence of a photocatalyst, no nitrate removal was observed, even at the highest irradiance (6.46×10^{22} photons/L or 0.107 einsteins/L), which was expected given that the borosilicate reactors and TiO_2 absorbed the nitrate photolysis wavelengths. Furthermore, <5% adsorption of nitrate was observed for any photocatalyst when experiments were performed in the dark. When formic acid was used as a hole scavenger (40 mM, which yields pH 2.57), all three catalysts reduced nitrate to varying extents; however, no nitrate removal was observed when water or equivalent molar quantities of oxalic acid (pH = 1.71) or sodium formate (pH = 6.43) were used. To determine repeatability of the experiments, P90 (1 g/L) was tested in duplicate with an initial nitrate and formic acid concentration of 100 mg-N/L and 40 mM, respectively (Figure 3.5). As shown, there is very little variance between the runs; therefore, further experiments were not conducted in duplicate.

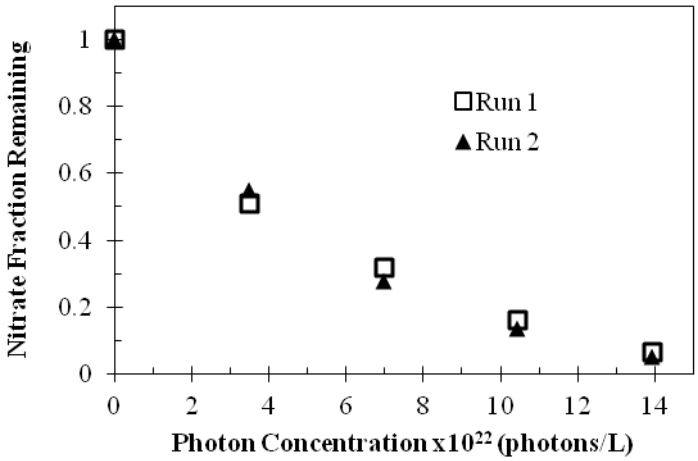


Figure 3.5. Nitrate fraction remaining as a function of photon concentration using an initial nitrate concentration of 100 mg-N/l and 40 mM formic acid

Figure 3.6 shows the percent nitrate removals for P25 and P90 using formic acid and under varying experimental conditions. P25 and P90 (1 g/L) achieved 64% and 77% removal, respectively, at the highest irradiance in model water, making P90 the most effective photocatalyst under the conditions evaluated. Nitrate removal decreased with lower dosages of catalyst but increased with removal of dissolved oxygen. UV100 (1 g/L) achieved only 8% removal of nitrate at the highest irradiance in model water (not shown), and was never greater than 10% under any pH, dissolved oxygen or hole scavenger condition tested. Consequently, UV100 was not included in further experiments pertaining to by-products, oxygen removal, and groundwater.

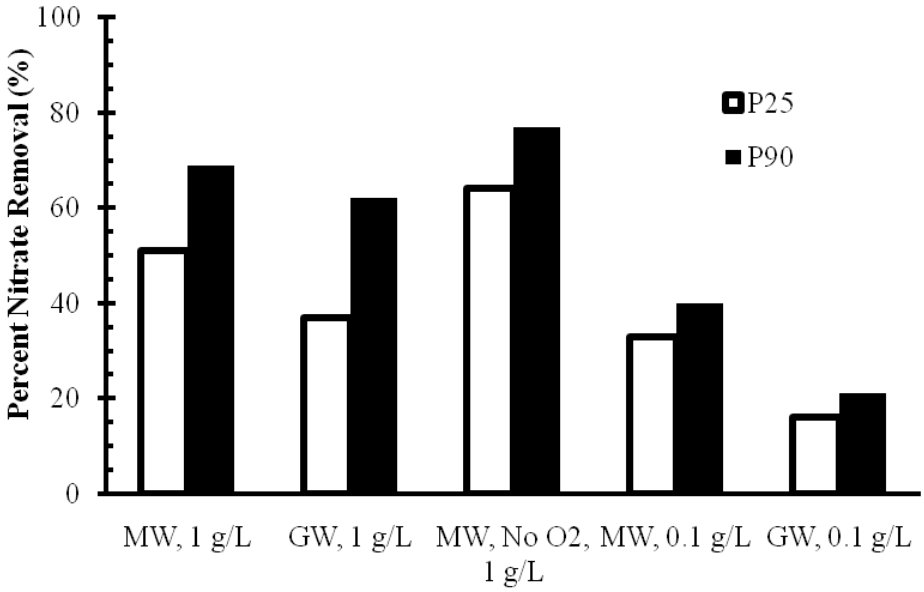


Figure 3.6. Percent nitrate removal after maximum irradiance (6.46 x 10^{22} photons/L). MW = model water, GW = groundwater, and 1 or 0.1 g/L represents the photocatalyst loading (40 mM formic acid and 100 mg-N/L nitrate initially). Removal of nitrate by UV100 (1 g/L) was 8% in model water.

Low levels of nitrite (< 0.5 mg-N/L) formed over the course of the experiments, which suggests nitrite is an intermediate in nitrate reduction. Very low levels of ammonium (<0.6 mg-N/L) also were detected at highest irradiance level tested. TDN measurements indicated that nitrate, ammonium, and nitrite were the only remaining aqueous nitrogen species. For example, when P25 was tested in model water using formic acid as a hole scavenger, the concentrations of nitrate, nitrite, ammonium and TDN were 36.4 mg-N/L, 0.492 mg-N/L, 0.384 mg-N/L and 36.6 mg-N/L, respectively. The small difference between TDN and the sum of nitrate, nitrite and ammonia (98%) is within analytical variance. Given that these experiments had initial nitrate concentrations of 100 mg-N/L, these by-product concentrations indicate a low selectivity for toxic, aqueous nitrogen species at the specified irradiance. However, when P90 was tested at a much

higher irradiance dosage (1.4×10^{23} photons/L) in model water with formic acid, nitrate was completely removed but the formation of ammonium increased to approximately 15 mg-N/L, which equates to approximately 15% selectivity. Nitrite was not detected, confirming its role as an intermediate. This suggests that as nitrate is removed, protons may begin to dominate the photocatalyst surface, making them available for ammonium formation.

The effect of oxygen on nitrate reduction was evaluated to determine the importance of electron availability. Oxygen in aqueous solution is a known scavenger of electrons (Gerischer & Heller, 1991) and required to oxidize organic hole scavengers. Because the natural presence of oxygen in water as well as oxygen produced from water oxidation may affect the reduction of nitrate or oxidation of the hole scavenger, experiments were conducted in which dissolved oxygen was stripped from the solution by bubbling argon gas through it (dissolved oxygen < 0.2 mg/L). Removal of oxygen resulted in <2% nitrate reduction when formic acid was not present. In all experiments containing formic acid, oxygen removal had a better nitrate reduction efficiency when compared to oxygen remaining in solution. For example, with formic acid and 1 g/L of catalyst, oxygen removal increased the nitrate reduction efficiency from 51% to 64% for P25 and from 69% to 77% for P90 (Figure 3.6). These results suggest that removal of oxygen increases the nitrate reduction efficiency by freeing up electrons that would otherwise be used to reduce oxygen.

Photocatalytic Nitrate Reduction in Groundwater

The photocatalytic reduction of nitrate in groundwater was evaluated because nitrate pollution is prevalent in groundwater, which is a concern because of its negative impact on drinking water quality. Groundwater contains anions and cations can affect surface reactions on the catalyst or can be involved in reactions with photoexcited electrons and holes (Chong et al., 2010). Groundwater was spiked to the same nitrate concentration (100 mg-N/L) used in model water experiments and then irradiated in the presence of formic acid and photocatalysts. Nitrate reduction occurred in groundwater, but at a somewhat slower rate than in model water (Figure 3.6). For example, nitrate removal at the highest irradiance for P90 decreased from 69% in model water to 62% in groundwater, and for P25 decreased from 51% in model water to 37% in groundwater.

Effect of Photocatalyst Surface Area

The results for P90 and P25 are useful for determining the effect that the specific surface area (SSA) has on the photocatalytic activity because they are similar materials except for surface area. A plot of the total photocatalyst surface area (m^2) for each P25 and P90 as a function of percent nitrate removal in a model water and groundwater is shown in Figure 3.7. Although only four points were available for regression analysis, there is a clear trend that suggests the SSA is the primary factor in the net differences in nitrate removal by these two otherwise identical materials. Under the highest photocatalyst surface area loading (187.2 m^2, 1 g/L P90), the percent nitrate removal was 69% in model water, and under the lowest photocatalyst surface area loading (9.18 m^2,

0.1 g/L P25), the percent nitrate removal was 33%. Thus, a 52% decrease in removal efficiency was observed for a 95% decrease in available photocatalyst surface area.

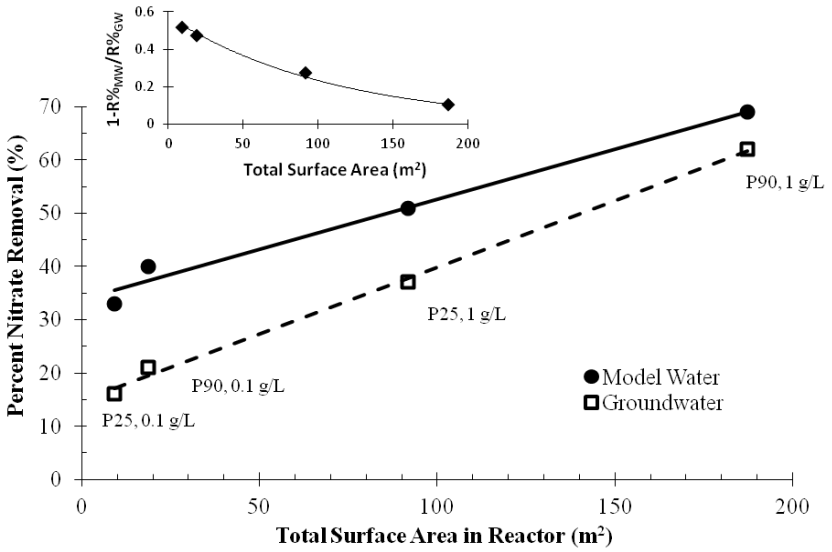


Figure 3.7. Relationship between percent nitrate removal and the total surface area of P25 and P90 photocatalysts in solution. Inset: The percent difference between the percent nitrate removals for model water and groundwater as a function of total catalyst surface area.

The effect of groundwater constituents fouling the photocatalyst surface may be mitigated by increasing the available photocatalyst surface area. The results are similar to those for the model water, in which nitrate removal efficiency increased with increasing photocatalyst surface area. As the surface area increases, the two lines for model water and groundwater begin to converge (Figure 3.7), indicating that surface area mitigates the effects of groundwater constituents. To highlight this convergence, the percent difference between the percent nitrate removal for model water and groundwater was plotted as a function of the total photocatalyst surface area (see Figure 3.7 inset). This relationship

shows that as total available photocatalyst surface area increases, the negative effects of groundwater are decreased. For example, at the highest surface area loading (187.2 m^2, 1 g/L P90), the difference between the percent nitrate removal for the model water and groundwater was only 10%, whereas at the lowest surface area loading (9.18 m^2, 0.1 g/L P25), the difference was a much more significant at 52%.

Kinetics and Quantum Yield of Photocatalytic Nitrate Reduction

Reactor kinetics and quantum efficiencies are necessary parameters for scaling up photoreactor design and comparing different photocatalysts. Nitrate reduction kinetics for P90 are plotted as a function of the time-dependent photon concentration in Figure 3.8. A pseudo-first-order relationship $\frac{d\left[NO_3^-\right]}{dh_\upsilon} = -k\left[NO_3^-\right]$, which generally fits the data well, is illustrated by regression analysis on the data. Regression was not fit through (0,0) as there appears to be a lag period due to unknown photocatalytic heterogeneous mechanisms. Table 3.2 summarizes the values of the rate constant, *k*, obtained from experiments with P25 and P90. UV100 is not included because it had insufficient loss of nitrate to accurately determine *k* values. In all cases, *k* was greater for P90 than for P25 under comparable experimental conditions. A tenfold decrease in the P90 concentration, from 1 to 0.1 g/L, decreased *k* from 0.18 (photons x 10^{22}/L)$^{-1}$ to 0.090 (photons x 10^{22}/L)$^{-1}$, which is only a 50% reduction in the pseudo-first-order rate constant. A tenfold decrease in the P25 concentration, from 1 to 0.1 g/L, decreased its *k* by 28%.

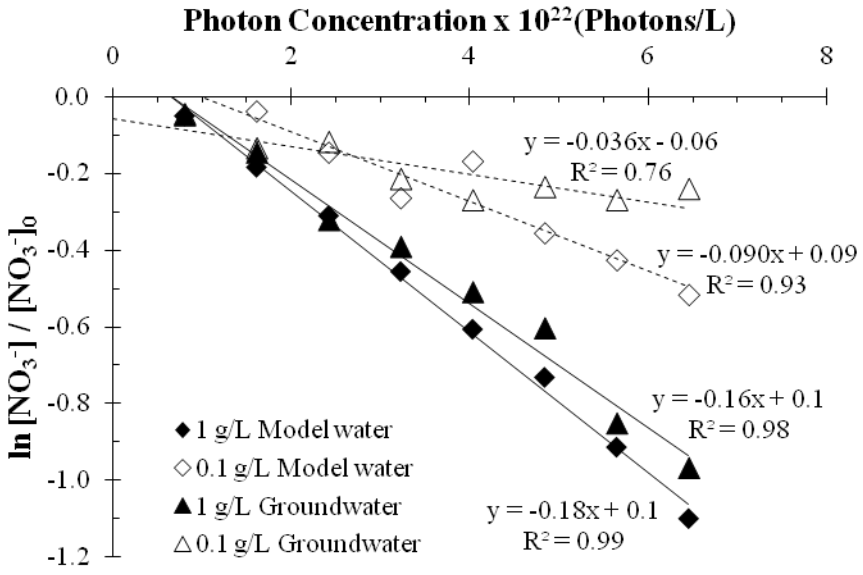


Figure 3.8. Pseudo first-order kinetics of nitrate removal as a function of photon concentration using P90 in the presence of formic acid.

Anions and other constituents present in groundwater also decreased the reduction rate constant. For example, compared to the model water, in groundwater the *k* value for nitrate reduction using P90 decreased by 11% for 1 g/L and by 27% for the 0.1 g/L catalyst dose. The same trend was observed for P25, where *k* decreased by 15% and 37% for 1 g/L and 0.1 g/L catalyst, respectively. Again, at a higher surface area (e.g., P90, 1 g/L), the decrease in rate constant was not as significant as observed when less surface area (i.e., sorption sites) was available.

Quantum yield provides a means to compare the true activity of photocatalysts using different lamps or reactors. Because of the difficulty in measuring the number of photons absorbed by the photocatalyst, an apparent quantum yield (photonic efficiency, ξ) was calculated by assuming that the photocatalyst absorbed 100% of the incident photons. Here, for our polychromatic light source, ξ_{poly} is defined as the ratio of moles of

nitrate reacted to the total moles of incident photons capable of TiO_2 bandgap excitation (Eq. 3.2) (Serpone, 1997; Serpone & Salinaro, 1999). The number of electrons reacted was calculated on the basis of experimental results that suggested nearly 100% of the nitrate molecules that reacted were converted to dinitrogen rather than to other nitrogen species. The conversion of nitrate to dinitrogen (N_2) consumes five moles of electrons per mole of nitrate (Eq. 3.3). ξ_{poly} values for P25 and P90 at the maximum irradiance in our experiments are summarized in Table 3.3. Values of ξ_{poly} follow trends similar to those in Figure 3.6. The ξ_{poly} for UV100 in model water with formic acid present, 0.017 (not shown in Table 3.3), was low compared to that of P25 and P90. Under other experimental conditions, nitrate removal for UV100 was too low to calculate a reliable ξ_{poly}.

Table 3.3. *k and ξ_{poly} Values for P25 and P90*

Experimental Conditions (in model water unless specified)	***k* values (photons x 10^{22}/L)$^{-1}$**				**ξ_{poly} at maximum irradiance**			
	P25		**P90**		**P25**		**P90**	
	0.1 g/L	1.0 g/L	0.1 g/L	1.0 g/L	0.1 g/L	1.0 g/L	0.1 g/L	1.0 g/L
Sodium formate	< 2% initial nitrate removal occurred				< 0.01			
Formic acid	0.071	0.098	0.090	0.18	0.07	0.17	0.09	0.23
Formic acid and oxygen removal	NA	0.16	NA	0.23	NA	0.20	NA	0.27
Groundwater with formic acid	0.045	0.083	0.066	0.16	0.04	0.09	0.10	0.17

NA = Not analyzed

$$\xi_{\text{poly}} = \frac{\text{moles of electrons reacted}}{\text{moles of incident photons}} \tag{3.2}$$

$$NO_3^- + 6H^+ + 5e^- \rightarrow \frac{1}{2}N_{2(g)} + 3H_2O; E^\circ(\text{NHE}) = 1.25\ \text{V} \tag{3.3}$$

Discussion

P90 has a smaller average anatase crystal size than P25, 12 vs. 16 nm, which results in a larger SSA, 104 m^2/g vs. 52 m^2/g. The higher SSA of P90 relative to P25 provides more active sites for adsorption of the nitrate anion, as well as more Ti(III) surface sites for trapping electrons, thus reducing recombination within the bulk of the particle (Ti(IV)-OH + e_{cb}^- $\rightarrow$ Ti(III)-OH). This effect was more pronounced when experiments were performed in groundwater (Figure 3.7 inset), where increasing the photocatalyst surface area decreased the negative effect that groundwater had on the nitrate reduction efficiency. The decrease in activity can be attributed to the presence of sulfate, carbonate, chloride, perchlorate, and phosphate in the groundwater (Abdullah, Low, & Matthews, 1990; F. X. Zhang et al., 2005). The presence of anions, as well as other ions and organics in the groundwater, may compete for surface sorption sites or for photogenerated electrons or holes (Chong et al., 2010). Thus, adding more catalyst can reduce the influence of dissolved substances in groundwater; however, high catalyst concentrations can reduce the penetration depth of irradiation, which reduces the photocatalytic efficiency. The SSA may not be the primary limiting variable regarding photocatalytic nitrate reduction because UV100, which has an estimated SSA of 400 m^2/g, had a poor nitrate reduction efficiency.

The rate of recombination is one of the most important variables affecting the activity of photocatalysts (Hoffmann et al., 1995; Linsebigler et al., 1995). When the recombination rate is discussed in relation to a heterogeneous matrix (i.e., not photocatalyst alone), it is dependent on many factors including the intrinsic rate at which the electron-hole pair recombines, the rate of charge trapping within/on the photocatalyst,

and the interfacial charge transfer rate to both the electron and hole acceptor. Regarding the intrinsic recombination rate, the availability of surface defects for charge carrier trapping and bulk defects as recombination centers (i.e., degree of crystallinity) is the main variable affecting the rate (Hoffmann et al., 1995).

Multi-phase photocatalysts, such as P25 and P90, have a slower rate of recombination due to the ability of the heterogeneous energy levels of rutile and anatase to separate charge carriers, which increases the lifetime of the electrons and holes and thus decreases the probability of recombination (Hurum, Gray, Rajh, & Thurnauer, 2005). In contrast, UV100, a single-phase photocatalyst, appears to have an electron-hole recombination rate that is competitive with the kinetics of electron transfer to nitrate anions. The recombination rate can be explained using ξ_{poly}; if recombination dominates, then ξ_{poly} will be low. In model water using formic acid as a hole scavenger, UV100 had a low ξ_{poly} (0.017) compared to P25 (0.17) and P90 (0.24), which can be attributed to the fast rate of recombination in UV100 due to the poor degree of crystallinity and its inability to separate the electron-hole pair. In this study, the rate of interfacial transfer of the electron-hole pair is dependent on the rate at which nitrate and the hole scavenger reacts with photogenerated electrons and holes, respectively. Formate and oxalate are similar compounds and both require two holes for complete mineralization and both form identical reducing radicals (Koppenol & Rush, 1987; Perissinotti, Brusa, & Grela, 2001; Surdhar, Mezyk, & Armstrong, 1989). Formic acid has been shown to undergo oxidation via a direct transfer of a hole, whereas other organic compounds, such as oxalate, are oxidized by an indirect hole transfer, i.e., hydroxyl radical oxidation (Mora-Sero et al., 2005). In our system, no nitrate reduction occurred when using oxalic acid, yet formic

acid performed very well. This observed difference may be due to the oxidation rate over TiO_2, where the rate of formic acid has been shown to be twice as fast as oxalic acid (McMurray et al., 2004).Theoretically, TiO_2 is thermodynamically capable of using water as a hole scavenger (i.e., electron donor) to produce oxygen, as illustrated in Figure 3.9. However, this and past studies have shown that, practically, TiO_2 is unable to reduce nitrate using water as a hole scavenger, even at acidic pH (Bems et al., 1999; W. Gao et al., 2004; Kominami et al., 2001a; Akihiko Kudo et al., 1992; Y. Li & Wasgestian, 1998; L. F. Liu et al., 2008; Ranjit, Varadarajan, et al., 1995; SÃ¡ et al., 2009; Sittinun Tawkaew, Yin, et al., 2001; Wehbe et al., 2009; F. X. Zhang et al., 2005). The kinetics of water oxidation using TiO_2 are very slow (Litter, 1999); thus, recombination may occur before the transfer of the hole. Consequently, the nitrate reduction efficiency is dependent upon the type of hole scavenger used. Choosing a hole scavenger with the fastest oxidation kinetics will increase the photocatalytic nitrate reduction efficiency by allowing more photons to be turned into chemical reactions.

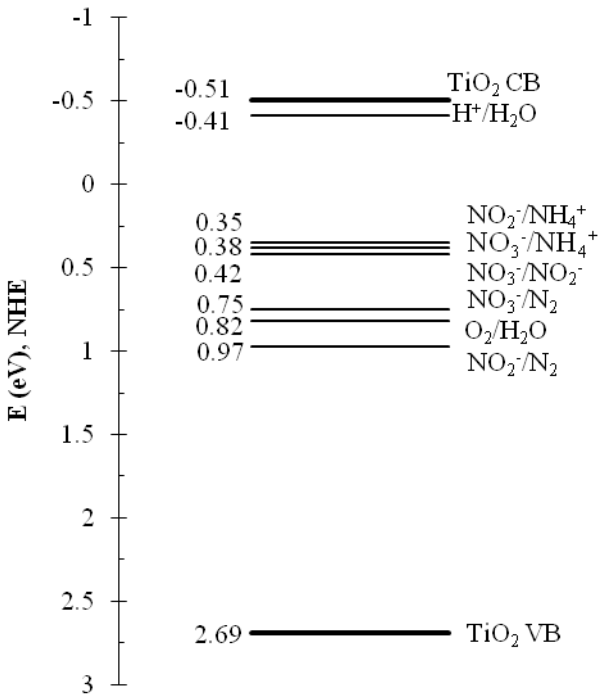


Figure 3.9. Standard reduction potentials (NHE) for nitrogen compounds in aqueous solution in relation to the band positions of anatase TiO_2. CB and VB represent the conduction and valence bands, respectively. The standard potentials of the nitrogen compounds were calculated for pH 7 (Pourbaix & De Zoubov, 1966). The band positions of TiO_2 at pH 7 were calculated for colloidal TiO_2 (Michael Gratzel, 1989).

Decreasing pH increases the photocatalytic activity (i.e., proton catalyst) by assisting in the nitrate reduction reaction, which requires twelve protons to convert nitrate to dinitrogen, as shown in Equation 3.3. Formic acid addition resulted in acidic conditions (pH 2.57), and nitrate reduction was observed (Figures 6 and 8). Sodium formate addition resulted in neutral conditions (pH 6.43), and no nitrate reduction was observed. These observations were independent of the type of catalyst (P25, P90), catalyst dose, or type of aqueous solution. The pH could also have an effect on the photocatalytic activity by altering the surface charge of the photocatalyst. At the pH of the experiments in the presence of formic acid (pH 2.57), the average zeta potentials of

P25 and P90 (zeta potential = 41 and 34 mV, respectively) are more positive than that of UV100 (zeta potential = 16 mV). Thus, the electrostatic attraction of anions such as nitrate and formate in the double layer may also be stronger for P25 and P90, which makes interfacial charge transfer more probable. However, given that oxalic acid had no activity at an experimental pH of 1.71, the rate of oxidation, which has a direct effect of the rate of recombination, appears to have a more limiting effect than pH on the nitrate reduction activity.

3.4 Summary

For the first time, this study conducted a side-by-side characterization of three common commercial titanium dioxide photocatalysts (P25, P90, and UV100) and compared their photocatalytic activity for the reduction of nitrate in a model water and in groundwater. Under the evaluated experimental conditions, nitrate was reduced to mostly non-aqueous by-products, with an ammonium selectivity of approximately 85% if full nitrate removal is achieved. The photocatalytic nitrate reduction activity was found to be dependent upon the rate of recombination, pH, and total photocatalyst surface area. The rate of recombination was the limiting variable controlling the reduction activity. When using formic acid as a hole scavenger, P90 and P25 exhibited much greater photocatalytic activity for nitrate reduction than UV100 because of their smaller recombination rates. Nitrate reduction proceeded in the presence of formate at acidic pH, but at neutral pH no nitrate reduction was observed for any of the photocatalysts, which may be attributed to the proton requirement for nitrate reduction or the change in surface charge. P90 exhibited greater photocatalytic activity than P25 due to its increased surface area, and an

increase in available surface area was successful in mitigating the negative effects of groundwater constituents.

Comparing our experimental results on nitrate reduction to results published in the literature is difficult because few studies provide the details necessary to calculate quantum yields. These comparisons are further complicated because some photocatalytic nitrate reduction studies use monochromatic lamps that emit light only at 254 nm, whereas others use polychromatic light sources. Irradiation at 254 nm is at a lower wavelength than the UV absorbance peaks at 302 and 354 nm for nitrate and nitrite, respectively. Therefore, different results are not completely surprising when various lamp types are used because direct photolysis may occur. In this study, we have showed that photocatalytic results can easily be reported as a function of irradiance (i.e., photon concentration).

While photocatalytic oxidation of pollutants has been studied extensively, photocatalytic reduction has received less attention. When using photocatalysis for oxidation reactions, oxygen reacts with conduction band electrons at a fast enough rate that recombination kinetics don't dominate and hole transfer occurs. However, if the pollutant of concern requires electrons (i.e., reduction), then water must behave as the hole scavenger. Oxidation of water over TiO_2 is slow such that recombination dominates and no reduction occurs. The results presented herein show that when designing materials for photocatalytic reduction of oxo-anions, perhaps more emphasis should be placed on decreasing the rate of recombination rather than increasing surface area or tailoring surface chemistry for selected pollutants. This study shows that P90 is a suitable replacement for P25 as a commercial photocatalyst standard, and that P25 and P90 can be

used as a standard to test the effect of surface area in photocatalytic experiments. Also, including UV100 may be an easy alternative to determine if recombination rate or surface area is the limiting variable. The advancement of photocatalytic nitrate reduction technologies should focus on creating commercial photocatalysts that are capable of using water as a hole scavenger and elucidating the chemical mechanisms of nitrate, the hole scavenger, and the photocatalyst.

CHAPTER 4

PHOTOCATALYTIC NITRATE REDUCTION IN WATER: MANAGING THE HOLE SCAVENGER AND REACTION BY-PRODUCT SELECTIVITY*

*Published: Doudrick, K., Yang, T., Hristovski, K., Westerhoff, P. Photocatalytic nitrate reduction: Managing the hole scavenger and by-product selectivity. *Applied Cat. B,* 136-137 (2013) 40-47.

Abstract

Nitrate contamination of groundwater limits it use as a drinking water supply unless the nitrate is removed. The aim of this study was to move toward implementing photocatalysis for nitrate treatment in drinking water systems by understanding the effects of experimental conditions and the mechanisms involved. Specifically, the photocatalytic reduction of nitrate in water was examined using titanium dioxide (Evonik P90) loaded with silver nanoparticles and formic acid as a hole scavenger (electron donor). For drinking water applications, minimization of residual formic acid is essential to prevent adverse effects in potable water distribution systems (e.g., carbon source for biofilm growth). Experimental parameters including pH, nitrate concentration, formate concentration, photocatalyst concentration, and silver loading were varied to demonstrate their effect on the rate of nitrate and formate removal as well as by-product selectivity. The addition of silver improved the rate of nitrate and formate removal significantly. The removal rates decreased with increasing pH, which suggests that the reaction is a proton-coupled electron transfer and that adsorption of the constituents is necessary. Under acidic conditions, nitrogen gases (~85%) and ammonium (~15%) were the final by-products. However, under neutral pH conditions, only nitrite formed, suggesting that a co-catalyst that is efficient at localizing protons is required to move beyond nitrite. The

experimental stoichiometric requirement for formic acid indicated that it acts as a two-hole scavenger, which suggests conduction band electrons, rather than radicals, are responsible for nitrate reduction. Using optimal operating conditions, nitrate and formate were efficiently removed at nearly a 1:1 ratio, showing that the residual hole scavenger concentration can be controlled while maintaining an acceptable rate.

4.1. Introduction

Nitrate is a stable, highly soluble ion that poses a risk to human health and has a large impact on the natural nitrogen cycle. It is a known cause of methemoglobinemia, or "blue baby" syndrome, and could be carcinogenic or an endocrine disruptor (Guillette & Edwards, 2005; Hamlin, 2006; Hamlin et al., 2008). The USEPA has set a drinking water maximum contaminant limit (MCL) for nitrate of 10 mg-N/L. A recent survey of 5,101 wells in the United States revealed that nitrate levels exceed the standard in approximately 8% of wells (20% agricultural, 3% urban, 4% major aquifers), affecting more than 24.6 million people (Burow et al., 2010). This makes nitrate the most ubiquitous contaminant found in drinking water sources (B. Nolan, 2004; B. T. Nolan & Hitt, 2006; B. T. Nolan et al., 2010; B. T. Nolan & Stoner, 2000), and these pollution levels continue to rise (Rupert, 2008). Ion exchange traditionally has been used to remove nitrate from drinking water sources, but this process leaves behind a highly concentrated brine solution that still requires treatment. Recent advances in biological and catalyst nitrate treatment technologies are promising (Seidel, Gorman, Darby, & Jensen, 2011), but technological disadvantages still remain. Photocatalysis as a reduction process is emerging as a potentially viable water treatment process (Hoffmann et al., 1995) but

requires further mechanistic understanding before optimization for drinking water treatment applications.

Photocatalysts are promising materials for water treatment because of their ability to create photogenerated conduction band electrons (e^-_{cb}) and valence band holes (h_{vb}^+), which enable redox reactions with adsorbed aqueous species (see SI for further discussion of photocatalytic mechanisms). Numerous studies report synthesis of new photocatalysts for nitrate reduction (Anderson, 2011; Bems et al., 1999; W. L. Gao et al., 2004; Hamanoi & Kudo, 2002; Jin et al., 2004; Kato & Kudo, 2002b; Kominami et al., 2001a; Kominami et al., 2005b; A. Kudo et al., 1987b; Akihiko Kudo et al., 1992; L. Y. Li et al., 2010; Y. Li & Wasgestian, 1998; L. F. Liu et al., 2008; Penpolcharoen et al., 2001; Ranjit, Krishnamoorthy, et al., 1995; Ranjit et al., 1994a; Ranjit, Varadarajan, et al., 1995; Ranjit et al., 1996; Ranjit & Viswanathan, 1997a, 1997c; Rengaraj & Li, 2007b; T. Sato et al., 1996; Sá et al., 2009; Sittinun Tawkaew, Yin, et al., 2001; Wehbe et al., 2009; F. X. Zhang et al., 2005). Tantalates have been used to reduce nitrate photocatalytically using water as a hole scavenger, but the removal rate and selectivity toward N_2 was poor (Kato & Kudo, 2002b). Of the photocatalysts examined, titanium dioxide (TiO_2) is the most efficient at reducing nitrate with a high selectivity toward innocuous by-products (e.g., dinitrogen) (Anderson, 2011; Bems et al., 1999; W. L. Gao et al., 2004; Kominami et al., 2001a; Kominami et al., 2005b; A. Kudo et al., 1987b; Akihiko Kudo et al., 1992; L. Y. Li et al., 2010; Y. Li & Wasgestian, 1998; L. F. Liu et al., 2008; Penpolcharoen et al., 2001; Ranjit, Varadarajan, et al., 1995; Ranjit & Viswanathan, 1997a, 1997c; Rengaraj & Li, 2007b; Sá et al., 2009; Sittinun Tawkaew, Yin, et al., 2001; Wehbe et al., 2009; F. X. Zhang et al., 2005); silver is the best co-

catalyst choice (Sá et al., 2009; F. X. Zhang et al., 2005). Silver is a strong co-catalyst for reactions involving reduction because it is excellent at trapping e^-_{cb} (Takai & Kamat, 2011). For nitrate reduction, TiO_2 requires the addition of an organic compound to fill valence band holes (i.e., electron donor) to either decrease recombination or produce reducing radicals. Formic acid is currently the most efficient hole scavenger for nitrate reduction over TiO_2 (K. D. Doudrick, Monzón, Mangonon, Hristovski, & Westerhoff, 2012; Sá et al., 2009; F. X. Zhang et al., 2005). Although studies have been dedicated to the synthesis of new photocatalytic materials for nitrate reduction, relatively little information is available on the applicability of photocatalytic nitrate reduction to drinking water systems, specifically on their rate and products as a function of pH or under conditions in which residual formic acid can be minimized. Residual formic acid in water distribution systems can serve as a carbon source for undesirable biofilm growth.

The aim of this study was to move toward implementing photocatalysis for nitrate treatment in drinking water systems by understanding the effects of experimental conditions and the mechanisms involved. TiO_2/Ag coupled with formic acid as a hole scavenger was used for this purpose. The objectives of this study were to (1) demonstrate the effect of the physical characteristics of the photocatalyst by varying the photocatalyst surface area and the amount of silver loading, (2) demonstrate the effect of the proton-dependent reaction by varying pH, (3) determine the optimal initial formate concentration to control residual formate, and (4) provide mechanistic insights on by-product formation and the role of the hole scavenger. Unlike the vast majority of previous studies that simply report "exposure time in photocatalytic reactor," we report our data with respect

to photon fluence to advance the application of photocatalytic reduction systems to engineered practice.

4.2. Experimental methods

Chemicals and materials

For this study, a new TiO_2/Ag photocatalyst composite was synthesized using P90 as the TiO_2 source, which is a more active commercial TiO_2 photocatalyst for nitrate reduction than P25 (K. D. Doudrick et al., 2012). P90 (Evonik, formerly Degussa, >99.5%) was obtained in powder form. It is synthesized using high-temperature flame hydrolysis of $TiCl_4$ in the presence of oxygen and hydrogen. It contains both anatase (88%, 12 nm) and rutile (12%, 18 nm) crystal structures, has a surface area of approximately 104 m^2/g, and has an average isoelectric point (IEP) of 6.4 (K. D. Doudrick et al., 2012). Sodium nitrate ($NaNO_3$, 99%, EMD) was used as the nitrate source and silver nitrate ($AgNO_3$, >99%, Sigma Aldrich) as the silver ion source. Formic acid (HCOOH, 98% Fluka) and sodium formate (HCOONa, 99.3%, Fisher) were used as formate sources. Silver nanopowder (576832, >99.5%, Sigma Aldrich) was used as received. Ultrapure deionized water was used for all experiments and prepared using a Nanopure® (18.3 MΩ-cm) treatment system.

P90/Ag synthesis

P90 was loaded with silver by an ultraviolet (UV) photoreduction method that reduces silver ions on the surface of P90. Briefly, 5 g of P90 was added to 500 mL of water and then bath sonicated (80 W/L, 40 kHz) for 30 minutes. An 8-mL aliquot of

methanol (CH_3OH, 99.9%, Fisher) was added to the suspension to act as a hole scavenger to increase the rate of silver deposition. The pH was adjusted to 10–11 using sodium hydroxide (NaOH, 97.0%, EMD) to form negative surface charges on P90 to assist with silver cation adsorption. The appropriate mass of silver ions for 0.5 to 5% loading from silver nitrate was then added to the suspension and mixed in the dark for 30 minutes to allow for adsorption. After mixing, the suspension was purged with argon for 15 minutes to remove dissolved oxygen (DO). The suspension was then covered, transferred to a photoreactor containing a 450-W medium pressure mercury lamp (Hanovia, PC451.050), and irradiated for approximately 30 minutes. After sufficient washing, the sample was dried in an air oven at 90ºC for 24 hours. The sample was heated in a muffle furnace in air at 450 °C to decompose silver oxides (Waterhouse, Bowmaker, & Metson, 2001), at which point the sample color changed from purple to light yellow.

Photocatalyst characterization

The crystal structure was determined using powder X-ray diffraction (XRD) on a D5000 (Siemens, USA) with a CuK_α source and an aluminum holder. Each sample was scanned from $2\theta = 20°$ to 60° to detect the characteristic TiO_2 peaks and from $2\theta = 30°$ to 120° to detect the characteristic Ag^0 peaks. Surface elemental composition and chemical state were analyzed using X-ray photoelectron spectroscopy (XPS) performed on a ESCALAB 220i-XL (Vacuum Generators, USA) with a monochromatic Al K_α source at $h\nu = 1486$ eV and a base pressure = 7×10^{-10} mbar. Images were obtained using a high-resolution scanning transmission electron microscope (STEM or TEM) with energy dispersive X-ray capabilities (EDS) (STEM Phillips CM-200). Inductively coupled

plasma-mass spectrometry (ICP-MS) (Thermo X-Series 2,Thermo Fisher Scientific Inc., Waltham, MA) was used to determine the mass of Ag loaded onto the photocatalyst. Duplicate samples were digested in a microwave using concentrated nitric acid, diluted, and then injected into the ICP-MS. The zeta potential was determined using the Phase Analysis Light Scattering technique (ZetaPALS, Brookhaven, NY) in 10 mM KNO_3 background electrolyte. The specific surface area was obtained with the Branauer, Emmett and Teller (BET) model using a Tristar II 3020 automated gas adsorption analyzer (Micromeritics, USA).

Photocatalytic experiments

Photocatalytic experiments were performed using a 200-mL photoreactor with a UV lamp located in the center. A borosilicate sleeve was placed around the lamp to filter out light wavelengths less than 280 nm to avoid direct photolysis of nitrate or formate. This was done to elucidate photocatalytic mechanisms; removing the sleeve simply increased the rate of removal, and no change in by-products was observed. The UV light source was a 450-W (Ace Glass power supply, 7830-60) medium-pressure mercury-vapor lamp (Ace Glass, 7825-34; Hanovia PC451.050) that was placed in a double-walled quartz immersion well (Ace Glass, 7854-25). The system temperature was maintained at 25 °C using a chiller. For each run, the photocatalyst was suspended using magnetic stirring in a solution of ultrapure water containing nitrate and formate.

The experimental design matrix included a baseline experiment (pH = 2.5, initial nitrate concentration = 7.14 mM, initial formic acid concentration = 40 mM, P90/Ag(1%) dosage = 1 g/L), which was assumed to be optimal on the basis of previous studies (F. X.

Zhang et al., 2005). From the baseline conditions, variables altered included photocatalyst concentration, silver loading, initial pH, initial nitrate concentration, and initial formic acid concentration; each was varied while keeping the other baseline conditions constant. P90/Ag(1%) dosage (0.1 to 1 g/L) and silver loading (0.5-5%) were varied to demonstrate their effect on the rate of nitrate removal and by-product selectivity. As a control, P90 (1 g/L) was mixed with 1% mass of Ag^0 nanoparticles to prove if a synergistic effect was present. The effect of pH was investigated at pH 2.5 to 10. pH was adjusted using the appropriate concentration of formic acid and sodium formate. The pH in control experiments containing no formate was adjusted using nitric acid (HNO_3). The effect of different nitrate and formate concentrations was investigated using three sets of experiments: (1) the initial concentration of formic acid was varied from 20 to 80 mM while keeping the initial nitrate concentration (7.14 mM) constant; (2) the initial nitrate concentration was varied from 0.714 to 35.7 mM while keeping the initial formic acid to nitrate molar ratio (FNR), 5.6, constant (i.e., the initial formic acid concentration was 4 to 200 mM); and (3) the initial nitrate concentration was varied from 0.714 to 35.7 mM while keeping the initial concentration of formic acid (40 mm) constant. The experimental design matrix is shown in Table SI-1. Prior to irradiation, the sample was stirred in the dark for 1 hr to eliminate non-photocatalytic removal (i.e., adsorption). On average, nitrate adsorption was <5% or ~2 molecules/nm^2. During kinetic photocatalysis experiments, samples were collected over time, filtered using a 0.45-µm nylon membrane to remove the photocatalyst, and stored in amber glass vials in the dark at ~3 °C until analysis within 48 hours.

Analytical methods

Samples were analyzed for nitrate (NO_3^-), nitrite (NO_2^-), ammonia (NH_4^+), and total dissolved nitrogen (TDN) to assess formation of aqueous by-products, and dissolved organic carbon (DOC) was measured to monitor changes in the concentration of formate (i.e., hole scavenger) over time. Ion chromatography was used to measure nitrate and nitrite anions (Dionex DX-120; AS12A column) and ammonium cations (Dionex IC-20; CS12A column) following EPA Standard Method 4110. TDN and DOC were measured using a total organic carbon/total nitrogen analyzer (Shimadzu TOC-V/ASI-V/TNM-1). Ion chromatography (Dionex DX-120; AS12A column) was used to confirm that all DOC present was formate and not an intermediate carbon compound. DO was measured using a handheld DO meter (YSI 550A). Previous studies on the photocatalytic reduction of nitrate detected only nitrite, ammonium, dinitrogen (N_2), and nitrous oxide (N_2O) as by-products (W. Gao et al., 2004; Kato & Kudo, 2002b; Kominami et al., 2001a; Kominami, Gekko, & Hashimoto, 2010; Kominami et al., 2005b; Sá et al., 2009; Wehbe et al., 2009; F. X. Zhang et al., 2005); therefore, the mass of gaseous nitrogen by-products was approximated on the basis of a nitrogen mass balance using nitrate, nitrite, ammonia, and TDN. Because this study focused on finished water quality (i.e., aqueous species for drinking water), the ratio of greenhouse gas (N_2O) to inert gas (N_2) was not measured. The selectivity toward nitrite (1), ammonium (2) , and N gaseous by-products (3) were defined according to:

(4.1) $S(NO_2^-)=\frac{[NO_2^-]_t}{[NO_3^-]_0-[NO_3^-]_t}$,

(4.2) $S(NH_4^+)=\frac{[NH_4^+]_t}{[NO_3^-]_0-[NO_3^-]_t}$,

and (4.3) $S(N_{gas})=\frac{[NO_3^-]_0-[NO_3^-]_t-[NO_2^-]_t-[NH_4^+]_t}{[NO_3^-]_0-[NO_3^-]_t}$, where $[X]_0$ is the concentration at time = 0 and $[X]_t$ is the concentration at time = t.

Lamp irradiance measurements

The lamp irradiance was measured using a UV-VIS fiber optic spectrometer (Avantes AvaSpec-2048) adapted with a cosine corrector. Irradiance was measured at a distance halfway between the lamp and reactor wall (1 cm) and at multiple points from the bottom to the top of the reactor to obtain the average irradiance. For this study, the total lamp irradiance in ultrapure water from 280 to 1050 nm was 29.2 mW/cm^2. With a bandgap of ~3.2 eV (K. D. Doudrick et al., 2012), the total irradiance absorbable by P90 (280–388 nm) was 6.5 mW/cm^2, or approximately 22% of the total lamp irradiance. Only the wavelengths absorbed by P90 were used for reporting experimental results. To make the results comparable with other materials and similar studies, they are reported as a function of irradiation rather than time. Because a polychromatic lamp was used, the irradiation is reported not as an energy fluence (e.g. J/cm^2) but as a photon fluence (P90 absorbable) to account for differences in photon energies.

4.3. Results and discussion

Photocatalyst characterization

Samples were characterized using microscopy, crystal structure, elemental, and surface analyses. Figure 4.1 shows TEM images of P90 with and without silver loading. Pristine P90 consists of nanocrystallites approximately 10–30 nm in diameter and has a distinct tetragonal structure (Figure 4.1a). After loading with silver there was an obvious change in the morphology of the crystallites owing to surface coverage with silver islands, which was confirmed by EDS (Figure 4.1b). The silver nanoparticles were approximately 2–3 nm in diameter.

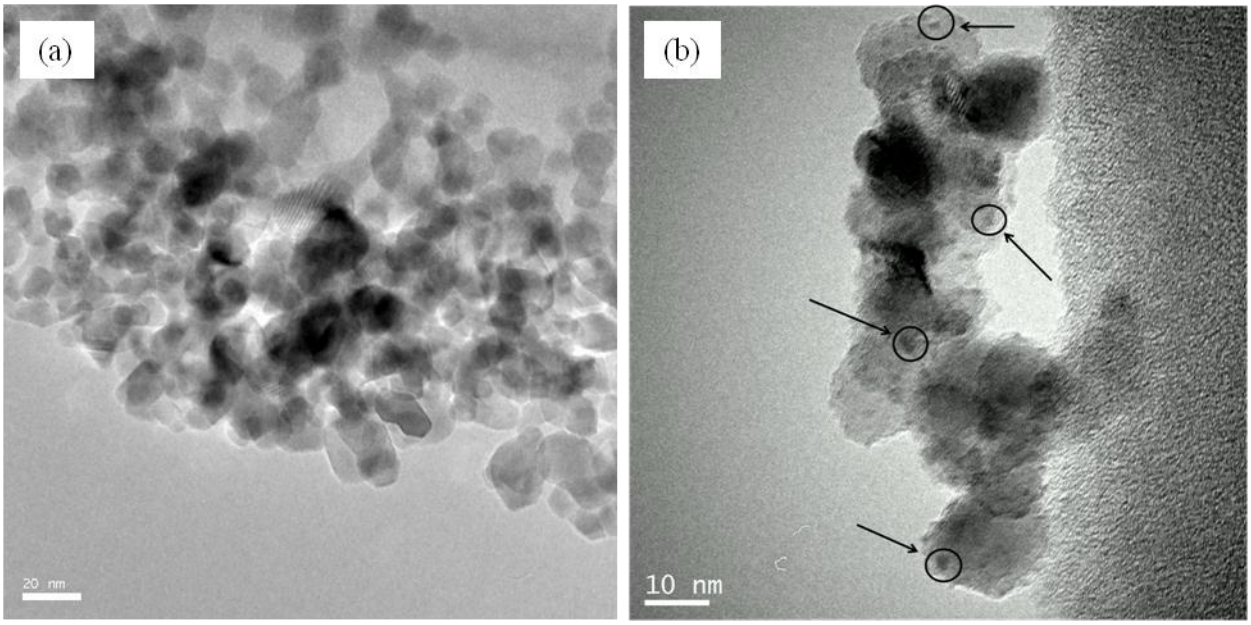


Figure 4.1. TEM images of (a) P90 and (b) P90/Ag(5%). Black particles in (b) are silver nanoparticles; some are highlighted with circles (~2–3 nm).

XRD and XPS were used to characterize the chemical state and composition of the silver nanoparticles (Figure SI-4.1a and Figure SI-4.1b, respectively). The results showed that the silver has a metallic core (Ag^0) with an unstable oxide shell, most likely Ag_2O.

ICP-MS results of acid-digested photocatalysts revealed silver mass loadings of 0.52, 1.10, 2.16, and 5.27% for theoretical loadings of 0.5, 1, 2, and 5%, respectively, indicating that nearly 100% of Ag^+ was photodeposited onto the P90 surface.

BET results showed that the specific surface areas for 0, 0.5, 1, 2, and 5% silver loadings were 104, 101, 94, 77, and 73 m^2/g, respectively. These results indicate that as the percentage of silver is increased, the surface area decreases. Because P90 is non-porous, this suggests that silver particles fill either surface sites on P90 that would otherwise be attributed to higher surface area or voids between P90 aggregates.

Zeta potential (ξ) analysis was performed from pH 2.5 to 10.5 (Figure SI-4.2). P90/Ag(1%) had a point of zero charge (pH_{zpc}) of 7.1, compared with 6.4 for P90 (K. D. Doudrick et al., 2012). Adding silver also resulted in a higher absolute surface charge under both acidic and basic conditions. For example, at pH = 4, P90/Ag(1%) was ~47 mV, and P90 was ~31 mV (Figure SI-4.2). A higher pH_{zpc} results in a lower adsorption energy requirement for anions when the pH is below the pH_{zpc}.

Photocatalytic removal of nitrate and formate

When formic acid and nitrate were mixed under dark or irradiated conditions ($\lambda >$ 280 nm), no nitrate reduction occurred without a photocatalyst. Therefore, formic acid does not act as a direct reductant under these experimental conditions; rather, it acts as a

hole scavenger. Figure 4.2 shows the concentrations of nitrogen compounds and formate as a function of photon fluence for the baseline experiment. Nitrite forms as an intermediate, and ammonium is a by-product; ammonium does not appear until after some nitrite has formed, which indicates that nitrate reduction is a step-wise process. After complete nitrate removal, the sum of NO_3^-, NO_2^-, and NH_4^+ accounted for ~90% of TDN for aqueous N species. The difference may be attributed to some nitrous acid (HNO_2, pK_a = 3.3) volatilization when samples were acidified for TDN measurement. This means that accumulation of significant amounts of other aqueous inorganic (e.g., hydroxylamine) or organic nitrogen species as aqueous intermediates or by-products from reactions with the hole scavenger are unlikely, which is in good agreement with previous studies (Sá et al., 2009; F. X. Zhang et al., 2005). Time-dependent concentrations of both nitrate and formate fit well ($R^2 > 0.95$) to a pseudo-first-order rate (Figure SI-4.3).

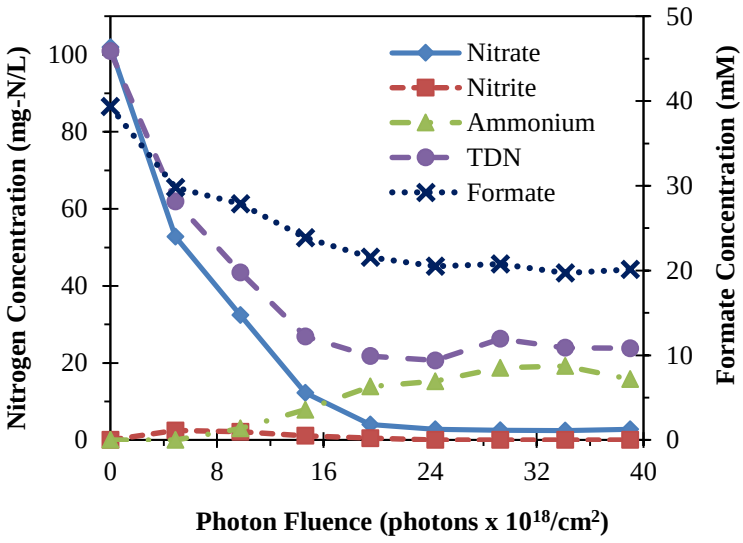


Figure 4.2. Concentrations of nitrogen compounds and formate as functions of photon fluence for the baseline experiment (7.14 mM NO_3^-, 40 mM HCOOH, 1 g/L P90/Ag(1%), pH = 2.5).

Effect of photocatalyst dosage and silver loading

When the suspended concentration of P90/Ag(1%) is increased, the rate of nitrate disappearance increases, reaching an apparent maximum at approximately 1 g/L (18.8 m^2), at which point the rate begins to decrease gradually (Figure SI-4.4a). The resulting inverse U-shaped curve indicates that increasing the photocatalyst surface area in the reactor results in improved nitrate reduction, but only to a limiting concentration at which the rate decreased, presumably due to irradiation shielding.

Loading silver onto P90 improved the rate of nitrate removal significantly (Figure SI-4.4b). For example, loading 1% silver onto P90 increased the pseudo-first-order rate constant for nitrate, $k_{nitrate}$, fivefold from 0.031 to 0.16 $cm^2/10^{18}$ photons $[T]^{-1}$. Above approximately 2% loading, $k_{nitrate}$ began to decrease. This may be attributed to too much P90 coverage, which would decrease the available irradiation area and cover up TiO_2 surface sites necessary for chemical reactions. Too much silver may also cause an increase in the silver particle size owing to silver cluster growth, which decreases its ability to store electrons (Takai & Kamat, 2011). Although silver particles appeared to adhere to the P90 surface (Figure 1b), the observed rate increase may have been caused by a synergistic effect between Ag^0 particles and P90. However, mixing Ag^0 nanoparticles with P90 did not indicate that a synergistic effect was responsible for the improved rate from silver loading.

Figure 4.3 shows the ammonium selectivity and the maximum nitrite concentration as functions of (a) photocatalyst concentration (P90/Ag(1%)) and (b) the percent mass of silver loaded onto P90. Because nitrite was an intermediate species, the

selectivity for each sample was zero after complete nitrate removal. Therefore, to compare the differences in nitrite intermediate formation in each sample, the maximum measured nitrite concentration was reported instead of selectivity. When the concentration of P90/Ag(1%) increased, both ammonium selectivity and the maximum nitrite concentration increased (Figure 4.3a). When the photocatalyst concentration was held constant and the percent silver loading increased, the selectivity to ammonium decreased, and the maximum nitrate concentration increased (Figure 4.3b). Adding a small amount of silver (0.5%) to P90 decreased the ammonium selectivity significantly (i.e., 29% to 19%), but it also increased the maximum nitrite intermediate concentration from 0.5 to 1.7 mg-N/L. Further increase in the mass percentage of silver did not significantly change the NH_4^+ selectivity, but the maximum nitrite concentration continued to increase. The improved reaction rate may be explained by silver's ability to build up excess electrons (K. D. Doudrick et al., 2012), thus promoting the reduction process. However, the rate of nitrite reduction to other nitrogen species decreased, suggesting that P90 sites, which decreased in number as silver loading increased, are responsible for nitrite reduction to further nitrogen intermediates.

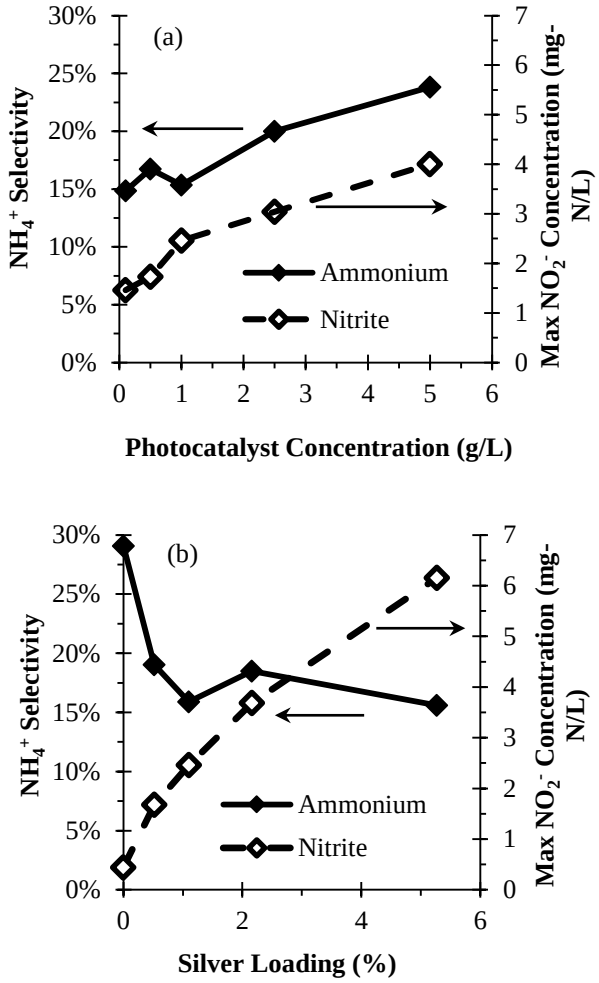


Figure 4.3. NH_4^+ selectivity and the maximum NO_2^- concentration as a function of (a) photocatalyst concentration (P90/Ag) in the reactor and (b) the percent mass of silver loaded onto P90. The silver loading in (a) is kept constant at 1%, and the photocatalyst concentration in (b) is constant at 1 g/L. Initial concentrations for nitrate (100 mg-N/L) and formic acid (40 mM, pH = 2.5) were constant. Photon fluence = 29×10^{18} photons/cm^2.

Effect of system pH on rate and selectivity

Across acidic to neutral pH conditions (2.5–6.8), approximately 100% nitrate removal was observed after 29×10^{18} photons/cm^2. Under alkaline conditions (pH = 10), no nitrate or formate removal was observed. $k_{nitrate}$ and the pseudo-first-order rate constant for formate, $k_{formate}$, decreased with increasing pH (Table SI-4.1). For example,

at pH = 2.5, $k_{nitrate}$ and $k_{formate}$ were 0.16 and 0.026 $cm^2/10^{18}$ photons, respectively, and when the pH was increased to 6.8, $k_{nitrate}$ and $k_{formate}$ decreased to 0.068 and 0.0083 $cm^2/10^{18}$ photons, respectively. Two processes could cause this decrease in observed pseudo-first-order removal rate, as increasing pH (1) decreases the number of protons available for reduction reactions and (2) increases the net negative surface charge of P90.

The multi-electron reduction of nitrate is more thermodynamically favorable (Eq. 4.4–4.6) than the single-electron reduction of nitrate (Eq. 4.7, $E° = –1.1$ V (Cook et al., 2001)). However, the multi-electron reaction requires protons, thus making pH a factor. At acidic pH, the reduction rate was faster than at neutral pH, and at alkaline pH, where the proton concentration was low, no nitrate removal was observed. Furthermore, P90 alone did not reduce nitrate at ambient pH (K. D. Doudrick et al., 2012), but the addition of silver made nitrate reduction possible. This suggests that silver may localize protons at its surface.

If nitrate and formate require direct electron and hole transfers, respectively, then their adsorption to the photocatalyst must occur before charge transfer. When the pH was 2.5, 6.8, and 10, the zeta potential of P90/Ag(1%) was +44, +6, and -46 mV, respectively. At pH = 2.5, the surface charge is highly positive, which promotes the adsorption of nitrate and formate by decreasing the energetic requirement for anion adsorption. At pH = 6.8 and in the absence of silver (i.e., P90 alone), the zeta potential was negative (ξ = -4 mV), and nitrate removal was not observed. With 1% silver on the P90 surface, the zeta potential was shifted to positive (ξ = +6 mV), anion adsorption thermodynamic requirements were still favorable, and nitrate removal was observed. At pH = 10, the thermodynamic adsorption barrier for anions was much greater, and nitrate removal was

not observed. These results suggest that adsorption of both formate and nitrate is important for direct transfer of charge carriers from the photocatalyst to the ion.

Figure 4.4 shows the selectivity for nitrite and ammonium at different pH levels after 39×10^{18} photons/cm^2. Each data point represents the final sample with approximately 100% nitrate removal. When pH $\leq$ 3.5, nitrite was an intermediate, presumably in the protonated form (Eq. 8), and ammonium was the main aqueous by-product (Eq. 4.5). Nitrogen gases, which were assumed to be N_2 (Eq. 4.6) and N_2O (Eq. 4.9), were presumably the main overall by-product. At 3.5 < pH < 5, nitrite became the dominant by-product in addition to some ammonium and nitrogen gases. At pH > 5, nitrite was the only by-product observed. One possible explanation for the sudden by-product switch between pH ~3.5 and 4 is that the pK_a for HNO_2/NO_2^- is approximately 3.3, and HNO_2 is known to disproportionate to NO and NO_2 at a fast rate (Eq. 4.10, k = 13.4×10^8 $M^{-1}s^{-1}$) (J. Y. Park & Lee, 1988); this may be the key limiting step for further reduction to N_2, N_2O, and NH_4^+. Therefore, a pH of ~3.5 can be used instead of pH = 2.5 to reduce formation of more harmful by-products (e.g., NH_4^+) while maintaining a similar rate of nitrate removal.

(4.4) $NO_3^- + 2e^- + 2H^+ \longrightarrow NO_2^- + H_2O$ ($E° = 0.84$ V)

(4.5) $NO_3^- + 8e^- + 10H^+ \longrightarrow NH_4^+ + 3H_2O$ ($E° = 0.88$ V)

(4.6) $2NO_3^- + 10e^- + 12H^+ \longrightarrow N_2 + 6H_2O$ ($E° = 1.25$ V)

(4.7) $NO_3^- + e^- \longrightarrow NO_3^{2-}$ ($E° = -1.1$ V)

(4.8) $NO_3^- + 2e^- + 3H^+ \longrightarrow HNO_2 + H_2O$ ($E° = 0.94$ V, $pK_a = 3.3$)

(4.9) $2NO_3^- + 8e^- + 10H^+ \longrightarrow N_2O + 5H_2O$ ($E° = 1.12$ V)

(4.10) $2HNO_2 \rightleftharpoons NO + NO_2 + H_2O$

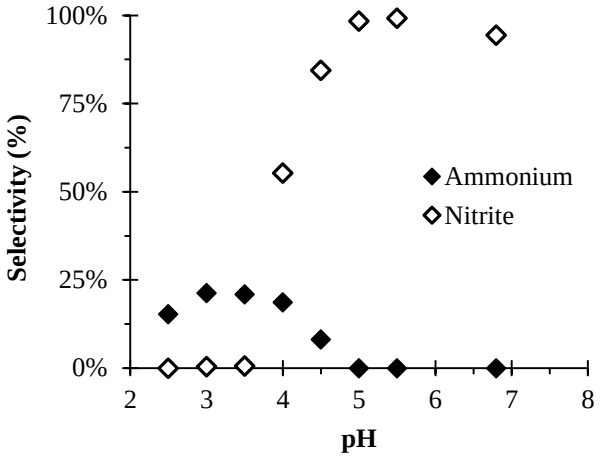


Figure 4.4. Nitrite and ammonium selectivity at different initial pH after 39 x 10^{18} photons/cm^2 (56 min) of irradiation and ~100% nitrate removal. Initial concentrations were 100 mg-N/L nitrate, 40 mM formate, and 1 g/L P90/Ag (1%).

Effect of varying nitrate and formic acid concentrations

Figure 4.5a shows $k_{nitrate}$ and $k_{formate}$ as functions of the initial formic acid to nitrate molar ratio (FNR) at a constant initial nitrate concentration of 7.14 mM. Complete nitrate removal was achieved at each FNR. For $k_{nitrate}$, increasing the FNR yielded no significant improvement; a minimum of 0.10 $cm^2/10^{18}$ photons occurred at FNR = 1.4, and a maximum of 0.19 $cm^2/10^{18}$ photons occurred at FNR = 4.2. However, when the FNR was less than 2.8, nitrate removal ceased after formate was removed from the system, indicating that the FNR was less than the stoichiometric requirement. $k_{formate}$ decreased with increasing FNR, indicating that increasing the formate concentration decreases the ability of the system to remove formate.

Figure 4.5b shows $k_{nitrate}$ and $k_{formate}$ as functions of the initial formate and nitrate concentrations at a constant FNR of 5.6. Except at low nitrate concentrations (<10 mg-

N/L), increasing the initial concentrations of nitrate and formate decreased both of their removal rates. We suspect this decrease was a result of an increase in ionic strength, which would decrease the ability of the photocatalyst to adsorb nitrate and formate ions. These results are important for modeling the reaction and transitioning experiments to larger scale experiments.

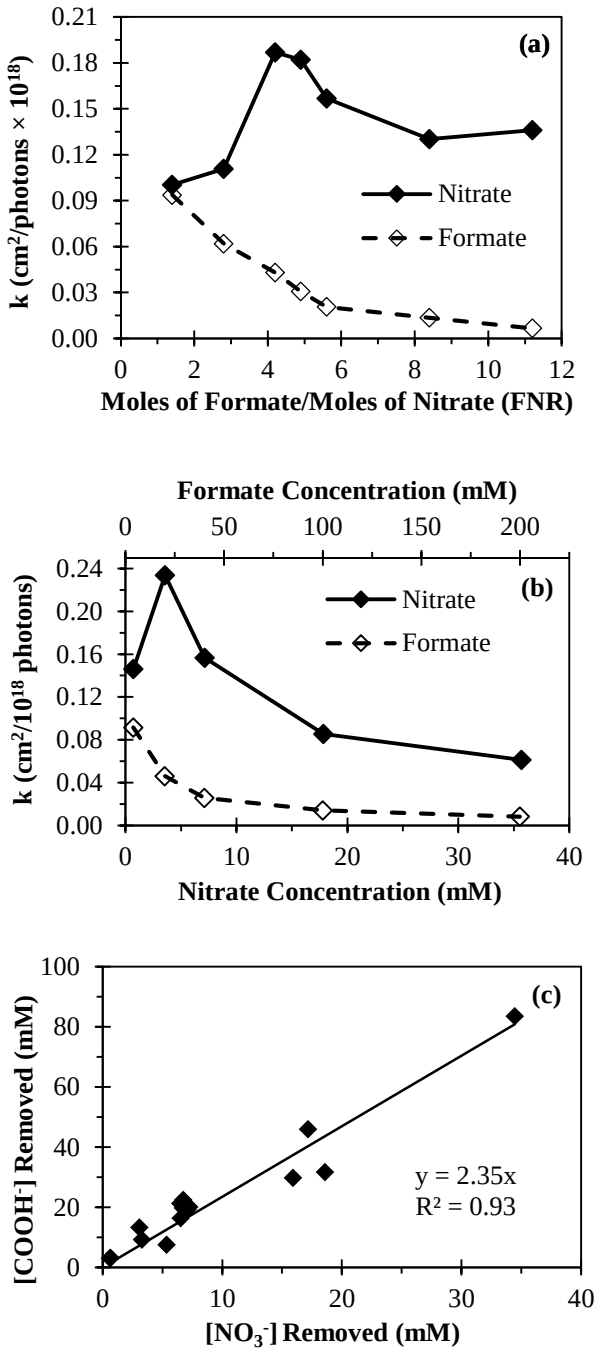


Figure 4.5. The pseudo-first-order rate constant, k, at pH = 2.5–2.7 for nitrate and formate as a function of (a) FNR at a constant initial nitrate concentration, 7.14 mM, and (b) nitrate and formate concentration at a constant FNR, 5.6. (c) Relationship between moles of formate removed and moles of nitrate removed for all of these experiments performed at pH = 2.5.

Controlling hole scavenger removal

For drinking water applications, residual organic hole scavenger (e.g., formate) is undesirable. Consequently, removal of the hole scavenger from the system is necessary, but doing so requires knowing the stoichiometric FNR. Figure 4.5c shows the relationship between moles of formic acid removed and moles of nitrate removed for all experiments at pH = 2.5. A simple linear regression model was used to fit the data (R^2 = 0.93); the slope indicates the average stoichiometric ratio (Figure 4.5c). This suggests that the average experimental FNR for all samples is approximately 2.4, which is close to the theoretical value of 2.7 for 85% N_2 and 15% NH_4^+ selectivity. This is also in good agreement with the formate requirement for biological denitrification (Smith, Miller, Brooks, Widdowson, & Killingstad, 2001).

By knowing the required stoichiometric FNR, we can adjust the photocatalyst concentration and the formic acid concentration such that 1:1 nitrate/formate removal and optimal kinetics are achieved. For example, for 17.85 mM nitrate (250 mg-N/L), 1 g/L P90/Ag, and FNR = 2.5, the required formic acid concentration would be 44.6 mM. When this was tested at pH = 2.5, similar $k_{nitrate}$ (0.040 $cm^2/10^{18}$ photons) and $k_{formate}$ (0.043 $cm^2/10^{18}$ photons) rates were obtained. Nitrate and formate were removed at a 0.94:1 ratio, which shows that both nitrate and the hole scavenger can be removed from the system by controlling the experimental parameters. And, as shown previously (i.e., Figure 4.5a), less than the required FNR can be added and partial nitrate removal still achieved, which is important in a continuous flow system.

Proposed mechanisms of formic acid

Some studies have suggested that strong reducing radicals produced from photocatalytic oxidation of formate, such as the carbon dioxide radical, $CO_2^{\bullet-}$ (Sá et al., 2009; F. X. Zhang et al., 2005) (E° = -1.8 V (Koppenol & Rush, 1987)), and the hydrogen radical, $H^{\bullet}$ (Wehbe et al., 2009) (E° = -2.3 V (Schwarz, 1981)), are responsible for nitrate reduction, rather than e_{cb}^-. Electron paramagnetic resonance (EPR) analysis showed that photocatalytic oxidation of formate over TiO_2 produced only $CO_2^{\bullet-}$ and that no $H^{\bullet}$ was present (Perissinotti et al., 2001). $H^{\bullet}/H_2$ reduction is more likely to occur over a hydrogenation co-catalyst such as Pd or Pt (Prüsse et al., 2000; Wehbe et al., 2009).

Nitrate reduction may proceed step-wise through either a one-electron reduction or a multi-electron reduction. If we examine the case in which nitrate is reduced to nitrite, two electrons are required in total (Eq. 4.4). Consequently, to maintain electroneutrality and avoid recombination, two holes would have to be reduced by one formic acid molecule (Eq. 4.11–4.12). Formic acid first adsorbs on the surface of TiO_2 and disproportionates to the formate anion and a proton (Eq. 4.13, $pK_a = 3.74$) (Diebold, 2003). TiO_2 is photoexcited, forming an h_{vb}^+ and an e_{cb}^- (Eq. 4.14). Formate reacts with one h_{vb}^+ to form the carbon dioxide anion radical, $CO_2^{\bullet-}$ (Eq. 4.15) (Harbour & Hair, 1979; Koppenol & Rush, 1987; Perissinotti et al., 2001; Somasundaram, Ming, Chenthamarakshan, Schelly, & Rajeshwar, 2004; Tachikawa, Tojo, Fujitsuka, & Majima, 2004), which is protonated below pH = 1.4 (Buxton & Sellers, 1973). If $CO_2^{\bullet-}$ alone was responsible for nitrate reduction to nitrite, then 1 mole of nitrate would require 2 moles of formate (i.e., $2HCOO^- = 2\ CO_2^{\bullet-} = 2e^-$; FNR = 2). However, experimental evidence presented herein has shown that the FNR is actually ~1.4, which means that $CO_2^{\bullet-}$ is not

solely responsible for the reduction of nitrate, and an additional electron is being used for this reduction reaction.

After $CO_2^{\bullet-}$ forms, we hypothesize that the further redox event may occur under three different scenarios: (1) $CO_2^{\bullet-}$ reacts with an h_{vb}^+ (Eq. 16), and two e_{cb}^- reduce nitrate to nitrite; (2) $CO_2^{\bullet-}$ injects an electron into the conduction band of TiO_2 (Eq. 4.17), and two e_{cb}^- reduce nitrate to nitrite; or (3) $CO_2^{\bullet-}$ reacts directly with nitrate to form NO_3^{2-} (Eq. 4.18), which is then further reduced to NO_2^- using one e_{cb}^-.

(4.11) $HCOOH + 2h_{vb}^+ \longrightarrow CO_2 + 2H^+ + 2e^-$ ($E° = –0.199$ V)

(4.12) $NO_3^- + HCOOH \longrightarrow NO_2^- + CO_2 + H_2O$

(4.13) $HCOOH_{ads} \longrightarrow H_{ads}^+ + COOH_{ads}^-$

(4.14) $TiO_2 + h\upsilon \longrightarrow h_{vb}^+ + e_{cb}^-$

(4.15) $HCOO_{ads}^- + h_{vb}^+ \longrightarrow HCO_2^{\bullet-} \rightleftharpoons H^+ + CO_2^{\bullet-}$ ($pK_a = 1.4$)

(4.16) $CO_2^{\bullet-} + h_{vb}^+ \longrightarrow CO_2$

(4.17) $CO_2^{\bullet-} \longrightarrow CO_2 + e_{cb}^-$ (injection to conduction band)

(4.18) $CO_2^{\bullet-} + NO_3^- \longrightarrow CO_2 + NO_3^{2-}$

(4.19) $CO_2^{\bullet-} + O_2 \longrightarrow CO_2 + O_2^{\bullet-}$

If nitrate reduction occurs via a multi-electron transfer, then Eq. 4.16 and 4.17 are most probable. If nitrate reduction occurs via a step-wise one-electron reduction to NO_3^{2-}, which has a high reduction potential ($E° = -1.1$ V), then Eq. 4.18 is the probable pathway because of the low potential of e_{cb}^- ($E° = -0.25$ V, Figure SI-4.5). Results

presented herein indicate that addition of a silver co-catalyst enhances nitrate reduction, presumably through electron storage, which would agree with Eq. 4.16–4.17. Furthermore, previous studies have shown that photocatalytic oxidation of formate can have a current doubling effect (Eq. 4.17) (Carraway, Hoffman, & Hoffmann, 1994; Hykaway, Sears, Morisaki, & Morrison, 1986; Tachikawa et al., 2004). However, an electron scavenger such as nitrate or oxygen can quench the radical before this occurs (i.e., Eq. 4.19). Reaction with oxygen is unlikely to be the dominant process, however, because nitrate is a more effective electron scavenger than oxygen (Martin, Herrmann, & Hoffmann, 1994), and nitrate removal was still observed with oxygen present in our system. Without doing further in-depth analytical studies, determining which scenario is occurring is difficult, but given the currently available information, nitrate reduction seems to proceed through a multi-electron reduction using e_{cb}^- and not radicals.

4.4 Implications for drinking water treatment

The results presented herein are integral to advancing photocatalytic nitrate treatment for drinking water systems. For TiO_2, the addition of an organic electron donor is necessary, which poses a problem for drinking water treatment. However, we have shown experimentally the required stoichiometric ratio of formate such that effluent DOC concentrations can be maintained during nitrate treatment. For TiO_2, pH still presents a barrier for drinking water treatment, and although the final pH is near 5, it would still need to be adjusted post-treatment, which can be costly.

To overcome some of the limitations of TiO_2 highlighted in this study and move toward direct drinking water treatment, ultimately, new materials must be developed. The

results presented herein will be important for designing these new photocatalysts. First, we have given evidence that radicals are unlikely to be responsible for nitrate reduction, so a photocatalyst base material with the proper Fermi level must be selected to meet the thermodynamic requirements. Second, pH was a factor in our experiments, so proton localization at the reaction sites will be important for treatment at ambient pH and for achieving innocuous by-products, which can be accomplished by selecting the proper co-catalysts (e.g., Ag, Cu). Although photocatalysis is not fully suitable for drinking water applications yet, P90/Ag removes nitrate efficiently and with a high selectivity, and it would be appropriate for offline treatment, such as that of ion-exchange brines.

4.5 Supplemental Information

Photocatalyst mechanisms

A photocatalyst can reduce nitrate when its electrons are excited to a free state in the conduction band. Once freed, these conduction band electrons can be transferred to nitrate ions adsorbed to the photocatalyst surface or in the electric double layer. Concurrently, the excitation of the electron creates a hole in the valence band of the photocatalyst (i.e., electron/hole pair). To maintain electoneutrality the hole must be filled with an electron either through the oxidation of compounds (i.e., electron donor) or from recombination of the electron/hole pair. Recombination is not desired, as this results in a loss of the photogenerated electron/hole pair, causing a decrease in photocatalytic activity. Adding a hole scavenger (i.e., electron donor) decreases the rate of recombination, which causes more electrons to become available for reduction reactions. Another way to decrease the recombination rate is to add a metal co-catalyst to the surface of the photocatalyst. The metal can act as an electron trap or sink for conduction band electrons, thus increasing the time available for the hole to be filled and the electrons to complete the interfacial transfer. Reduction of adsorbed species is thermodynamically possible if the conduction band is more negative than the redox potential of the species. Oxidation is thermodynamically possible if the valence band is more positive than the species. For example, at pH = 0, the potential of NO_3^-/NO_2^- is +0.82 eV and that of TiO_2 is -0.5 eV, so the reduction reaction is possible.

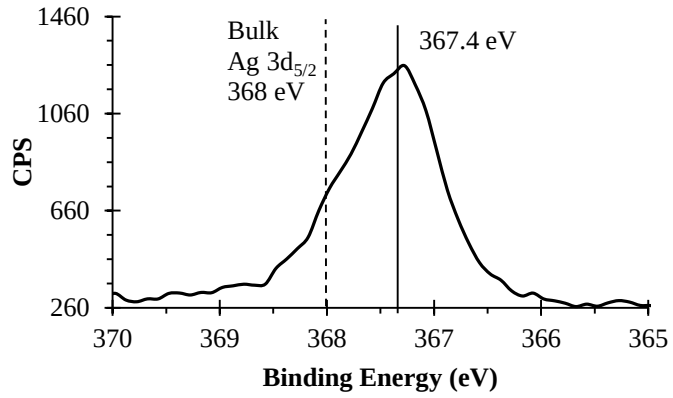


Figure SI-4.1. XPS spectrum of P90/Ag(2%). The dotted line represents the "Bulk Ag $3d_{5/2}$" peak position for silver.

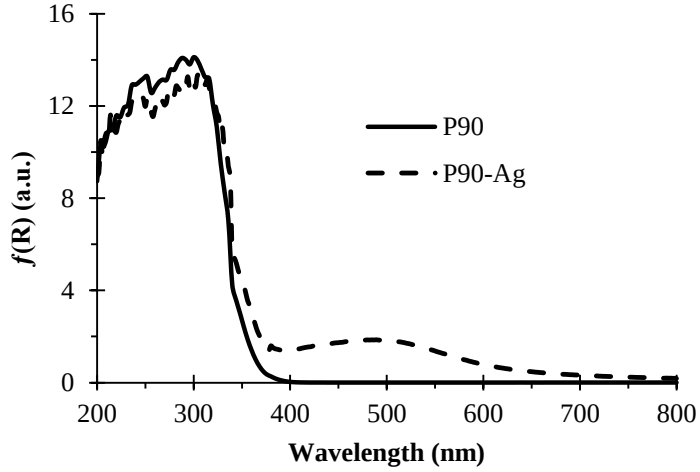


Figure SI-4.2. Kubelka-Munk absorbance as a function of photon wavelength for P90 and P90/Ag(1%).

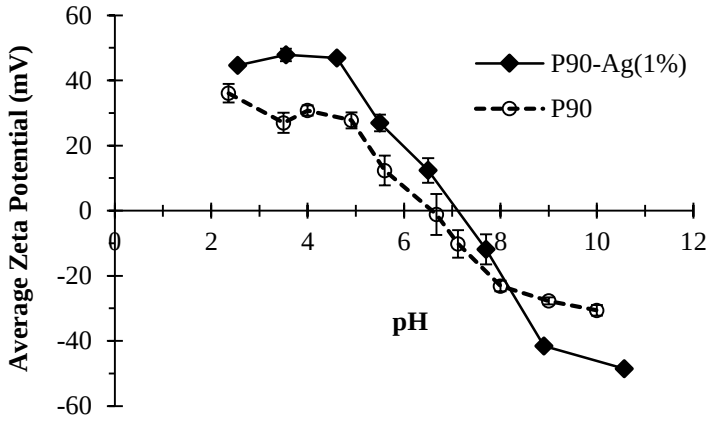


Figure SI-4.3. Zeta potential analysis for P90 and P90/Ag(1%).

Photocatalytic removal

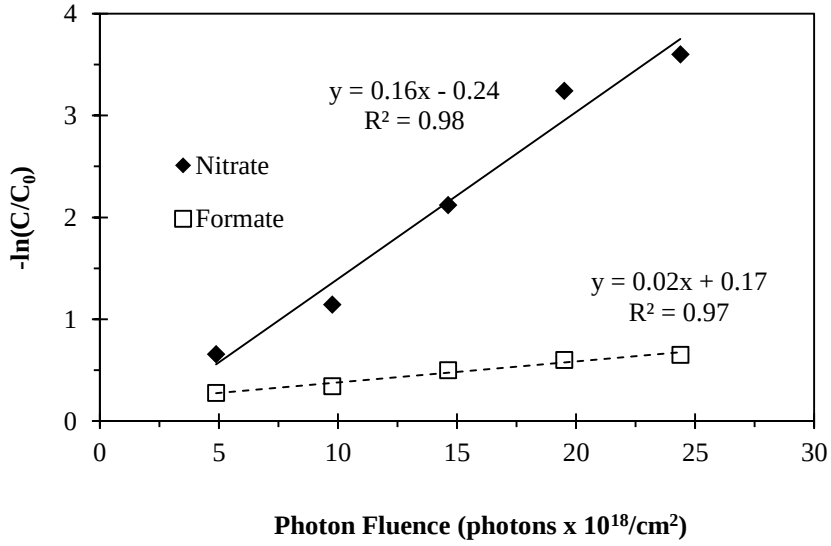


Figure SI-4.4. Pseudo-first-order kinetics for nitrate and formate as a function of photon fluence for the baseline experiment (7.14 mM NO_3^-, 40 mM HCOOH, 1 g/L P90/Ag(1%), pH = 2.5).

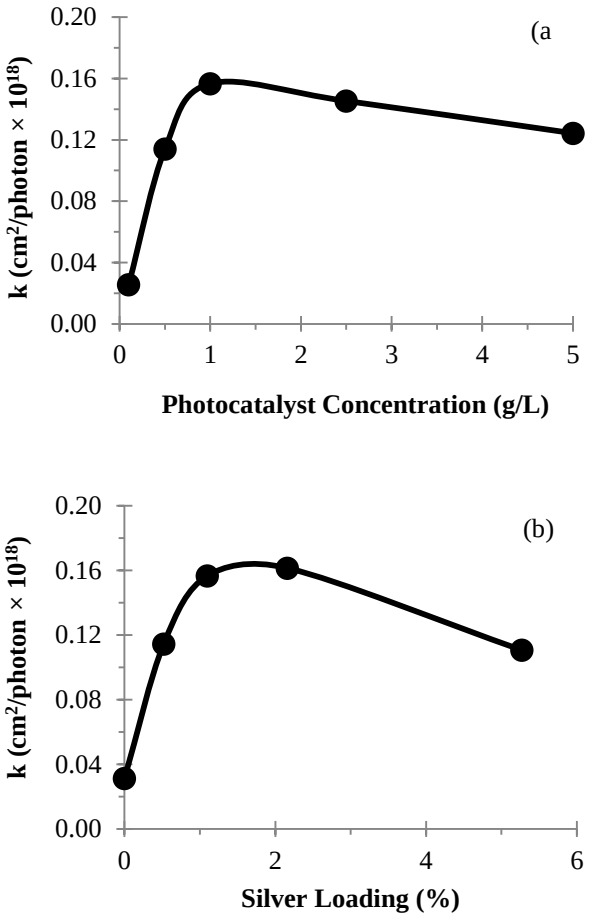


Figure SI-4.5. The pseudo-first-order rate constant, k, for nitrate as a function of (a) photocatalyst concentration (P90/Ag(1%)) in the reactor and (b) the percent mass of silver loaded onto P90 (1 g/L). All samples had initial concentrations of 7.14 mM nitrate and 40 mM formic acid (pH = 2.5).

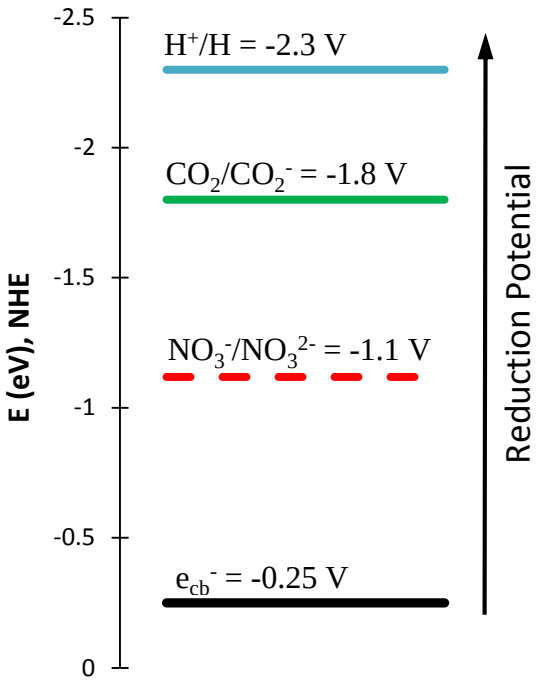


Figure SI-4.6. Electrochemical potential of the one-electron nitrate couple and relevant reductants.

Table SI-4.1. *Experimental matrix with first order rate constants for nitrate and formate*

Exp. #	Nitrate Concentration (mg-N/L, mM)	Formate concentration (mM)	pH	Photocatalyst concentration (g/L)	Silver mass %	$k_{nitrate}$ ($cm^2/10^{18}$ photons)	$k_{formate}$ ($cm^2/10^{18}$ photons)
1	100, 7.14	10	2.5	1	1	0.1	0.094
2	100, 7.14	20	2.5	1	1	0.11	0.062
3	100, 7.14	30	2.5	1	1	0.19	0.043
4	100, 7.14	35	2.5	1	1	0.18	0.031
5	**100, 7.14**	**40**	**2.5**	**1**	**1**	**0.16**	**0.021**
6	100, 7.14	60	2.5	1	1	0.13	0.014
7	100, 7.14	80	2.5	1	1	0.14	0.0066
8	100, 7.14	40	3	1	1	0.11	0.019
9	100, 7.14	40	3.5	1	1	0.11	0.02
10	100, 7.14	40	4	1	1	0.088	0.012
11	100, 7.14	40	4.5	1	1	0.077	0.007
12	100, 7.14	40	5	1	1	0.057	0.0056
13	100, 7.14	40	5.5	1	1	0.064	0.0057
14	100, 7.14	40	6.8	1	1	0.068	0.0083
15	100, 7.14	40	10	1	1	NR	NR
16	10, 0.714	40	2.5	1	1	0.094	0.0098
17	10, 0.714	4	2.5	1	1	0.15	0.091
18	50, 3.57	40	2.5	1	1	0.12	0.009
19	50, 3.57	20	2.5	1	1	0.23	0.046
20	250, 17.9	40	2.5	1	1	0.039	0.034
21	250, 17.9	44.6	2.5	1	1	0.04	0.043
22	250, 17.9	100	2.5	1	1	0.085	0.014
23	500, 35.7	40	2.5	1	1	0.02	0.059
24	500, 35.7	200	2.5	1	1	0.061	0.0082
25	100, 7.14	40	2.5	0.1	1	0.026	DNM
26	100, 7.14	40	2.5	0.5	1	0.11	DNM
27	100, 7.14	40	2.5	2.5	1	0.15	DNM
28	100, 7.14	40	2.5	5	1	0.12	DNM
29	100, 7.14	40	2.5	1	0	0.031	DNM
30	100, 7.14	40	2.5	1	0.5	0.11	DNM
31	100, 7.14	40	2.5	1	2	0.16	DNM
32	100, 7.14	40	2.5	1	5	0.11	DNM
33	100, 7.14	17.85	2.5	0.45	1	0.073	0.05
34	10, 0.714	4	2.5	0.1	1	0.077	0.031

NR = No removal
DNM = Did not measure

CHAPTER 5

PHOTOCATALYTIC REDUCTION OF NITRATE USING TITANIUM DIOXIDE FOR REGENERATION OF ION EXCHANGE BRINE*[a]

*Published: Yang, T., Doudrick, K., Westerhoff, P. Photocatalytic reduction of nitrate using titanium dioxide for regeneration of ion exchange brine. *Water Research*, 47(3), 1299–1307, 2013.

[a]Contributing author. The experimental work for this chapter was conducted by both Ting Yang and myself. Ting Yang was the main author of this paper and I was an editor, contributing to figure design, editing, and writing style. Overall, I contributed approximately 25% to this study.

Abstract

Nitrate is often removed from groundwater by ion exchange (IX) before its use as drinking water. Accumulation of nitrate in IX brine reduces the efficiency of IX regeneration and the useful life of the regeneration brine. For the first time, we present a strategy to photocatalytically reduce nitrate in IX brine, thereby extending the use of the brine. Titanium dioxide (Evonik P90), acting as photocatalyst, reduced nitrate effectively in both synthetic brines and sulfate-removed IX brine when formic acid (FA) was used as the hole scavenger (i.e., electron donor) and the initial formate to nitrate molar ratio (IFNR) was 5.6. Increasing the NaCl level in the synthetic brine slowed the nitrate reduction rate without affecting by-product selectivity of ammonium and gaseous N species (e.g., N_2, N_2O). In a non-modified IX brine, nitrate removal was greatly inhibited owing to the presence of sulfate, which competed with nitrate for available surface sites on P90. After removing sulfate through barium sulfate precipitation, nitrate was effectively reduced; approximately 1.8×10^{19} photons/cm^2 absorbable energy was required to reduce each 100 mg-N/L nitrate. To make optimum use of FA and control the

residual FA level in treated brine, the IFNR was varied. High IFNRs (e.g., 4, 5.6) were found to be more efficient for nitrate reduction but left higher residual FA in brine. IX column tests were performed to investigate the impact of residual FA for brine reuse. The residual FA in the brine did not significantly affect the nitrate removal capacity of IX resins, and formate contamination of treated water could be eliminated by rinsing with one bed volume of fresh brine.

5.1 Introduction

Nitrate contamination of groundwater, mainly resulting from intensive agricultural activities using nitrogen fertilizers, has become a widespread problem throughout the world (Burow et al., 2010; B. Singh & Sekhon, 1979; Strebel, Duynisveld, & Bottcher, 1989; W. L. Zhang, Tian, Zhang, & Li, 1996). High levels of nitrate (NO_3^-) in groundwater pose a great risk to human health when groundwater is used as a supply of drinking water. In the gastrointestinal tract, nitrate is reduced to nitrite, which reacts with hemoglobin, preventing blood cells from transferring oxygen and resulting in infant methemoglobinemia, or blue baby syndrome. Intake of nitrate may also cause formation of carcinogenic N-nitroso compounds and increase the risk for gastric cancer and other diseases (Mirvish, 1985). To limit the health impact of nitrate, 10 mg-N/L as NO_3^- was recommended by the United States Environmental Protection Agency (U.S. EPA) as the maximum contaminant level (MCL) in drinking water, and 50 mg/L as NO_3^- (11.3 mg-N/L) was prescribed by the World Health Organization (WHO) as the maximum permissible limit.

Among available nitrate removal technologies, ion exchange (IX) is used frequently in drinking water applications because of its effectiveness, low cost, and operational simplicity in producing reliable drinking water. However, the IX process generates large volumes of waste brine containing nitrate, chloride, sulfate, and other oxyanions (McAdam & Judd, 2008). Disposal of IX brine has become a costly challenge from economic and environmental standpoints. Various other technologies aim to convert nitrate into harmless nitrogen gas (N_2); these include biological denitrification (Karanasios, Vasiliadou, Pavlou, & Vayenas, 2010; McAdam & Judd, 2006a; M. I. M. Soares, 2000), catalytic reduction (Gasparovicova & Kralik, 2000; Pintar, Batista, & Musevic, 2004), and electrochemical reduction (Inam Ul & Tariq, 2010; M. Li et al., 2009). Biological denitrification has not been widely adopted for drinking water applications because of its high capital costs, lengthy lead times for biofilm establishment, and post-treatment requirements for the removal of biomass and dissolved organics. Other reduction technologies also have disadvantages (e.g., poor by-product selectivity, hydrogen requirement, high energy input) that limit their practical applications and will not soon replace IX in drinking water treatment.

Integration of IX with brine denitrification processes is promising because the combination could reduce IX costs for brine disposal and minimize problems associated with each denitrification approach for drinking water treatment. Biological denitrification to remove nitrate from IX brine has been studied extensively (B. U. Bae, Jung, Han, & Shin, 2002; Cang, Roberts, & Clifford, 2004; Clifford & Liu, 1993; Lehman, Badruzzaman, Adham, Roberts, & Clifford, 2008; McAdam & Judd, 2008; McAdam, Pawlett, & Judd, 2010; Van Ginkel et al., 2008; Vanderhoek, Vanderven, & Klapwijk,

1988). By treating IX brine instead of the drinking water itself, quality concerns, such as bacterial, organic matter, and hazardous by-product contamination caused by bioprocesses, are minimized. However, IX systems are often operated intermittently (i.e., a few times per month to meet peak water demands), which makes inclusion of biological processes challenging. Electrochemical reduction can selectively treat nitrate in high salt solutions, but it may produce Cl_2, which can damage the structure of IX resins (Dortsiou et al., 2009; Paidar, Bouzek, Jelinek, & Matejka, 2004). An attempt to reduce nitrate using zero-valent iron nanoparticles showed that the nitrate removal rate was greatly slowed in 6% NaCl solution, and ammonium was the predominant by-product accounting for 62% of the reduced nitrate (Xiong, Zhao, & Pan, 2009). Therefore, a need exists to develop an effective nitrate reduction technology for IX brine treatment that overcomes these disadvantages.

Photocatalytic reduction of nitrate over semiconductor materials is a relatively new technique, but it has shown high efficacy and great potential for nitrate removal. Titanium dioxide (TiO_2) is the most frequently studied photocatalyst; such studies include applications using metal-modified TiO_2 to improve the kinetics and selectivity away from undesirable aqueous by-products (e.g., NO_2^-, NH_4^+) (Anderson, 2012; Bifen Gao, Ma, Cao, Yang, & Yao, 2006; W. L. Gao et al., 2004; Hirayama, Kondo, Miura, Abe, & Kamiya, 2012; Kominami et al., 2001b; Kominami et al., 2005b; A. Kudo, Domen, Maruya, & Onishi, 1987a; L. Li et al., 2010; Ranjit & Viswanathan, 1997c; Rengaraj & Li, 2007a; Sa et al., 2009; F. X. Zhang et al., 2005). When irradiated with incident light whose energy is larger than that of the band gap of the semiconductor, electrons are excited to the conduction band (e^-_{cb}) and positive holes form in the valence

band (h_{vb}^{+}). The electrons and holes generated can be utilized for reduction and oxidation, respectively. However, the photo-generated electron-hole pairs can recombine within a few nanoseconds (Rothenberger, Moser, Gratzel, Serpone, & Sharma, 1985; Serpone, Lawless, Khairutdinov, & Pelizzetti, 1995); this can be overcome by adding a hole scavenger (i.e., electron donor) to trap the holes, leaving the photo-generated electrons available for nitrate reduction. Common hole scavengers such as methanol (Mori, Suzuki, Fujimoto, Watanabe, & Hasegawa, 1999b), ethanol (Hirayama et al., 2012), oxalic acid (W. L. Gao et al., 2004; Kominami et al., 2001b), acetic acid (Sa et al., 2009), formic acid (FA), and sodium formate (Sa et al., 2009; F. X. Zhang et al., 2005) have been investigated for nitrate reduction. Among them, FA exhibits the highest activity (Sa et al., 2009; F. X. Zhang et al., 2005).The overall redox reactions between nitrate and FA with photocatalysts under UV irradiation can be expressed as follows:

$$NO_3^- + HCOO^- + H^+ \rightarrow NO_2^- + CO_2 + H_2O,\ FNR = 1 \quad (5.1)$$

$$2NO_3^- + 5HCOO^- + 7H^+ \rightarrow N_2 + 5CO_2 + 6H_2O,\ FNR = 2.5 \quad (5.2)$$

$$NO_3^- + 4HCOO^- + 6H^+ \rightarrow NH_4^+ + 4CO_2 + 3H_2O,\ FNR = 4 \quad (5.3)$$

Both formate ions and protons are consumed during nitrate reduction. The theoretical formate to nitrate stoichiometric ratios (FNRs) to reduce nitrate to nitrite, to dinitrogen, and to ammonium are 1, 2.5, and 4, respectively. Though a FNR of 2.5 is an ideal stoichiometric ratio for 100% N_2 selectivity, a higher FNR value than 2.5 is usually necessary for effective nitrate reduction. For example, an initial formate to nitrate molar ratio (IFNR) of 5.6 was reported to be optimal in terms of both nitrate reduction kinetics

and by-product selectivity (Sa et al., 2009; F. X. Zhang et al., 2005). Thus, complete removal of nitrate and formate simultaneously is currently difficult to achieve, though recent research shows it may be possible to control the residual FA levels (Anderson, 2012). In addition, 100% dinitrogen selectivity is hard to achieve on bare or modified photocatalysts (e.g., TiO_2), and ammonium is commonly formed as the aqueous by-product of photocatalytic nitrate reduction (Anderson, 2012; W. L. Gao et al., 2004; Ranjit & Viswanathan, 1997c; Rengaraj & Li, 2007a; Sa et al., 2009). Although these biologically unstable hole scavengers (e.g., FA) and aqueous nitrogen by-products (e.g., ammonium) are not desirable in drinking water, indirect contact with drinking water through photocatalytic nitrate reduction of spent IX brine may make them acceptable.

This study is the first to evaluate the ability of photocatalytic reduction using TiO_2 to remove nitrate from IX brine wastes. The specific objectives of this study were to (1) investigate the ability of TiO_2 and silver-modified TiO_2 to remove nitrate from IX brines and (2) evaluate the possibility of reusing the photocatalytically treated brine for IX resin regeneration.

5.2 Materials and methods

Materials

Titanium dioxide (Evonik P90) was obtained in powder form and used as received. P90 is a commercially available product containing both anatase (88%, 12 nm) and rutile (12%, 18 nm) crystal phases; compared with P25 (the most frequently used TiO_2), it has a higher surface area and was previously found to have a higher rate of nitrate reduction **(**Doudrick et al., 2012a). P90 loaded with silver (P90/Ag) was

synthesized according to a method reported elsewhere **(**Doudrick et al., 2012b). Sodium nitrate ($NaNO_3$, 99% EMD) and FA (HCOOH, 98% Fluka) were used as the nitrate source and hole scavenger, respectively. Sodium hydroxide (NaOH, EMD) was used for pH adjustment. A model water was prepared using a Nanopure® (18.3 MΩ-cm) treatment system. Sodium chloride (NaCl, 99.5% Sigma-Aldrich) was added to model water to create synthetic NaCl brines. A real IX brine was obtained from a nitrate IX system for groundwater treatment used by a confidential water company in Arizona. The major characteristics of this brine are summarized in Table 5.1.

Table 5.1. *Characteristics of real IX brine*

Parameter	**Value**	**Unit**
pH	7.81	-
Dissolved organic carbon	23.9	mg-C/L
Total dissolved nitrogen	1793	mg-N/L
Nitrate	1740	mg-N/L
Nitrite	1.1	mg-N/L
Ammonium	3.6	mg-N/L
Conductivity	127.4	mS
Sulfate	6000	mg/L
Sodium chloride	4.2%	-
Magnesium	20.6	mg/L
Calcium	27.2	mg/L
Total Hardness	350	mg/L as $CaCO_3$

Photocatalytic experiments

Different concentrations of synthetic NaCl brines (0%, 3%, 6%, and 10% by weight) were prepared by adding NaCl to model water spiked with 500 mg-N/L nitrate (35.7 mM). The real IX brine contained a much higher nitrate level of 1740 mg NO_3^--N/L (124.3 mM). Then, 1 g/L P90 was mixed into the brines as the photocatalyst. An IFNR of

5.6 was used in all experiments except those in which IFNR values were varied. 200- and 700-mM FA were added to the synthetic brines and the real brine, respectively. In select experiments using the real IX brine, barium chloride dihydrate ($BaCl_2 \cdot 2H_2O$, 99% Aldrich) was added to the brine for sulfate precipitation. The mixture was sonicated for 20 minutes, vigorously stirred for 2 hours, and allowed to sit for 30 minutes to settle out the precipitate. Then, the supernatant was filtered using a GF/F glass fiber filter. Barium sulfate precipitation brought the dissolved sulfate concentration in IX brine down to less than 50 mg/L.

Photocatalytic reactions were carried out in a double-wall quartz reactor. A 450-W medium-pressure mercury lamp (Ace Glass, 7825-34) was put in a double-walled quartz immersion well (Ace Glass, 7854-25), which was placed in the middle of the reactor for irradiation. In different experiments, 200-mL samples of real or synthetic brine with different P90 and FA concentrations were prepared and poured into the reactor after sonication. No effort was made to remove dissolved oxygen. A chiller was used to maintain a constant solution temperature of 25 °C. A magnetic stir bar was used to keep the suspension well dispersed. A small part of the solution was withdrawn periodically, filtered with a 0.45-µm nylon membrane, and then diluted and analyzed.

Using an Avantes UV-VIS Fiber Optic Spectrometer (AvaSpec-2048) with a cosine corrector, the lamp intensity was measured in water at multiple points between the bottom and the top of the reactor to obtain the average irradiance. The lamp irradiance starts at approximately 230 nm, and the irradiance absorbable by TiO_2 (230–388 nm) is 7.1 mW/cm^2, which is used here as the actual energy consumed by P90. Variation of fluence was used instead of accumulation of operating time to make our results

comparable to other studies. Because a polychromatic lamp was used, the irradiation is shown as photon fluence instead of energy fluence (e.g. J/cm^2) to account for the energy difference at different wavelengths.

IX system

Purolite A-520E, a commercially available macroporous strong base anion exchange resin, was used. This resin has quaternary ammonium functional groups and is specifically designed for the removal of nitrate. The resin particles have sizes between 0.3 and 1.2 mm. 50-mL of resin were packed into an IX column (OD = 2.5 cm), regenerated using 6% NaCl, and rinsed prior to use. Model water spiked with 200 mg-N/L nitrate was pumped downward at a flow rate of 40 mL/min (48 BV/h), which corresponds to an empty bed contact time of 1.25 min. After nitrate breakthrough, the resins were rinsed and regenerated using 6% NaCl containing 400-mM FA (the pH was adjusted to 3.0 using sodium hydroxide) at a flow rate of 10 mL/min for 50 min. In select experiments, an additional regeneration process was followed using 6% NaCl at a flow rate of 5 mL/min for 10 min.

Analytical methods

Concentrations of nitrate, chloride, and sulfate were analyzed using ion chromatography (Dionex DX-120; AS12A column). Nitrite and ammonium in brines could not be analyzed using our ion chromatography setup due to overlapping of chloride and sodium peaks with nitrite and ammonium peaks, respectively. Thus, nitrite and ammonium concentrations were measured using colorimetry (nitrite TNT plus 839,

wavelength = 515 nm; ammonia TNT plus 830, wavelength = 694 nm) on an ultraviolet-visible light absorption spectrometer (Hach DR5000, Loveland, CO). Total dissolved nitrogen (TDN) was measured, along with dissolved organic carbon (DOC), using a Shimadzu TOC-V instrument. Samples were acidified and purged with air prior to TDN analysis. TDN measures the sum of non-volatile N species (e.g., NO_3^-, NO_2^-, NH_4^+, or other aqueous N-species). DOC indicates the concentration of FA added initially as the hole scavenger. X-ray photoelectron spectroscopy (XPS) was performed on an ESCALAB 220i-XL (Vacuum Generators) with a monochromatic Al K_α source at $h\nu$ = 1486 eV and a base pressure = 7×10^{-10} mbar. Conductivity and pH were measured using VWR model 2052 and Beckman model PHI 410 meters, respectively.

5.3 Results and discussion

Nitrate reduction in synthetic NaCl brines

Figure 5.1 compares the rate of nitrate reduction with UV irradiation only (UV alone) and of photocatalytic reduction using P90 (1 g/L) and FA (200 mM) under irradiation (P90+FA+UV). Nitrate was slowly reduced with UV alone (Fig. 5.1a), which suggests photolysis of nitrate occurred; nitrite was the major by-product, accounting for more than 90% of the reduced nitrate. Inclusion of P90 and FA substantially increased the rate of nitrate reduction (Fig. 5.1b). Approximately 25% of the reduced nitrate converted to ammonium and 75% to unknown non-aqueous N species (e.g., N_2, N_2O). No nitrite concentration was detected throughout the experiment. In separate experiment in which nitrite (500 mg-N/L) was added initially to model water instead of nitrate, the rate of nitrogen loss in the presence of P90 and FA was significantly enhanced. For example,

the first-order rate $k_{nitrite}$ (3.53 $cm^2/10^{19}$ photons ×) was an order of magnitude higher than $k_{nitrate}$ (0.37 $cm^2/10^{19}$ photons). This could suggest that nitrite may be produced as an intermediate during nitrate reduction but was rapidly reduced and unlikely to be detected in solution. The sum of nitrate, nitrite and ammonium concentrations agreed well with measured TDN levels in all conditions, indicating that levels of other aqueous N species were negligible. In the absence of FA, P90 had a slower nitrate reduction rate than did UV alone, probably because the presence of P90 particles created a light scattering effect that reduced the photon absorption of nitrate. The nitrate removal efficiency of P90+UV was greatly slowed in comparison with that of P90+FA+UV, thus verifying the indispensable role of FA as a hole scavenger in the photocatalytic system.

Figure 5.1 also reveals the influence of NaCl concentration (0%, 3%, 6%, and 10% by weight) on nitrate removal efficiency. With UV alone, increasing the ionic strength through NaCl addition slightly increased the rate of nitrate removal (Fig. 5.1a). In contrast, the nitrate removal efficiency decreased as the NaCl concentration increased from 0% to 3% with P90+FA+UV, but additional NaCl addition up to 10% further decreased nitrate removal little (Fig. 5.1b). For example, the absorbable photon fluence required to reduce each 100 mg-N/L nitrate at the different NaCl concentrations (0%, 3%, 6%, and 10%) was calculated to be 1.7, 2.2, 2.3, and 2.4 × 10^{19} photons/cm^2, respectively. Greater than 98% nitrate reduction was achieved at all NaCl levels studied after 1.3 × 10^{20} photons/cm^2 irradiation. This suggests that the existence of high levels of chloride slowed the rate of nitrate reduction, but P90 is still capable of effectively reducing nitrate in NaCl brines and is especially competitive in extremely high NaCl

concentrations, e.g., 10%. Addition of NaCl did not significantly change the selectivity toward N-species by-products for either UV alone or P90+FA+UV.

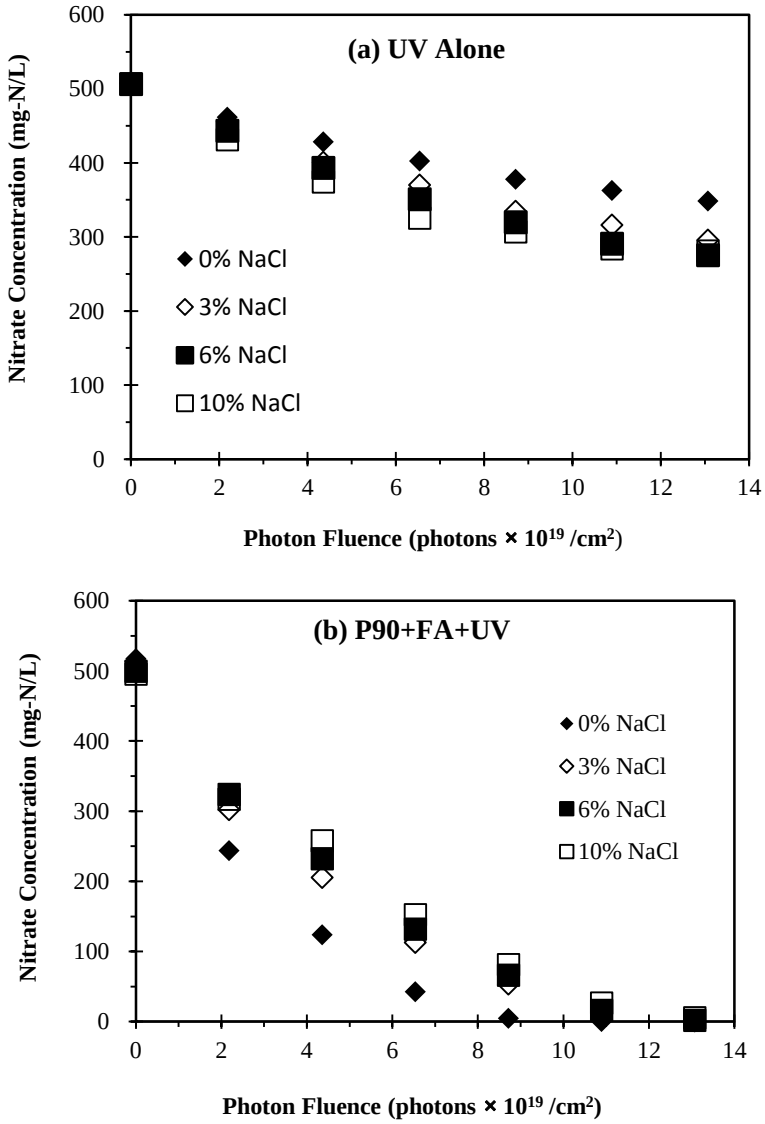


Figure 5.1. Nitrate removal in synthetic NaCl brines (0%, 3%, 6%, and 10% by weight) as a function of photon fluence absorbable by TiO_2 using (a) UV alone and (b) P90+FA+UV. The initial concentration of nitrate was ~500 mg-N/L for all samples. For P90+FA+UV samples, 1-g/L P90 and 200-mM formic acid were initially added to the solution.

In an effort to increase the nitrate reduction rate and improve selectivity toward gaseous N species, experiments were conducted using P90/Ag. Titanium dioxide loaded with silver nanoparticles has been shown to have much faster kinetics and higher innocuous by-product selectivity in model water (Zhang et al., 2005; Sa et al., 2009; Doudrick et al., 2012b). When P90/Ag was tested in a synthetic NaCl brine, however, no better performance was observed in contrast to non-modified P90. This may be due to chloride interacting with the silver and causing it to dissolve; a similar phenomenon is seen with chloride and copper (Chaplin, Roundy, Guy, Shapley, & Werth, 2006). Dissolution of the silver into AgCl would eliminate its ability to enhance the rate of nitrate reduction, thus explaining the similar reduction rates of P90 and P90/Ag.

Nitrate reduction in a real IX brine

Figure 5.2 shows the conversion of nitrate in a non-modified real IX brine in the presence of P90+FA+UV. Nitrate removal was also tested in a synthetic brine (4.2% NaCl solution, 1740 mg-N/L nitrate) for comparison. The difference between the IX brine and synthetic brine suggested a potential role of anions other than chloride in nitrate reduction. Previous studies have shown that the presence of sulfate or carbonate anions decreases the kinetics of photocatalytic nitrate reduction employing TiO_2 (F. X. Zhang et al., 2005). In this IX brine, carbonate and bicarbonate anions were unlikely to cause interference because they were converted to carbonic acid by the addition of 700-mM FA before irradiation. The sulfate concentration in the IX brine was as high as 6000 mg/L, and its concentration did not decrease during the photocatalytic treatment process. After removing sulfate from the IX brine through barium sulfate precipitation, the nitrate

reduction efficiency was significantly improved, and the nitrate removals of the sulfate-removed brine and synthetic 4.2% NaCl brine were in good agreement (Fig. 5.2), which indicates that sulfate is the major disturbance factor for nitrate removal in brine. XPS results for P90 after photocatalytic treatment of non-modified real brine (with sulfate) showed no fouling of the photocatalyst (Fig. SI-5.1). This indicates that the presence of chloride, sulfate, and other components of the brine did not deactivate the photocatalyst surface and that P90 could be used as a stable photocatalyst for brine treatment. The isoelectric point for P90 is reported to be approximately 6.4 **(**Doudrick et al., 2012a), which suggests that the surface of P90 is positively charged in acidic media (pH < 6.4) owing to presence of titanol (Ti-OH) on the surface (Hoffmann et al., 1995; Kormann, Bahnemann, & Hoffmann, 1991) and that anions (i.e., NO_3^-, NO_2^-, and formate) are absorbed to surface sites of P90 particles before photocatalytic reaction occurs. Sulfate and chloride compete with nitrate for available surface sites on P90, which slows the rate of nitrate reduction in the brine. SO_4^{2-} is divalent and may be preferentially adsorbed by P90 under acidic conditions. Figure SI-5.2 shows that 1000 mg/L sulfate (a sulfate-to-nitrate molar ratio of 0.08) was sufficient to decrease the nitrate removal rate by 20% in the real brine. However, removal of sulfate from the real brine (by barium sulfate precipitation) prior to photocatalysis allowed nitrate to be effectively removed. On average, approximately 1.8×10^{19} photons/cm^2 absorbable energy input was required to reduce each 100 mg-N/L nitrate, which is similar to the amount needed in synthetic brines, as discussed in previously. No nitrite was detected, and the selectivity of ammonium and gaseous nitrogen compounds was 17% and 83%, respectively (Fig. SI-

5.3). According to DOC measurement, nearly 400-mM FA was left at 2.6×10^{20} photons/cm^2 of irradiation.

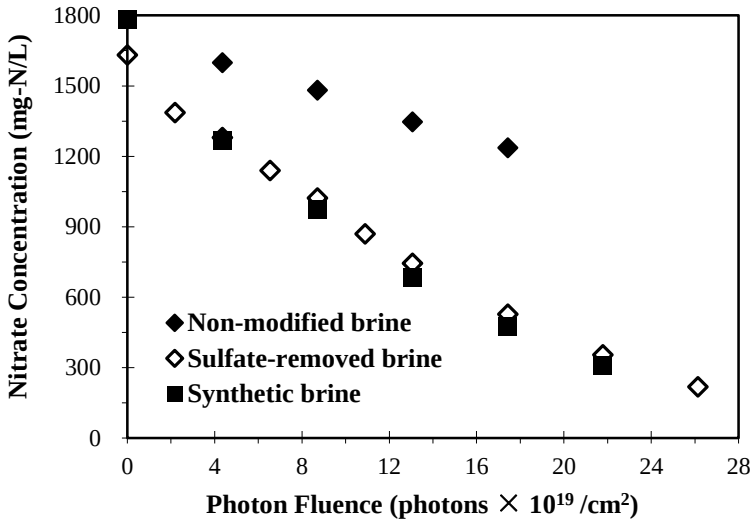


Figure 5.2. Nitrate removal in a non-modified IX brine, synthetic brine (4.2% NaCl solution, 1740 mgN/L nitrate), and sulfate-removed IX brine as a function of photon fluence absorbable by TiO_2. The nitrate concentration in the IX brine was 1740 mgN/L. The concentration of P90 in solution was constant at 1 g/L. In all samples, 700 mM formic acid was added initially.

To make optimum use of FA as the hole scavenger and control the residual FA in the treated brine, the initial FA concentration added to the sulfate-removed brine was varied at IFNR = 1, 2.5 and 4 other than IFNR of 5.6 (shown above); the results are shown in Figure 5.3. Figure 3(a) compares the nitrate removal efficiency in brine at different IFNR values. The nitrate reduction rate was fastest for IFNR 5.6. For all IFNR values, similar initial nitrate removal rates were observed at less than 7.9×10^{19} photons/cm^2 of irradiation. However, whereas IFNR 5.6 and IFNR 4 maintained the same nitrate removal rate throughout the experiment, nitrate reduction at IFNR 1 became slower and slower. In addition, turning point occurred for IFNR 2.5 at 1.6×10^{20} photons/cm^2 irradiation, after which nitrate reduction was much slower. Table SI-5.1

shows the changes in FNR and pH as the nitrate reduction proceeds. For IFNR 4 and IFNR 5.6, FNR values increased as nitrate concentration decreased, which suggests sufficient formate was available during the nitrate reduction process. The pH values for IFNR 4 and IFNR 5.6 increased from 2.0 to 3.3 and 1.9 to 3.0, respectively, indicating that adequate protons were available to be consumed. Thus, complete nitrate removal may be achieved with prolonged irradiation. For IFNR 1 and IFNR 2.5, FNR values gradually decreased as the nitrate in the brine decreased. A sharp increase in pH occurred with IFNR 1 (2.6–8.1) and IFNR 2.5 (2.2–7.8), which suggests a deficiency of protons in the solution. Lack of formate as a hole scavenger and insufficient protons at neutral pH could explain the slower nitrate reduction rates for IFNR 1 and IFNR 2.5 in the later period (e.g., more than 1.6×10^{20} photons/cm^2 of irradiation). Moreover, in experiments with sufficient formate and protons (IFNR 4, IFNR 5.6), nitrate was converted into N gases and a small portion of ammonium (~17%) without detection of nitrite. However, in experiments with IFNR 1 and IFNR 2.5, nitrite was formed (> 40 mg-N/L); a similar portion of ammonium was produced. The presence of nitrite in treated brine may cause drinking water contamination if the treated brine was reused for IX resin regeneration. Therefore, a higher IFNR value (e.g. 4, 5.6) seems more appropriate for nitrate reduction in IX brine. Formate was consumed in accordance with nitrate reduction (Fig. 3(b)), and 400, 240, 83, and 11 mM of formate remained in the treated brine after 2.4×10^{20} photons/cm^2 irradiation for IFNR = 1, 2.5, 4, and 5.6, respectively.

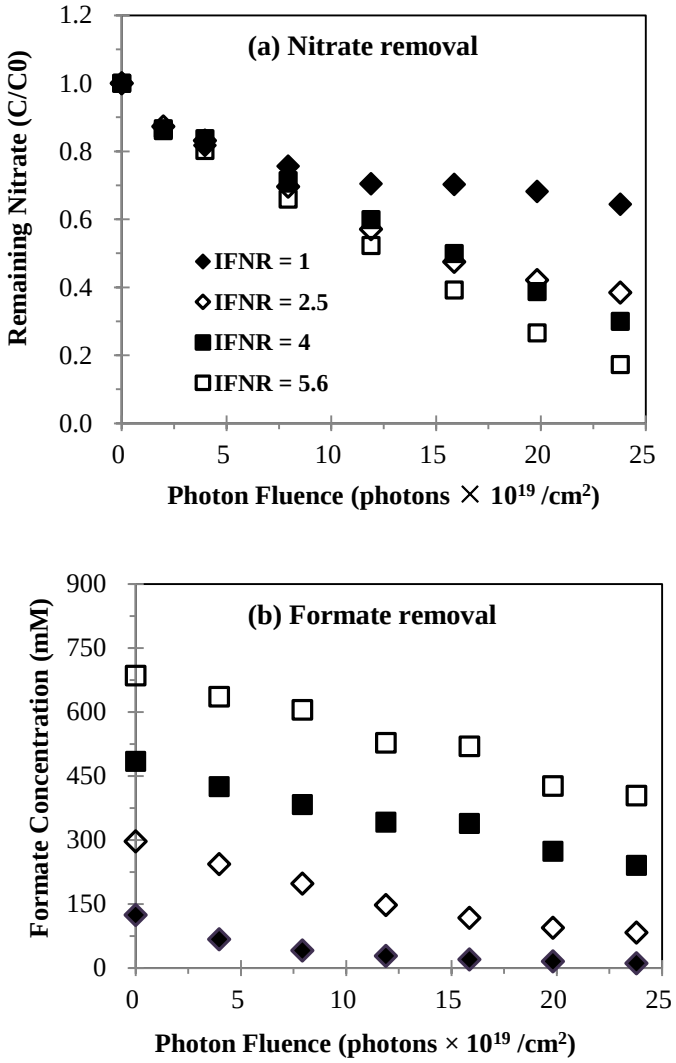


Figure 5.3. Nitrate and formate removal as a function of photon fluence adsorbable by TiO_2 in sulfate-removed brine for varying initial formate to nitrate molar ratios (IFNRs). The concentration of P90 in solution was constant at 1 g/L.

Managing FA during IX resin regeneration

Photocatalytic reduction using P90 can remove nitrate from IX brines with higher IFNRs (e.g., 4, 5.6), with formation of approximately 17% ammonium as the aqueous by-product. As anion exchange resins are used for nitrate removal, accumulation of ammonium has an insignificant effect on IX resin performance and the treated drinking

water quality, as proved by Paidar and co-workers (Paidar et al., 2004). Thus, a scheme combining IX with photocatalytic nitrate treatment of IX brine may be able to remove nitrate from drinking water sources (Fig. 5.4). The subsequent question is what influence the residual FA from photocatalytic denitrification has on IX resin regeneration. Oxidation of all of the formate to CO_2 during photolysis may be feasible, but we wanted to investigate the fate of any residual FA by measuring DOC. An IX column was operated to study the impact of residual FA in the brine on IX resin regeneration. The higher residual FA of 400 mM from the IFNR 5.6 experiment was added to synthetic brine (6% NaCl) for IX resin regeneration. To maintain the same formate concentration, the pH of the synthetic brine was adjusted using sodium hydroxide to 3.0, the pH of the treated brine from the IFNR 5.6 experiment.

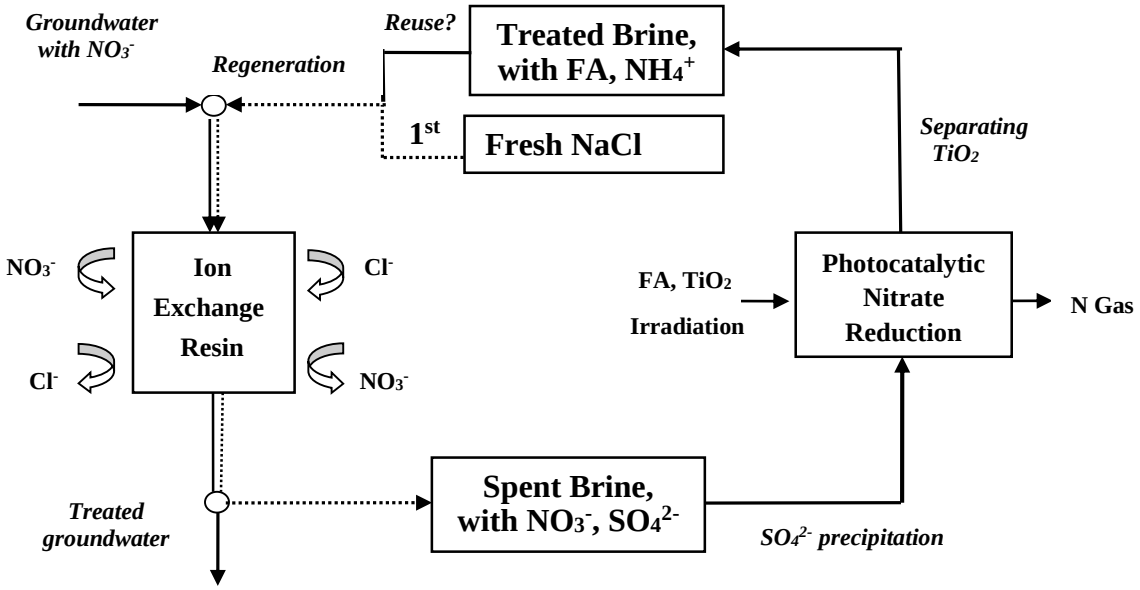


Figure 5.4. Schematic of an ion exchange system integrated with photocatalytic nitrate reduction of IX brine for reuse. FA represents formic acid.

Figure 5.5 shows the nitrate and formate breakthrough curves as a function of bed volumes (BVs) of treated water. We used a high influent nitrate concentration (100 mg-N/L) to accelerate IX column tests. Similar nitrate breakthrough curves were observed for fresh resin (a) and regenerated resin (b, c). Using 10 mg-N/L (EPA MCL) as the breakthrough threshold, the amount of nitrate-containing model water can be treated during (a), (b), and (c) is 62, 61, and 59 BVs, respectively. The small differences indicate that the residual formate in treated IX brine resulted in minimal loss of the nitrate removal capacity of IX resins. However, after regeneration using FA-containing brine, formate was detected in treated water (Fig. 5.5b) in the first 40 BVs, with a maximum of 2.8 mM (127.5 mg/L) at approximately 6 BVs. We speculate that formate anions in the brine occupied resin exchange sites during the regeneration process and were displaced by nitrate in the model water in the following exhaustion runs, causing treated water contamination. Assuming the impact of FA in treated brine is exchange based, 50 mL (1 BV) of fresh 6% NaCl was applied as a follow-up regeneration process to replace formate brought from regeneration using FA-containing brine. This approach eliminated formate leakage into treated water (Fig. 5.5c), which further supported the exchange based assumption. As a result, the negative effect of a high concentration of residual FA in IX brine was completely overcome, and the reliable performance of the IX process could be ensured. By reusing the photocatalytically treated brine for regeneration, costs for NaCl consumption and brine disposal can be greatly reduced.

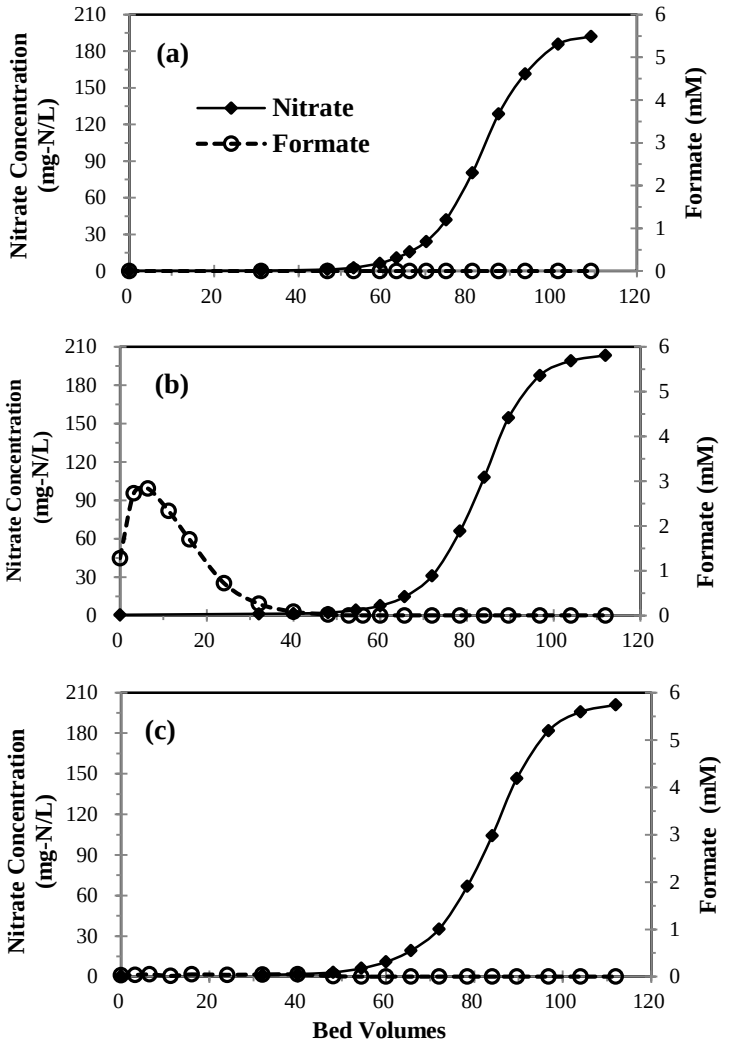


Figure 5.5. Breakthrough curves of nitrate and formate for fresh IX resin (a) and regenerated resin (b, c). The regenerant used before (b) was 6% NaCl containing 400-mM FA (500 mL), pH = 3.0; the regenerant used before (c) was 6% NaCl containing 400-mM FA (500 mL), pH=3.0, followed by 50 mL fresh 6% NaCl.

5.4 Conclusions

This study investigated the feasibility of photocatalytic reduction using TiO_2 (Evonik P90) to remove nitrate from IX brine and analyzed the possibility of reusing the treated brine containing residual FA for resin regeneration. Photocatalytic reduction using P90 could effectively remove nitrate from synthetic NaCl brines and real IX brine. No

nitrite was detected as a by-product. Most of the reduced NO_3^- converted to volatile N species and a small portion to ammonium. High levels of chloride slowed the rate of nitrate reduction, but the presence of sulfate in IX brine is the major disturbance factor that inhibited nitrate removal, likely because sulfate competes with nitrate for available surface sites on titanium dioxide. A higher IFNR (e.g., 4, 5.6) was found to be more appropriate for nitrate reduction but left higher residual FA in the treated brine. IX column tests showed that 400-mM residual FA in treated brine had an insignificant effect on IX resin capacity loss, and its contamination of treated water could be eliminated by rinsing with 1 BV of fresh NaCl. Accumulation of ammonium in the brine would not affect the performance of anion exchange resins though eventually requires further treatment. Thus, the photocatalytically treated brine with residual FA and ammonium is potentially suitable for continuous reuse after separating the TiO_2 nanoparticles.

Based on the findings in this study, we believe that IX integrated with photocatalytic denitrification of the spent brine could be a feasible and effective technology to remove nitrate from drinking water. This integrated process could reduce the salt consumption and costs of brine disposal as well as produce reliable drinking water without the need for extensive post-treatment. Adequately sized photocatalytic systems (e.g., the Photo-Cat system from Purifics) that include ceramic membranes for catalyst recovery are commercially available and could be used to treat IX brines in the fashion described above. The next step would be to conduct pilot tests to obtain performance data and information for an economic analysis.

5.5 Supplemental Information

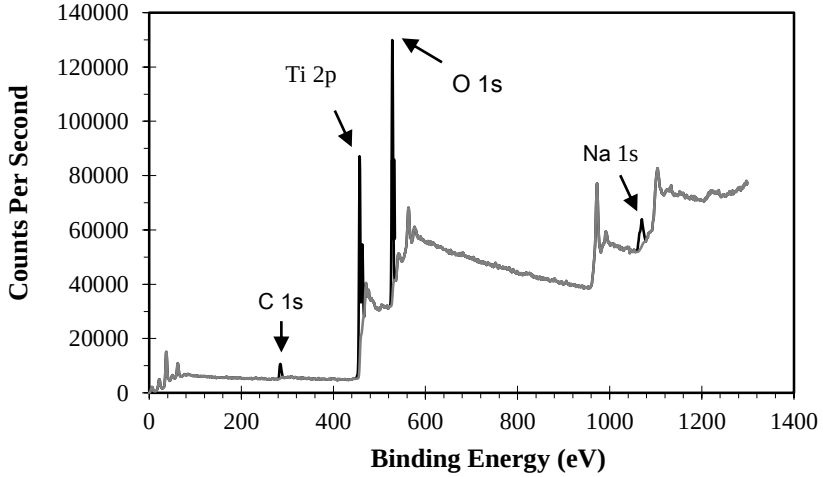


Figure SI-5.1. X-ray photoelectron spectrum of recycled P90 (TiO_2) after nitrate reduction in non-modified ion exchange brine.

XPS measures the elemental composition and chemical state in the surface of the titanium dioxide (P90). Apart from titanium and oxygen, small peaks of sodium and carbon were found, which is probably resulting from the P90 synthesizing process. There was absence of sulfur, suggesting that the surface of P90 was not contaminated by sulfate in the IX brine.

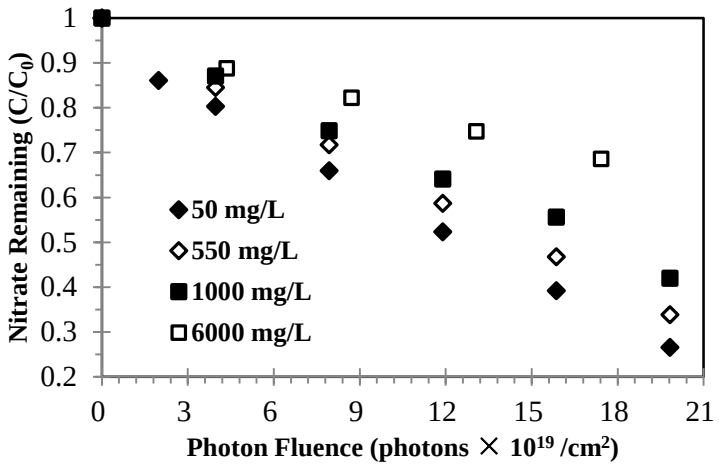


Figure SI-5.2. Nitrate removal in the real ion exchange brine with different sulfate concentrations varying at 50, 550, 1000, and 6000 mg/L as a function of photon fluence absorbable by TiO_2. The concentration of P90 in solution was constant at 1 g/L. Initially, 700-mM formic acid was added.

Nitrate reduction in the real brine with sulfate was fit well by the zero-order rate law. The zero-order rate constants ($k_{nitrate}$) for different sulfate concentrations of 50, 550, 1000 and 6000 mg/L were 4.83, 4.07, 3.49 and 2.27 $mMcm^2/10^{19}$ photons respectively, which suggesting nitrate removal was inhibited by 16%, 28% and 53% with existence of sulfate at 550, 1000 and 6000 mg/L, respectively. Figure SI-5.2 indicates that the influence of sulfate on nitrate removal should not be neglected when removing nitrate from the IX brine.

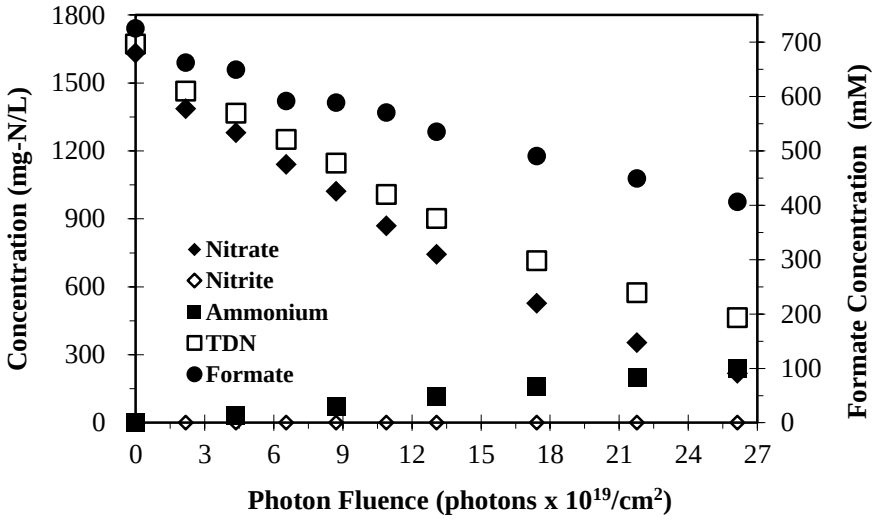


Figure SI-5.3. Removal of nitrate, formate, and total dissolved nitrogen (TDN) as well as formation of nitrogen reduction by-products (NO_2^-, NH_4^+) as a function of photon fluence absorbable by TiO_2 in sulfate-removed brine. The concentration of P90 in solution was constant at 1 g/L. Initially, 700-mM formic acid was added.

Nitrate in the sulfate-removed brine was effectively reduced that approximately 87% nitrate removal was achieved at 2.6×10^{20} photons/cm^2 irradiation (6 hrs). No nitrite was detected, and the selectivity of ammonium and gaseous N species were 17% and 83%, respectively. The sum of nitrate, nitrite and ammonium concentrations agreed well with measured TDN levels, indicating negligible levels of other aqueous N species existed. DOC was measured to track the concentration of formate, and nearly 400 mM formate was left in brine at 2.6×10^{20} photons/cm^2 of irradiation.

Table SI-5.1. *Changes in FNR (formate to nitrate molar ratio) and pH for experiments with different IFNRs (initial formate to nitrate molar ratios)*

Photon fluence (photons × 10^{19} /cm^2)		0	4.0	7.9	11.9	15.9	19.8	23.8
IFNR=1	FNR	1.0	0.7	0.4	0.3	0.2	0.2	0.1
	pH	2.6	NM	NM	NM	NM	NM	8.1
IFNR=2.5	FNR	2.4	2.4	2.3	2.1	2.0	1.8	1.8
	pH	2.2	NM	NM	NM	NM	NM	7.8
IFNR=4	FNR	4.0	4.1	4.4	4.7	5.5	5.8	6.6
	pH	2.0	NM	NM	NM	NM	NM	3.3
IFNR=5.6	FNR	5.6	6.5	7.5	8.3	10.9	13.2	19.2
	pH	1.9	NM	NM	NM	NM	NM	3.0

NM: Not measured.

CHAPTER 6

EXPLORATION OF CO-CATALYSTS FOR THE PHOTOCATALYTIC REDUCTION OF NITRATE OVER TITANIUM DIOXIDE

6.1 Introduction

Co-catalysts are used in photocatalysis to improve the reaction rate and/or shift selectivity to a desired by-product. The desired reaction outcome will determine the type of co-catalyst that should be used. For example, platinum (Pt) is used to facilitate hydrogen production because it lowers the overpotential (Sayama & Arakawa, 1996). Loading metal oxides with nano-sized metal particles can to shift the chemical potential of the semiconductor to more negative potentials (i.e., more powerful reduction potential), and it can facilitate the charge separation as well as promote interfacial charge transfer at the electrolyte interface (Subramanian, Wolf, & Kamat, 2001; Subramanian, Wolf, & Kamat, 2004). Figure 6.1 shows the energy diagram of a typical n-type semiconductor. In theory, if the work function (Φ) of the metal oxide semiconductor is less than that of the metal, a Schottky contact/barrier will be formed. The benefit of a Schottky contact over an ohmic contact is that electrons can be trapped or stored with a Schottky contact. The work function of bulk TiO_2 has been estimated to be approximately 4.6 to 4.7 eV, Pt to be 5.5 eV, and Ag to be 4.2-4.7 eV (S. L. Lee, Scott, Chiang, & Amal, 2009). However, these are bulk values and the work function is known to increase with decreasing particle size (Zhou & Zachariah, 2012). Consequently, larger Schottky contacts can be made when small metal nanoparticles are loaded onto larger nano-crystals (e.g., Chapter 4 – P90/Ag). Even though the work function of Pt and Pd are appropriate to

form Schottky contacts, when loaded onto TiO_2 as nanoparticles, ohmic contacts are formed; whereas, with coinage metals, such as Ag and Cu, Schottky contacts are made (Takai & Kamat, 2011). Because the ohmic contact is not efficient at storing electrons, these metals might not be good for nitrate reduction given the multi-electron requirement (e.g., Chapter 4).

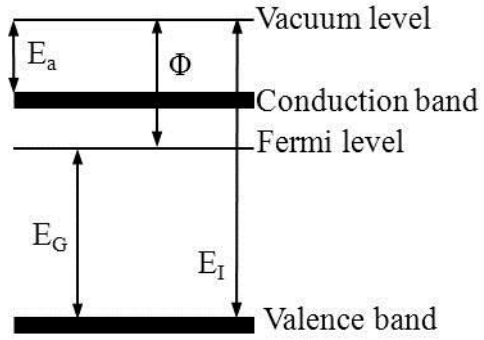


Figure 6.1. Energy diagram of a typical n-type semiconductor. E_a is the electron affinity, E_G is the bandgap, Φ is the work function, and E_I is the ionization energy.

Although metal nanoparticles can make excellent co-catalysts, they are often made of expensive and rare metals such as Pd, Pt, Ir, and Au. To move away from relying on these metals, more abundant and sustainable co-catalysts must be explored. Recently carbon nanotubes (CNTs) (Bouazza, Ouzzine, Lillo-Rodenas, Eder, & Linares-Solano, 2009; H. Z. Chen, Yang, Yu, Ju, & Sun, 2011; L. Chen, Zhang, Qu, & Yu, 2005; M. L. Chen, Zhang, & Oh, 2009; Y. S. Chen, Crittenden, Hackney, Sutter, & Hand, 2005; Cong et al., 2011; Eder & Windle, 2008; Fan, Gao, & Sun, 2006; B. Gao, Chen, & Puma, 2009; B. Gao, Peng, Chen, & Puma, 2008; L. H. Huang, Wang, Liu, Jiao, & Shao, 2010; Q. Huang & Gao, 2003; Jiang, Zheng, Wang, Li, & Sun, 2011; Kalbac et al., 2007; Kang,

Cui, & Mu, 2007; Leary & Westwood, 2011; X. H. Li, Niu, Zhang, Li, & Liu, 2003; B. Liu & Zeng, 2008; Lu et al., 2010; Oh, Zhang, & Chen, 2009; Orlanducci et al., 2006; Ou, Lin, Fang, & Liao, 2006; Qian & Lu, 2009; Sharif Zein & Boccaccini, 2008; Y. H. Tseng, Yen, Yen, & Ma, 2010; H. Wang, Wang, Jiang, & Li, 2009; S. Wang et al., 2008; Williams, Seger, & Kamat, 2008; Woan, Pyrgiotakis, & Sigmund, 2009; J. M. Wu, Yao, Yang, Fan, & Xu, 2010; Xia et al., 2007; Y. Xie, Heo, Yoo, Ali, & Cho, 2010; Y. J. Xu, Zhuang, & Fu, 2010; H. P. Yang, Shi, Dai, Duan, & Wu, 2011; Y. Yao, Li, Ciston, Lueptow, & Gray, 2008; Yu, Quan, Chen, & Zhao, 2007; Yu, Quan, Chen, Zhao, & Zhang, 2008; W. Zhang, Cul, & Jiang, 2008; L. P. Zhao & Gao, 2004; Zhu, Zhou, Yu, Nomura, & Fugetsu, 2006) and graphene (C. Chen et al., 2010; Lambert et al., 2009; Leary & Westwood, 2011; Ng, Lightcap, Goodwin, Matsumura, & Kamat, 2010; Williams et al., 2008; H. Zhang, Lv, Li, Wang, & Li, 2010; X. Y. Zhang, Li, Cui, & Lin, 2010; Y. H. Zhang, Tang, Fu, & Xu, 2010) have been evaluated as possible co-catalysts for photocatalysis due to their ability to capture and shuttle electrons. CNTs consist of carbon-carbon bonds, which occur as sp^2 hybridized bonds in its purest state, and they give CNTs unique physical and chemical properties. There are three main categories of CNTs including single-walled (SWCNTs), multi-walled (MWCNTs), and a special type of MWCNT called double-walled (DWCNTs). SWCNTs can be either semiconducting or conducting depending on their chirality with bandgaps ranging from 0 to 2.4 eV (Baughman, Zakhidov, & de Heer, 2002). MWCNTs are a zero bandgap material and are considered metallic no matter the chirality of the individual shells (H. Li, Yin, Banerjee, & Mao, 2008). DWCNTs are similar to SWCNTs, yet their inner shell properties are maintained if the outer shell is damaged, giving them a unique ability to maintain high

conductivity with defects present. Recent literature has suggested the work function of MWCNTs could be around 4.3 to 5.1 eV depending on the crystallinity (i.e., number of defects) (Ago et al., 1999). This suggests that MWCNTs would be able to form a Schottky barrier with TiO_2 (or other semiconductors) and act as an electron localization site.

The charge transfer mechanisms associated with TiO_2 and carbon nanotube bonds (C-O-Ti) are not fully understood. Kamat and co-workers (Kongkanand & Kamat, 2007) reported that when TiO_2 is bonded to a SWCNT, the SWCNT is able to accept electrons and store up to 1 electron per 32 carbon atoms. Sigmund and co-workers (Woan et al., 2009) have speculated that there are three possible scenarios for charge transfer between MWCNTs and TiO_2: (1) TiO_2 absorbs a photon which excites an electron to the CB. The electron is then transferred to the CNT, which acts as an electron storage material and is similar to a Schottky barrier junction in metal/ TiO_2 composites. (2) The CNT absorbs a photon which excites an electron to the CB. The free electron is then transferred to the space charge region (conduction band) of TiO_2, where it can act in reduction reactions. At the same time, the hole in the VB of the CNT is transferred to the surface region of the TiO_2 VB where it can to take part in oxidation reactions. (3) The third mechanism suggests that the Ti-O-C bond extends light absorption to longer wavelengths (visible-light). Furthermore, this bond tends to act as a defect with the TiO_2 structure. So, the freed electron in the space charge region of TiO_2 does not directly transfer to the CNT and it does not recombine, rather it is transferred to the impurity associated with the Ti-O-C bond (i.e., trapped). However, since MWCNTs are known to be metallic in nature,

scenario (b) can be ruled out because excitons in metallic solids recombine at a fast rate, such that it would not be efficient for photocatalytic oxidation-reduction reactions.

Defects in the CNT structure transforms the sp^2 bonds to sp^3 and decreases the conductivity and strength of the CNT. High temperature annealing (or graphitization) has been shown to reduce defects and produce CNTs of high crystallinity (Andrews, Jacques, Qian, & Dickey, 2001; Bom et al., 2002; J. Chen et al., 2007; Gong et al., 2007; W. Huang, Wang, Luo, & Wei, 2003; Kajiura, Nandyala, & Bezryadin, 2005; Kim, Hayashi, Osawa, Dresselhaus, & Endo, 2003; Kim et al., 2004; Mattia et al., 2006; Yao Wang, Wu, & Wei, 2003). Consequently, annealing also increases the MWCNT oxidation point approximately 200 °C in air (Bom et al., 2002), which is indicative of the improved structural quality. For acid-treated CNTs, annealing is important because Wang and co-workers (Yao Wang et al., 2003) have shown that annealed CNTs avoid sidewall destruction better than non-annealed CNTs after being acid treating them in boiling H_2SO_4/HNO_3 (3:1) at 140 °C for 30 minutes. Because high-temperature annealing improves the structural integrity of the nanotube, the conductivity is increased as well. After annealing CVD produced MWCNTs, the conductivity increased from 100 S/cm to 2,000 S/cm, which is around the maximum value of that found for arc-discharge produced MWCNTs (Mattia et al., 2006). As such, CNTs were annealed in this study prior to use as a co-catalyst.

The purpose of this study was to explore different co-catalysts loaded onto P90 (TiO_2) for photocatalytic nitrate reduction. Well known photocatalytic co-catalysts including copper, platinum, palladium, nickel, and iridium were examined to determine their effect of the rate of nitrate reduction and by-product selectivity. To move toward

more sustainable co-catalysts that utilize more abundant materials, CNTs, graphene, and C_{60} were also evaluated.

6.2 Experimental Methods

Materials

Materials used for synthesis of TiO_2 composites included P90 titanium dioxide (Evonik), Poly(sodium 4-styrenesulfonate) (PSS, M_W~70,000, Sigma Aldrich 243051, titanium (IV) oxysulfate ($TiOSO_4$, 99.99% purity, ~15% Ti as TiO_2 by weight, Sigma Aldrich 495379), titanium isopropoxide (TTIP, $Ti[OCH(CH_3)_2]_4$, 97% Sigma Aldrich 205273), copper (II) chloride dehydrate ($CuCl_2$, Sigma Aldrich 467847, 99.99%), palladium (II) nitrate ($Pd(NO_3)_2$, Sigma Aldrich 76070, ~40% Pd), sodium hexachloroiridate (III) hydrate (Na_3IrCl_6 x H_2O, Sigma Aldrich 288160), chloroplatinic acid hexahydrate (H_2PtCl_6 x $6H_2O$, Sigma Aldrich 206083, 99.95%, 37.5% Pt), nickel (ii) nitrate hexahydrate ($Ni(NO_3)_2$ x $6H_2O$, Alfa Aesar), fullerenol salt ($C_{60}(OH)_x(ONa)_y$, MER Corporation, y = 6-8, x+y = 24), chemical vapor deposition carbon nanotubes (>95% 7-15 nm outer diameter, 3-6 nm inner diameter, 0.5-200 μm length, Sigma Aldrich 694185), graphene nanoplatelets (GNP, Angstron Materials N006-P), and graphene oxide (GO, TW-Nano, 1:1 O:C ratio).

Synthesis of Metal-Loaded Titanium Dioxide

P90 was loaded with the metal co-catalysts using a photoreduction method as described in Chapter 4. Briefly, the metal salt was first dissolved in water and then the appropriate amount was added to a pre-sonicated suspension of P90. The pH was then

adjusted accordingly and was dependent upon the charge on the metal ion. For example, platinum chloride ion is negatively charged so the pH was adjusted to positive values to ensure adsorption of the metal on the surface of P90. The sample was then irradiated using a 450-W medium pressure lamp for approximately 30 minutes. After irradiation, the sample was washed with water via centrifugation and then dried in at air at 90 °C.

Synthesis of TiO_2/CNT Composites

CNTs were first annealed at ~2000 °C in a helium atmosphere for 1 hr to remove defects. Then, a 1% by weight solution of PSS (~10 mg/mL) was prepared in 0.5 M sodium chloride. 150 mg/L of CNTs were then added to 350 mL of the PSS solution, stirred magnetically, and then sonicated for 30 minutes. The mixture was then centrifuged (12,000 g for 1 hr) and washed with water multiple times. The CNTs were then resuspended in 150 mL water, and remained stable, indicating successfully wrapping with PSS. 4.4 mL (500 mg) of $TiOSO_4$ (10:1 TiO_2:CNT) was slowly added to 100 mL of water while mixing vigorously (~1,000 RPM). The $TiOSO_4$ solution was then added drop-by-drop to the 150 mL CNT suspension, and then bath sonicated for 30 minutes. The mixture was then gradually heated on a hotplate to 80 °C for 4 hrs. Following heating, the mixture was peptized using NaOH (1.25 M) until the solution pH (initial pH = 1.26) was approximately 5.5, at which point TiO_2 formation was apparent as a result of precipitation. The precipitate was allowed to age for 1 hr and then dried in air at 90 °C.

Synthesis of TiO_2/GNP and TiO_2/GO Composites

TiO_2/GNP and TiO_2/GO composites were synthesized using an *ex-situ* sol-gel method. Amorphous TiO_2 nanoparticles were first synthesized using TTIP as a precursor. Water was used to hydrolyze the TiO_2 and HNO_3 was used to peptize the TiO_2 agglomerates. The molar ratio of TTIP:H_2O:HNO_3 used was 1:232:0.6. 1.9 mL of HNO_3 was added to 220 mL H_2O and mixed briefly. Then, 16 mL of TTIP was slowly added to the acidified water during rapid mixing (>1,500 RPM). The mixture was allowed to mix for approximately 2 days or until it was a bluish translucent color, which indicates the presence of nanoparticles less than 5 nm. After preparing the TiO2 sol, 2% by weight of GNPs or GO were added to the TiO_2 sol, probe sonicated for 3 minutes at 50% intensity, and then mixed indefinitely. The mixture was dried at 90 °C in air to obtain a powder and then calcinated at 500 °C for 1 hr.

Thin Film Preparation

Thin films of TiO_2/GNP and TiO_2/GO were prepared on FTO electrodes from the suspensions used to create the powders. Thin films were made by pipetting 75 uL of the suspension directly on the FTO glass. The liquid was continuously spread while trying to maintain homogeneity. After drying, the thin films were annealed at 500 °C for 1 hr.\

Micrograph Images

Images were obtained using a high-resolution scanning transmission electron microscope (STEM or TEM) with energy dispersive X-ray capabilities (EDS) (STEM Phillips CM-200).

Photocatalytic Experiments

Photocatalytic experiments were performed using a 200-mL photoreactor with a UV lamp located in the center. A borosilicate sleeve was placed around the lamp to filter out light wavelengths less than 280 nm to avoid direct photolysis of nitrate or formate. The UV light source was a 450-W (Ace Glass power supply, 7830-60) medium-pressure mercury-vapor lamp (Ace Glass, 7825-34; Hanovia PC451.050) that was placed in a double-walled quartz immersion well (Ace Glass, 7854-25). The system temperature was maintained at 25 °C using a chiller. For each run, the photocatalyst was suspended using magnetic stirring in a solution of ultrapure water containing nitrate and formic acid. Thin films were tested in a similar manner, but in a 250 mL borosilicate beaker using a silver wire as a counter electrode.

Photocurrent Experiments

The photocurrent of the thin films was evaluated using the setup shown in Figure 6.2. The thin film was excited using a 200-W xenon lamp with water circulation to filter out infrared light (Newport Corporation, United States). Photocurrent was measured using an SP-200 potentiostat with EC-Lab software (BioLogic Scientific Instruments, United States). For each experiment 7.14 mM nitrate and 40 mM formic acid were used. The photoelectrode was a thin film prepared on FTO glass as described above, and the counter electrode was a silver wire (diameter = 2 mm).

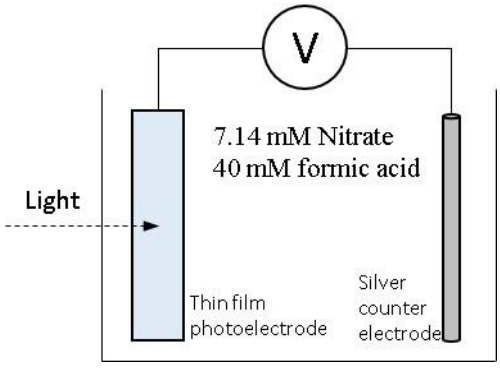


Figure 6.2. Photocurrent measurement setup.

6.3 Results

Metal Co-Catalysts

Metal nanoparticle co-catalysts were successfully loaded onto P90 (e.g., Pt Figure 6.3). Pd has been suggested to be active for reducing nitrite (NO_2^-) to dinitrogen (N_2) without an additional hole scavenger, but in that particular case 10 g/L of photocatalyst and only 0.7 mg-N/L was used, so the effectiveness is difficult to gauge (Kominami et al., 2005a). Under more realistic conditions tested herein (100 mg-N/L, 1 g/L photocatalyst), no improvement in the selectivity was observed over P90/Pd; in fact, the nitrate reduction rate decreased compared to the P90/Ag material presented in Chapter 3. Pd was also loaded in tandem with Cu or Ag, but no improvement was observed over Pd alone for either composite. The Pt and Ir loaded materials performed similar to Pd. On the other hand, Cu performed similar to Ag, but selectivity for ammonium was ~45%, which is worse than Ag. Au had similar selectivity as Ag, but the efficiency was lower. These results suggest that a Schottky contact is necessary for co-catalysts and the photocatalytic nitrate reduction reaction. For Pt and Pd, an ohmic contact was assumed, which means that the electrons are free to flow from the semiconductor to the metal and

back. While this does extend the lifetime of the exciton, the electrons are not trapped and the rate of recombination is still faster than nitrate reduction. For the coinage metals (i.e., Au, Cu, Ag)**,** a Schottky barrier is formed, thus electrons flow into the metal and become trapped. This allows for electron storage, thus facilitating the multi-electron nitrate reduction reactions.

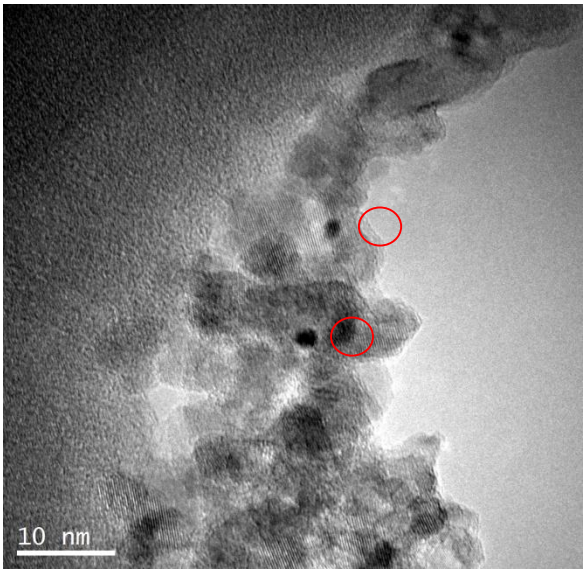


Figure 6.3. TEM image of P90 loaded with 1% Pt nanoparticles (examples circled in red).

Carbonaceous Co-Catalysts

MWCNTs were successfully loaded with TiO_2 nanoparticles (e.g., Figure 6.4) using a PSS bridge. When tested as a heterogeneous particulate photocatalysts (i.e., suspension), no nitrate removal was observed for the MWCNT/TiO_2 composites. This was attributed to the electron localization at the center of the composite. Upon excitation, electrons are shuttled away from the surface and to the CNT at the center of the composite, leaving an abundance of holes at the TiO2 surface. While this may be ideal

for oxidation reactions, this was not good for nitrate reduction, which requires a pooled source of electrons. However, the lack of nitrate removal also highlights the ability of CNT composite to move electrons away from the TiO_2, which is significant for electrode materials in photoelectrochemical processes.

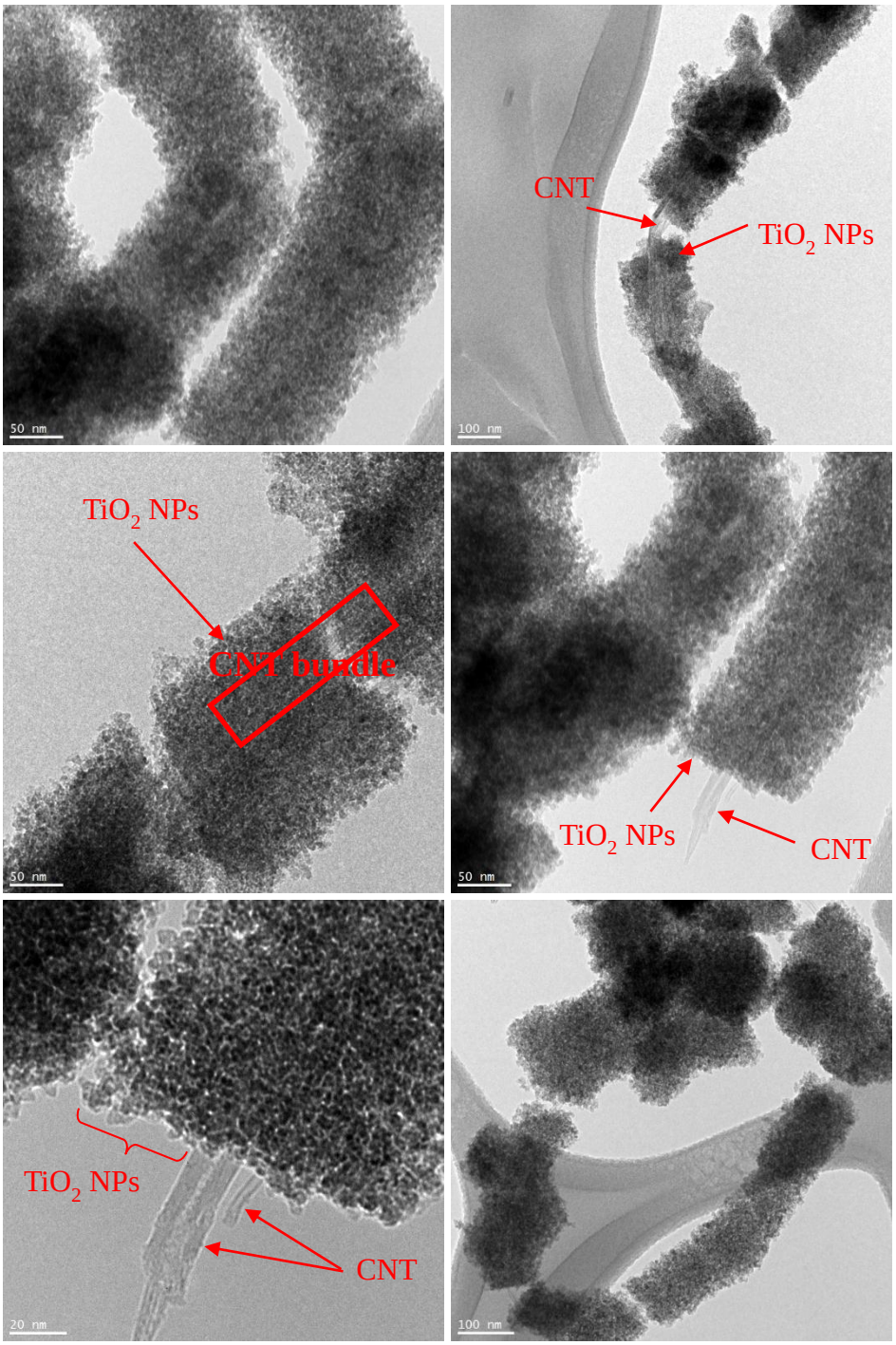


Figure 6.4. TEM images of MWCNTs coated with TiO_2.

To utilize the unique electron shuttling capabilities of carbon/TiO_2 composites, CNTs and graphene were used to improve TiO_2 thin films in a photoelectrochemical

system. In this scenario, the electrons are shuttled to the electrode and then to the counter electrode where reduction reactions occur. Graphene, which is simply an unrolled CNT, is more conductive than CNTs and, consequently, makes a more suitable electrode composite co-catalyst. Graphene nanoplatelets (GNP), consisting of 1-10 graphene sheets, and graphene oxide (GO), consisting of single sheets of graphene with a 1:1 oxygen:carbon ratio, were used for the graphene composites.

The photocurrent was examined for various TiO_2/graphene composites (Figure 6.5). The peaks signify when the light was on and the troughs signify when the light was off, thus creating a chopped curve. TiO_2 alone had a photocurrent of approximately 0.05 mA/cm^2 (not shown). When GO was loaded onto P90 no significant change in photocurrent was observed. When GO was loaded with a sol-gel synthesized nano-TiO2 (Sol-gel), the photocurrent doubled to 1 mA/cm^2. When the Sol-gel was loaded with GNP (Figure 6.6), the photocurrent improved significantly by approximately six-fold to 0.03 mA/cm^2. There a few reasons why the electron transfer efficiency to the electrode was reduced for GO compared to GNP. One reason is that the GO samples area insulating and may be forming recombination sites for the electron-hole pairs. The other possibility is that during annealing most of the GO was oxidized to CO/CO_2, which would have left gaps between TiO_2 particles, thus reducing the interparticle contact between particles and reducing the number of pathways for electrons to travel. Nitrate removal after three hours of irradiation was approximately 15% with no other aqueous nitrogen compounds being formed as by-products. Compared to a particulate system (e.g., Chapters 3 and 4), this thin film system is slow. The main reason for this is the available surface area of the film.

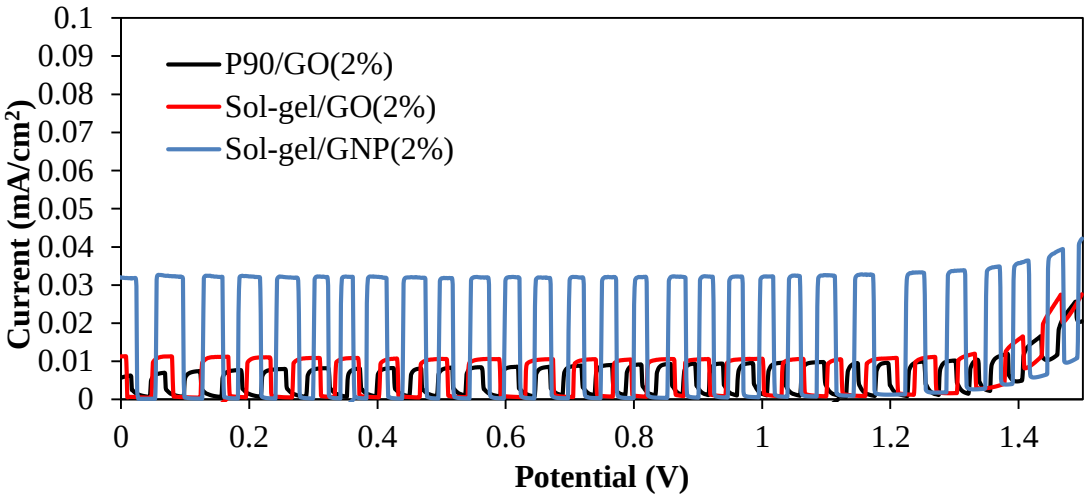


Figure 6.5. Current-potential diagram showing photocurrent for three graphene composites.

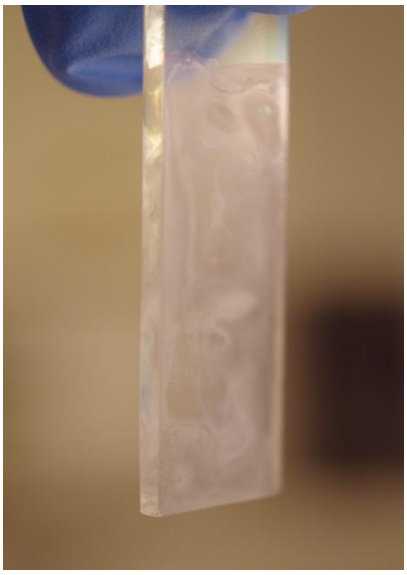


Figure 6.6. Image of TiO_2 sol/GNP(2%) coated FTO glass.

6.4 Conclusions

Metal co-catalysts are only effective for nitrate reduction if they serve as an electron localization site (i.e., Schottky contact). Even then, those metals may promote

selectivity toward hazardous by-products, such as the case with copper. While some metal co-catalysts may be successful at improving the rate of nitrate reduction and by-product selectivity (e.g., Ag), these are often expensive or non-abundant materials. Carbonaceous nanomaterials are more abundant, but they are not suitable co-catalysts for reduction reactions due to transfer of electrons away from the surface. This quality, however, makes them excellent candidates for photoelectrode co-catalysts in photoelectrochemical systems that spatially separate the oxidation-reduction reactions. Of the co-catalyst materials examined in this study, only carbon nanotubes and graphene do not currently have a standardized detection method. To maintain responsible engineering, development of detection method for carbon nanotubes and graphene warrants additional studies.

CHAPTER 7

DETECTION OF CARBON NANOTUBES AND GRAPHENE[a] IN ENVIRONMENTAL MATRICES USING PROGRAMMED THERMAL ANALYSIS*

*Published CNT portion: Doudrick, K., P. Herckes, P. Westerhoff. Detection of carbon nanotubes in environmental matrices using programmed thermal analysis. *Environ. Sci. Technol.*, 46(22), 12246–12253, 2012.

[a]Graphene section can be found in the supplemental information at the end of the chapter.

Abstract

Carbon nanotube (CNT) production is rapidly growing, and there is a need for robust analytical methods to quantify CNTs at environmentally relevant concentrations in complex organic matrices. Because physical and thermal properties vary among different types of CNTs, we studied 14 single-walled (SWCNTs) and multiwalled CNTs (MWCNTs). Our aim was to apply a classic analytical air pollution method for separating organic (OC) and elemental carbon (EC) (thermal optical transmittance/reflectance, TOT/R) to environmental and biological matrices and CNTs. The TOT/R method required significant modification for this analysis, which required a better understanding of the thermal properties of CNTs. An evaluation of the thermal properties of CNTs revealed two classes that could be differentiated using Raman spectroscopy: thermally "weak" and "strong." Using the programmed thermal analysis (PTA) method, we optimized temperature programs and instituted a set of rules for defining the separation of OC and EC to quantify a broad range of CNTs. The combined Raman/PTA method was demonstrated using two environmentally relevant matrices (cyanobacteria (CB) and urban air). Thermal evaluation of CB revealed it to be a complex matrix with interference occurring for both weak and strong CNTs, and thus a pretreatment method was

necessary. Strong CNT masses of 0.51, 2.7, and 11 µg, corresponding to concentrations of 10, 54, and 220 µg CNT/g CB, yielded recoveries of 160 ± 29%, 99 ± 1.9%, and 96 ± 3.0%, respectively. Urban air was also a complex matrix and contained a significant amount (12%) of background EC that interfered with greatly weak CNTs and minimally with strong CNTs. The current detection limit at 99% confidence for urban air samples and strong CNTs is 55 ng/m^3 (0.33 µg). Overall, the PTA method presented here provides an initial approach for quantifying a wide range of CNTs, and we identify specific future research needs to eliminate potential interferences and lower detection limits.

7.1 Introduction

Carbon nanotube (CNT) production and usage is increasing, and consequently, concern is growing over the fate and toxicity of CNTs in the environment (Lam, James, McCluskey, Arepalli, & Hunter, 2006). Multiwalled carbon nanotubes (MWCNTs) account for the majority of nanoscale carbon production. Capacity estimates reached 3,400 ton/yr in 2010 with a projected increase to 9,400 ton/yr in 2015; actual production is less than 20% of capacity (Innovative Research and Products, 2011). Large-scale production of CNTs is usually accomplished using one of two methods: electric-arc discharge (arc) or catalytic chemical vapor deposition (CVD). CVD is the most common method for large-scale production and produces yields of high purity (>90–95%), whereas the arc method is used less frequently and produces yields of lower purity (20–60%) (*Carbon Nanotubes: Science and Applications*, 2005). Post-production, CNTs are usually purified, functionalized, or annealed to change their physical and chemical properties for specified applications. The production and treatment methods affect the

mechanical, electrical, and thermal properties of the CNTs (*Carbon Nanotubes: Science and Applications*, 2005).

CNTs are challenging to quantify using traditional techniques such as mass spectrometry because of their heterogeneity in diameter, length, surface functionality, and, for single-walled CNTs (SWCNTs), chirality. Several techniques have been explored for CNT quantification (Table SI-1), including optical methods such as UV-VIS-NIR absorption (Bahr, Mickelson, Bronikowski, Smalley, & Tour, 2001; Jeong et al., 2007; Z. F. Li et al., 2006), fluorescence (H. Huang et al., 2011; O'Connell et al., 2002), and Raman spectroscopy (Salzmann, Chu, Tobias, Llewellyn, & Green, 2007); tagging approaches such as isotopic (Petersen, Huang, & Weber, 2008; L. W. Zhang, Petersen, & Huang, 2011), fluorescence (Xiao et al., 2006), and probe labeling; size-exclusion methods such as gel electrophoresis (R. H. Wang et al., 2009; R. H. Wang et al., 2011); and thermal analysis methods such as thermogravimetric analysis (TGA) (Pang, Saxby, & Chatfield, 1993; Plata, Reddy, & Gschwend, Submitted 2011), temperature programmed oxidation (TPO) (Alvarez, Kitiyanan, Borgna, & Resasco, 2001; Herrera & Resasco, 2003), chemothermal oxidation (CTO) (Sobek & Bucheli, 2009), total organic carbon (TOC) (Tamura et al., 2011), and thermal optical transmittance/reflectance (TOT/R) (Hyung, Fortner, Hughes, & Kim, 2007; Myojo et al., 2009; Ono-Ogasawara, Serita, & Takaya, 2009). These approaches have limitations, including specificity to particular CNTs or inapplicability to more complex matrices. With these current limitations and concerns over CNT fate and toxicity, there is a need to develop a strategy for CNT analysis in complex environmental matrices.

Thermal-based analytical methods are promising owing to the unique thermodynamic stability of CNTs. TGA was coupled with mass spectrometry to quantify CNTs in marine sediments using isotopic ratios of carbon in CNTs, and a detection limit of 4 µg SWCNT/40 mg sample was obtained (Plata et al., Submitted 2011). Similarly, CTO 375 °C, a soot analysis method (Gustafsson et al., 2001), was used to quantify a range of CNTs in ultrapure water and in marine sediments (Sobek & Bucheli, 2009). Recovery values were highly dependent on the type of CNT, especially in the more complex sediment samples, and large CNT concentrations were used (25 mg CNT/g sediment). TOC was coupled successfully with an elaborate pre-oxidation method to quantify MWCNTs in rat lungs (Tamura et al., 2011); however, the chemical and thermal oxidation pretreatments used were very harsh and are known to oxidize CNTs to CO_2 (I. D. Rosca, Watari, Uo, & Akaska, 2005). TOT/R is a standard method for detecting refractory or elemental carbon (EC) (e.g., soot) in air samples (Health, 1998), and it has been used to quantify MWCNTs alone (Myojo et al., 2009; Ono-Ogasawara et al., 2009) or in a simple matrix consisting of ultrapure water and natural organic matter (NOM) (Hyung et al., 2007). Interlaboratory comparisons of organic carbon (OC)/EC separation methods (including TGA, CTO, and TOT/R) have shown that TOT/R is the most reliable technique for detecting EC in environmental matrices (Hammes et al., 2007; Schmid et al., 2001; Watson, Chow, & Chen, 2005). However, little evidence supports its validity for a wide range of CNTs exhibiting different thermal and physical properties. Furthermore, the thermal behavior of various environmental matrices using TOT/R is unknown, and this will be important for detecting CNTs. The CNT quantification strategy

described herein is built around the TOT/R method owing to its reliability in detecting soot in air and sediment samples.

This study aims to evaluate the thermal stability of many different CNTs alone to develop a thermal analysis strategy for CNT quantification. Environmentally relevant air, water, sediment, and biological matrices were analyzed to assess potential interferences in CNT measurement from pyrolized organic matter and the presence of natural EC in water (surface and tap water, wastewater, chemical dispersants), sediments, urban air, and biological samples (urine, serum, milk, lung tissue). Our study is unique because we use 14 different CNTs produced by a range of processes that result in a span of physical and chemical properties. We discuss optimization of analysis methods for CNT detection. Demonstration of CNT detection in two relevant environmental matrices (cyanobacteria (CB) and urban air) was completed to investigate the potential inferences on CNT quantification.

7.2 Experimental Details

CNT Sources and Sample Preparation

CNTs (n = 14) used in this study are listed in Table 7.1. An array of MWCNTs were studied, including raw CVD (MW-O, MW-Mitsui, MW-15, MW-20, MW-30, MW-100), purified CVD (MW-P), functionalized CVD (MW-F, MW-OH, MW-COOH), annealed CVD (MW-15G), and raw arc (MW-Arc). Two SWCNTs were studied including a raw (SW) and purified (SW-65) CVD. Manufacturer details are provided in the Supplemental Information (SI).

Table 7.1. *Properties of CNTs used in this study*

CNT ID	CNT Type	State	Purity[a]	Metal Content[b]	Outer Diameter (nm)	Inner Diameter (nm)	Length (µm)
MW-O	MWCNT	Raw	>95%	<6%	20-30	5-10	10-30
MW-P	MWCNT	Purified	>98%	<2%	20-30	5-10	10-30
MW-F	MWCNT	Functionalized	>99.9%	<0.01%	20-30	5-10	10-30
MW-15	MWCNT	Raw	>95%	<5%	7-15	3-6	0.5-200
MW-20	MWCNT	Raw	>95%	<5%	10-20	5-10	0.5-200
MW-30	MWCNT	Raw	>95%	<5%	10-30	5-10	0.5-500
MW-100	MWCNT	Raw	>95%	<5%	60-100	5-10	0.5-500
MW-OH	MWCNT	Functionalized	>95%	<1.5%	8-15	3-5	10-50
MW-COOH	MWCNT	Functionalized	>95%	<1.5%	8-15	3-5	10-50
MW-15G[c]	MWCNT	Annealed	>97%	<1%	7-15	3-6	0.5-200
MW-Mitsui	MWCNT	Raw	>98%	<1%	20-70	NA	NA
MW-Arc	MWCNT[d]	Raw	<50%	0%	5-10[e]	NA	NA
SW	SWCNT	Raw	<50%	<10%	1.1	NA	0.5-100
SW-65	SWCNT	Purified	<75%	<10%	0.8	NA	0.45-2

[a]CNT content reported by manufacturer. MW-P and MW-F calculated assuming no amorphous carbon remaining.
[b]Metal content reported by manufacturer except for MW-F and MW-P determined using energy dispersive X-ray spectroscopy and MW-15G using thermogravimetric analysis.
[c]MW-15 annealed at ~2000 °C in UHP He.
[d]Synthesized using arc method; all others are CVD.
[e]Obtained from TEM images; all others reported by manufacturer.

CNTs were massed using a microbalance (Sartorius Micro M 500 P). CNT stock solutions were prepared by adding CNTs (10 mg/10 mL) to ultrapure water (Nanopure®, 18.3 MΩ-cm) followed by bath sonication (Branson 2510, 40 kHz) for approximately 30 minutes. Except for MW-F CNTs, Triton X-114 was added as a dispersant at a 4:1 dispersant to CNT mass ratio. X-114 had no marked effect on the thermal stability of the CNTs. Samples, ranging from 1 to 100 µL, were loaded onto pre-fired quartz fiber filters (QFF, Pallflex Tissuquartz Filters, 2500 QAT-UP). Filters were heated to 870 °C prior to sample preparation to remove any carbonaceous contamination acquired during storage

(e.g., dust). Aqueous samples were loaded by pipetting the desired sample volume (1–100 uL) onto the center of the filter and then allowing it to dry at approximately 90 °C.

Environmental and Biological Matrices

Four dispersants (Sigma Aldrich) commonly used to create homogeneous CNT stock solutions, polydiallydimethylammonium chloride (PDDA, #409014, 20% in H_2O, average MW = 100,000–200,000 g/mol), Triton X-114 (X-114, #X-114, average MW = 537 g/mol), sodium dodecyl sulfate (SDS, #436143, >99%), and sodium deoxycholate (SDOC, #D6750, >97%) were used as received. Reservoir surface water (Saguaro Lake, DOC = 5.6 mg/L) and tap water (Tempe, AZ, DOC = 2.7 mg/L) samples were collected in July 2010. Representative wastewater samples were obtained from a laboratory activated sludge sequencing batch reactor (Yifei Wang, Westerhoff, & Hristovski, 2011). Urban air (Arizona State University, Tempe, AZ) was collected for 24 hrs on a pre-fired QFF using a high volume air sampler. Sediments were collected from the Bread and Butter Creek, SC, an intertidal mudflat sediment containing 4.7% TC (of dry sediment mass). Biological matrices included synthetic urine (prepared as described previously (Wenzler-Rottele et al., 2006)), human serum (Sigma Aldrich, H4522), and cow's milk (Shamrock Farms, 2%).

Extraction of CNTs from Cyanobacteria

Cyanobacteria (*Synechocystis* sp. PCC6803) were collected from a lab culture and then freeze dried. MW-Mitsui CNTs were spiked into a 50 mg sample of cyanobacteria and allowed to mix. Samples were digested with 10 mL of tetramethylammonium

hydroxide (TMAH, 25% in H_2O, Sigma Aldrich 331635) at 65 °C for 24 hrs, followed by centrifugation at 13,000 g. The pellet, containing non-digestible OC and CNTs, was transferred to a QFF and heat treated in air at 500 °C for 15 minutes to remove low-stability organic carbon. The treated pellet was then used for further analyses.

Analytical Methods

Thermal analysis was performed using a commercial OC-EC analyzer equipped with optical correction (Sunset Laboratory, Inc., Forest Grove, OR). The instrument is commonly used for NIOSH soot determinations as well as atmospheric OC and EC measurements in air pollution studies. Instrument details are provided in the SI, and a schematic of the instrument setup is shown in Figure SI-7.1.

The EC-OC instrument is controlled through user-defined temperature programs, which emerged as critical for CNT analysis. These programs allow the temperature, temperature residence time, and carrier gas to be adjusted according to the type of sample under analysis. Although this instrument is standard for analysis of air pollutants, its operation is briefly described because optimization for CNT analysis requires a basic understanding. For this study, an inert (100% He) and an oxidizing carrier gas (90%He/10% O_2) were used with temperatures ranging from 0 to 910 °C. Samples were first heated under inert conditions to remove volatile OC. The sample chamber was then cooled and switched to oxidizing conditions. OC that does not volatilize may undergo pyrolysis becoming pyrolytically generated elemental carbon (PEC; i.e., char), which has thermal properties similar to EC. Fixed or variable residence times can be used at each temperature step, where variable residence times are defined by a minimum and

maximum time that allows for complete desorption at each temperature step. Variable residence times were used during the inert phase to allow for complete desorption of OC so as to minimize interferences with EC during the oxidizing phase. Both variable and fixed residence times were used during the oxidizing phase and depended on the sample matrix and CNT type.

As the sample is analyzed, the volatilized and combusted carbon travels to an oxidizing oven (MnO_2 catalyst at 870 °C), where it is transformed into carbon dioxide (CO_2). The CO_2 passes through a methanator (Ni firebrick–supported catalyst) and is reduced to methane (CH_4). The CH_4 signal is measured using a flame ionization detector (FID) and is converted to TC using a CH_4 standard. TC is split into two types of carbon post-analysis: OC and EC. The portion of TC that is OC or EC is defined by the method, which determines where the OC-EC split is placed post-analysis. This split can be automatic on the basis of automatic optical correction; the optical transmittance or reflectance is observed throughout analysis using a 632 nm laser, and the split is placed where the transmittance/reflectance returns to the initial reading. For samples in which optical correction does not work, a manual split defined by the analyst should be used. For samples containing no PEC, the split can be placed between the two carrier gas modes; everything to the left of the split (inert conditions) would be OC, and everything to the right (oxidizing conditions) would be EC. This method is based on the assumption that EC is stable under inert conditions and that OC is not. If PEC is present but combusts at lower temperatures than the EC under analysis, then a manual split can be placed between OC and EC, usually at a defined temperature. If the PEC overlaps with the EC, then the manual split must be placed where interference is minimal. Figure SI-2 shows a

sample thermogram of sucrose using the NIOSH temperature program (Birch & Cary, 1996; Health, 1998) and how OC, EC, and PEC are traditionally defined using optical correction.

The automatic optical correction (i.e., TOT/R) is successful when using well dispersed CNTs that can be loaded homogeneously on the filter at concentrations that allow for proper transmittance [23]. However, optical correction will err when dealing with CNT samples that are more indicative of that found in the environment (e.g., aggregated, low concentrations), such that only a few aggregates are heterogeneously dispersed on the filter (Hammes et al., 2007; Schmid et al., 2001). For all CNTs examined (Table 1), the optical correction method was not reliable, and a manual split method was required for aqueous and solid samples (see the SI for further discussion). Because of the lack of optical correction, the thermal analysis method discussed herein for CNTs is referred to as programmed thermal analysis (PTA).

Raman spectroscopy was performed on a custom-built instrument in 180° geometry. The sample was excited using a 532-nm laser with 100-mW maximum power, which was controlled using neutral density filters. The data were collected using an Acton 300i spectrograph and a back thinned Princeton Instruments liquid nitrogen cooled CCD detector with a spatial resolution <1 μm and spectral resolution of ~1 cm^{-1}.

For analysis of the CNTs, dry powders were loaded onto quartz slides, and spectral analysis was done in triplicate. Analysis of CNTs in environmental matrices was performed directly on the QFF. For all samples, the background was subtracted from the spectra.

7.3 Results and Discussion

CNT Thermal Stability and Method Optimization

Using the manual split method to quantify CNTs in complex matrices requires a deeper understanding of the thermal behavior of CNTs under both inert and oxidizing conditions. This method cannot be developed around one type of CNT because CNTs have different thermal properties depending on whether they are single-walled, multiwalled, functionalized, annealed, etc. To optimize a set of temperature programs for a range of CNTs, we first analyzed a representative group of CNTs (Table 1) under inert conditions to determine the maximum temperature at which no CNT loss occurs, and then analyzed them under oxidizing conditions to determine the minimum temperature at which the CNTs begin to combust.

Figure 7.1 shows the fraction of CNT mass remaining after heating to 870 °C under inert conditions for several CNTs. This is the maximum temperature used in the NIOSH program and previous CNT thermal studies (Health, 1998; Hyung et al., 2007; Myojo et al., 2009). Mass loss curves for this and subsequent figures were generated by integrating the thermogram FID signal (e.g., Figure SI-7.4). In Figure 7.1, the raw CVD MWCNTs (MW-O, MW-15, MW-20, MW-30, MW-100) were represented by MW-O and MW-15, the functionalized MWCNTs (MW-F, MW-OH, MW-COOH) by MW-F, the purified MWCNTs by MW-P, the graphitized or ordered MWCNTs (MW-Arc, MW-15G, MW-Mitsui) by MW-Arc, and the SWCNTs (SW, SW-65) by SW-65. Figure 7.1 shows that only the graphitized MWCNTs were stable under inert conditions up to 870 °C. The MW-P CNTs were the least stable, exhibiting nearly 100% mass loss after ~1000 seconds at 870 °C. All CVD MWCNTs were unstable at 870 °C, and they exhibited mass

loss with what appears to be a zero-order rate. Thus, using the temperature programs outlined in existing methods is not valid for all CNTs.

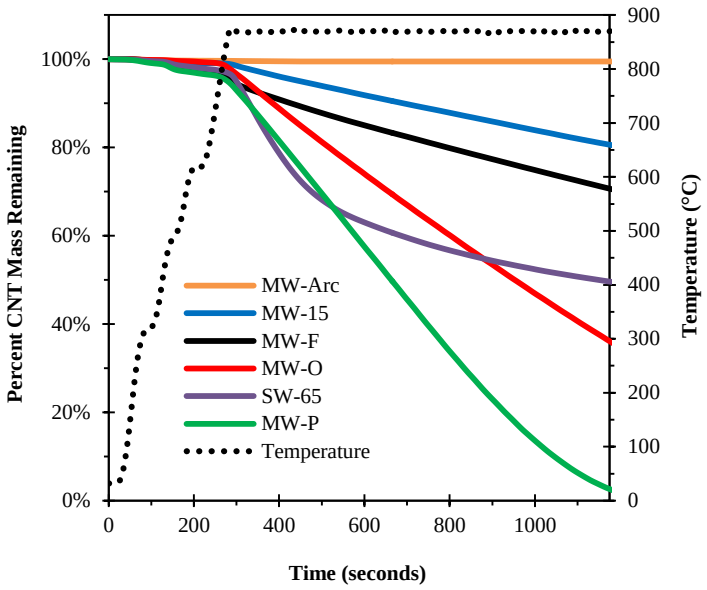


Figure 7.1. Percent CNT mass remaining after heating to 870 °C under inert conditions for several CNTs.

Several factors could have influenced the observed range of CNT thermal stability including functional group content, metal catalyst content, and defect density. If oxygenated groups were responsible for the observed mass loss (Figure 7.1) then the expected order of mass loss rate should follow MW-O ~ MW-P < MW-F; however, the rate of mass loss followed MW-P < MW-O < MW-F. The MW-O had the most metal (oxide) impurities (4.49% Ni/0.76% Fe), but they were more stable than MW-P (1.80% Ni/0.08% Fe). Furthermore, the MW-Mitsui CNTs, which contained ~10% iron impurities, did not exhibit any mass loss. This suggests that, for MWCNTs, oxygen associated with functional groups or metals does not affect the rate of mass loss under

inert conditions. The difference in thermal stabilities between CNTs under inert conditions may be explained by the defect density rather than the abundance of oxygenated functional groups or metal oxides. MWCNTs produced by CVD will generate additional defects when heated under inert conditions until a limiting temperature is reached, at which point the defects begin to heal (Bhalerao, Sinha, & Sathe, 2008). If this temperature is not reached, then defects may continue to develop. High-temperature annealing of CNTs reorders the sp^3 bonds to sp^2, which makes them more thermally stable (Andrews et al., 2001; Bom et al., 2002; Kim et al., 2003; Ray et al., 2009; D. K. Singh, Iyer, & Giri, 2010; H. Zhang, Sun, Li, Li, & Cheng, 2006). For CNTs created or treated at high temperatures (>2500 °C), such as MW-Arc and MW-15G, respectively, no defects were introduced because they had already reached a high state of thermodynamic stability. Also, no mass loss was observed for MW-15G, unlike MW-15; the only difference between the two was thermal treatment. Although defects are likely the cause of mass loss under inert conditions, the mechanisms behind this are unknown. Sublimation has been shown to occur for C_{60} under inert heating conditions (Milliken et al., 1991), but similar behavior has yet to be shown to occur for CNTs.

To optimize the temperature program for the CNTs exhibiting mass loss under inert conditions, the MW-O, MW-P, MW-F, and SG-65 CNTs were analyzed at several maximum temperatures, including 675, 700, 750, and 870 °C (MW-O shown in Figure SI-7.5). No significant (<5%) CNT mass loss occurred below 675 °C for any CNTs in this study. The minimal CNT mass loss (<5%) observed at temperatures as low as ~250 °C was attributed to either oxidation caused by oxygen associated with surface C atoms or amorphous carbon (Figure SI-7.4).

The thermal behavior of CNTs was examined under oxidizing conditions to determine the temperature at which CNTs begin to combust as well as the maximum temperature required to completely oxidize the CNTs. Figure 7.2 shows the fraction of CNT mass remaining with increasing temperature under oxidizing conditions. MW-F and MW-O CNTs were representative of all other MWCNTs not shown in Figure 7.2 (all mass loss curves are shown in Figure SI-7.6). The purified SWCNTs (SW-65) were the least stable CNTs, with almost 100% mass loss occurring before 650 °C. Most of the weak CNTs began combusting at ~650 °C and reached a maximum rate at ~700 °C. MW-15 also started combustion between 650 and 700 °C, but at a slower rate than other weak CNTs, which suggests that MW-15 represents the upper limit of the weak CNTs. Similar to inert conditions, under oxidizing conditions MW-Arc, MW-Mitsui, and MW-15G were more stable than all other CNTs; their initial oxidation temperatures ranged from ~750 to 800 °C. When a weak CNT (MW-15) was annealed at ~2000 °C (MW-15G), the rate of mass loss was decreased. The MW-Arc CNTs, which are synthesized at greater than 3000 °C, were the most stable; most of their oxidation occurred above 900 °C. This is consistent with previous studies that showed MWCNTs produced by arc were much more stable than those produced using CVD (Behler, Osswald, Ye, Dimovski, & Gogotsi, 2006; Watts, Hsu, Kroto, & Walton, 2003). No linear correlation was found between thermal stability and CNT diameter, unlike as shown previously for CNTs synthesized by a common method (D. K. Singh et al., 2010), which in our case may be attributed to the differences in CNT production temperature rather than diameter.

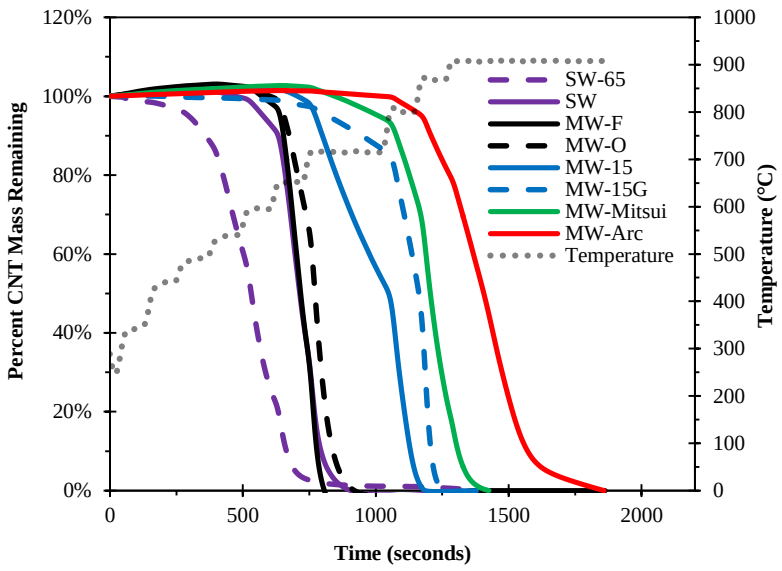


Figure 7.2. Percent CNT mass remaining after heating to 910 °C under oxidizing conditions. MW-F and MW-O were representative of all other raw CVD MWCNTs not shown.

On the basis of these results, the CNTs can be grouped into two thermal classifications: CNTs that are stable at the maximum temperature (870 °C) under inert conditions and did not begin oxidation until ~750-800 °C were classified as thermally "strong," and CNTs that are not stable above ~700 °C under inert conditions were classified as thermally "weak." The range of weak CNTs was much broader; the SG-65 and MW-15 represent the lower and upper bounds, respectively. Whereas MWCNTs are classified by their defect density, SWCNTs are classified as weak because of their small diameter and high percentage (~100%) of surface atoms, which decreases thermal stability due to an increase in bond strain (N. Yao et al., 1998) and a larger number of carbon atoms exposed to oxygen, respectively.

"Weak" and "Strong" Classification Using Raman Spectroscopy

Raman spectroscopy has been shown to be a reliable characterization tool for CNTs with spectral peaks that are specific to graphitic carbon (Dresselhaus, Dresselhaus, Saito, & Jorio, 2005). Between 1300 and 1600 cm^{-1}, there are two distinct peaks for CNTs, called the D-band (~1350 cm^{-1}) and the G-band (~1580 cm^{-1}) (Figure SI-7.7a). The D-band indicates disorder present within the CNT sample, and its intensity is proportional to defect density. The G-band is a result of C-C bond stretching unique to sp^2 hybridizations found in graphitic carbon. The ratio of the D-band and G-band intensities (I_D/I_G) is often used to quantify the defectiveness of CNTs, and this ratio can be used to estimate the thermal stability of CNTs (Behler et al., 2006; Bhalerao et al., 2008; J. Chen et al., 2007; Kim et al., 2003; D. K. Singh et al., 2010; Tran, Tridech, Alfrey, Bismarck, & Shaffer, 2007). Another advantage of Raman spectroscopy is that it can be used to distinguish between SWCNTs and MWCNTs by inspection of the radial breathing mode (RBM) at lower frequencies (Dresselhaus et al., 2005). For SWCNTs, there will be multiple peaks between 100 and 300 cm^{-1}, whereas MWCNTs will have no characteristic peaks (Figure SI-7.7b). If RBM peaks are present, then the sample will be classified as weak, independent of the I_D/I_G ratio.

Raman spectroscopy was used to distinguish thermally "strong" from "weak" CNTs. There is a strong linear relationship ($R^2 = 0.96$) between the I_D/I_G ratio and the temperature at 50% CNT mass loss (Figure 7.3, Table SI-7.2). MWCNTs with $I_D/I_G >$ 0.60 and SWCNTs were synonymous with weak CNTs, and MWCNTs with $I_D/I_G \leq 0.60$ with strong CNTs. This suggests that Raman spectroscopy can be used to determine the thermal stability classification of the CNT (i.e., weak or strong), which can then be used

to determine the approximate temperature at which the CNTs will combust. The key to using Raman for CNT thermal classification will be to eliminate background Raman peaks by extracting the CNTs from the sample. If the CNT type cannot be determined using Raman spectroscopy, then assuming the CNTs to be weak would be an appropriate conservative estimate.

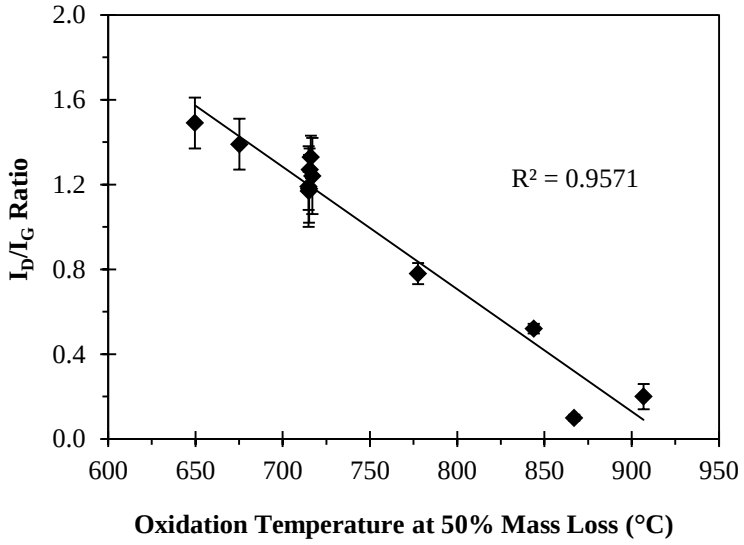


Figure 7.3. I_D/I_G ratio as a function of oxidation temperature at 50% mass loss for all MWCNTs.

Thermal Behavior of Environmental and Biological Matrices

Under inert conditions organic matter can form PEC, and this may cause interference if it combusts in the same temperature range as CNTs. Furthermore, environmental samples that have been exposed to anthropogenic EC such as wastewater sludge, air, soils, and sediments can also cause interference. We define all "non-CNT EC" evolving during the oxidizing phase as NEC, and this includes PEC, anthropogenic EC (e.g., soot), and natural EC.

Figure 5a shows the percent NEC (µg NEC/µg TC × 100%) generated under inert conditions for several environmental and biological matrices. The NEC percentage was independent of the TC loading and used to quantify charring of organic matter and the presence of background EC. The dispersants, which are free of background EC, had negligible NEC (<1%), which indicates little PEC formation. Of the environmental matrices, surface water and lab activated sludge had less than 10% NEC, and the urban air and sediment samples had a substantial amount of NEC, which is most likely attributed to the background EC (e.g., soot). Of the biological matrices, urine had very little NEC, whereas lung tissue, milk, and human serum had high NEC percentages, most likely owing to charring of fats and proteins rather than background EC. Matrices that had less than 10% NEC content were defined as "simple," and those that that had greater than 10% NEC were defined as "complex."

Figure 7.4b shows the percent NEC mass remaining for complex matrices and percent EC mass remaining for three CNTs with increasing temperature under oxidizing conditions. MW-F and MW-15 CNTs represent the average and upper bound of the thermally weak CNTs, respectively, and MW-Arc represents the thermally strong CNTs. Of the environmental and biological samples examined, the simple matrices had less than 5% interference at combustion temperature ranges similar to both the weak and strong CNTs, whereas the complex matrices had more substantial interferences depending on the CNT classification. All of the complex matrices were observed to overlap with all weak CNTs to some degree. The most substantial interference with weak CNTs was observed for the sediment and urban air samples, which may be due to thermally stable EC (e.g., soot). The biological samples exhibited <5% interference with the upper bound

weak CNTs (MW-15), but approximately 10% and 20% of the urban air and sediment samples, respectively, remained when the MW-15 CNTs began oxidizing. No matrices exhibited any significant (>5%) interference with the strong CNTs. On the basis of these results, complex matrices will interfere with weak CNTs during the oxidizing phase (Figure 7.2). Furthermore, these complex matrices have OC that desorbs at the same temperature as the weak CNTs under inert conditions (Figure 7.1); this makes interference even more significant, especially if long residence times at temperatures greater than 700ºC are required to remove the OC.

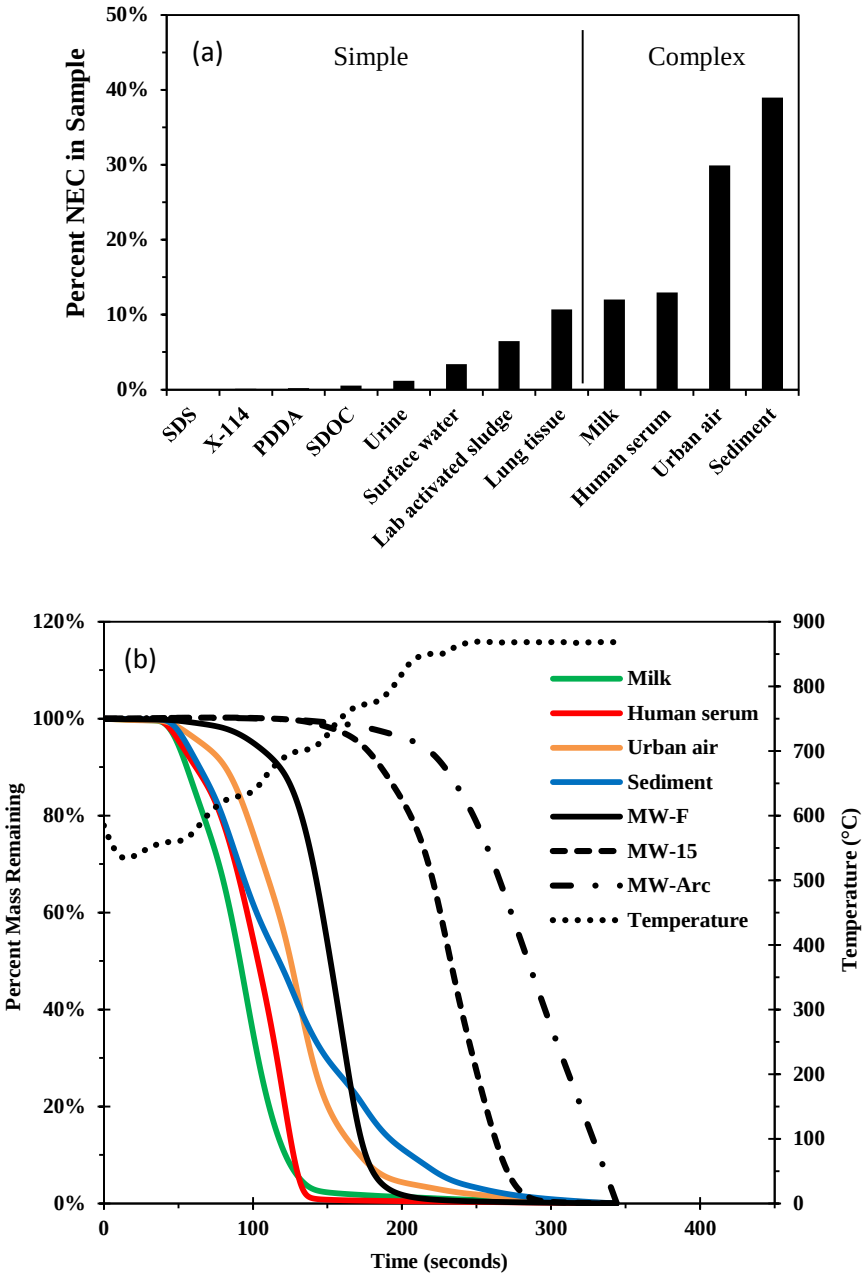


Figure 7.4. (a) Percent of NEC (NEC/TC × 100%) present in various laboratory, environmental, and biological matrices. (b) Percent NEC mass remaining from various matrices and percent mass remaining for three CNTs representing the lower (MW-F) and upper (MW-15) range of weak CNTs and strong (MW-Arc) CNTs. NEC mass is the percent remaining after treatment under inert conditions such that all volatile OC has been removed.

Given the small sample size of the matrices tested, even the smallest amount of interference can compound in a larger environmental sample to overshadow the CNT signal. For example, 5.0 µL of human serum contained 200 µg of TC, of which 26 µg was considered NEC and 15 µg (7.5%) and 0.16 µg (0.08%) interfered with weak and strong CNTs, respectively. A procedure was developed to account for these potential interferences. First, an optimized temperature program for thermally strong and weak CNTs, differentiated using Raman spectroscopy, must be used. Second, digestion techniques must be used to degrade organic matter to prevent PEC formation (see below). However, the digestion technique should be non-selective for CNTs such that they will not be degraded to CO_2, as is observed with harsh chemical oxidant digestion methods. Techniques to separate graphitic EC from CNTs in soils, sediments, sludge, and air will be more challenging to develop because of their similar chemical and thermal properties

Demonstration of CNT Detection in Environmental Matrices

We have outlined a method that can be used to identify the thermal classification of CNTs using Raman spectroscopy followed by quantification using PTA. Using two different environmental matrices, cyanobacteria and urban air, the applicability of this method is demonstrated for a strong CNT (MW-Mitsui). Weak CNTs require development of more elaborate extraction methods that are beyond the scope of this study. CB were selected because they are a ubiquitous primary producer in surface waters, and research has suggested that they may be a good indicator organism for ecotoxicity tests (Ando et al., 2007; Aslim & Ozturk, 2009). Similarly, green algae have

been used as an indicator organism to examine the toxicity effects of CNTs (Basiuk, Ochoa-Olmos, & De la Mora-Estrada, 2011; Blaise, Gagne, Ferard, & Eullaffroy, 2008; Schwab et al., 2011; Wei et al., 2010).

CB (50 mg dry-weight) was spiked with 0.51, 2.7, and 11 µg of MW-Mitsui MWCNTs corresponding to a mass ratio of 10, 54, and 220 µg CNTs/g CB, respectively. Recovery is expressed as the mean and standard error of triplicate samples. After pre-treatment, samples were loaded onto a QFF and then analyzed with Raman spectroscopy. CNT aggregates were easily located using the Raman microscope due to their opacity, and a spectrum with clear CNT peaks was obtained with relatively low noise (Figure SI-7.8). The important steps for isolating CNT aggregates for Raman spectroscopy were: (1) extracting the CNTs by digesting the CB and (2) centrifuging the sample to aggregate the CNTs. The I_D/I_G ratio was 0.26 ± 0.08, which would appropriately classify the CNTs as "strong." After Raman analysis, the samples were analyzed using PTA with an OC/EC split point at 750 °C. CNT mass recovery for 10 µg CNTs/g CB, 54 µg CNTs/g CB, and 220 µg CNTs/g CB was 160 ± 29%, 99 ± 1.9%, and 96 ± 3.0%, respectively. Although CB is a relatively simple matrix (i.e., no background EC), a small amount (~0.20 µg) of interference is still caused by PEC formation, which evolves at the same temperature as the MW-Mitsui CNTs. Although the interference had little effect on larger CNT masses (e.g., 2.7 and 11 µg) and excellent recoveries were obtained, it was significant enough that when the CNT mass was closer to the interference mass, the recovery was less accurate. PTA is appropriate for exposure studies using CB as an indicator organism, but dosage levels should be greater than 10 µg CNTs/g CB (dry) to obtain reliable recoveries.

Graphitic particles are ubiquitous in soils, sediments, air, and wastewater sludge, and these will have a thermal stability very close to if not greater than CNTs. Urban air contains EC that combusts at the same temperature as the weak CNTs (i.e., Figure 7.4b), thus making it difficult to detect a low concentration of CNTs in an urban air sample with a large EC content (Figure SI-7.9a). However, less interference occurs with the strong CNTs (Figure SI-7.9b). Urban air samples (1.5 cm^2 filter punch) were spiked with 2.8 μg (465 ng/m^3) of MW-Mitsui CNTs and analyzed using PTA. Recovery is expressed as the mean and standard error of nine replicates. The CNTs began combusting at ~750 °C, which was used to develop the temperature program and the location of the split point. A non-spiked urban air sample from the same filter contained 45 μg (7,477 ng/m^3) of TC, with 12% (5.5 μg, 914 ng/m^3) EC as determined by optical correction, and 0.46% (0.21 μg, 35 ng/m^3) combusting after 750 °C. The mean mass of nine replicates was 2.8 μg with a standard deviation of 0.11 μg resulting in a recovery of 100 ± 4.0%. The EPA standard method was used to calculate detection limits (EPA). The method detection limit (MDL) with 99% confidence was calculated to be 55 ng/m^3 (0.33 μg). The lower critical limit (LCL) and the upper critical limit (UCL) for 95% confidence were calculated to be 22 ng/m^3 (0.13 μg) and 76 ng/m^3 (0.46 μg), respectively. The limit of detection (LOD) and limit of quantitation (LOQ) were calculated to be approximately 136 ng/m^3 (0.82 μg) and 183 ng/m^3 (1.1 μg), respectively.

7.4 Applicability and Future Development Needs

A temperature program specific to different CNTs and environmental matrices is required for reliable quantification. CNTs have a wide range of initial oxidation

temperatures ranging from approximately 500 °C to 800 °C; most initial oxidation occurs at ~650 °C. The temperature programs will depend on the matrix under analysis and the split point on the type of CNT. For weak CNTs, the maximum temperature that should be used during inert conditions is 675 °C, and if higher temperatures are required, then small residence times should be employed to reduce CNT mass loss. During oxidizing conditions, the highest temperature should be a minimum of 800 °C to ensure complete CNT oxidation.

Currently, the method described herein is ideal for working at concentrations commonly used in toxicity studies (Firme & Bandaru, 2010; Lam et al., 2006; Petersen, Akkanen, Kukkonen, & Weber, 2009; Uo, Akasaka, Watari, Sato, & Tohji, 2011; X. C. Zhao & Liu, 2012) for strong CNTs and some weak CNTs in controlled experiments (e.g., toxicity tests, lab-scale removal tests). The future challenge will be processing large volumes of CNT-containing sample (e.g., wastewater) or CNTs in samples containing large amounts of interfering carbon (e.g., soils). Extraction, separation, and purification steps are key to working with such samples. Our work with TMAH represents the first step in such a pre-treatment strategy, but additional work is needed on the Raman/PTA approach demonstrated here before it can be applied to environmental monitoring at trace levels.

7.5 Supplemental Information

Carbon Nanotube Details

Carbon nanotubes (CNTs) are cylindrical and can be single-walled (SWCNT) or multi-walled (MWCNT). SWNTs are essentially a single sheet of graphite (called graphene) rolled up and connected end to end. MWCNTs are concentric SWCNTs of increasing diameter. Because of their unique properties, double-walled carbon nanotubes (DWCNTs) are considered a separate class of MWCNT. All CNTs have unique and excellent electrical, thermal, and physical properties with a high strength to weight ratio, which makes them ideal for a variety of applications (Aitken, Chaudhry, Boxall, & Hull, 2006). The method of production affects the mechanical, electrical, and thermal properties of the CNTs (*Carbon Nanotubes: Science and Applications,* 2005). Laser ablation is common for SWCNTs, and it produces CNTs similar to the Arc technique. Laser ablation is not currently used for large-scale production of MWCNTs.

The CVD process operates at low temperatures (<1000 °C) to produce CNTs with a high defect density (i.e., disorder), and the arc process operates at much higher temperatures (>3000 °C) to produce CNTs with a low defect density. Consequently, the CVD CNTs have a lower thermal stability and less desirable mechanical and electrical properties as compared with arc CNTs. For SWCNTs, a metal catalyst is necessary for synthesis, and the raw product can contain a high percentage of metal catalyst impurities, up to 50% of the total weight. When MWCNTs are synthesized using the arc process, no metal catalyst is required, and thus there is no metal contamination. Arc produces a low yield of CNTs, generally 20-60%; the remaining mass is fullerenes, multilayer polygonal carbon nanoparticles, graphitic nanoparticles, amorphous carbon nanoparticles, and, for

SWCNTs, metal catalysts. Generally, before arc CNTs are used they are purified with a gas- or liquid-phase chemical treatment or through physical separation such as centrifugation or filtration (Hou, Liu, & Cheng, 2008). Often CNTs are chemically treated to add surface functional groups to make them hydrophilic or for particle supports. Unfortunately, chemical oxidation induces defects in the CNTs and decreases their thermal stability. Physical and chemical destruction of the bonds occurs when the sp^2 orbitals are transformed to sp^3 orbitals, which are represented by non-hexagonal polygons (e.g., a pentagon). Physical destruction includes folding, tearing, twisting, or stretching of the CNT structure, and chemical or thermal destruction includes oxidation of the CNT or breaking of the C-C bonds.

Three MWCNTs representing the CNT treatment process included a raw (MW-O), purified (MW-P), and functionalized (MW-F) MWCNT. The MW-Os were obtained from Cheaptubes, Inc., and were used as received. The MW-Ps are the MW-Os purified with dilute HNO_3 to remove metal and amorphous carbon impurities. The MW-Fs are the MW-Ps further treated using microwave-assisted acid treatment (HNO_3/H_2SO_4) to add functional groups to the surface to make them hydrophilic (5.27% –COOH, 0.03% $–SO_3$) (Y. B. Wang, Iqbal, & Mitra, 2006). FTIR analysis revealed that no oxygenated functional groups were present for MW-O and MW-P. The zeta potential (pH 7) for MW-O, MW-P, and MW-F was -14.5, -8.73, and -50.30, respectively, which provides further evidence for the presence of oxygenated functional groups on MW-F. MWCNTs synthesized by the Arc method were obtained from Alfa Aesar in raw form and used as received (Cat. #42886). Two commercial functionalized MWCNTs were obtained from Cheaptubes, Inc. They contained –OH (MW-OH, 2.5%) and –COOH (MW-COOH,

3.7%) functionalities on the surface as listed by the manufacturer. MWCNTs that had similar properties but with varying diameters were obtained from Sigma Aldrich (Cat. #636835, 636509, 636525, 694185) to examine the thermal stability as a function of diameter. One Sigma Aldrich MWCNT (MW-15) was annealed (graphitized) under inert conditions at 2000 °C to represent graphitized CNTs (MW-15G). Mitsui MWCNTs (MW-Mitsui) are commonly used in toxicology studies and were obtained from the University of Rochester. Low-purity (as received) SWCNTs were obtained from Sigma Aldrich (Cat. #636797) and contained mixed chirality. Purified SWCNTs (>90% carbon, >75% SWCNTs, <10% Mo/Co) of >50% semiconducting chirality (6,5) were obtained from SouthWest NanoTechnologies, Inc.

Analytical Method Details

Samples were analyzed using a thermal optical transmittance (TOT) OC/EC instrument show in detail in Figure SI-7.1. As the sample is analyzed, the volatilized and combusted carbon travels to an oxidizing oven (MnO_2 catalyst at 870 °C), where it is transformed into carbon dioxide (CO_2). The CO_2 passes through a methanator (Ni firebrick–supported catalyst) and is reduced to methane (CH_4). The CH_4 signal is measured using a flame ionization detector (FID). At the end of the sample run, a known mass of CH_4 is injected into the sample oven to calibrate the FID; this known mass is used for quantification. An external standard of sucrose is used to validate the instrument calibration.

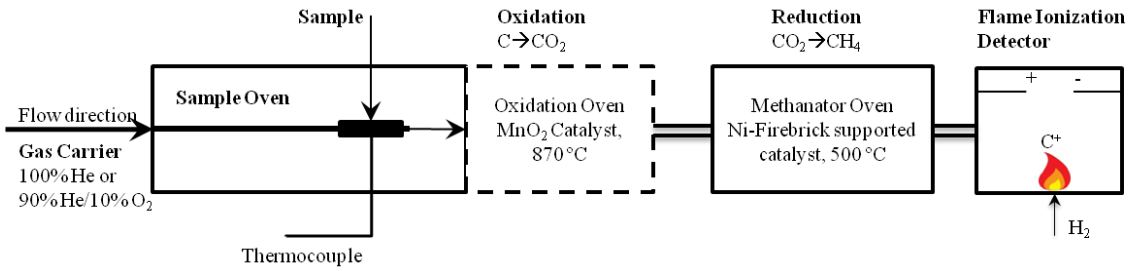


Figure SI-7.1. Instrument schematic.

Samples are first heated under non-oxidizing conditions (100% He carrier gas) to remove volatile OC. The sample chamber is then cooled, switched to oxidizing conditions (90% He/10% O_2), and heated again. For this instrument, temperatures range from 0 to 920 °C and are set by the user. OC that does not volatilize instead undergoes pyrolysis to become char or PEC, which has thermal properties similar to EC. Because the sample darkens as it chars and then lightens as the carbon evolves, optical correction is used to separate PEC (OC) from EC. A laser (632 nm) is used to measure the transmittance or reflectance of the sample throughout analysis, and the split between OC and EC is automatically placed where the transmission returns to its original value after the char has been removed. Optical correction is only valid if the assumption that OC and PEC will evolve at lower temperatures than EC is true.

For this study, ultra-high purity gases were used, and an oxygen/moisture trap (Restek #20601) was put in line with the helium tank. QFFs are constructed of pure quartz and have a 99.9% aerosol retention efficiency for 0.3-µm particles according to the ASTM standard method, D2986-95a ("ASTM Standard D2986-95a, 1999, "Standard practice for evaluation of air assaymedia by the monodisperse DOP (dioctyl phthalate) smoketest"," 1999). Because this study uses aqueous samples, the retention size cannot

be used to estimate the nominal pore size, and thus the performance of these filters for aqueous samples is unknown. Upon use of QFFs to filter the aqueous CNT suspensions, which were well dispersed, a black filtrate was evident, and thus filtration through QFF was deemed a failure for this method.

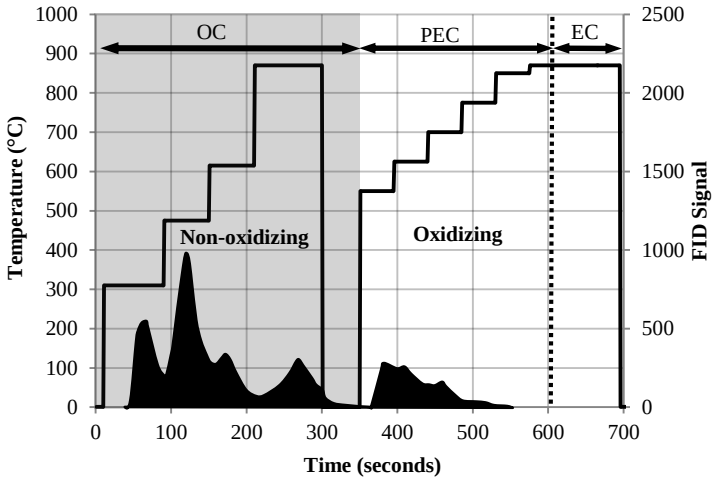


Figure SI-7.2. Thermogram example (sucrose) showing how OC, PEC, and EC are traditionally defined using the NIOSH temperature program. A 100% He carrier gas is used for non-oxidizing conditions, and a 90% He/10% O_2 carrier gas is used for oxidizing conditions.

Thermal optical analysis has been used frequently for analysis of black carbon in air and sediment samples, and because of the difficulty in analyzing black carbon against a carbon matrix, there is no concurrence on analytical method that should be used (Hammes et al., 2007; Watson et al., 2005). For high loadings of black carbon where the sample is too opaque to render a good optical reading, or non-homogenous filter loadings, such as with sediment samples, optical correction is not possible (Hammes et al., 2007; Schmid et al., 2001). We evaluated the validity of optical correction for MW-F CNTs using different split methods for OC/EC separation including two optical splits,

transmittance and reflectance, and a manual split that was placed between the two carrier gas conditions. The manual split is considered valid on the basis of the assumption that when only CNTs are present, all carbon evolving under inert and oxidizing conditions is OC and EC, respectively. Maximum temperatures of 675 °C and 910 °C were used during inert and oxidizing conditions, respectively. The MW-F sample was used to evaluate the OC/EC split methods because it is relatively free of amorphous carbon (99.9% CNTs) and is assumed to be ~100% CNTs. A control filter (blank) showed that no OC/EC contamination was present owing to exposure of the filters to the air during drying. The manual gas split was placed between transitioning carrier gas conditions (i.e., 100% He to 90% He/10% O_2), and the automatic transmittance/reflectance splits were based on optical correction as determined by the laser reading and analytical software. The gas split provided the most reliable value; approximately 97% of the TC was defined as EC (i.e., CNTs). The mass lost during the non-oxidizing phase may be attributed to the oxygenated surface defects, as it is assumed there is no amorphous carbon remaining on the surface of the CNTs. If no loss had occurred during the non-oxidizing phase, 100% of the TC would be CNTs. The transmission and reflectance optical correction splits fared worse, retaining only 80% and 64% of the CNT mass, respectively. This was because the split was located where the CNTs evolved, due to a very low optical reading from the blackness of the CNTs. Therefore, this finding means that when analyzing CNTs, a manual split, whether it is based on the carrier gases or a specified temperature, should be used.

Figure SI-7.3 shows a calibration curve for the MW-F stock solution for 2-100 μg, indicating a good analytical linear range. The method detection limit (MDL) for a

weak CNT in a simple matrix was calculated using the EPA Method with nine replicates of MW-F CNTs in a tap water-X-114 mixture (~0.85%). Using a mean mass of approximately 3.70±0.25 μg, an MDL (99%) of approximately 0.72 μg was calculated. The lower critical limit (LCL) and the upper critical limit (UCL) for 95% confidence were calculated to be 0.30 μg and 1.02 μg, respectively. The limit of detection (LOD) and limit of quantitation (LOQ) were calculated to be approximately 1.8 μg and 2.5 μg, respectively.

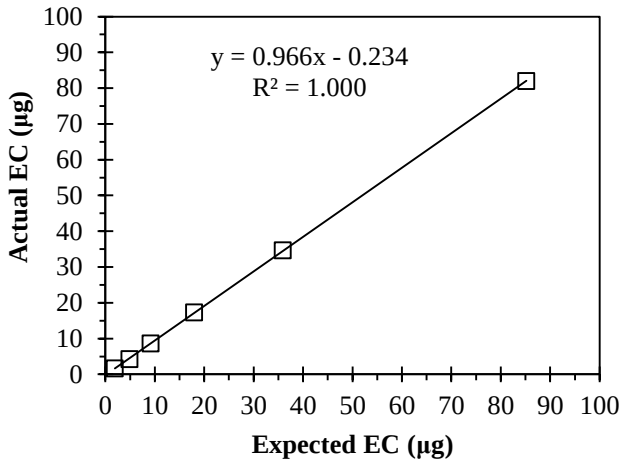


Figure SI-7.3. Calibration curve for MW-F CNT stock solution (0.85 g/L) using a manual gas split.

CNT Thermal Behavior

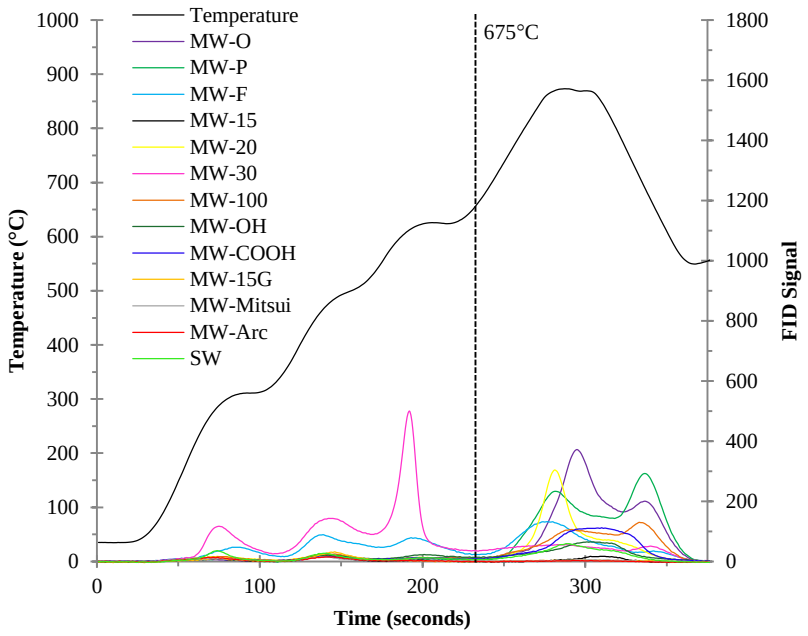


Figure SI-7.4. Thermograms of CNTs under non-oxidizing conditions using the NIOSH temperature program.

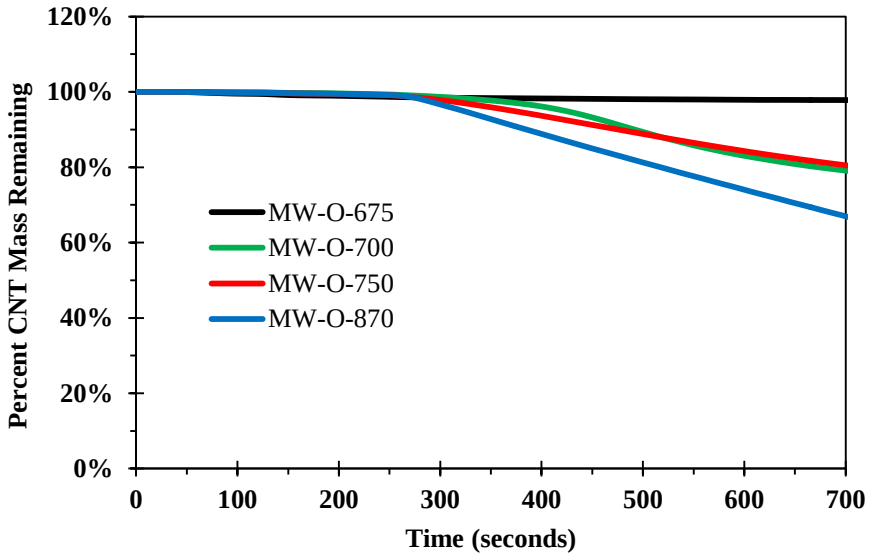


Figure SI-7.5. Percent MW-O mass remaining after analysis under non-oxidizing conditions at various maximum temperatures.

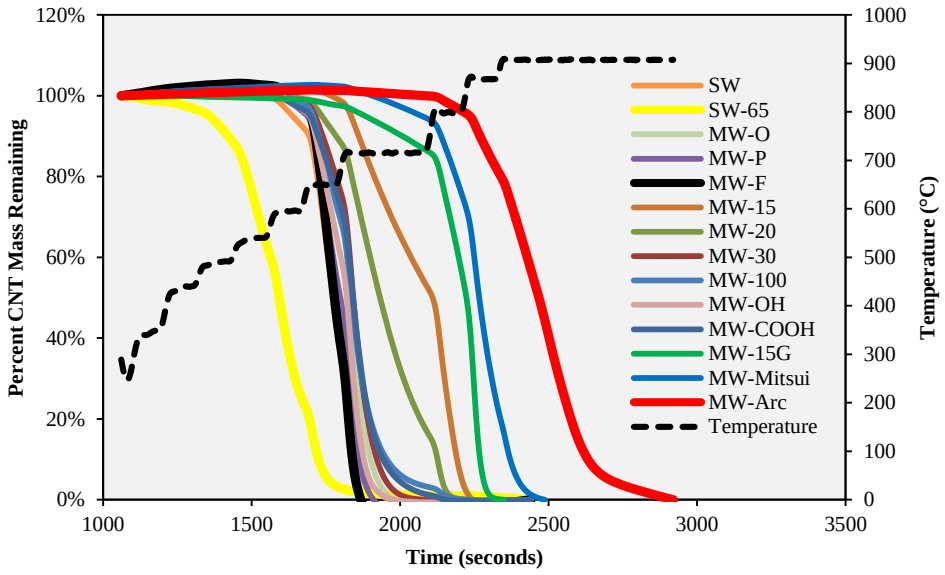


Figure SI-7.6. Mass loss curves of CNTs under oxidizing conditions.

Raman Spectroscopy

Figure SI-7.7a shows the Raman spectrograms of the D and G bands for a robust (MW-P) and a weak (MW-Arc) MWCNT. The robust MWCNT had a large D-band peak compared to the weak MWCNT, and its I_D/I_G ratio was much larger. SWCNTs (not shown) had similar ratios as the MW-Arc, but because SWCNTs are not as stable as the MW-Arc, the I_D/I_G ratio alone cannot be used to estimate the thermal stability of the CNTs in a sample. However, combined with the RBM (Figure SI-7.7b), Raman spectroscopy can be a powerful tool for characterization of the thermal stability of CNTs in an environmental or biological sample.

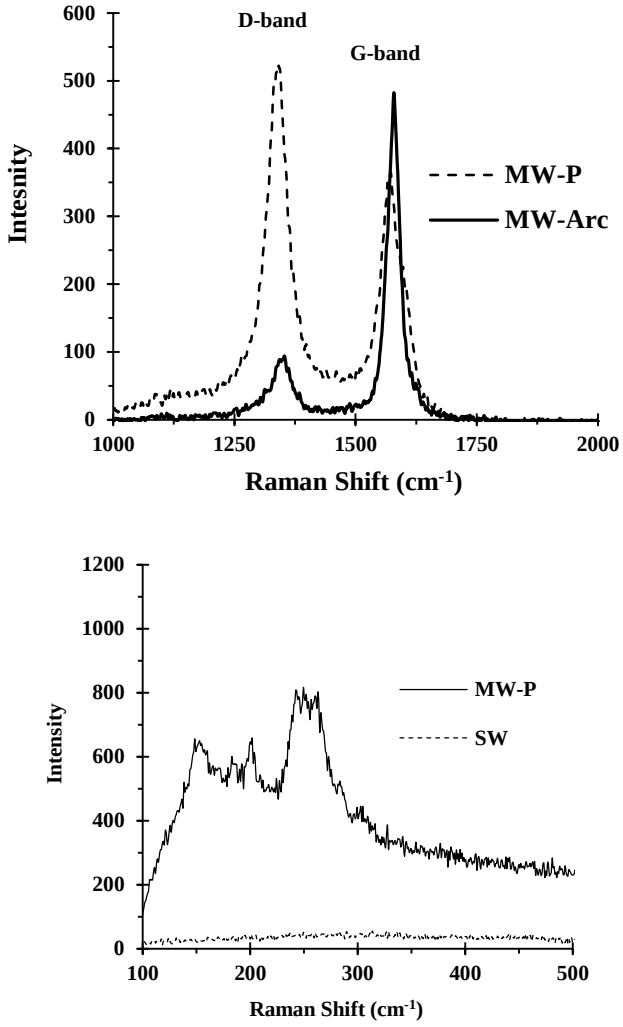


Figure SI-7.7. Raman spectroscopy of (a) MW-Arc and MW-P D-band and G-band peaks and (b) of the radial breathing mode for SWCNTs (SW) and MWCNTs (MW-P). SWCNTs (not shown) have a very similar D-band/G-band peak ratio as the MW-Arc.

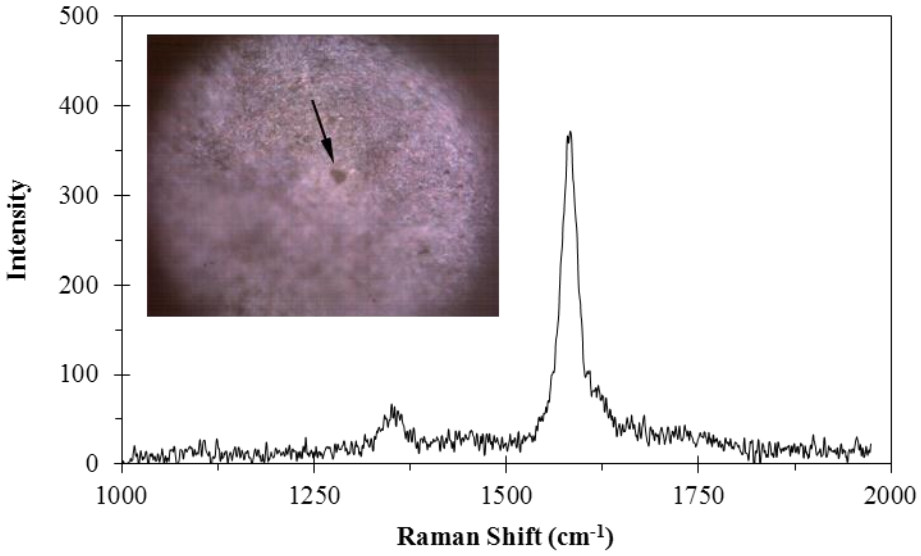
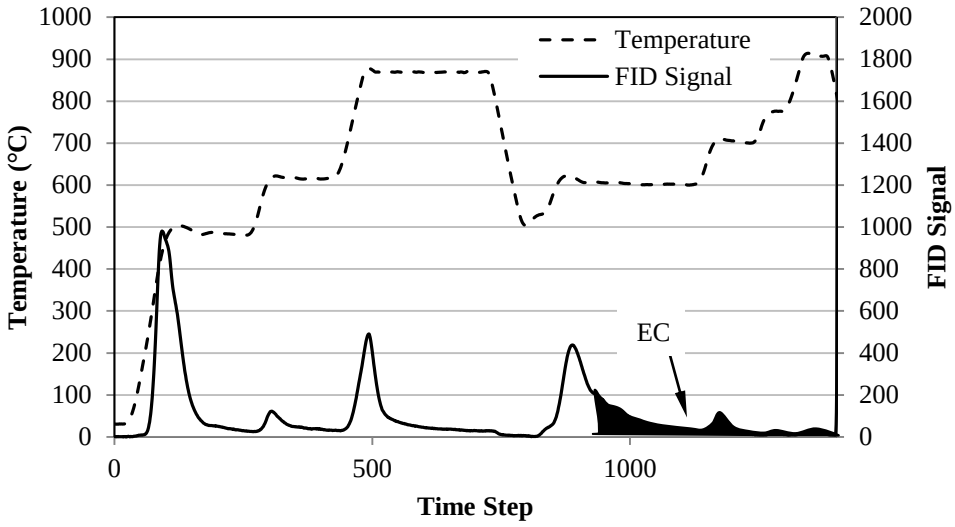


Figure SI-7.8. Raman spectroscopy of MW-Mitsui in a digest Cyanobacteria matrix loaded onto a quartz-fiber filter. Inset: Raman microscope image shows the CNT aggregate (indicated by arrow) used to gather the Raman spectrum.

(a)



(b)

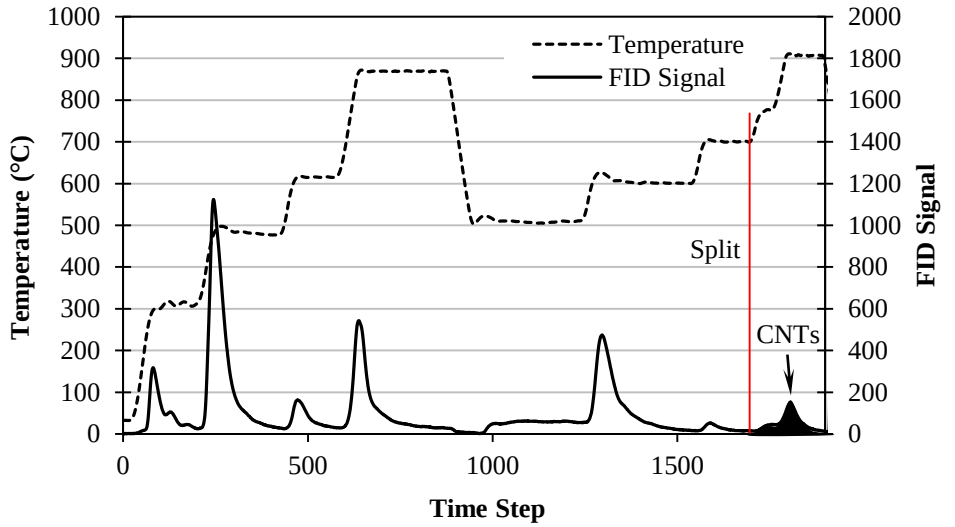


Figure SI-7.9. Thermograms of (a) urban air and (b) urban air spiked with 3 µg MW-Mitsui CNTs. The EC in (a) was determined by conventional air analysis using optical correction, and the CNTs in (b) by a manual split as discussed in this study.

Table SI-7.1. *Quantification methods for carbon nanotubes*

Method	Matrix	Application	Advantages	Disadvantages	Reference
Near-infrared fluorescence (NIRF)	Ultrapure water, D_2O	Extracted SWCNT samples	Low detection limit ~1 µg	Only valid for semiconducting SWCNTs; CNTs must be fully dispersed; clean matrix only in D_2O	(H. Huang et al., 2011; O'Connell et al., 2002)
Ultraviolet-visible light near infrared absorbance (UV-VIS NR)	Ultrapure water	Stock suspensions in water; extracted samples	Simple, economic, readily available	Clean matrix only with H_2O; good dispersion required	(Bahr et al., 2001; Z. F. Li et al., 2006)
Fluorescence probe labeling	Yeast cells	Toxicity studies; fate and transport	Excellent detection limit (2.5 fg); no background interferences; not biased to CNT type	Difficult; expensive; CNTs must be labeled first; may alter physicochemical surface properties	(Xiao et al., 2006)
Isotopic labeling	Lumbriculus variegates Peat	Toxicity studies; fate and transport	Good for any type of matrix, no CNT bias	Difficult, expensive, isotope labeled CNTs must be used	(Petersen et al., 2008; L. W. Zhang et al., 2011)
Gel electrophoresis	Tissue cells	Liquid samples	Very good detection limit (5 ng); no CNT bias	Low volume samples (60 uL max); internal calibration needed each time because of variation in gel, light intensity, and scan	(R. H. Wang et al., 2009; R. H. Wang et al., 2011)
Thermogravimetric analysis (TGA)	CNT only	Characterization of dry CNTs	Simple, economic	Only valid for CNTs by themselves	(Pang et al., 1993)
Advanced[1] TGA coupled with MS (TGA-MS)	Marine sediments	Environmental matrices	Good separation of CNTs from organic and elemental carbon	Detection limit ~10 ug; complex instrument	(Plata et al., Submitted 2011)
Temperature programmed oxidation (TPO)	CNT only	Dry CNT samples	Simple, economic	CNT only matrix	(Alvarez et al., 2001; Herrera & Resasco, 2003)
Chemothermal oxidation, 375 °C (CTO-375)	Marine sediments	CNTs in environmental matrices	Simple, economic, can separate CNTs from black carbon	Recovery is dependent on type of CNT (e.g., low for CNTs with high defect	(Sobek & Bucheli, 2009)

				density and/or small diameter)	
Advanced[2] CTO	Rat lung tissue	Highly graphitic CNTs in complex matrices	Simple, economic, readily available	Can't distinguish between CNTs and carbon background unless a very stable CNT is used (i.e., low defect density)	(Tamura et al., 2011)
Thermal optical transmittance (TOT)	CNT only, diesel particulate, NOM in water	Stock suspensions, CNTs in environmental matrices	Simple, economic, valid for all CNT types; good detection limit (1 µg); separation from black carbon	Optical separation only valid for homogeneously loaded samples	(Hyung et al., 2007; Myojo et al., 2009; Ono-Ogasawara et al., 2009)

[1]Hydrogen assisted thermal degradation was used

[2]Pre-oxidative steps were employed to remove background organic/elemental carbon

Table SI-7.2. *CNT I_D/I_G ratios and the temperature at 50% CNT mass loss under oxidizing conditions*

CNT ID	I_D/I_G	Oxidation Temperature (°C)[a]	CNT Thermal Classification
MW-O	1.3 ± 0.10	715	Thermally "Weak"
MW-P	1.4 ± 0.12	675	
MW-F	1.5 ± 0.12	650	
MW-15	0.78 ± 0.050	778	
MW-20	1.3 ± 0.10	716	
MW-30	1.2 ± 0.090	715	
MW-100	1.2 ± 0.16	715	
MW-OH	1.2 ± 0.18	717	
MW-COOH	1.2 ± 0.19	715	
SW	0.080 ± 0.060	651	
SG-65	0.13 ± 0.90	593	
MW-15G	0.52 ± 0.023	844	Thermally "Strong"
MW-Mitsui	0.10 ± 0.014	867	
MW-Arc	0.20 ± 0.060	907	

Detection of Graphene

Graphene is essentially a SWCNT unrolled or a single sheet of graphite thickness of one carbon atom. As such, the same quantification method developed for CNTs, PTA, can be applied to graphene. Figure SI-7.10 shows the fraction of graphene remaining as a function of time and temperature under oxidizing conditions (90% O_2/10% He). GNPs had a 50% mass loss temperature of approximately 950 °C, which classifies it as strong. GO, on the other hand, had a 50% mass loss temperature of approximately 750 °C, which puts it in the weak category, and, as a result, makes it much more difficult to detect GO in complex matrices using PTA. This weakness is due to the large amount of oxygen (1:1 O:C ratio). There was also a significant mass loss during the inert phase for the GO, which was attributed to the oxygenated functional groups. The I_D/I_G ratios for GNP and GO were 0.24 ± 0.08 and 1.0 ± 0.05, respectively, which agrees with the thermal stability classifications. PTA is ideal for GNPs and other non-oxidized forms of graphene, but oxygenated forms will require reduction pretreatments in order to utilize the PTA method.

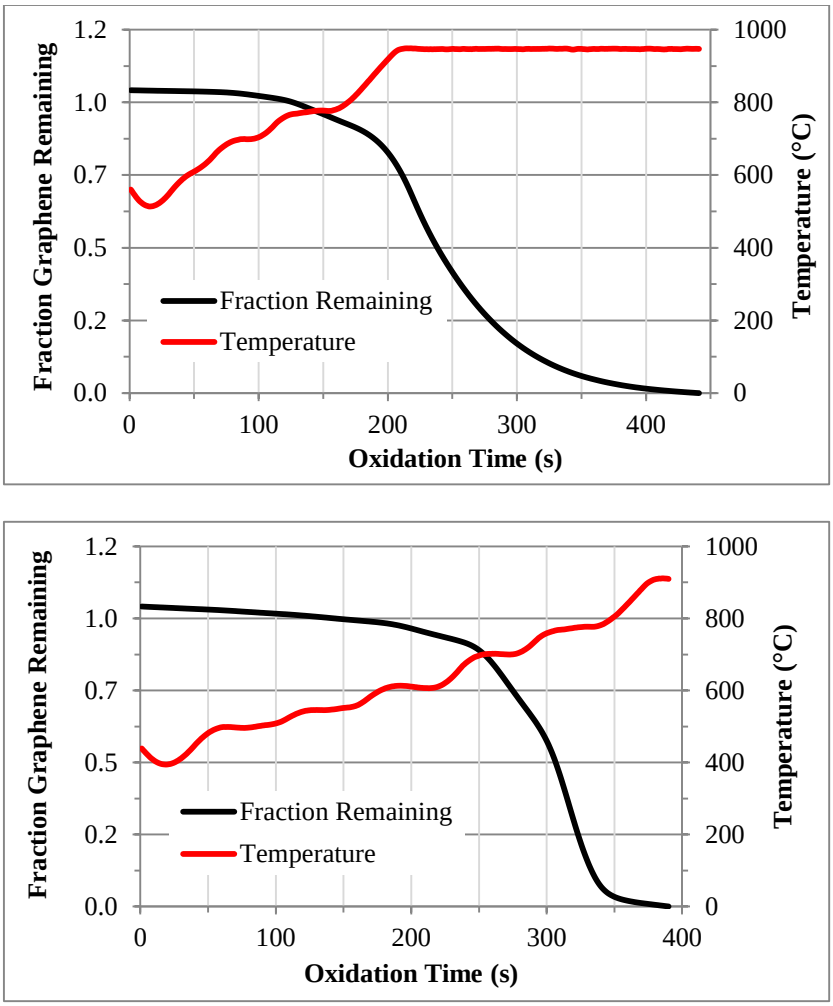


Figure SI-7.10. PTA analysis of GNP and GO – Fraction of graphene remaining as a function of oxidation time and temperature for (a) GNPs and (b) GO.

CHAPTER 8

EXTRACTION OF CARBON NANOTUBES FROM COMPLEX ORGANIC MATRICES WITH APPLICATION TO RAT LUNG TISSUE*

*To be submitted: Doudrick, K., Corson, N., Oberdörster, G., Eder, A., Herckes, P., Halden, R., Westerhoff, P. Extraction of carbon nanotubes from complex organic matrices with application to rat lung tissue. *Nanotoxi*.

Abstract

Various treatment methods including Solvable (2.5% sodium hydroxide/surfactant mixture), ammonium hydroxide, nitric acid, sulfuric acid, hydrochloric acid, hydrofluoric acid, hydrogen peroxide, and proteinase K were examined for their ability to extract carbon nanotubes (CNTs) from rat lung tissue. The defining metric was the percent recovery of CNTs from rat lung tissue after treatment, which was quantified using programmed thermal analysis (PTA). The recovery was affected by the damage done to the CNTs as a result of harsh treatment methods and the amount of interfering carbon from the rat lung tissue as a result of incomplete digestion. Solvable emerged as the optimal treatment method because it (1) digested rat lung tissue while keeping the CNTs intact, (2) maintained a stable centrifuge pellet during sample washing, and (3) did no damage to the PTA instrument. Although Solvable was the optimal method, a small amount of interfering carbon (~0.2 µg) still remained, and the addition of a second treatment step using pro K was necessary to remove this. When approximately 3 µg of CNTs were spiked into a whole rate lung and then extracted using the two-step digestion method, a percent recovery of 93±15% was obtained. This extraction method is ideal for *in vivo* studies, and it is applicable to other complex matrices as well (e.g., wastewater sludge).

8.1 Introduction

Carbon nanotubes (CNTs) are steadily becoming a viable component in consumer products, drug-delivery systems, composite materials, and electronics (Endo, Strano, & Ajayan, 2008). Their increased demand and production warrants consideration of their environmental and human health impacts. Inhalation and dermal exposure from CNT manufacturing and through CNT product degradation poses the highest risk for CNT exposure, with inhalation being the most probable pathway (Aschberger et al., 2010; Han et al., 2008; Kuhlbusch, Asbach, Fissan, Gohler, & Stintz, 2011; Maynard et al., 2004). Typically, rats are used as model organisms for *in vivo* studies that look at the inflammatory response caused by CNTs. There have been a number of studies that explore the effect of CNTs, but currently no information exists on the clearance rates of CNTs from the lung (e.g., dose metrics). This is mainly due to the lack of methods available for extracting CNTs from complex matrices (e.g., tissue, wastewater) (Petersen & Henry, 2012).

Chemical digestion methods are commonly used to extract metals from soils, sediments, sludges, plants, and animal tissues (USEPA, 1995). These methods use oxidant, acidic, and alkaline chemicals to break chemical bonds of the solid matrix through hydrolysis or oxidation (i.e., dissolves solid). Common chemicals used to digest samples include nitric acid (HNO_3), sulfuric acid (H_2SO_4), hydrofluoric acid (HF), hydrochloric acid (HCl), hydrogen peroxide (H_2O_2), alkalis (e.g., sodium hydroxide), and enzymes (e.g., proteinase K). For CNTs in complex matrices, the major challenge is digesting the matrix while keeping the CNTs intact. Unfortunately, some of the chemicals used in standard methods, such nitric acid and sulfuric acid, are known to break carbon-

carbon bonds in CNTs, oxidize the surface, or degrade the CNTs to CO and CO_2 (Peng & Liu, 2006; I. D. Rosca et al., 2005; Tchoul, Ford, Lolli, Resasco, & Arepalli, 2007).

For this study, we use a previously developed method to quantify CNTs, called programmed thermal analysis (PTA), that utilizes the unique thermal stability of CNTs (K. Doudrick, Herckes, & Westerhoff, 2012). Although CNTs are one of the most thermodynamically stable forms of carbon, these digestion processes may result in carbon mass loss and/or a decrease in the thermal strength. For lung tissues, alkalis and enzymes have been shown to effectively dissolve the tissue while keeping minimizing damage to graphitic-like carbon (Griffis et al., 1983; Searl & Cullen, 1997).

The aim of this study was to develop a method for extracting CNTs from rat lung tissue. To achieve this we wanted to dissolve the rat lung tissue while maximizing CNT recovery. Commonly used acids, alkalis, oxidants, and enzymes were examined. The percent recovery of CNTs from rat lung tissue was quantified using programmed thermal analysis (PTA) (K. Doudrick et al., 2012). In this study, two types of multiwalled CNTs (MWCNT) were used to represent the broad thermal stability spectrum of CNTs (K. Doudrick et al., 2012). The thermal fingerprint of the CNTs obtained during PTA was important for determining the change in the thermal stability of the CNTs after treatment. Raman spectroscopy was also used to determine if CNT structural damage was evident (Osswald, Havel, & Gogotsi, 2007). For application to rat lung tissue, we considered the treatment method to be unsuccessful if it (a) destroyed CNTs or (b) did not effectively dissolve the rat lung. The results of this study will expand the knowledge on carbon nanomaterial extraction from complex matrices, and it will have an impact on carbon nanomaterial inhalation toxicity studies.

8.2 Experimental Methods

Materials

Two types of CNTs were used to represent a thermally weak (W-CNT) and strong (S-CNT) CNT, as determined previously, to represent the thermal stability upper and lower of the broad spectrum of CNTs (K. Doudrick et al., 2012). The W-CNT (Cheaptubes, Inc., MWCNT, 20-30 nm diameter, 10-30 μm length as reported by manufacturer) and the S-CNT (Mitsui & Co., MWCNT, 40-50 nm diameter, 10-20 μm length as reported by manufacturer) were suspended in ultrapure water with the aid of a dispersion media similar to that used in rat lung CNT exposure studies (Porter et al., 2008). The dispersion media consisted of bovine serum albumin (Sigma Aldrich A-2058, >97%), 1,2-dipalmitoyl-*sn*-glycero-3-phosphcholine (DSPC, Sigma Aldrich P-0763, >99%), and sodium chloride (NaCl, Sigma Aldrich S7653, >99.5%). Chemicals used for digestion included, 67-70% (15.8 M) HNO_3 (EMD NX0409-2), 98% (18.4 M) H_2SO_4 (JT Baker 6902-05), 30% (9.8 M) H_2O_2 (JT Baker 5155-01), 32-36% (11 M) HCl (EMD HX0603-3), 40% (22.6 M) HF (JT Baker 6904-05), 28-30% (14.8 M) NH_4OH (Sigma Aldrich 320145), Solvable (Perkin Elmer; 2.5% NaOH, 2.5-10% N, N-dimethyldodecylamine N-oxide, 2.5-10% polyethylene glycol trimethylnonyl ether), proteinase K (20 g/L) and ATL buffer (QIAGEN 19131, 19076). The ATL buffer composition is mostly propriety; the known components include sodium dodecyl sulfate (2.5-10%) and edetic acid. Rat lungs were obtained from male Sprague Dawley rats (Rockland, Inc.), dried at 110 °C, and then ground using an agate pestle and mortar.

Preparation of CNT Suspensions

First, 10 mL of dispersion medium (DM) was prepared using 3.99 mL 0.9% NaCl, 6 mL of BSA (1 mg/mL in 0.9% NaCl), and 0.01 mL of DSPC (10 mg/mL in ethanol, made fresh each stock batch). CNTs were added to obtain a concentration of 0.5 mg/mL (5 mg). The dispersion was stirred briefly and then probe sonicated (Misonix Sonicator 4000, ¼ inch tip) in an ice bath for 10 minutes at 50 % power.

Digestion of CNTs and Rat Lung Tissue

The procedure for digesting rat lung tissue and CNTs is outlined in Figure 8.1. Briefly, S-CNT, W-CNT, or rat lung tissue samples were placed in a 2 mL plastic centrifuge tube and the appropriate chemical was added. For the CNTs, approximately 25 µg were added to 1 mL of chemical. The pro K mixture was prepared by mixing 20 µL pro K, 180 µL of buffer ATL, and 800 µL of water (total volume = 1 mL). For chemical digestion screening for rat lung tissue, approximately 10 mg of dried rat lung tissue was added to identical amounts of chemical as that for the CNTs. For recovery experiments, whole lung tissue was dried in a furnace at ~110 °C, placed in a 15 mL centrifuge vial, and 5 mL of chemical was added. For all experiments, samples were heated at 60 °C and mixed intermittently (30 s on at 700 RPM, 5 min off) for 24 hrs. For the rat lung tissue, initial success was deemed by visual examination; those samples that were dissolved (i.e., no visible tissue remaining) were considered successful, while those that still had tissue remaining were deemed unsuccessful. After treatment, the CNTs were washed three times with a salt solution (e.g., 0.1 M potassium nitrate to promote aggregation) and water via centrifugation at 25,000 G's for 15 minutes. Acidic and alkaline samples were

neutralized with 1 M NaOH and 1 M HNO_3 during the initial washing steps (~30 µL was added). After washing, CNT pellets were loaded onto pre-fired quartz-fiber filters (QFF), wrapped in pre-fired aluminum foil, dried in air, and then dried in a furnace at 90 °C.

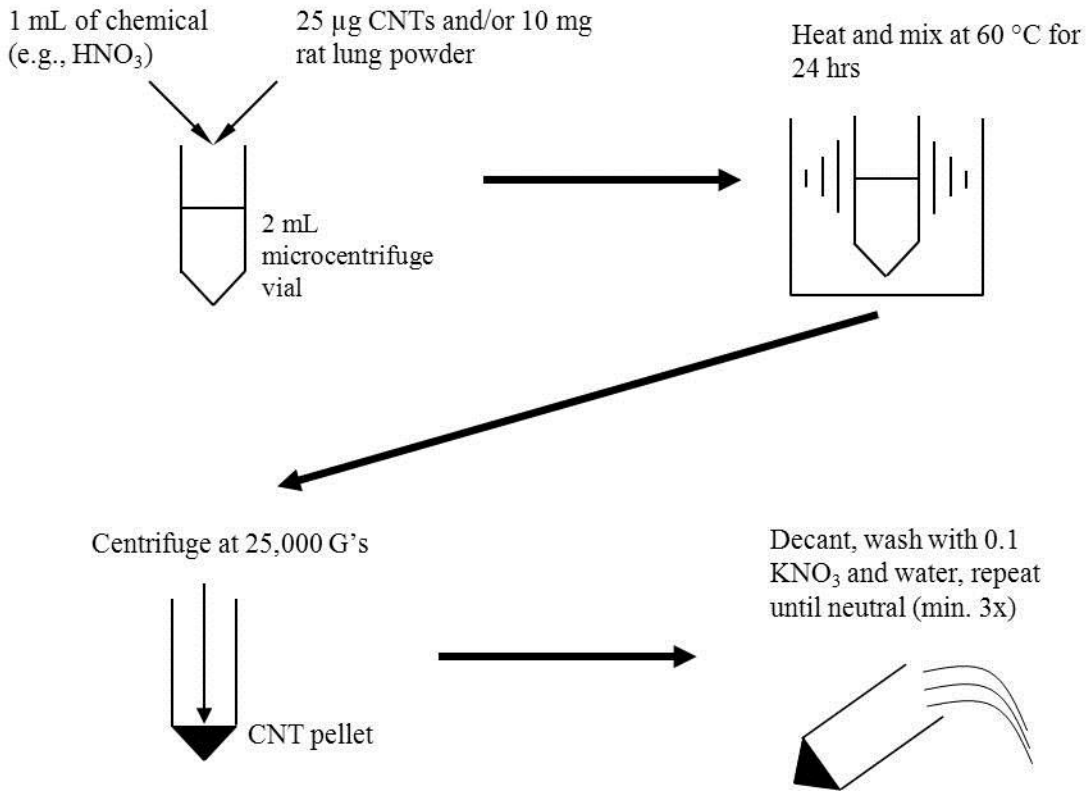


Figure 8.1. Digestion procedure for rat lung tissue and CNTs.

Programmed Thermal Analysis

PTA was used to determine the thermal stability of the treated CNTs under inert and oxidizing conditions, and to quantify the CNTs; its operation is described in detail elsewhere (K. Doudrick et al., 2012). Briefly, samples were heated using a CNT specific temperature ramp program (Figure SI-8.1) under 100% He and then heated under

90%He/10%O_2. The maximum temperature under inert conditions was set to avoid loss of W-CNTs, as found previously (K. Doudrick et al., 2012). The inert heating process is used to remove any organic carbon remaining after digestion, and the oxidizing heating program is used to develop the CNT thermal fingerprint. The time required to reach 50% CNT mass loss was used to determine the effect of the digestion methods on the thermal fingerprint of the CNT.

Raman Spectroscopy

Raman spectroscopy was performed on a custom-built instrument in 180° geometry. The sample was excited using a 532-nm laser with 100-mW maximum power, which was controlled using neutral density filters. The data were collected using an Acton 300i spectrograph and a back thinned Princeton Instruments liquid nitrogen cooled CCD detector with a spatial resolution <1 μm and spectral resolution of ~1 cm^{-1}. The CNT defect peak (D-band) and the graphitic peak (G-band) were analyzed at four different points for each sample. The average I_D/I_G ratio was calculated.

8.3 Results and Discussion

CNT Thermal Analysis

PTA was used to evaluate the effect of various chemicals on CNTs. Figure 8.2 shows the CNT percent recovery for S-CNTs and W-CNTs. Solvable resulted in the highest recovery for both CNT types. For some of the digestion methods, good recovery was not possible because the CNTs could not form a stable pellet throughout the washing steps, or they adhered to the sides of the centrifuge vials. H. peroxide and hydrochloric

acid samples stuck to the centrifuge vials and did not form a stable pellet resulting in a loss of CNTs during decantation. Hydrofluoric acid, pro K, and water samples formed semi-stable pellets, meaning there was still some slight sticking to the centrifuge tube sides or the pellet was not fully compact. Solvable and ammonium hydroxide formed very solid pellets without sticking to the vials; although, pellet formation decreased for ammonium hydroxide during the washing steps. For the samples that did not produce more compact pellets, increasing the centrifugation speed (up to 25,000 G's) or increasing the time (up to 1 hr) did not improve the pellet formation. A functionalized version of the W-CNT (F-CNT) was used to determine the applicability of centrifuging using the most optimal method, Solvable. Even though the functionalized W-CNTs are very stable in water, pellet formation was identical to the non-functionalized W-CNTs (Figure SI-8.2), indicating the effectiveness of using Solvable for hydrophilic CNTs as well. Because of the issues forming pellets during the washing steps, the recovery results are not a true indicator of the damage induced by the different methods. As such, other analyses, such as thermal fingerprint analysis and Raman spectroscopy, were completed to validate the recovery results.

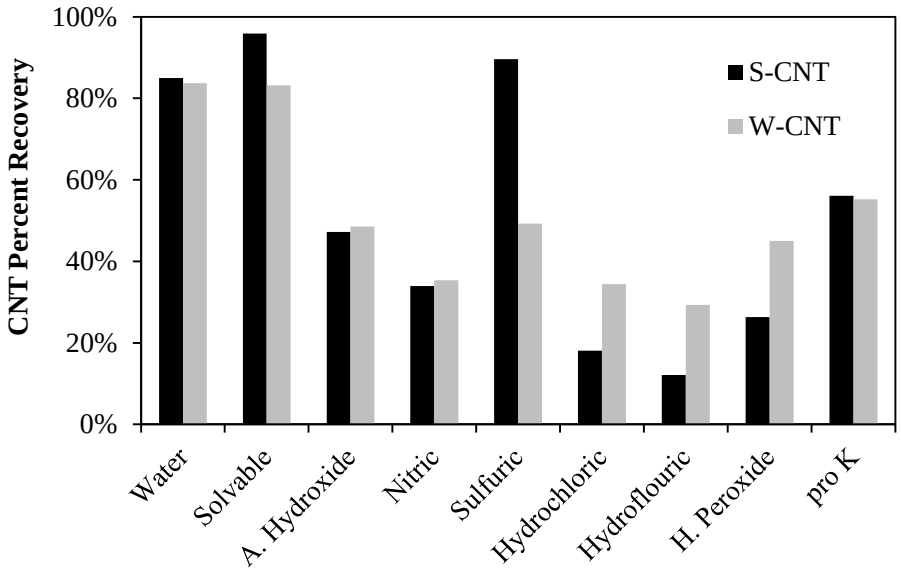


Figure 8.2. Percent recovery for S-CNTs and W-CNTs following various digestion methods (single run).

The thermal fingerprints of the CNTs (Figure SI-8.3) were analyzed to determine if the chemical digestion methods had an effect on the oxidation temperature. This is important for two reasons: (1) a significant decrease in oxidation temperature may indicate mass loss during the digestion, and (2) decreasing the oxidation temperature of the CNTs results in an increase in interference with matrices containing carbon with low oxygen content (i.e., more thermally stable). Figures 8.3 and 8.4 show the peak fraction of the total CNT area for each temperature step and the time required for 50% mass loss after treatment under oxidizing conditions with various methods for an W-CNT and a S-CNT, respectively. Each temperature step (500, 550, 600, 650, 700, 750, 800, 910 °C) corresponds to a peak (peaks 1–8) in thermal fingerprint of the CNT (e.g., Figure SI-8.3). The untreated sample (i.e., the raw CNT analyzed as a dry powder) was used as a control. W-CNTs evolved during peaks 1–6, and S-CNTs evolved during peaks 5–8. The

normalized area of each peak gives a good idea of the change in the thermal fingerprint of the CNT after each treatment method. The key factor to thermal stability was the availability of oxygen on the surface of the CNT.

For both CNT types, the water sample, containing only CNTs and water, was one of the weakest CNT in terms of thermal stability. This was attributed to the dispersant, which remained wrapped around the CNT during washing and contributed oxygen during the thermal analysis. For other methods, the dispersant was destroyed (i.e., oxidized, hydrolyzed) during the treatment processes. Similarly, the F-CNT was the weakest CNT overall due to the large amount of oxygenated surface (~6%). The addition of oxygenated functional groups caused a shift in the maximum peak oxidation temperature of 150 °C (i.e., peak 6 to peak 3).

For W-CNT samples that had a significant decrease in the time to 50% mass loss (e.g., hydrogen peroxide), the maximum peak oxidation temperature was shifted 50 °C (i.e., peak 6 to peak 5), and in general, an increase in the CNT fraction evolving at lower temperatures. These results show that Solvable, hydrofluoric acid, hydrochloric acid, and pro K treatments had minimal effect on the W-CNT oxidation temperature. Ammonium hydroxide, sulfuric acid, nitric acid, and hydrogen peroxide did the most damage to the W-CNT.

For S-CNT samples that had a marked decrease in the time to 50% mass loss (e.g., sulfuric acid), the peak oxidation temperature remained at 910 °C, but the amount of CNT evolving during that step (i.e., peak 8) decreased. Solvable, nitric acid, hydrofluoric acid, hydrogen peroxide, and pro K did not significantly affect the oxidation temperature of S-CNTs. Ammonium hydroxide, sulfuric acid, hydrochloric acid

treatments induced some damage to the S-CNT structure, but not enough that the oxidation temperature was shifted significantly.

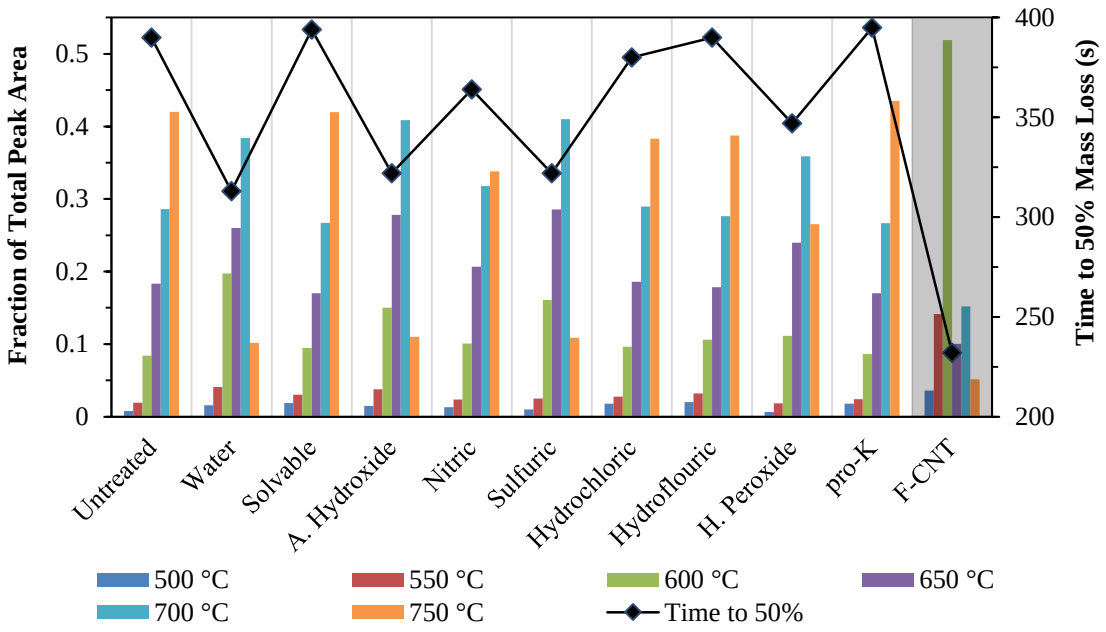


Figure 8.3. Peak fraction of the total CNT area for each temperature step and time required for 50% mass loss for a W-CNT under oxidizing conditions after treatment with various methods. Grey shaded area is the functionalized W-CNT (F-CNT) after treatment with Solvable.

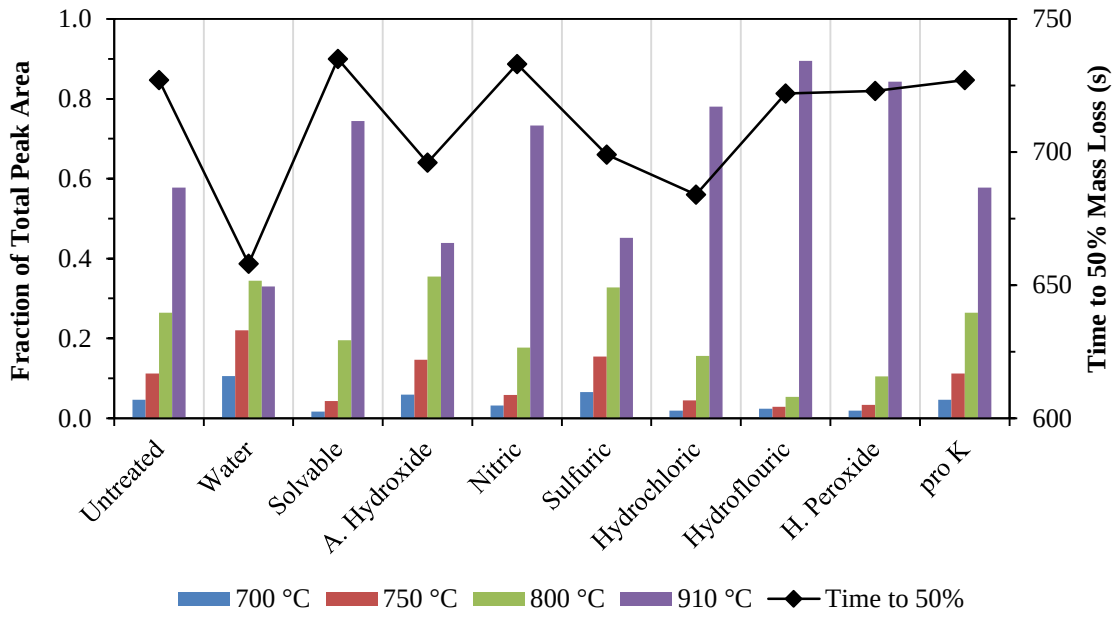


Figure 8.4. Peak fraction of the total CNT area for each temperature step and time required for 50% mass loss for an S-CNT under oxidizing conditions after treatment with various methods.

For both CNT types, ammonium hydroxide and sulfuric acid were the most detrimental to the CNT, and the slight differences between the other treatments and both CNTs was probably due to the difference in initial defects and the way the different treatments react with defects. For example, a mixture of sulfuric and nitric acids has been shown to first attack available defects and then create new defects (Chiang, Lin, & Chang, 2011). Beyond CNT damage, some of the harsher treatments resulted in damage to the PTA instrument tubing and metal from residual acids/alkalis (e.g., sulfuric acid, nitric acid). While this risk could be minimized with additional washing steps, this decreases the recovery of CNTs.

Raman Spectroscopy of CNTs

Raman spectroscopy has been shown to be a promising characterization tool for CNTs with spectral peaks that are specific to CNTs or graphite and to no other form of carbon (Dresselhaus et al., 2005). Between 1300 and 1600 cm^{-1}, there are two distinct peaks for CNTs, called the D-band and the G-band. The D-band is present because of defects or disorder present within the CNT sample and increases in intensity with increasing disorder. The G-band is the graphitic band, and a higher, narrower peak indicates a more ordered CNT. The ratio of the D-band to the G-band (I_D/I_G) is often used to determine the defectiveness of CNTs, and it may be possible that this ratio can be used to estimate the thermal stability of CNTs (Behler et al., 2006; Bhalerao et al., 2008; J. Chen et al., 2007; Kim et al., 2003; D. K. Singh et al., 2010; Tran et al., 2007).

Figure 8.5 shows the I_D/I_G ratio for S-CNTs and W-CNTs after treatment with various chemicals. For the S-CNTs, hydrochloric acid and ammonium hydroxide were the only treatments that had any statistical difference from the control, which is in good agreement with the thermal analysis. For example, ammonium hydroxide increased the I_D/I_G ratio from ~0.3 to 0.4, which suggests that some damage occurred but not enough to have a marked effect on the oxidation temperature. For the W-CNTs, there was not a change in the I_D/I_G ratio for any of the treatment methods. The absence of change is expected because the W-CNTs already have a high initial defect density, which leaves little room for the formation of additional defects (Schonfelder et al., 2012). Although Raman is a useful tool to detect CNTs and determine the oxidation peak temperature of the CNTs (K. Doudrick et al., 2012), it is not sensitive enough to evaluate the treatment

methods for CNT loss, and it should only be used to complement the thermal results of S-CNTs.

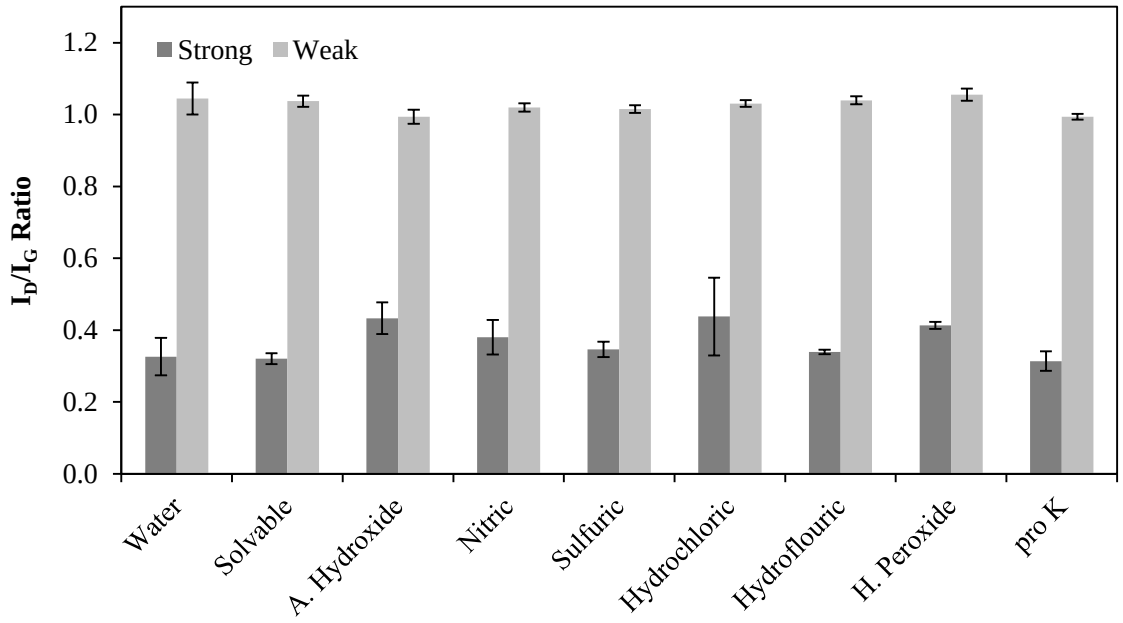


Figure 8.5. I_D/I_G ratios obtained from Raman spectroscopy for CNTs after treatment with using various chemicals (60 °C for 24 hrs).

Rat lung tissue digestion

When dissolving organic matter (e.g., tissue) with acids, alkalis, oxidants, or enzymes, generally some thermal energy beyond room temperature is needed for activity to occur in a timely manner. Typically the boiling point of the liquid (i.e., temperature at reflux) generates the highest activity; this can range from high (e.g., H_2SO_4 – 337 °C) to low (e.g., HCl – 84 °C) temperatures. However, at higher temperatures, controlling the activity of the treatment becomes more difficult (i.e., reacts too fast). For this study, treating CNTs at the respective reflux temperatures resulted in major CNT loss for strong

acids and oxidants (e.g., H_2SO_4, H_2O_2). As a results, the rat lung tissue treatment methods were evaluated at a mild temperature, 60 °C.

A visual inspection of the samples before and after treatment was used to determine the efficacy of the treatment methods (Figure 8.6). All alkalis (Solvable, ammonium hydroxide, tetramethylammonium hydroxide (TMAH), potassium hydroxide/ethanol (KOH-EtOH)) were effective at dissolving the tissue within the first hour. However, KOH-EtOH and TMAH are not discussed further because KOH-EtOH melted the QFFs during PTA, and TMAH produced triethylamines upon heating, which makes its use non-ideal due to the offensive odor that is produced. The resultant liquid for the alkalis was transparent yellow and a small pellet was formed consisting of non-digestible carbon (Figures 8.6a and 8.6b). Nitric acid was very effective dissolving the tissue within 30 minutes, resulting in a transparent yellow solution with no obvious pellet (Figure 8.6c). Sulfuric acid, hydrochloric acid, and hydrofluoric acid all dissolved the tissue, but the result was a dark liquid consisting of high refractory soluble carbon and black particulates remained (Figures 8.6d-8.6f), indicating incomplete digestion. Hydrogen peroxide dissolved most of the tissue, but white visible particulates remained after 24 hrs, which formed a large pellet of undigestable carbon (Figure 8.6g). Of the enzymes examined, only pro K (w/ATL buffer) was successful at dissolving the tissue in the allotted time (Figure 8.6h). Without ATL buffer present, pro K showed no activity within 24 hrs, indicating the need for activation. Of the various chemicals examined for dissolving rat lung tissue, Solvable, ammonium hydroxide, nitric acid, and pro K were deemed the most successful.

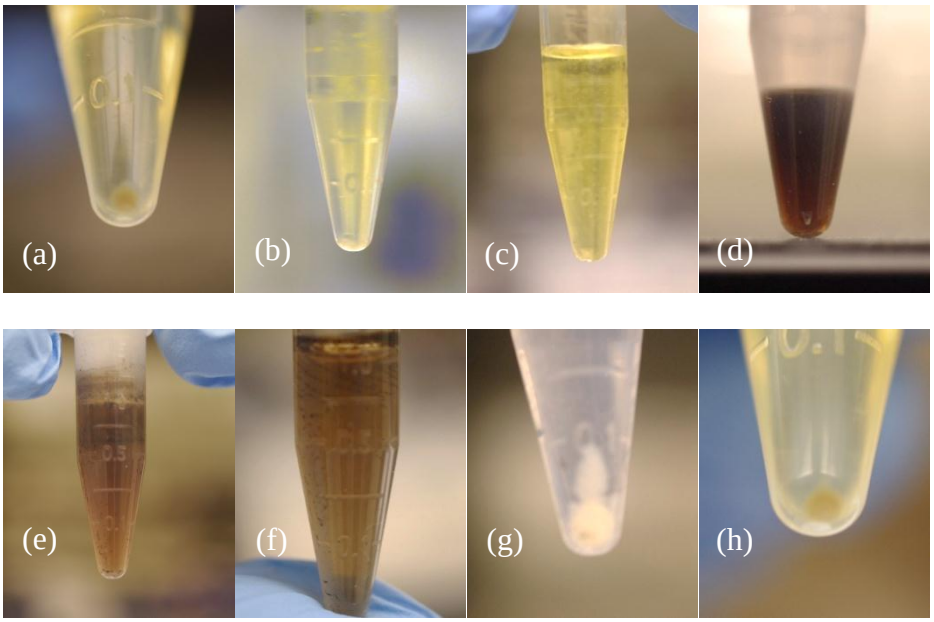


Figure 8.6. Rat lung tissue after various digestion methods and centrifugation. (a) Solvable, (b) ammonium hydroxide, (c) nitric acid, (d) sulfuric acid, (e) hydrochloric acid, (f) hydroflouric acid, (g) hydrogen peroxide, and (h) pro K.

Demonstration of Final Digestion Method: Recovery of S-CNTs from Rat Lung Tissue

Screening results of the different treatment methods indicated that Solvable was the most effective for dissolving rat lung tissue without causing extensive CNT loss. Solvable was also effective because of its ability to form stable CNT pellets during washing and the low risk of damage to the instrument (i.e., 5% -OH compared to 30% for NH_4OH). Figure 8.6a shows the thermal fingerprint for rat lung tissue during the oxidation phase after treatment with Solvable (no CNTs). Although Solvable was successful at hydrolyzing the tissue and removing most of the interfering carbon, some hydrolysate still remained in the pellet (e.g., Figure 8.5a), resulting in a small amount (~0.2 µg) of interfering carbon remaining. Pro K, which is known to be very effective at cleaving peptide bonds and catalyzing the hydrolysis process, was used as a follow-up

digestion method. Figure 8.6b shows the fingerprint of the rat lung tissue after Solvable treatment followed by pro K treatment. The pro K was successful at eliminating the remaining interfering carbon. This two-step method was selected as the final method for recovery of CNTs from rat lung tissue.

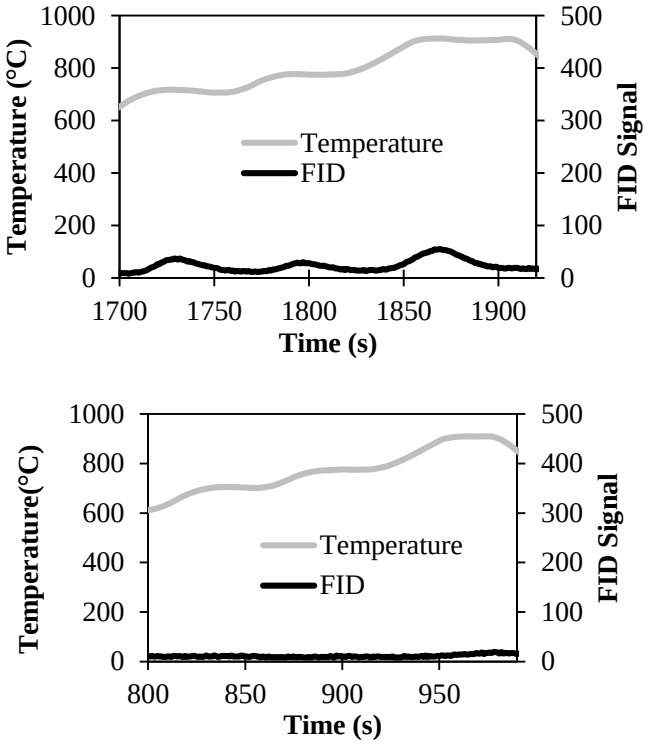


Figure 8.6. Thermograms for a whole rat lung after treatment with (a) Solvable followed by (b) pro K. Data has been cropped to show only the temperatures that S-CNTs oxidize at (i.e., ~650-900 °C).

The final digestion method was used to determine recovery of approximately 3 µg S-CNTs from whole rat lungs (dry weight ~0.2g). As a control, 3.6 µg of S-CNTs was treated with the two-step digestion method. The average recovery for triplicate samples was 3.3±0.09 µg, or about 91% recovery. This indicates minimal loss of S-CNTs as a result of the two-step digestion method with intermittent centrifugal washing.

The process was repeated for whole lungs spiked with S-CNTs. The average recovery for triplicate samples was 2.8±0.44 µg or approximately 93±15%. This shows that interfering carbon from the rat lung tissue was removed and S-CNTs were successfully recovered from the rat lungs using the two-step digestion method developed herein.

8.4 Summary and Conclusion

This study examined a number of chemicals commonly used to extract metals from complex matrices for application to CNTs. The results were applied to rat lung tissue, but will have an impact other studies focused on other complex matrices such as composite materials and sediments. Solvable proved to be the most effective at dissolving rat lung tissue while maintaining a high percent recovery of CNTs. Removing all interfering carbon from the rat lung tissue required the development of a two-step digestion method using Solvable and pro K.. Recovery of S-CNTs from rat lung tissue was efficient with a percent recovery of approximately 93%, indicating the ability of this method to be used in *in vivo* studies.

8.5 Supporting Info

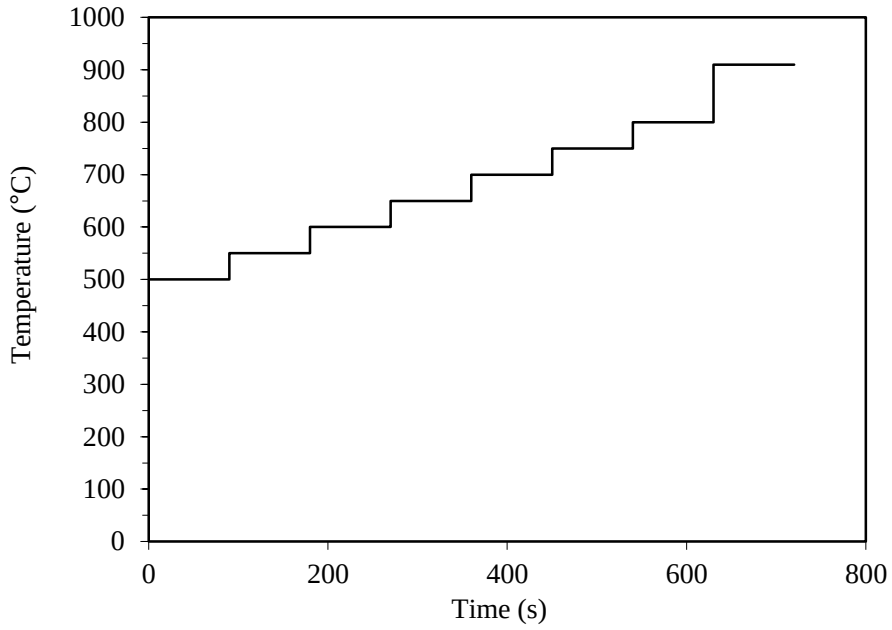


Figure SI-8.1. PTA program for evaluating CNTs

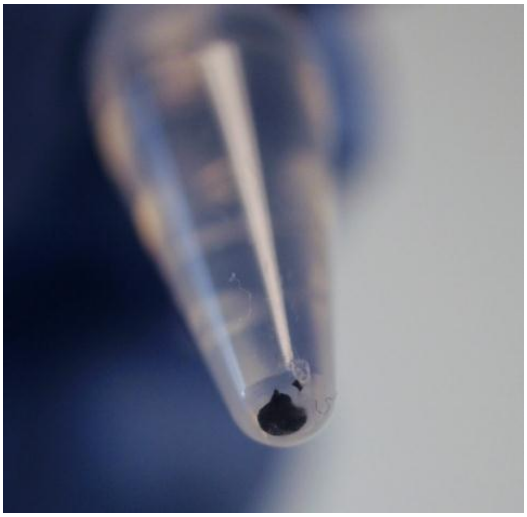


Figure SI-8.2. Image of functionalized W-CNT pellet after treatment with Solvable.

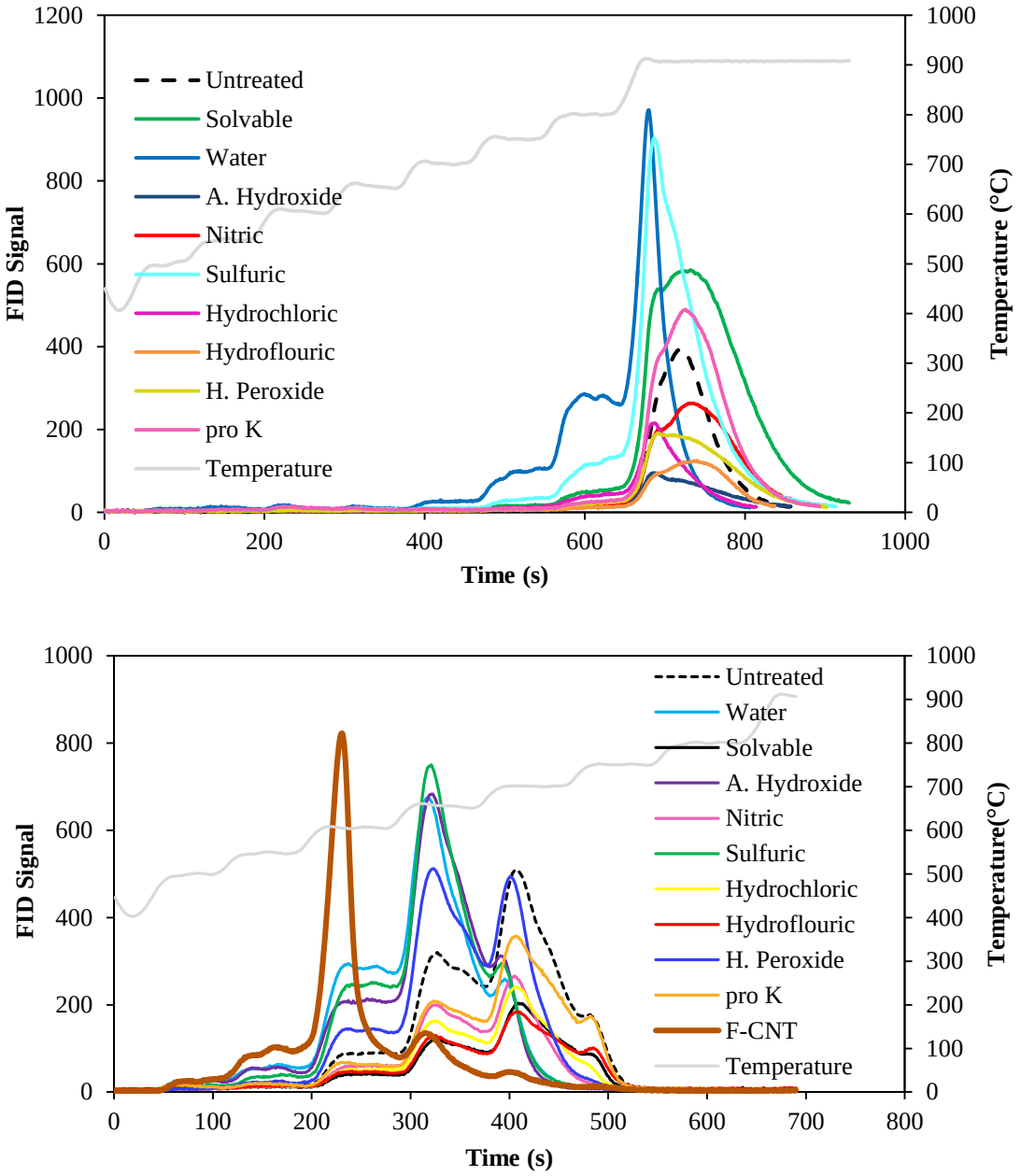


Figure SI-8.3. Thermograms for (a) S-CNTs and (b) W-CNTs after various treatments.

CHAPTER 9

SYNTHESIS CHAPTER: A FRAMEWORK FOR ENGINEERING PHOTOCATALYSTS FOR NITRATE TREATMENT

Introduction

As the human population increases so will the demand for food and water. In order to meet food demands, we will need to use more fertilizer, and as a result, nutrient pollution in our waters will increase. Of these fertilizer nutrients, nitrate remains the most problematic, causing depleted oxygen zones and reducing the amount of potable water. Production of nitrate-based fertilizers have also unbalanced the natural nitrogen cycle by taking nitrogen from the atmosphere without returning it. The physico-chemical properties of nitrate makes it problematic for nitrate removal in a water treatment plant. Currently, ion-exchange and separation (e.g., reverse osmosis) are the most commonly used methods. These are physical removal processes that leave a concentrated brine waste solution requiring further treatment or disposal, and they does not solve the nitrogen cycle issue.

New treatment methods such as biological and catalytic denitrification are destructive turning nitrate into nitrogen gas, but they have disadvantages that make them unsuitable as a permanent solution. For example, biological treatment carries the risk of cross-contamination, and the systems are slow to start up and difficult to maintain. Catalysts are effective and reusable, but they require a non-renewable energy source such as hydrogen and expensive materials such as palladium, making them an unsustainable option. Photocatalysis holds the promise of catalysts and uses a renewable energy source,

sunlight. The key to engineering new photocatalysts will be using abundant and stable materials that absorb a majority of the solar spectrum.

The goal of this chapter is to use the results presented in this dissertation to develop a framework for engineering more efficient nitrate-selective photocatalysts. First, a summary of the photocatalytic mechanisms of nitrate reduction found in the literature and presented in this dissertation is given. This summary is used to develop a conceptual framework for designing photoelectrochemical systems (e.g., heterogeneous photocatalysts) specifically for nitrate treatment in water. The strategy used to develop this framework is applicable for other water pollutants (e.g., chromate), among other things (e.g., CO_2 to fuel). When engineering photocatalysts specifically for nitrate treatment in water there are five things that we must design for including (1) efficient removal at neutral pH, (2) ability to use water as a hole scavenger, (3) N_2 by-product selectivity, (4) stability in water, and (5) non-toxic to humans and the environment.

Photocatalytic Reduction of Nitrate

The one-electron reduction potential for nitrate (NO_3^-) to the nitrate ion ($NO_2^{\bullet}$) is very high ($E° = -1.1$ V) (Cook et al., 2001), which is more negative than most semiconductor chemical potentials. So, the most probable first step in the photocatalytic nitrate reduction process is nitrate to nitrite ($NO_3^- + 2H^+ + 2e^- \rightarrow NO_2^- + H_2O$), which requires two electrons and has a more positive redox potential ($E° = 0.88$ V). Because this is a multi-electron transfer ($n = 2$), the reaction will be most efficient when two electrons are transferred simultaneously (i.e., electron-coupling). Because protons are also involved in nitrate reduction, protons should also be localized near the coupled electrons. This

overall process is considered a multi proton-coupled electron-transfer (PCET). For nitrate reduction over TiO_2, the multi-PCET pathway is very important as shown in Chapters 2 and 3, where no nitrate reduction occurred at neutral pH. Also shown was that nano-silver islands loaded onto the surface of TiO_2 allowed for nitrate reduction at neutral pH. Silver (Ag) is an effective source for pooling and localizing electrons (Takai & Kamat, 2011), which facilitates the multi-electron reactions and may lower the overpotential for nitrate reduction steps. At acidic pH, nitrate reduction was observed under all conditions tested and no aqueous nitrogen by-products (e.g., ammonium) remained. Getting past nitrite is possible at acidic pH, but not at neutral pH, even when an electron localization/trapping site (i.e., Ag) is present. This suggests that proton localizing near the electron trap site is very important for moving past nitrite and achieving reduction to N_2 at neutral pH. Examining the pK_a of nitrite, which is about 3.3, may shed some light on this matter. Near this pH is where the by-product swing from N_2/NH_4^+ to NO_2^- occurs. This suggests that moving past nitrite requires HNO_2, which is in good agreement with the proton localization theory since the proton would already be coupled to the nitrite ion and readily available to participate in the PCET reaction. So, the two-electron reduction of nitrate to nitrite has a significant potential barrier, and the barrier for moving beyond nitrite seems to be even greater as a result of non-localized protons. Determining the activation magnitudes and designing for these barriers will be key to developing an N_2 selective photocatalyst at neutral pH.

The oxidation reaction must also be considered when looking at the probability of a successful photocatalytic reaction and the mechanisms of nitrate reduction. In the case of using an organic compound as the hole scavenger (e.g., formate), powerful reducing

radicals may be produced (e.g., CO_2^-), and these could facilitate the one-electron reduction of nitrate. However, as discussed in Chapter 3, in the case of formate and on the basis of stoichiometry, formate is used as a two-hole scavenger and there is no clear evidence that these radicals are being produced when using TiO_2 for photocatalytic nitrate reduction. This evidence adds to the importance of designing for the PCET reactions. To move beyond using an organic hole scavenger and move toward using water as a hole scavenger, we must consider the water oxidation process carefully. Water splitting is one of great interest to the energy community and has taken a front seat as one of the most promising options for sustainable energy. Water oxidation to oxygen gas requires four holes and is most efficient using a PCET (Gagliardi, Vannucci, Concepcion, Chen, & Meyer, 2012; Gagliardi et al., 2010; Huynh & Meyer, 2007; F. Liu et al., 2008). Similar to nitrate, the intermediate one-electron steps are slow and require a large potential barrier (e.g., $OH•/H_2O$ = 2.31 eV). If the two reactions are coupled together, competing multi-electron, multi-proton reactions occur, resulting in a kinetically slow redox reaction. Furthermore, the intermediates from nitrate reduction are likely to compete for the hole site with the more difficult water oxidation reactions, further limiting the overall redox reaction. So, in order for the photocatalyst to be efficient at reducing nitrate using water as a hole scavenger, a water oxidation specific photocatalyst/co-catalyst will be required and the reaction will have to be tailored to reduce the back-reaction of intermediates (e.g., NO_2^-, H_2).

Choosing the Photocatalyst

The first step to designing a photocatalyst for nitrate reduction is selection of the photocatalyst materials. For the photocatalyst, the bandgap, the chemical potential, the type (i.e., n-type or p-type), and the material composition (e.g., metal oxide or metal sulfide) will all be important. These material properties will affect the oxidation-reduction potential, absorption properties, surface charge, toxicity, aqueous stability, and pollutant selectivity.

Through bandgap excitation, the photocatalyst generates the electrons and holes that are necessary for oxidation-reduction reactions. The conduction band (CB) minimum of the photocatalyst is often used to estimate the electrochemical potential (i.e., the energy binding an electron inside the semiconductor), but the Fermi level or chemical potential is a better measure of the true electrochemical potential. For example, in an n-type semiconductor, the Fermi level lies very near the CB, but in a p-type the Fermi level is closer to the valence band (VB) maximum. Generally, an n-type semiconductors will have a more reductive potential and a p-type a more oxidative potential. This is the first characteristic that should be considered when selecting a photocatalyst for a specific pollutant because if the potential does not have the appropriate magnitude then treatment of the pollutant(s) will be (theoretically) impossible. Generally, this potential should be greater than the theoretical value due to kinetic overpotential barriers (e.g., reduction of nitrate to nitrite). In the case of a heterogeneous photocatalyst, where all reactions are occurring on the same surface, both the oxidation and reduction potentials must be considered. For oxidation to occur, the VB must be more positive than the oxidation potential, and for reduction to occur the CB must be more negative than the reduction

potential. In other words, the bands should straddle the redox reactions of concern. An example of this is shown in Figure 9.1 and Figure 9.2 for a number of metal oxide and metal sulfide photocatalysts, respectively, with the nitrate reduction (to NO_2^-) and the water oxidation (to O_2) potentials listed as a reference.

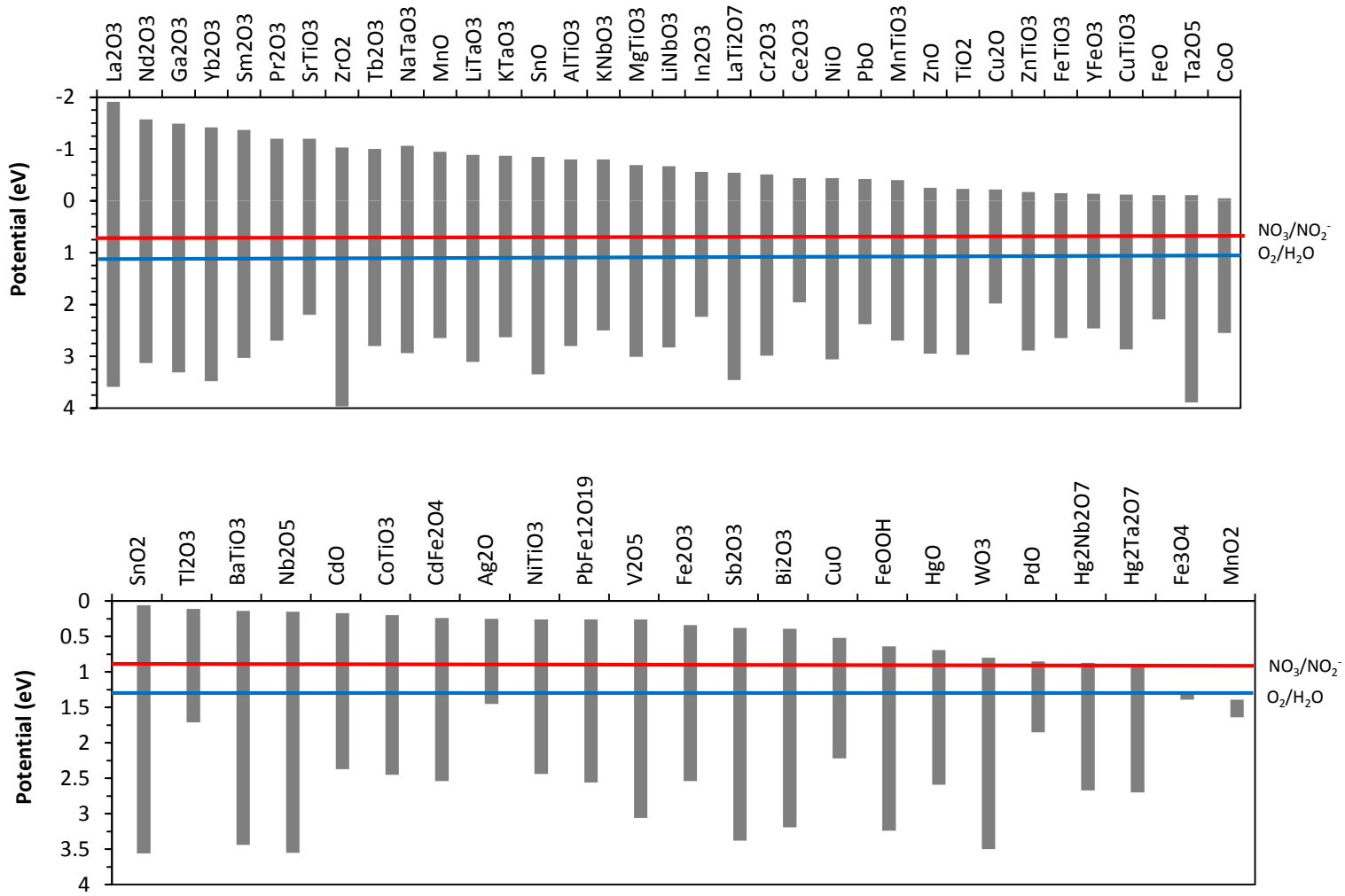


Figure 9.1. Band gaps of various metal oxides along with the reduction potentials for nitrate (to nitrite) and water (to oxygen). Data adapted from (Y. Xu & Schoonen, 2000). All numbers are subscripts.

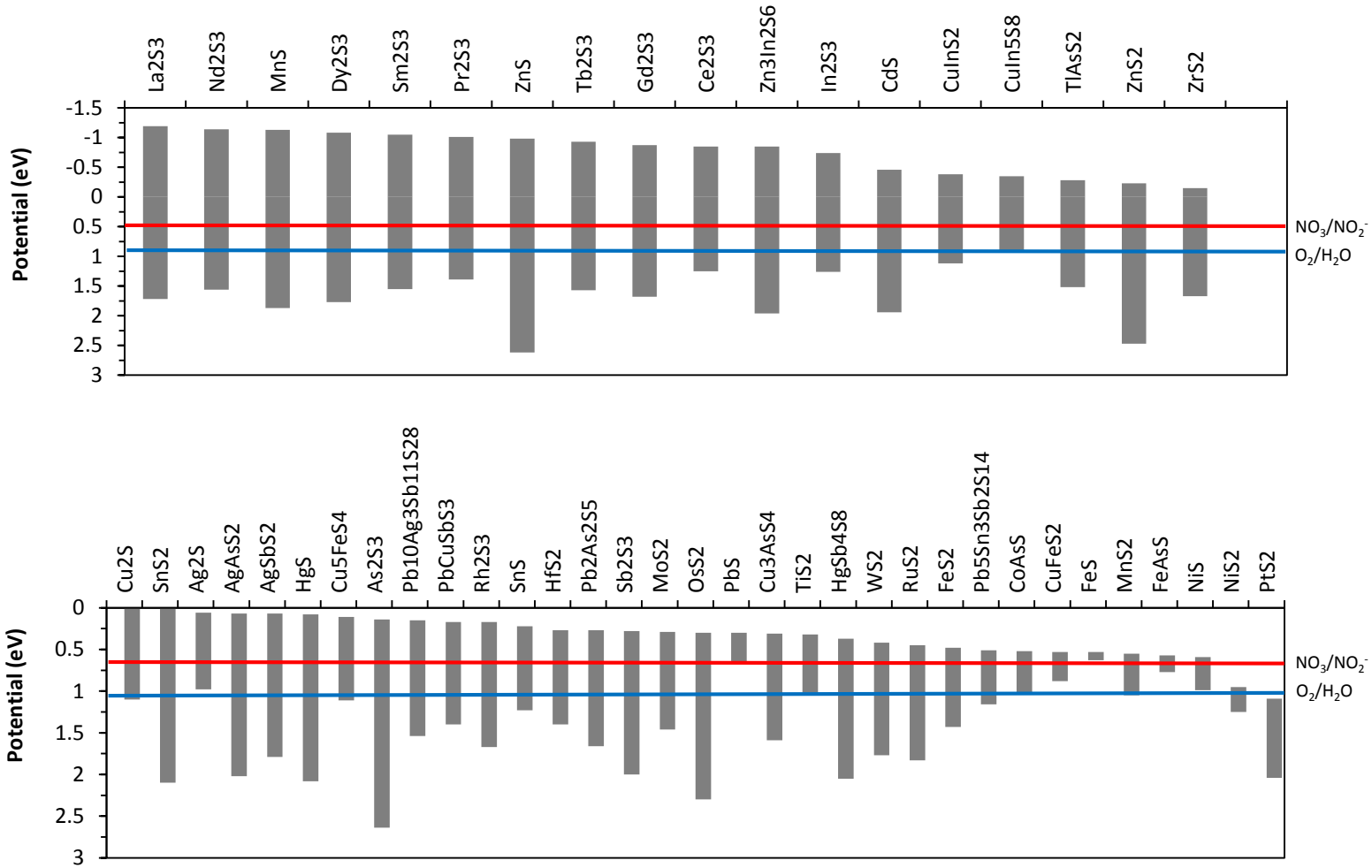


Figure 9.2. Band gaps of various metal sulfides along with the reduction potentials for nitrate (to nitrite) and water (to oxygen). Data adapted from (Y. Xu & Schoonen, 2000). All numbers are subscripts.

Metal oxides tend to have better oxidation potentials than metal sulfides because of the O 2p orbitals that put the VB around 3 eV. Metal sulfides will have nearly the same reduction potentials as metal oxides because of the metal forming CBs, but with more negative oxidation potentials because of the s-shell formed valence bands. This results in a photocatalyst with a smaller bandgap that is ideal for reduction reactions. Unfortunately, most metal sulfides are not stable in water and suffer from self-oxidation. Some metal oxides, such as the rare-earth oxides and ZrO_2, have both a high reduction and oxidation potential, but this results in a large bandgap, which requires more energy for activation. Combining two small bandgap semiconductors in tandem that have both a strong oxidation and reduction potential will be the key to developing a nitrate reduction photocatalyst.

Besides oxidation-reduction potential, the structure of the bandgap also affects the efficiency of the reaction. The bandgap takes two forms: direct and indirect. A direct bandgap is defined as the CB minimum and the VB maximum having the same momentum, thus the transfer of the electron is direct. An indirect bandgap has an unequal momentum, and, thus, a phonon must be used to overcome the crystal momentum. As a result, the direct bandgap is more efficient at absorbing light and generating charge carriers compared to the indirect bandgap, which requires the extra step of momentum transfer. However, more efficient charge generation in the direct bandgap also results in a more efficient radiative recombination rate. Ideally, the photocatalyst will be a direct bandgap to ensure efficient charge transfer and this will be coupled with an additional material that inhibits radiative recombination (e.g., Schottky barrier, indirect bandgap

material). In the case of an indirect bandgap material, non-radiative recombination would dominate (e.g., point defects and grain boundaries).

Stability is another concern when choosing a photocatalyst for water treatment applications. Metal oxides such as TiO_2 and ZrO_2 are generally stable. There are exceptions, such as ZnO, which is unstable at acidic and basic pH. Chalcogenides such as sulfides (e.g., ZnS) are also unstable. For those photocatalysts that are unstable, the photocatalyst oxidizes itself in the absence of a sacrificial hole scavenger other than water.

Heterojunction Photocatalyst

A heterojunction is formed when two photocatalysts are joined to form one composite material. Heterojunctions are important for separating the charge carriers, improving the oxidation and reduction potentials, separating oxidation and reduction reactions, and reducing the rate of recombination. A good example of a heterogeneous photocatalyst is P25 or P90, mixed phase TiO_2 photocatalysts consisting of anatase and rutile. Anatase has an indirect bandgap and rutile has a direct bandgap. The mixed-phase characteristic of this commercial material is believed to contribute to its high activity (Hurum et al., 2006; Hurum, Agrios, Gray, Rajh, & Thurnauer, 2003; Hurum et al., 2005). In this case, excited electrons are transferred to the CB of rutile, which lies below that of the anatase CB, thus facilitating charge separation and preventing the likelihood of recombination. When designing for a photocatalyst for nitrate reduction, a heterojunction can be utilized by selecting two photocatalysts that are ideal for the oxidation and reduction reactions.

Choosing the Co-Catalyst

The main purpose of the co-catalyst is to control the by-product selectivity and to improve reaction kinetics. The co-catalyst material is generally loaded onto the surface of the photocatalyst in a particulate heterogeneous system. For nitrate reduction and metal co-catalysts, choosing a co-catalyst that forms a Schottky barrier with the semiconductor is ideal because it creates electron storing in the metal (e.g., Chapter 4). Metals that form ohmic contacts result in lowered nitrate reduction activity because of the lack of potential barrier between the metal and the semiconductor. Results presented herein have shown that silver is the best choice as a co-catalysts for photocatalytic reduction of nitrate because of its ability to store electrons and ideal by-product selectivity. In a photoelectrochemical system, silver would serve as the counter electrode for nitrate reduction.

Water as a Hole Scavenger

When dealing with nitrate reduction in water, typically nitrate is more selective for electrons than protons (with some material exceptions, e.g., Pt). However, with regards to interfacial transfer in TiO_2, the rate of recombination is faster than the rate at which electrons transfers to the nitrate molecule. This is because the rate of water oxidation (i.e., hole scavenger) is very slow, thus leaving the hole available for recombination. As such, nitrate reduction over TiO_2 using water as a hole scavenger is not efficient. Generally, this limitation is overcome by adding a hole scavenger, one that has fast oxidation kinetics, to the system to retard the rate of recombination, thus

allowing for nitrate reduction. However, for drinking water applications, addition of a hole scavenger is not desired.

There have been a number of photocatalysts that have been shown to be efficient at oxidizing water (A. Kudo & Miseki, 2009). The most efficient photocatalysts were selected and tested for nitrate reduction with and without an additional hole scavenger. Additionally, various co-catalysts were loaded to examine their ability to catalyze the water oxidation reaction. Photocatalysts that were examined are listed in Table 9.1. Some were purchased from commercial source (listed), others were synthesized (see Chapter 6). Photocatalysts were examined at 1 g/L using 100 mg-N/L nitrate. Interestingly, none of the photocatalysts tested had any nitrate removal activity using water as a hole scavenger after two hours exposure using the 450-W UV lamp photoreactor described in Chapter 3. Even when formic acid was added, no removal was observed, with the exception of ZrO_2, which had some activity. Lanthanum doped sodium tantalate loaded with nickel oxide ($NaTaO_3$:La/NiO) has the highest water oxidation reported (Kato et al., 2003). This material was tested for 15 hrs achieving approximately 75% nitrate removal and 25% selectivity to nitrogen gas was observed, with the rest being nitrite. This was attributed to the back reaction of nitrite to nitrate at the hole site, which is preferential over water oxidation, and similar results have been observed previously for TiO_2 (Kominami et al., 2010). So, designing a photocatalytic system that separates the nitrate reduction and water oxidation reactions will be necessary to achieve efficient nitrate reduction using water as a hole scavenger.

Table 9.1. *Summary of materials tested for photocatalytic nitrate reduction using water as a hole scavenger. HT: Hydrothermal; photo-loaded: photoreduction method; SS: solid-state.*

Photocatalyst	Synthesis Method
$NaTaO_3$ (Commercial)	Commercial, Materion
$NaTaO_3$	Hydrothermal
$NaTaO_3$	Sol-gel
$NaTaO_3$	Solid state synthesis
$NaTaO_3$/Pd	HT/photo-loaded
$NaTaO_3$/IrO2	HT/photo-loaded
$NaTaO_3$/Pd-IrO2	HT/photo-loaded
$NaTaO_3$/Ni	HT/photo-loaded
$NaTaO_3$/Ni-450 C	HT/photo-loaded
$BiVO_4$	Commercial, Materion
$BiVO_4$/Ag (1%)	Commercial, Materion/photo-loaded
$BiVO_4$:Mo SS (5%)	Solid state synthesis
WO_3	Commercial, Sigma
$SrTiO_3$	HT
$SrTiO_3$/Rh(1%)	HT/chemical loaded
$SrTiO_3$/Rh(2%)	HT/chemical loaded
$SrTiO_3$/Rh(1%)-RuO_2	HT/chemical loaded
ZrO_2	Commercial, Sigma
$NaTaO_3$:La(1%)	Solid state
$NaTaO_3$:La(1%)/NiO	Solid state/chemical loaded

Engineering a Nitrate Reducing, Water Oxidizing Photoelectrochemical System

This study has laid out a framework for developing a nitrate-specific photocatalytic system. In order to use water as a hole scavenger, the nitrate reduction and water oxidation reactions must be spatially separated to prevent the back reaction of nitrite to nitrate. Additionally, a co-catalyst for each reaction is need to ensure good efficiency and appropriate by-product selectivity (i.e., N_2). In the case of nitrate, this co-catalyst should be efficient at electron storage and proton localization.

Figure 9.3 shows a conceptual design of a tandem photoelectrochemical cell that meets these criteria. For the nitrate reduction reaction, the photocatalyst should be a p-

type photocatalysts with a CB position below -1 eV and a bandgap less than 3 eV. For the water oxidation reaction, the photocatalysts should be an n-type with a VB position above 2 eV and a bandgap also below 3 eV. The overall redox potential of the two-photon tandem system covers a large range without the need for a wide bandgap photocatalyst (i.e., > 5 eV). The photoelectrodes are separate, thus eliminating back reaction, and each can be tailored with co-catalysts specific for the reduction and oxidation reactions.

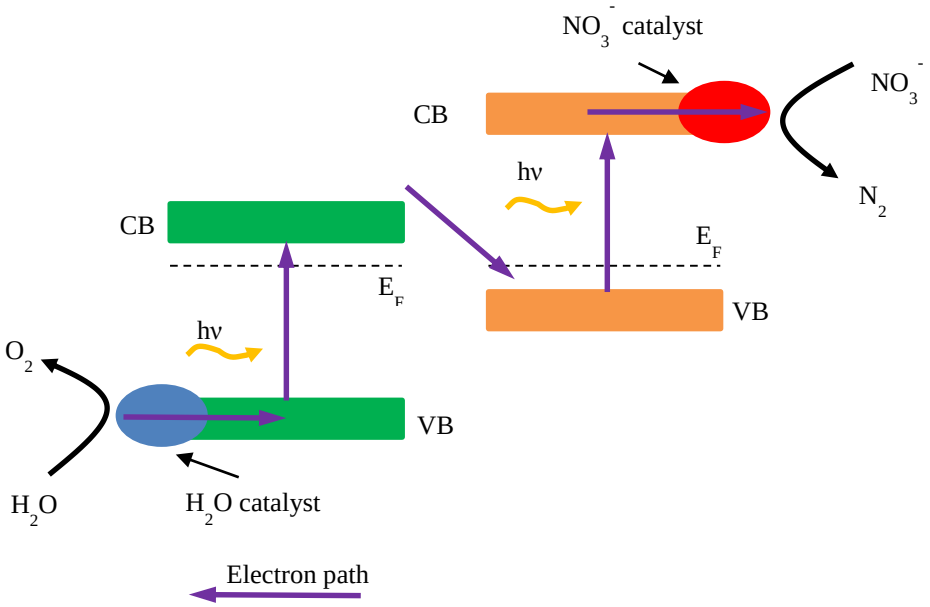


Figure 9.3. Conceptual design of a tandem photoelectrochemical system for nitrate reduction and water oxidation. E_F is the Fermi level. CB and VB are conduction band and valence band, respectively.

In order to develop this tandem cell, information on the atomic-scale mechanisms will be required for selecting the appropriate materials (i.e., photocatalyst, co-catalyst). We know that TiO_2 is a good photocatalyst and silver is a good co-catalyst for nitrate reduction, but we do not know exactly why (e.g., does it adsorb to silver?). *In-situ* surface studies, such as attenuated total reflectance-Fourier transform infrared spectroscopy

(ATR-FTIR) and Raman spectroscopy, as well as theoretical studies, such as density functional theory (DFT), are needed to determine exactly why TiO_2 and silver are unique for nitrate. The results of these types of studies will be imperative for engineering a photoelectrochemical system specifically for nitrate treatment.

CHAPTER 10

SUMMARY, CONCLUSIONS, AND FUTURE RECOMMENDATIONS

10.1 Summary

This overarching goal of this dissertation was to gain additional insight into the mechanisms and develop new materials for the photocatalytic reduction of nitrate in water. The dissertation was organized into different chapters to separate the main objectives that were completed to meet this goal.

Dissertation Objectives

1. Evaluate the ability of three similar, yet distinct, commercial TiO_2 photocatalytic nanomaterials for the reduction of nitrate in groundwater, and determine the material characteristics controlling the nitrate reduction efficiency. (Chapter 3)
2. Determine the effect of experimental parameters such as pH, nitrate concentration, hole scavenger concentration, and photocatalyst dose on the photocatalytic nitrate reduction activity. Provide insight into the role of silver as a co-catalyst. (Chapter 4)
3. Use TiO_2 to photocatalytic treat ion-exchange brine and test the ability of the treated brine to regenerate the ion-exchange sites. (Chapter 5)
4. Examine metal and carbonaceous nanomaterials as TiO_2 co-catalysts for the photocatalytic reduction of nitrate. (Chapter 6)

5. Develop a method for detecting carbon nanotubes in complex environmental and biological matrices. (Chapter 7)
6. Develop a method for extracting carbon nanotubes from rat lung tissue. (Chapter 8)
7. Develop a framework for engineering photocatalysts specifically for nitrate treatment in water. (Chapter 9)

Observations

Chapter 3: Nitrate Reduction in Water Using Commercial Titanium Dioxide Photocatalysts (P25, P90, and Hombikat UV100)

- Surface area is not the limiting characteristic as expected. Instead, the rate of recombination, which is dependent on the material properties such as defects, crystal size, and crystal phase, is the limiting factor. For photocatalysts with similar recombination rates, surface area was the next limiting factor, and increasing surface area help to mitigate the negative effects resulting from groundwater constituents.
- No nitrate removal was observed at neutral pH, which signifies a potential barrier existing due to either lack of coupled electrons and protons, which are necessary for the reduction reaction.

Chapter 4: Photocatalytic nitrate reduction in water: Managing the hole scavenger and reaction by-product selectivity

- Silver plays an important role as a co-catalyst, separating charge carriers and storing electrons. Silver facilitated the multi-electron proton coupled nitrate reduction reaction and nitrate removal was achieved at neutral pH.
- Although removal was observed at neutral pH, the by-product selectivity was 100% nitrite, indicating that limiting reaction is nitrite reduction (e.g., to NO), and that proton localization is necessary to move beyond nitrite.
- Formate was observed to act as a two-hole scavenger and not a radical producer, which provides further evidence that a multi-electron transfer is necessary as the one-electron reduction of nitrate has a very negative potential.
- The stoichiometric requirement of formate was determined such that a 1:1 removal of nitrate and formate was achieved, which reduces costs and the risk of effluent DOC contamination.

Chapter 5: Photocatalytic Reduction of Nitrate Using Titanium Dioxide for Regeneration of Ion Exchange Brine

- In synthetic brines, increasing NaCl was found to decrease the photocatalytic rate of nitrate removal, but beyond 3% NaCl, the decrease was not significant.
- Sulfate was found to be the major inhibitor in the ion-exchange brines. Barium sulfate precipitation successfully removed the sulfate and increased the nitrate removal rate.

- More than the stoichiometric requirement of formic acid calculated in Chapter 3 was required for efficient nitrate removal. This was attributed to the capture of electrons by competing anions such as chloride and sulfate.
- Residual formic acid in the brine did not inhibit ion exchange performance after regeneration, and a single washing of the column removed adsorbed formic acid, leaving the treated drinking water free of cross-contamination.
- High chloride concentrations found in brine negated the benefits of adding silver, most likely due to silver chloride complexation.

Chapter 6: Exploration of Co-catalysts for the Photocatalytic Reduction of Nitrate over Titanium Dioxide

- The addition of palladium and platinum on P90 retarded the nitrate removal rate, owing to the ohmic nature of their contact and their preference for hydrogen production.
- Beside silver, other coinage metals such as copper and gold were able to increase the nitrate removal rate, although, not as good as silver. Copper had a higher by-product selectivity for ammonium than silver or P90 alone.
- TiO_2 coated CNTs showed no activity for nitrate removal in a heterogeneous system (i.e., particulate). This was attributed to the electron shuttling away from the surface of the composite to the CNT core.
- TiO_2/CNTs and TiO_2/Graphene are excellent candidates for electrode materials. TiO_2/Graphene thin films exhibited a photocurrent six times that of TiO_2 thin films as a result of improved charge transfer to the electrode.

Chapter 7: Detection of Carbon Nanotubes in Environmental Matrices Using Programmed Thermal Analysis

- A method for detecting CNTs, termed programmed thermal analysis or PTA, was developed for quantifying carbon nanotubes.
- Two thermal categories of CNTs were discovered, termed "weak" and "strong," and refers to their thermal stability under inert and oxidizing conditions.
- Raman spectroscopy was found to be successful for identifying whether a CNT fell into the weak or strong category. Those that had an I_D/I_G ratio less than 0.75 were strong, and they had little interference with complex matrices. Weak CNTs had an I_D/I_G ratio greater than 0.75 and were more difficult to separate from complex matrices containing very thermal stable organic (e.g., milk) or anthropogenic elemental carbon (e.g., soot).
- Strong CNT masses of 0.51, 2.7, and 11 µg, corresponding to concentrations of 10, 54, and 220 µg CNT/g cyanobacteria, yielded recoveries of 160 ± 29%, 99 ± 1.9%, and 96 ± 3.0%, respectively.
- The current detection limit at 99% confidence for urban air samples and strong CNTs is 55 ng/m^3 (0.33 µg).

Chapter 8: Extraction of Carbon Nanotubes from Complex Organic Matrices with Application to Rat Lung Tissue

- A method was developed for extracting CNTs from rat lung tissue.

- Weak alkaline hydrolysis combined with surfactants (Solvable) was found to be the most effective method for dissolving rat lung tissue while maintaining high CNT percent recoveries.
- Proteinase K enzyme was used as a follow up method to the alkaline step to remove remaining interfering carbon that remained after the Solvable step.
- 3 µg S-CNTs were spiked into whole rat lungs (dry weight ~0.2g), and the average recovery for triplicate samples was 2.8±0.44 µg or approximately 93±15%.

Chapter 9: Synthesis Chapter: A Framework for Engineering Photocatalysts for Nitrate Treatment

- Photocatalytic nitrate reduction in water is a step process requiring multiple PCETs.
- A co-catalyst capable of storing electrons such as copper or silver is necessary to complete the multi-PCETs.
- A co-catalyst capable of adsorbing and transferring protons is also required.
- Of the photocatalysts examined, titanium dioxide is far beyond other materials in terms of activity. The hypothesized reason that water oxidizing photocatalysts were not successful is because of the back reaction of nitrite to nitrate at the hole site. This can be overcome by separating the oxidation and reduction reactions.
- The key will be to design a tandem photoelectrochemical system that is comprised of two photoelectrodes, one specifically for reduction (photocathode) and one specifically for oxidation (photoanode). Each of these should consist of an

electron mediator such as graphene, and the photoelectrodes should be loaded with a co-catalysts that facilitates the reactions.

10.2 Conclusions

Nitrate is currently a wide-spread water pollutant that will continue to grow as the demand for food increases. Current nitrate treatment technologies are not sustainable, and they do not solve the ultimate problem of completing the nitrogen cycle by returning nitrate back to dinitrogen. Photocatalysis is an ideal candidate for solving the nitrate problem because it can utilize solar energy, it is reusable, and it can be tailored to reduce nitrate to dinitrogen. This dissertation has contributed to the understanding of the photocatalytic reduction of nitrate. Herein, I presented one of the first studies to focus on using photocatalysis for a specific pollutant. I also highlighted the need for responsible engineering when developing new materials, which is to ensure that detection methods are available for these materials to assist with risk assessment analyses.

One of this biggest issues limiting photocatalysis development for nitrate reduction was the lack of knowledge on the mechanisms. This dissertation work highlighted the macro-scale mechanisms and the appropriate application of current photocatalysis materials. I showed that photocatalytic nitrate reduction proceeds in a series of step-wise proton-coupled electron transfers, which emphasizes the need for electron and proton localization at nitrate reduction sites. Commercially available materials, such as TiO_2, were limited to non-direct treatment of nitrate such as ion-exchange brine wastes because of inability to efficiently use water as a hole scavenger. To overcome this barrier, we should move away from single heterogeneous

photocatalysts systems and toward tandem systems that separate the oxidation and reduction reactions.

10.3 Future Recommendations

In order to advance the photocatalytic treatment of nitrate, nitrate-specific photocatalysts will need to be developed. Before this can occur, we must know more about the atomic-scale mechanisms, such as how nitrate interacts with the photocatalyst and co-catalyst surfaces. One suggestion is to use a theoretical model, such as density functional theory (DFT), and couple that with *in-situ* techniques, such as attenuated total reflectance Fourier transform infrared spectroscopy (ATR-FTIR). We also need to develop high-throughput methods for synthesizing and testing an array of photocatalysts and experimental conditions. These tools will be necessary for engineering photocatalysts to be pollutant-specific.

For nitrate, a tandem photoelectrochemical system consisting of a nitrate reducing photocathode and a water oxidizing photoanode, will be needed to achieve nitrate reduction under neutral conditions and using water as a hole scavenger. For the nitrate electrode, a co-catalyst that is good at localizing electrons and protons, and one that is sustainable (i.e., not Pd) needs to be developed. For the water oxidizing electrode, there is already a number of studies focused on creating these water oxidizing co-catalysts, and these should be screened for nitrate specific photoelectrochemical systems.

REFERENCES

Abdullah, M., Low, G. K. C., & Matthews, R. W. (1990). EFFECTS OF COMMON INORGANIC ANIONS ON RATES OF PHOTOCATALYTIC OXIDATION OF ORGANIC-CARBON OVER ILLUMINATED TITANIUM-DIOXIDE. *Journal of Physical Chemistry, 94*(17), 6820-6825.

Ago, H., Kugler, T., Cacialli, F., Salaneck, W. R., Shaffer, M. S. P., Windle, A. H., & Friend, R. H. (1999). Work functions and surface functional groups of multiwall carbon nanotubes. *Journal of Physical Chemistry B, 103*(38), 8116-8121.

Aitken, R. J., Chaudhry, M. Q., Boxall, A. B. A., & Hull, M. (2006). Manufacture and use of nanomaterials: current status in the UK and global trends. *Occupational Medicine-Oxford, 56*(5), 300-306. doi: 10.1093/occmed/kq1051

Alvarez, W. E., Kitiyanan, B., Borgna, A., & Resasco, D. E. (2001). Synergism of Co and Mo in the catalytic production of single-wall carbon nanotubes by decomposition of CO. *Carbon, 39*(4), 547-558.

Anderson, J. A. (2011). Photocatalytic nitrate reduction over Au/TiO(2). *Catalysis Today, 175*(1), 316-321. doi: 10.1016/j.cattod.2011.04.009

Anderson, J. A. (2012). Simultaneous photocatalytic degradation of nitrate and oxalic acid over gold promoted titania. *Catalysis Today, 181*(1), 171-176. doi: 10.1016/j.cattod.2011.05.027

Ando, T., Nagase, H., Eguchi, K., Hirooka, T., Nakamura, T., Miyamoto, K., & Hirata, K. (2007). A novel method using cyanobacteria for ecotoxicity test of veterinary antimicrobial agents. *Environmental Toxicology and Chemistry, 26*(4), 601-606. doi: 10.1897/06-195r.1

Andrews, R., Jacques, D., Qian, D., & Dickey, E. C. (2001). Purification and structural annealing of multiwalled carbon nanotubes at graphitization temperatures. *Carbon, 39*(11), 1681-1687.

Anpo, M., Yamashita, H., Ichihashi, Y., Fujii, Y., & Honda, M. (1997). Photocatalytic reduction of CO_2 with H_2O on titanium oxides anchored within micropores of zeolites: Effects of the structure of the active sites and the addition of Pt. *Journal of Physical Chemistry B, 101*(14), 2632-2636.

Anpo, M., Yamashita, H., Ikeue, K., Fujii, Y., Ichihashi, Y., Zhang, S. G., . . . Yoo, J. W. (1998). Photocatalytic reduction of CO_2 with H_2O on titanium oxides anchored within zeolites. In T. Inui, M. Anpo, K. Izui, S. Yanagida & T. Yamaguchi (Eds.), *Advances in Chemical Conversions for Mitigating Carbon Dioxide* (Vol. 114, pp. 177-182). Amsterdam: Elsevier Science Publ B V.

Aschberger, K., Johnston, H. J., Stone, V., Aitken, R. J., Hankin, S. M., Peters, S. A. K., Christensen, F. M. (2010). Review of carbon nanotubes toxicity and exposure-Appraisal of human health risk assessment based on open literature. *Critical Reviews in Toxicology, 40*(9), 759-790. doi: 10.3109/10408444.2010.506638

Aslim, B., & Ozturk, S. (2009). Toxicity of herbicides to cyanobacterial isolates. *Journal of Environmental Biology, 30*(3), 381-384.

ASTM Standard D2986-95a, 1999, "Standard practice for evaluation of air assaymedia by the monodisperse DOP (dioctyl phthalate) smoketest". (1999). West Conshohocken, PA: ASTM International.

Atsdr. (2007). Case Studies in Environmental Medicine Nitrate/nitrite Toxicity.

Avery, A. A. (1999). Infantile methemoglobinemia: Reexamining the role of drinking water nitrates. *Environmental Health Perspectives, 107*(7), 583-586.

Bae, B. U., Jung, Y. H., Han, W. W., & Shin, H. S. (2002). Improved brine recycling during nitrate removal using ion exchange. *Water Research, 36*(13), 3330-3340. doi: 10.1016/s0043-1354(02)00012-x

Bae, S. E., & Gewirth, A. A. (2008). Differential reactivity of Cu(111) and Cu(100) during nitrate reduction in acid electrolyte. *Faraday Discussions, 140*, 113-123. doi: 10.1039/b803088j

Bahnemann, D., Henglein, A., Lilie, J., & Spanhel, L. (1984). Flash photolysis observation of the absorption spectra of trapped positive holes and electrons in colloidal titanium dioxide. *The Journal of physical chemistry, 88*(4), 709.

Bahr, J. L., Mickelson, E. T., Bronikowski, M. J., Smalley, R. E., & Tour, J. M. (2001). Dissolution of small diameter single-wall carbon nanotubes in organic solvents? *Chemical Communications*(2), 193-194.

Balazs, N., Mogyorosi, K., Sranko, D. F., Pallagi, A., Alapi, T., Oszko, A., . . . Sipos, P. (2008). The effect of particle shape on the activity of nanocrystalline TiO_2 photocatalysts in phenol decomposition. *Applied Catalysis B-Environmental, 84*(3-4), 356-362. doi: 10.1016/j.apcatb.2008.04.018

Bamwenda, G. R., Uesigi, T., Abe, Y., Sayama, K., & Arakawa, H. (2001). The photocatalytic oxidation of water to O-2 over pure CeO2, WO3, and TiO2 using Fe3+ and Ce4+ as electron acceptors. *Applied Catalysis a-General, 205*(1-2), 117-128.

Barrabes, N., & Sa, J. (2011). Catalytic nitrate removal from water, past, present and future perspectives. *Applied Catalysis B-Environmental, 104*(1-2), 1-5. doi: 10.1016/j.apcatb.2011.03.011

Barrabés, N., Just, J., Dafinov, A., Medina, F., Fierro, J. L. G., Sueiras, J. E., . . . Cesteros, Y. (2006). Catalytic reduction of nitrate on Pt-Cu and Pd-Cu on active carbon using continuous reactor: The effect of copper nanoparticles. *Applied Catalysis B: Environmental, 62*(1-2), 77.

Basiuk, E. V., Ochoa-Olmos, O. E., & De la Mora-Estrada, L. F. (2011). Ecotoxicological Effects of Carbon Nanomaterials on Algae, Fungi and Plants. *Journal of Nanoscience and Nanotechnology, 11*(4), 3016-3038. doi: 10.1166/jnn.2011.3767

Baughman, R. H., Zakhidov, A. A., & de Heer, W. A. (2002). Carbon nanotubes - the route toward applications. *Science, 297*(5582), 787-792.

Behler, K., Osswald, S., Ye, H., Dimovski, S., & Gogotsi, Y. (2006). Effect of thermal treatment on the structure of multi-walled carbon nanotubes. *Journal of Nanoparticle Research, 8*(5), 615-625. doi: 10.1007/s11051-006-9113-6.

Bems, B., Jentoft, F. C., & Schlogl, R. (1999). Photoinduced decomposition of nitrate in drinking water in the presence of titania and humic acids. *Applied Catalysis B-Environmental, 20*(2), 155.

Benderskii, V. A., Krivenko, A. G., & Ponomarev, E. A. (1989). ELECTROCHEMISTRY OF SHORT-LIVED INTERMEDIATES FORMED BY REDUCTION OF NITRATE-IONS TO HYDROXYLAMINE. *DOKLADY AKADEMII NAUK SSSR, 308*(5), 1159-1163.

Bhalerao, G. M., Sinha, A. K., & Sathe, V. (2008). Defect-dependent annealing behavior of multi-walled carbon nanotubes. *Physica E-Low-Dimensional Systems & Nanostructures, 41*(1), 54-59. doi: 10.1016/j.physe.2008.06.006

Bhatkhande, D. S., Pangarkar, V. G., & Beenackers, A. (2002). Photocatalytic degradation for environmental applications - a review. *JOURNAL OF CHEMICAL TECHNOLOGY AND BIOTECHNOLOGY, 77*(1), 102-116.

Birch, M. E., & Cary, R. A. (1996). Elemental carbon-based method for monitoring occupational exposures to particulate diesel exhaust. *Aerosol Science and Technology, 25*(3), 221-241. doi: 10.1080/02786829608965393

Blaise, C., Gagne, F., Ferard, J. F., & Eullaffroy, P. (2008). Ecotoxicity of selected nano-materials to aquatic organisms. *Environmental Toxicology, 23*(5), 591-598. doi: 10.1002/tox.20402

Bohdziewicz, J., Bodzek, M., & Wasik, E. (1999). The application of reverse osmosis and nanofiltration to the removal of nitrates from groundwater. *Desalination, 121*(2), 139-147. doi: 10.1016/s0011-9164(99)00015-6

Bom, D., Andrews, R., Jacques, D., Anthony, J., Chen, B. L., Meier, M. S., & Selegue, J. P. (2002). Thermogravimetric analysis of the oxidation of multiwalled carbon nanotubes: Evidence for the role of defect sites in carbon nanotube chemistry. *Nano Letters, 2*(6), 615-619. doi: 10.1021/nl020297u

Bouazza, N., Ouzzine, M., Lillo-Rodenas, M. A., Eder, D., & Linares-Solano, A. (2009). TiO_2 nanotubes and CNT-TiO_2 hybrid materials for the photocatalytic oxidation of propene at low concentration. *Applied Catalysis B-Environmental, 92*(3-4), 377-383. doi: 10.1016/j.apcatb.2009.08.017

Bruningfann, C. S., & Kaneene, J. B. (1993). THE EFFECTS OF NITRATE, NITRITE AND N-NITROSO COMPOUNDS ON HUMAN HEALTH - A REVIEW. *Veterinary and Human Toxicology, 35*(6), 521-538.

Buresh, R. J., & Moraghan, J. T. (1976). CHEMICAL REDUCTION OF NITRATE BY FERROUS IRON. *Journal of Environmental Quality, 5*(3), 320-325.

Burow, K. R., Nolan, B. T., Rupert, M. G., & Dubrovsky, N. M. (2010). Nitrate in Groundwater of the United States, 1991-2003. *Environmental Science & Technology, 44*(13), 4988-4997. doi: 10.1021/es100546y

Buxton, G. V., & Sellers, R. M. (1973). ACID DISSOCIATION-CONSTANT OF CARBOXYL RADICAL - PULSE-RADIOLYSIS STUDIES OF AQUEOUS-SOLUTIONS OF FORMIC-ACID AND SODIUM FORMATE. *Journal of the Chemical Society-Faraday Transactions I, 69*(3), 555-559. doi: 10.1039/f19736900555

Cang, Y., Roberts, D. J., & Clifford, D. A. (2004). Development of cultures capable of reducing perchlorate and nitrate in high salt solutions. *Water Research, 38*(14-15), 3322-3330. doi: 10.1016/j.watres.2004.04.020

Carbon Nanotubes: Science and Applications. (2005). Boca Raton, FL: CRC Press LLC.

Carpenter, S. R., Caraco, N. F., Correll, D. L., Howarth, R. W., Sharpley, A. N., & Smith, V. H. (1998). NONPOINT POLLUTION OF SURFACE WATERS WITH PHOSPHORUS AND NITROGEN. *Ecological Applications, 8*(3), 559-568.

Carraway, E. R., Hoffman, A. J., & Hoffmann, M. R. (1994). PHOTOCATALYTIC OXIDATION OF ORGANIC-ACIDS ON QUANTUM-SIZED SEMICONDUCTOR COLLOIDS. *Environmental Science & Technology, 28*(5), 786-793. doi: 10.1021/es00054a007

Cevaal, J. N., Suratt, W. B., & Burke, J. E. (1995). Nitrate removal and water quality improvements with reverse osmosis for Brighten, Colorado. *Desalination, 103*(1-2), 101-111. doi: 10.1016/0011-9164(95)00091-7

Chaplin, B. P., Reinhard, M., Schneider, W. F., Schuth, C., Shapley, J. R., Strathmann, T. J., & Werth, C. J. (2012). Critical Review of Pd-Based Catalytic Treatment of Priority Contaminants in Water. *Environmental Science & Technology, 46*(7), 3655-3670. doi: 10.1021/es204087q

Chaplin, B. P., Roundy, E., Guy, K. A., Shapley, J. R., & Werth, C. J. (2006). Effects of natural water ions and humic acid on catalytic nitrate reduction kinetics using an alumina supported Pd-Cu catalyst. *Environmental Science & Technology, 40*(9), 3075-3081. doi: 10.1021/es0525298

Chen, C., Cai, W. M., Long, M. C., Zhou, B. X., Wu, Y. H., Wu, D. Y., & Feng, Y. J. (2010). Synthesis of Visible-Light Responsive Graphene Oxide/TiO_2 Composites with p/n Heterojunction. *Acs Nano, 4*(11), 6425-6432. doi: 10.1021/nn102130m

Chen, H. Z., Yang, S. G., Yu, K., Ju, Y. M., & Sun, C. (2011). Effective Photocatalytic Degradation of Atrazine over Titania-Coated Carbon Nanotubes (CNTs) Coupled with Microwave Energy. *Journal of Physical Chemistry A, 115*(14), 3034-3041. doi: 10.1021/jp109948n

Chen, J., Shan, J. Y., Tsukada, T., Munekane, F., Kuno, A., Matsuo, M., . . . Endo, M. (2007). The structural evolution of thin multi-walled carbon nanotubes during isothermal annealing. *Carbon, 45*(2), 274-280. doi: 10.1016/j.carbon.2006.09.028

Chen, L., Zhang, B. L., Qu, M. Z., & Yu, Z. L. (2005). Preparation and characterization of CNTs-TiO_2 composites. *Powder Technology, 154*(1), 70-72. doi: 10.1016/j.powtec.2005.04.028

Chen, M. L., Zhang, F. J., & Oh, W. C. (2009). Synthesis, characterization, and photocatalytic analysis of CNT/TiO_2 composites derived from MWCNTs and titanium sources. *New Carbon Materials, 24*(2), 159-166. doi: 10.1016/s1872-5805(08)60045-1

Chen, Y. S., Crittenden, J. C., Hackney, S., Sutter, L., & Hand, D. W. (2005). Preparation of a novel TiO_2-based p-n junction nanotube photocatalyst. *Environmental Science & Technology, 39*(5), 1201-1208. doi: 10.1021/es049252g

Chi, I., Zhang, S. T., Lu, X., Dong, L. H., & Yao, S. L. (2004). Chemical reduction of nitrate by metallic iron. *Journal of Water Supply Research and Technology-Aqua, 53*(1), 37-41.

Chiang, Y. C., Lin, W. H., & Chang, Y. C. (2011). The influence of treatment duration on multi-walled carbon nanotubes functionalized by H_2SO4/HNO_3 oxidation. *Applied Surface Science, 257*(6), 2401-2410. doi: 10.1016/j.apsusc.2010.09.110

Chong, M. N., Jin, B., Chow, C. W. K., & Saint, C. (2010). Recent developments in photocatalytic water treatment technology: A review. *Water Research, 44*(10), 2997-3027. doi: 10.1016/j.watres.2010.02.039

Clifford, D., & Liu, X. S. (1993). ION-EXCHANGE FOR NITRATE REMOVAL. *Journal American Water Works Association, 85*(4), 135-143.

Cong, Y., Li, X. K., Qin, Y., Dong, Z. J., Yuan, G. M., Cui, Z. W., & Lai, X. J. (2011). Carbon-doped TiO_2 coating on multiwalled carbon nanotubes with higher visible light photocatalytic activity. *Applied Catalysis B-Environmental, 107*(1-2), 128-134. doi: 10.1016/j.apcatb.2011.07.005

Cook, A. R., Dimitrijevic, N., Dreyfus, B. W., Meisel, D., Curtiss, L. A., & Camaioni, D. M. (2001). Reducing radicals in nitrate solutions. The NO_3^{2-} system revisited. *Journal of Physical Chemistry A, 105*(14), 3658-3666. doi: 10.1021/jp0038052

Cueto, L. F., Martinez, G. T., Zavala, G., & Sanchez, E. M. (2010). Surface Characterization and CO2 Reduction Using Electrodeposited Silver Particles over TiO_2 Thin Film. *Journal of Nano Research, 9*, 89-100. doi: 10.4028/www.scientific.net/JNanoR.9.89

da Cunha, M., De Souza, J. P. I., & Nart, F. C. (2000). Reaction pathways for reduction of nitrate ions on platinum, rhodium, and platinum-rhodium alloy electrodes. *Langmuir, 16*(2), 771-777. doi: 10.1021/la990638s

Dash, B. P., & Chaudhari, S. (2005). Electrochemical denitrificaton of simulated ground water. *Water research, 39*(17), 4065-4072.

Daub, K., Wunder, V. K., & Dittmeyer, R. (2001). CVD preparation of catalytic membranes for reduction of nitrates in water. *Catalysis Today, 67*(1-3), 257-272. doi: 10.1016/s0920-5861(01)00313-3

Devadas, A., Vasudevan, S., & Epron, F. (2011). Nitrate reduction in water: Influence of the addition of a second metal on the performances of the Pd/CeO_2 catalyst. *Journal of Hazardous Materials, 185*(2-3), 1412-1417. doi: 10.1016/j.jhazmat.2010.10.063

Dey, G. R. (2007). Chemical reduction of CO_2 to different products during photo catalytic reaction on TiO_2 under diverse conditions: an overview. *Journal of Natural Gas Chemistry, 16*(3), 217-226.

Dhar, N. R. (1934). Denitrification in sunlight. *Nature, 134*, 572-573.

Dhar, N. R., Tandon, S. P., Biswas, N. N., & Bhateacharya, A. K. (1934). Photo-oxidation of nitrite to nitrate. *Nature, 133*, 213-214.

Diebold, U. (2003). The surface science of titanium dioxide. *Surface Science Reports, 48*(5-8), 53-229. doi: 10.1016/s0167-5729(02)00100-0

Doll, T. E., & Frimmel, F. H. (2004). Kinetic study of photocatalytic degradation of carbamazepine, clofibric acid, iomeprol and iopromide assisted by different TiO_2 materials - determination of intermediates and reaction pathways. *Water Research, 38*(4), 955-964. doi: 10.1016/j.watres.2003.11.009

Doll, T. E., & Frimmel, F. H. (2005). Photocatalytic degradation of carbamazepine, clofibric acid and iomeprol with P25 and Hombikat UV100 in the presence of natural organic matter (NOM) and other organic water constituents. *Water Research, 39*(2-3), 403-411. doi: 10.1016/j.watres.2004.09.016

Domen, K., Kudo, A., & Onishi, T. (1986). MECHANISM OF PHOTOCATALYTIC DECOMPOSITION OF WATER INTO H-2 AND O-2 OVER NIO - $SRTIO_3$. *Journal of Catalysis, 102*(1), 92-98.

Domen, K., Naito, S., Onishi, T., & Tamaru, K. (1982). PHOTOCATALYTIC DECOMPOSITION OF LIQUID WATER ON A NIO $SRTIO_3$ CATALYST. *Chemical Physics Letters, 92*(4), 433-434.

Dortsiou, M., Katsounaros, I., Polatides, C., & Kyriacou, G. (2009). Electrochemical removal of nitrate from the spent regenerant solution of the ion exchange. *Desalination, 248*(1-3), 923-930. doi: 10.1016/j.desal.2008.10.012

Doudrick, K., Herckes, P., & Westerhoff, P. (2012). Detection of carbon nanotubes in environmental matrices using programmed thermal analysis. *Environmental Science and Technology, 46*(22), 12246-12253.

Doudrick, K. D., Monzón, O., Mangonon, A., Hristovski, K., & Westerhoff, P. K. (2012). Nitrate Reduction in Water Using Commercial Titanium Dioxide Photocatalysts (P25, P90, and Hombikat UV100). *ASCE Journal of Environmental Engineering, In Press*.

Dresselhaus, M. S., Dresselhaus, G., Saito, R., & Jorio, A. (2005). Raman spectroscopy of carbon nanotubes. *Physics Reports-Review Section of Physics Letters, 409*(2), 47-99. doi: 10.1016/j.physrep.2004.10.006

Duca, M., Kavvadia, V., Rodriguez, P., Lai, S. C. S., Hoogenboom, T., & Koper, M. T. M. (2010). New insights into the mechanism of nitrite reduction on a platinum electrode. *Journal of Electroanalytical Chemistry, 649*(1-2), 59-68. doi: 10.1016/j.jelechem.2010.01.019

Duca, M., Khamseh, S., Lai, S. C. S., & Koper, M. T. M. (2010). The Influence of Solution-Phase HNO(2) Decomposition on the Electrocatalytic Nitrite Reduction

at a Hemin-Pyrolitic Graphite Electrode. *Langmuir, 26*(14), 12418-12424. doi: 10.1021/la101172f

Duca, M., & Koper, M. T. M. (2012). Powering denitrification: the perspectives of electrocatalytic nitrate reduction. *Energy & Environmental Science, 5*(12), 9726-9742. doi: 10.1039/c2ee23062c

Duca, M., van der Klugt, B., & Koper, M. T. M. (2012). Electrocatalytic reduction of nitrite on transition and coinage metals. *Electrochimica Acta, 68*, 32-43. doi: 10.1016/j.electacta.2012.02.037

Eder, D., & Windle, A. H. (2008). Carbon-inorganic hybrid materials: The carbon-nanotube/TiO2 interface. *Advanced Materials, 20*(9), 1787

El Midaoui, A., Elhannouni, F., Taky, M., Chay, L., Sahli, M. A. M., Echihabi, L., & Hafsi, M. (2002). Optimization of nitrate removal operation from ground water by electrodialysis. *Separation and Purification Technology, 29*(3), 235-244. doi: 10.1016/s1383-5866(02)00092-8

Elmidaoui, A., Elhannouni, F., Sahli, M. A. M., Chay, L., Elabbassi, H., Hafsi, M., & Largeteau, D. (2001). Pollution of nitrate in Moroccan ground water: removal by electrodialysis. *Desalination, 136*(1-3), 325-332. doi: 10.1016/s0011-9164(01)00195-3

Endo, M., Strano, M. S., & Ajayan, P. M. (2008). Potential applications of carbon nanotubes. *Carbon Nanotubes, 111*, 13-61.

Energy, D. o. (2008). New Science for a Secure and Sustainable Energy Future. In J. Hemminger (Ed.).

EPA, U. S. PART 136—GUIDELINES ESTABLISHING TEST PROCEDURES FOR THE ANALYSIS OF POLLUTANTS. Definition and Procedure for the Determination of the Method Detection Limit—Revision 1.11 (Vol. Federal Register, 49 FR 43430 (10/26/84), 50 FR 694 (1/4/85),and 51 FR (6/30/86).).

Epron, F., Gauthard, F., & Barbier, J. (2002a). Catalytic reduction of nitrate in water on a monometallic Pd/CeO2 catalyst. *Journal of Catalysis, 206*(2), 363-367. doi: 10.1006/jcat.2001.3498

Epron, F., Gauthard, F., & Barbier, J. (2002b). Influence of oxidizing and reducing treatments on the metal-metal interactions and on the activity for nitrate reduction of a Pt-Cu bimetallic catalyst. *Applied Catalysis a-General, 237*(1-2), 253-261.

Fan, W. G., Gao, L., & Sun, J. (2006). Anatase TiO_2-coated multi-wall carbon nanotubes with the vapor phase method. *JOURNAL OF THE AMERICAN CERAMIC SOCIETY, 89*(2), 731-733.

Fanning, J. C. (2000). The chemical reduction of nitrate in aqueous solution. *Coordination Chemistry Reviews, 199*, 159-179.

Firme, C. P., & Bandaru, P. R. (2010). Toxicity issues in the application of carbon nanotubes to biological systems. *Nanomedicine-Nanotechnology Biology and Medicine, 6*(2), 245-256. doi: 10.1016/j.nano.2009.07.003

Formenti, M., Juillet, F., Meriaude.P, & Teichner, S. J. (1971). HETEROGENEOUS PHOTOCATALYSIS FOR PARTIAL OXIDATION OF PARAFFINS. *Chemical Technology* (NOV), 680.

Formenti, M., Juillet, F., & Teichner, S. J. (1970). PHOTOOXIDATION OF PARAFFINS AND OLEFINS IN PRESENCE OF ANATASE AT AMBIENT TEMPERATURE. *Comptes Rendus Hebdomadaires Des Seances De L Academie Des Sciences Serie C, 270*(2), 138-&.

Formenti, M., Teichner, S. J., Juillet, F., Courbon, H., Lissatch.A, Meriaude.P, & Martin, J. R. (1972). PHOTOINTERACTION BETWEEN OXYGEN AND NONPOROUS PARTICLES OF ANATASE. *Journal of Vacuum Science & Technology, 9*(2), 947-&.

Frank, S. N., & Bard, A. J. (1977). HETEROGENEOUS PHOTOCATALYTIC OXIDATION OF CYANIDE AND SULFITE IN AQUEOUS-SOLUTIONS AT SEMICONDUCTOR POWDERS. *Journal of Physical Chemistry, 81*(15), 1484-1488.

Fujishima, A., & Honda, K. (1972). ELECTROCHEMICAL PHOTOLYSIS OF WATER AT A SEMICONDUCTOR ELECTRODE. *Nature, 238*(5358), 37.

Fujishima, A., & Zhang, X. (2006). Titanium dioxide photocatalysis: present situation and future approaches. *Comptes Rendus Chimie, 9*(5-6), 750.

Gagliardi, C. J., Vannucci, A. K., Concepcion, J. J., Chen, Z. F., & Meyer, T. J. (2012). The role of proton coupled electron transfer in water oxidation. *Energy & Environmental Science, 5*(7), 7704-7717. doi: 10.1039/c2ee03311a

Gagliardi, C. J., Westlake, B. C., Kent, C. A., Paul, J. J., Papanikolas, J. M., & Meyer, T. J. (2010). Integrating proton coupled electron transfer (PCET) and excited states. *Coordination Chemistry Reviews, 254*(21-22), 2459-2471. doi: 10.1016/j.ccr.2010.03.001

Gao, B., Chen, G. Z., & Puma, G. L. (2009). Carbon nanotubes/titanium dioxide (CNTs/TiO2) nanocomposites prepared by conventional and novel surfactant wrapping sol-gel methods exhibiting enhanced photocatalytic activity. *Applied Catalysis B-Environmental, 89*(3-4), 503-509. doi: 10.1016/j.apcatb.2009.01.009

Gao, B., Ma, Y., Cao, Y., Yang, W., & Yao, J. (2006). Great enhancement of photocatalytic activity of nitrogen-doped titania by coupling with tungsten oxide. *Journal of Physical Chemistry B, 110*(29), 14391-14397. doi: 10.1021/jp0624606

Gao, B., Peng, C. A., Chen, G. Z., & Puma, G. L. (2008). Photo-electro-catalysis enhancement on carbon nanotubes/titanium dioxide ($CNTs/TiO_2$) composite prepared by a novel surfactant wrapping sol-gel method. *Applied Catalysis B-Environmental, 85*(1-2), 17-23. doi: 10.1016/j.apcatb.2008.06.027

Gao, W., Guan, N., Chen, J., Guan, X., Jin, R., Zeng, H., Zhang, F. (2003). Titania supported Pd-Cu bimetallic catalyst for the reduction of nitrate in drinking water. *Applied Catalysis B: Environmental, 46*(2), 341.

Gao, W., Jin, R., Chen, J., Guan, X., Zeng, H., Zhang, F., & Guan, N. (2004). Titania-supported bimetallic catalysts for photocatalytic reduction of nitrate. *Catalysis Today, 90*(3-4), 331.

Gao, W. L., Jin, R. C., Chen, M. X., Guan, X. X., Zeng, H. S., Zhang, F. X., & Guan, N. J. (2004). Titania-supported bimetallic catalysts for photocatalytic reduction of nitrate. *Catalysis Today, 90*(3-4), 331-336. doi: 10.1016/j.cattod.2004.04.043

Garron, A., & Epron, F. (2005). Use of formic acid as reducing agent for application in catalytic reduction of nitrate in water. *Water Research, 39*(13), 3073-3081. doi: 10.1016/j.watres.2005.05.012

Gasparovicova, D., & Kralik, M. (2000). Catalytic reduction of nitrates in drinking water over Pd-Cu catalysts. *Chemicke Listy, 94*(5), 308-313.

Gauthard, F., Epron, F., & Barbier, J. (2003). Palladium and platinum-based catalysts in the catalytic reduction of nitrate in water: effect of copper, silver, or gold addition. *Journal of Catalysis, 220*(1), 182-191. doi: 10.1016/s0021-9517(03)00252-5

Gayle, B. P., Boardman, G. D., Sherrard, J. H., & Benoit, R. E. (1989). Biological denitrification of water. *Journal of Environmental Engineering-Asce, 115*(5), 930-943.

Gašparovičová, D., Králik, M., Hronec, M., Vallušová, Z., Vinek, H., & Corain, B. (2007). Supported Pd–Cu catalysts in the water phase reduction of nitrates: Functional resin versus alumina. *Journal of Molecular Catalysis A: Chemical, 264*(1-2), 93.

Gerischer, H., & Heller, A. (1991). The role of oxygen in photooxidation of organic molecules on semiconductor particles. *The Journal of physical chemistry, 95*(13), 5261.

Gong, Q. M., Li, Z., Wang, Y., Wu, B., Zhang, Z., & Liang, J. (2007). The effect of high-temperature annealing on the structure and electrical properties of well-aligned

carbon nanotubes. *Materials Research Bulletin, 42*(3), 474-481. doi: 10.1016/j.materresbull.2006.06.023

Gratzel, M. (1989). *Heterogeneous Photochemical Electron Transfer*. Boca Raton, FL: CRC Press, Inc.

Gratzel, M. (2001). Photoelectrochemical cells. *NATURE, 414*(6861), 338-344.

Griffis, L. C., Wolff, R. K., Henderson, R. F., Griffith, W. C., Mokler, B. V., & McClellan, R. O. (1983). CLEARANCE OF DIESEL SOOT PARTICLES FROM RAT LUNG AFTER A SUBCHRONIC DIESEL EXHAUST EXPOSURE. *Fundamental and Applied Toxicology, 3*(2), 99-103. doi: 10.1016/s0272-0590(83)80063-3

Guan, G. Q., Kida, T., & Yoshida, A. (2003). Reduction of carbon dioxide with water under concentrated sunlight using photocatalyst combined with Fe-based catalyst. *Applied Catalysis B-Environmental, 41*(4), 387-396.

Guillette, L. J., & Edwards, T. M. (2005). Is nitrate an ecologically relevant endocrine disruptor in vertebrates? *Integrative and Comparative Biology, 45*(1), 19-27.

Guo, Y. N., Cheng, J. H., Hu, Y. Y., & Li, D. H. (2012). The effect of TiO_2 doping on the catalytic properties of nano-Pd/SnO2 catalysts during the reduction of nitrate. *Applied Catalysis B-Environmental, 125*, 21-27. doi: 10.1016/j.apcatb.2012.05.012

Gustafsson, O., Bucheli, T. D., Kukulska, Z., Andersson, M., Largeau, C., Rouzaud, J. N., Eglinton, T. I. (2001). Evaluation of a protocol for the quantification of black carbon in sediments. *Global Biogeochemical Cycles, 15*(4), 881-890. doi: 10.1029/2000gb001380

Guy, K. A., Xu, H. P., Yang, J. C., Werth, C. J., & Shapley, J. R. (2009). Catalytic Nitrate and Nitrite Reduction with Pd-Cu/PVP Colloids in Water: Composition, Structure, and Reactivity Correlations. *Journal of Physical Chemistry C, 113*(19), 8177-8185. doi: 10.1021/jp810049y

Hagfeldt, A., & Gratzel, M. (1995). LIGHT-INDUCED REDOX REACTIONS IN NANOCRYSTALLINE SYSTEMS. *Chemical Reviews, 95*(1), 49-68.

Hamanoi, O., & Kudo, A. (2002). Reduction of nitrate and nitrite ions over Ni-ZnS photocatalyst under visible light irradiation in the presence of a sacrificial reagent. *Chemistry Letters*(8), 838-839.

Hamlin, H. J. (2006). Nitrate toxicity in Siberian sturgeon (Acipenser baeri). *Aquaculture, 253*(1-4), 688-693. doi: 10.1016/j.aquaculture.2005.08.025

Hamlin, H. J., Moore, B. C., Edwards, T. M., Larkin, I. L. V., Boggs, A., High, W. J., . . . Guillette, L. J. (2008). Nitrate-induced elevations in circulating sex steroid concentrations in female Siberian sturgeon (Acipenser baeri) in commercial aquaculture. *Aquaculture, 281*(1-4), 118-125. doi: 10.1016/j.aquaculture.2008.05.030

Hammes, K., Schmidt, M. W. I., Smernik, R. J., Currie, L. A., Ball, W. P., Nguyen, T. H., . . . Ding, L. (2007). Comparison of quantification methods to measure fire-derived (black/elemental) carbon in soils and sediments using reference materials from soil, water, sediment and the atmosphere. *Global Biogeochemical Cycles, 21*(3), 18. doi: Gb301610.1029/2006gb002914

Han, J. H., Lee, E. J., Lee, J. H., So, K. P., Lee, Y. H., Bae, G. N., . . . Yu, I. J. (2008). Monitoring multiwalled carbon nanotube exposure in carbon nanotube research facility. *Inhalation Toxicology, 20*(8), 741-749. doi: 10.1080/08958370801942238

Harbour, J. R., & Hair, M. L. (1979). RADICAL INTERMEDIATES IN THE PHOTOSYNTHETIC GENERATION OF H2O2 WITH AQUEOUS ZNO DISPERSIONS. *Journal of Physical Chemistry, 83*(6), 652-656. doi: 10.1021/j100469a003

Hatchard, C. G., & Parker, C. A. (1956). A NEW SENSITIVE CHEMICAL ACTINOMETER .2. POTASSIUM FERRIOXALATE AS A STANDARD CHEMICAL ACTINOMETER. *Proceedings of the Royal Society of London Series a-Mathematical and Physical Sciences, 235*(1203), 518-536.

Health, N. I. f. O. S. a. (1998). Elemental Carbon (Diesel Particulate): Method 5040. NIOSH Manual of Analytical Methods (4th Edition ed.).

Hell, F., Lahnsteiner, J., Frischherz, H., & Baumgartner, G. (1998). Experience with full-scale electrodialysis for nitrate and hardness removal. *Desalination, 117*(1-3), 173-180. doi: 10.1016/s0011-9164(98)00088-5

Herrera, J. E., & Resasco, D. E. (2003). In situ TPO/Raman to characterize single-walled carbon nanotubes. *Chemical Physics Letters, 376*(3-4), 302-309. doi: 10.1016/s0009-2614(03)00987-4

Herrmann, J. M. (1999). Heterogeneous photocatalysis: fundamentals and applications to the removal of various types of aqueous pollutants. *Catalysis Today, 53*(1), 115-129.

Hirayama, J., Kondo, H., Miura, Y. K., Abe, R., & Kamiya, Y. (2012). Highly effective photocatalytic system comprising semiconductor photocatalyst and supported bimetallic non-photocatalyst for selective reduction of nitrate to nitrogen in water. *Catalysis Communications, 20*, 99-102. doi: 10.1016/j.catcom.2012.01.011

Hiscock, K. M., Lloyd, J. W., & Lerner, D. N. (1991). Review of natural and artificial denitrification of groundwater. *Water Research, 25*(9), 1099-1111. doi: 10.1016/0043-1354(91)90203-3

Hitoki, G., Ishikawa, A., Takata, T., Kondo, J. N., Hara, M., & Domen, K. (2002). Ta3N5 as a novel visible light-driven photocatalyst (lambda < 600 nm). *Chemistry Letters*(7), 736-737.

Hitoki, G., Takata, T., Kondo, J. N., Hara, M., Kobayashi, H., & Domen, K. (2002). An oxynitride, TaON, as an efficient water oxidation photocatalyst under visible light irradiation (lambda <= 500 nm). *Chemical Communications*(16), 1698-1699. doi: 10.1039/b202393h

Hoffmann, M. R., Martin, S. T., Choi, W. Y., & Bahnemann, D. W. (1995). ENVIRONMENTAL APPLICATIONS OF SEMICONDUCTOR PHOTOCATALYSIS. *Chemical Reviews, 95*(1), 69-96.

Horold, S., Vorlop, K. D., Tacke, T., & Sell, M. (1993). DEVELOPMENT OF CATALYSTS FOR A SELECTIVE NITRATE AND NITRITE REMOVAL FROM DRINKING-WATER. *Catalysis Today, 17*(1-2), 21-30. doi: 10.1016/0920-5861(93)80004-k

Hou, P. X., Liu, C., & Cheng, H. M. (2008). Purification of carbon nanotubes. *Carbon, 46*(15), 2003-2025. doi: 10.1016/j.carbon.2008.09.009

Howe, R. F., & Gratzel, M. (1985). ELECTRON-PARAMAGNETIC-RES OBSERVATION OF TRAPPED ELECTRONS IN COLLOIDAL TIO2. *Journal of Physical Chemistry, 89*(21), 4495-4499.

Hsiao, C.-Y., Lee, C.-L., & Ollis, D. F. (1983). Heterogeneous photocatalysis: Degradation of dilute solutions of dichloromethane (CH_2Cl_2), chloroform (CHCl3), and carbon tetrachloride (CCl4) with illuminated TiO_2 photocatalyst. *Journal of Catalysis, 82*(2), 418-423.

Hsu, C. L., Wang, S. L., & Tzou, Y. M. (2007). Photocatalyfic reduction of Cr(VI) in the presence of NO_3^- and Cl^- electrolytes as influenced by Fe(III). *Environmental Science & Technology, 41*(22), 7907-7914.

Huang, H., Zou, M., Xu, X., Liu, F., Li, N., & Wang, X. (2011). Near-infrared fluorescence spectroscopy of single-walled carbon nanotubes and its applications. *TrAC Trends in Analytical Chemistry, 30*(7), 1109-1119.

Huang, L. H., Wang, H. J., Liu, Y. L., Jiao, Z. B., & Shao, Z. B. (2010). TiO_2/Carbon Nanotube Composites and Their Synergistic Effects on Enhancing the Photocatalysis Efficiency. *Progress in Chemistry, 22*(5), 867-876.

Huang, Q., & Gao, L. (2003). Immobilization of rutile TiO_2 on multiwalled carbon nanotubes. *JOURNAL OF MATERIALS CHEMISTRY, 13*(7), 1517-1519.

Huang, W., Wang, Y., Luo, G. H., & Wei, F. (2003). 99.9% purity multi-walled carbon nanotubes by vacuum high-temperature annealing. *Carbon, 41*(13), 2585-2590. doi: 10.1016/s0008-6223(03)00330-0

Hurum, D. C., Agrios, A. G., Crist, S. E., Gray, K. A., Rajh, T., & Thurnauer, M. C. (2006). Probing reaction mechanisms in mixed phase TiO2 by EPR. *Journal of Electron Spectroscopy and Related Phenomena, 150*(2-3), 155-163. doi: 10.1016/j.elspec.2005.01.294

Hurum, D. C., Agrios, A. G., Gray, K. A., Rajh, T., & Thurnauer, M. C. (2003). Explaining the enhanced photocatalytic activity of Degussa P25 mixed-phase TiO2 using EPR. *Journal of Physical Chemistry B, 107*(19), 4545-4549. doi: 10.1021/jp0273934

Hurum, D. C., Gray, K. A., Rajh, T., & Thurnauer, M. C. (2005). Recombination pathways in the Degussa P25 formulation of TiO_2: Surface versus lattice mechanisms. *Journal of Physical Chemistry B, 109*(2), 977-980. doi: 10.1021/jp015395d

Huynh, M. H. V., & Meyer, T. J. (2007). Proton-coupled electron transfer. *Chemical Reviews, 107*(11), 5004-5064. doi: 10.1021/cr0500030

Hykaway, N., Sears, W. M., Morisaki, H., & Morrison, S. R. (1986). CURRENT-DOUBLING REACTIONS ON TITANIUM-DIOXIDE PHOTOANODES. *Journal of Physical Chemistry, 90*(25), 6663-6667. doi: 10.1021/j100283a014

Hyung, H., Fortner, J. D., Hughes, J. B., & Kim, J. H. (2007). Natural organic matter stabilizes carbon nanotubes in the aqueous phase. *Environmental Science & Technology, 41*(1), 179-184. doi: 10.1021/es061817g

Igarashi, M., Fukuda, M., Taki, M., Tago, T., Minowa, T., Okada, Y., & Nishimura, J. (1995). PHOTOREDUCTION OF WATER BY THE SYSTEM OF C-60-PLATINUM-METHYLVIOLOGEN. *Fullerene Science and Technology, 3*(1), 37-43.

Inam Ul, H., & Tariq, M. (2010). Electrochemical Reduction of Nitrate: A Review. *Journal of the Chemical Society of Pakistan, 32*(3), 396-418.

Indrakanti, V. P., Kubicki, J. D., & Schobert, H. H. (2009). Photoinduced activation of CO2 on Ti-based heterogeneous catalysts: Current state, chemical physics-based insights and outlook. *Energy & Environmental Science, 2*(7), 745-758. doi: 10.1039/b822176f

Indusekhar, V. K., Trivedi, G. S., & Shah, B. G. (1991). REMOVAL OF NITRATE BY ELECTRODIALYSIS. *Desalination, 84*(1-3), 213-221. doi: 10.1016/0011-9164(91)85131-d

Innovative Research and Products, I. (2011). Production and applications of carbon nanotubes, carbon nanofibers, fullerenes, graphene, and nanodiamonds: A global technology survey and market analysis (pp. 531).

Inoue, T., Fujishima, A., Konishi, S., & Honda, K. (1979). PHOTOELECTROCATALYTIC REDUCTION OF CARBON-DIOXIDE IN AQUEOUS SUSPENSIONS OF SEMICONDUCTOR POWDERS. *Nature, 277*(5698), 637-638.

Iwase, A., Kato, H., & Kudo, A. (2010). A Simple Preparation Method of Visible-Light-Driven BiVO4 Photocatalysts From Oxide Starting Materials (Bi_2O_3 and V_2O_5) and Their Photocatalytic Activities. *Journal of Solar Energy Engineering-Transactions of the Asme, 132*(2), 5. doi: 02110610.1115/1.4001172

Jeong, S. H., Kim, K. K., Jeong, S. J., An, K. H., Lee, S. H., & Lee, Y. H. (2007). Optical absorption spectroscopy for determining carbon nanotube concentration in solution. *Synthetic Metals, 157*(13-15), 570-574. doi: 10.1016/j.synthmet.2007.06.012

Jiang, G. H., Zheng, X. Y., Wang, Y., Li, T. W., & Sun, X. K. (2011). Photo-degradation of methylene blue by multi-walled carbon nanotubes/TiO_2 composites. *Powder Technology, 207*(1-3), 465-469. doi: 10.1016/j.powtec.2010.11.029

Jin, R. C., Gao, W. L., Chen, J. X., Zeng, H. S., Zhang, F. X., Liu, Z. G., & Guan, N. J. (2004). Photocatalytic reduction of nitrate ion in drinking water by using metal-loaded MgTiO3-TiO2 composite semiconductor catalyst. *Journal of Photochemistry and Photobiology a-Chemistry, 162*(2-3), 585-590. doi: 10.1016/s1010-6030(03)00420-9

Kajitvichyanukul, P., Ananpattarachai, J., & Pongpom, S. (2005). Sol-gel preparation and properties study of TiO2 thin film for photocatalytic reduction of chromium(VI) in photocatalysis process. *Science and Technology of Advanced Materials, 6*(3-4), 352-358. doi: 10.1016/j.stam.2005.02.014

Kajiura, H., Nandyala, A., & Bezryadin, A. (2005). Quasi-ballistic electron transport in as-produced and annealed multiwall carbon nanotubes. *Carbon, 43*(6), 1317-1319. doi: 10.1016/j.carbon.2004.12.004

Kalbac, M., Frank, O., Kavan, L., Zukalova, M., Prochazka, J., Klementova, M., & Dunsch, L. (2007). Heterostructures from single-wall carbon nanotubes and TiO_2 nanocrystals. *Journal of the Electrochemical Society, 154*(8), K19-K24. doi: 10.1149/1.2741132

Kang, S.-Z., Cui, Z., & Mu, J. (2007). Composite of Carboxyl-Modified Multi-walled Carbon Nanotubes and TiO2 Nanoparticles: Preparation and Photocatalytic Activity. *Fullerenes, Nanotubes and Carbon Nanostructures, 15*(2), 81.

Kapoor, M. P., Inagaki, S., & Yoshida, H. (2005). Novel zirconium-titanium phosphates mesoporous materials for hydrogen production by photoinduced water splitting. *Journal of Physical Chemistry B, 109*(19), 9231-9238. doi: 10.1021/jp045012b

Karanasios, K. A., Vasiliadou, I. A., Pavlou, S., & Vayenas, D. V. (2010). Hydrogenotrophic denitrification of potable water: A review. *Journal of Hazardous Materials, 180*(1-3), 20-37. doi: 10.1016/j.jhazmat.2010.04.090

Kato, H., Asakura, K., & Kudo, A. (2003). Highly efficient water splitting into H-2 and O-2 over lanthanum-doped NaTaO3 photocatalysts with high crystallinity and surface nanostructure. *Journal of the American Chemical Society, 125*(10), 3082-3089. doi: 10.1021/ja027751g

Kato, H., & Kudo, A. (1999). Highly efficient decomposition of pure water into H-2 and O-2 over NaTaO3 photocatalysts. *Catalysis Letters, 58*(2-3), 153-155.

Kato, H., & Kudo, A. (2002a). Photocatalytic reduction of nitrate ions over tantalate photocatalysts. *Physical Chemistry Chemical Physics, 4*(12), 2833-2838. doi: 10.1039/b110511f

Kato, H., & Kudo, A. (2002b). Photocatalytic reduction of nitrate ions over tantalate photocatalysts. *Physical Chemistry Chemical Physics, 4*(12), 2833.

Katsounaros, I., Dortsiou, M., Polatides, C., Preston, S., Kypraios, T., & Kyriacou, G. (2012). Reaction pathways in the electrochemical reduction of nitrate on tin. *Electrochimica Acta, 71*, 270-276. doi: 10.1016/j.electacta.2012.03.154

Katsounaros, I., Ipsakis, D., Polatides, C., & Kyriacou, G. (2006). Efficient electrochemical reduction of nitrate to nitrogen on tin cathode at very high cathodic potentials. *Electrochimica Acta, 52*(3), 1329.

Katsounaros, I., & Kyriacou, G. (2008). Influence of nitrate concentration on its electrochemical reduction on tin cathode: Identification of reaction intermediates. *Electrochimica Acta, 53*(17), 5477-5484.

Kesore, K., Janowski, F., & Shaposhnik, V. A. (1997). Highly effective electrodialysis for selective elimination of nitrates from drinking water. *Journal of Membrane Science, 127*(1), 17-24. doi: 10.1016/s0376-7388(96)00282-7

Ketir, W., Bouguelia, A., & Trari, M. (2009). NO_3^- removal with a new delafossite $CuCrO_2$ photocatalyst. *Desalination, 244*(1-3), 144-152.

Kho, Y. K., Iwase, A., Teoh, W. Y., Madler, L., Kudo, A., & Amal, R. (2010). Photocatalytic H-2 Evolution over TiO_2 Nanoparticles. The Synergistic Effect of Anatase and Rutile. *Journal of Physical Chemistry C, 114*(6), 2821-2829. doi: 10.1021/jp910810r

Kim, Y. A., Hayashi, T., Osawa, K., Dresselhaus, M. S., & Endo, M. (2003). Annealing effect on disordered multi-wall carbon nanotubes. *Chemical Physics Letters, 380*(3-4), 319-324. doi: 10.1016/j.cplett.2003.09.027

Kim, Y. A., Muramatsu, H., Hayashi, T., Endo, M., Terrones, M., & Dresselhaus, M. S. (2004). Thermal stability and structural changes of double-walled carbon nanotubes by heat treatment. *Chemical Physics Letters, 398*(1-3), 87-92. doi: 10.1016/j.cplett.2004.09.024

Kirchnerova, J., Cohen, M. L. H., Guy, C., & Klvana, D. (2005). Photocatalytic oxidation of n-butanol under fluorescent visible light lamp over commercial TiO_2 (Hombicat UV100 and Degussa P25). *Applied Catalysis a-General, 282*(1-2), 321-332. doi: 10.1016/j.apcata.2004.12.045

Kitano, M., & Hara, M. (2010). Heterogeneous photocatalytic cleavage of water. *Journal of Materials Chemistry, 20*(4), 627-641. doi: 10.1039/b910180b

Koci, K., Mateju, K., Obalova, L., Krejcikova, S., Lacny, Z., Placha, D., . . . Solcova, O. (2010). Effect of silver doping on the TiO_2 for photocatalytic reduction of CO_2. *Applied Catalysis B-Environmental, 96*(3-4), 239-244. doi: 10.1016/j.apcatb.2010.02.030

Koci, K., Obalova, L., & Lacny, Z. (2008). Photocatalytic reduction of CO_2 over TiO_2 based catalysts. *Chemical Papers, 62*(1), 1-9. doi: 10.2478/s11696-007-0072-x

Koci, K., Obalova, L., Matejova, L., Placha, D., Lacny, Z., Jirkovsky, J., & Solcova, O. (2009). Effect of TiO_2 particle size on the photocatalytic reduction of CO2. *Applied Catalysis B-Environmental, 89*(3-4), 494-502. doi: 10.1016/j.apcatb.2009.01.010

Kominami, H., Furusho, A., Murakami, S., Inoue, H., Kera, Y., & Ohtani, B. (2001a). Effective photocatalytic reduction of nitrate to ammonia in an aqueous suspension of metal-loaded titanium(IV) oxide particles in the presence of oxalic acid. *Catalysis Letters, 76*(1-2), 31.

Kominami, H., Furusho, A., Murakami, S., Inoue, H., Kera, Y., & Ohtani, B. (2001b). Effective photocatalytic reduction of nitrate to ammonia in an aqueous suspension of metal-loaded titanium(IV) oxide particles in the presence of oxalic acid. *Catalysis Letters, 76*(1-2), 31-34. doi: 10.1023/a:1016771908609

Kominami, H., Gekko, H., & Hashimoto, K. (2010). Photocatalytic disproportionation of nitrite to dinitrogen and nitrate in an aqueous suspension of metal-loaded titanium(IV) oxide nanoparticles. *Physical Chemistry Chemical Physics, 12*(47), 15423-15427. doi: 10.1039/c0cp00794c

Kominami, H., Nakaseko, T., Shimada, Y., Furusho, A., Inoue, H., Murakami, S., . . . Ohtani, B. (2005a). Selective photocatalytic reduction of nitrate to nitrogen molecules in an aqueous suspension of metal-loaded titanium(IV) oxide particles. *Chemical Communications, 45*(23), 2933-2935. doi: 10.1039/b502909k

Kominami, H., Nakaseko, T., Shimada, Y., Furusho, A., Inoue, H., Murakami, S., . . . Ohtani, B. (2005b). Selective photocatalytic reduction of nitrate to nitrogen molecules in an aqueous suspension of metal-loaded titanium(IV) oxide particles. *Chemical Communications*(23), 2933-2935. doi: 10.1039/b502909k

Kongkanand, A., & Kamat, P. V. (2007). Electron Storage in Single Wall Carbon Nanotubes. Fermi Level Equilibration in Semiconductorâ€“SWCNT Suspensions. *ACS Nano, 1*(1), 13.

Koppenol, W. H., & Rush, J. D. (1987). REDUCTION POTENTIAL OF THE CO2/CO2.- COUPLE - A COMPARISON WITH OTHER C1 RADICALS. *Journal of Physical Chemistry, 91*(16), 4429-4430.

Korgel, B. A., & Monbouquette, H. G. (1997). Quantum confinement effects enable photocatalyzed nitrate reduction at neutral pH using CdS nanocrystals. *Journal of Physical Chemistry B, 101*(25), 5010.

Kormann, C., Bahnemann, D. W., & Hoffmann, M. R. (1991). PHOTOLYSIS OF CHLOROFORM AND OTHER ORGANIC-MOLECULES IN AQUEOUS TIO2 SUSPENSIONS. *Environmental Science & Technology, 25*(3), 494-500. doi: 10.1021/es00015a018

Kudo, A. (2006). Development of photocatalyst materials for water splitting. *International Journal of Hydrogen Energy, 31*(2), 197-202. doi: 10.1016/j.ijhydene.2005.04.050

Kudo, A. (2007). Recent progress in the development of visible light-driven powdered photocatalysts for water splitting. *International Journal of Hydrogen Energy, 32*(14), 2673-2678. doi: 10.1016/j.ijhydene.2006.09.010

Kudo, A., Domen, K., Maruya, K., & Onishi, T. (1987a). PHOTOCATALYTIC REDUCTION OF NO3- TO FORM NH3 OVER PT-TIO_2. *Chemistry Letters*(6), 1019-1022. doi: 10.1246/cl.1987.1019

Kudo, A., Domen, K., Maruya, K., & Onishi, T. (1987b). Photocatalytic Reduction of NO_3- to Form NH_3 over PT-TiO_2. *CHEMISTRY LETTERS*(6), 1019-1022
.
Kudo, A., Domen, K., Maruya, K.-i., & Onishi, T. (1992). Reduction of nitrate ions into nitrite and ammonia over some photocatalysts. *Journal of Catalysis, 135*(1), 300-303.

Kudo, A., & Kato, H. (2000). Effect of lanthanide-doping into NaTaO3 photocatalysts for efficient water splitting. *Chemical Physics Letters, 331*(5-6), 373-377.

Kudo, A., Kato, H., & Tsuji, I. (2004). Strategies for the development of visible-light-driven photocatalysts for water splitting. *Chemistry Letters, 33*(12), 1534-1539.

Kudo, A., & Miseki, Y. (2009). Heterogeneous photocatalyst materials for water splitting. *Chemical Society Reviews, 38*(1), 253-278. doi: 10.1039/b800489g

Kuhlbusch, T. A. J., Asbach, C., Fissan, H., Gohler, D., & Stintz, M. (2011). Nanoparticle exposure at nanotechnology workplaces: A review. *Particle and Fibre Toxicology, 8*, 18. doi: 10.1186/1743-8977-8-22

Lam, C. W., James, J. T., McCluskey, R., Arepalli, S., & Hunter, R. L. (2006). A review of carbon nanotube toxicity and assessment of potential occupational and environmental health risks. *Critical Reviews in Toxicology, 36*(3), 189-217. doi: 10.1080/10408440600570233

Lambert, T. N., Chavez, C. A., Hernandez-Sanchez, B., Lu, P., Bell, N. S., Ambrosini, A., . . . Huber, D. L. (2009). Synthesis and Characterization of Titania-Graphene Nanocomposites. *Journal of Physical Chemistry C, 113*(46), 19812-19823. doi: 10.1021/jp905456f

Leary, R., & Westwood, A. (2011). Carbonaceous nanomaterials for the enhancement of TiO2 photocatalysis. *Carbon, 49*(3), 741-772. doi: 10.1016/j.carbon.2010.10.010

Lee, K.-C., & Rittmann, B. E. (2002). Applying a novel autohydrogenotrophic hollow-fiber membrane biofilm reactor for denitrification of drinking water. *Water research, 36*(8), 2040.

Lee, S. L., Scott, J., Chiang, K., & Amal, R. (2009). Nanosized metal deposits on titanium dioxide for augmenting gas-phase toluene photooxidation. *Journal of Nanoparticle Research, 11*(1), 209-219. doi: 10.1007/s11051-008-9469-x

Lehman, S. G., Badruzzaman, M., Adham, S., Roberts, D. J., & Clifford, D. A. (2008). Perchlorate and nitrate treatment by ion exchange integrated with biological brine treatment. *Water Research, 42*(4-5), 969-976. doi: 10.1016/j.watres.2007.09.011

Li, H., Yin, W.-Y., Banerjee, K., & Mao, J.-F. (2008). Circuit Modeling and Performance Analysis of Multi-Walled Carbon Nanotube Interconnects. *IEEE Transactions on Electron Devices, 55*(6), 1328-1337.

Li, L., Xu, Z., Liu, F., Shao, Y., Wang, J., Wan, H., & Zheng, S. (2010). Photocatalytic nitrate reduction over Pt-Cu/TiO2 catalysts with benzene as hole scavenger. *Journal of Photochemistry and Photobiology a-Chemistry, 212*(2-3), 113-121. doi: 10.1016/j.jphotochem.2010.04.003

Li, L. Y., Xu, Z. Y., Liu, F. L., Shao, Y., Wang, J. H., Wan, H. Q., & Zheng, S. R. (2010). Photocatalytic nitrate reduction over Pt-Cu/TiO_2 catalysts with benzene as hole scavenger. *Journal of Photochemistry and Photobiology a-Chemistry*, *212*(2-3), 113-121. doi: 10.1016/j.jphotochem.2010.04.003

Li, M., Feng, C. P., Zhang, Z. Y., Lei, X. H., Chen, R. Z., Yang, Y. N., & Sugiura, N. (2009). Simultaneous reduction of nitrate and oxidation of by-products using electrochemical method. *Journal of Hazardous Materials, 171*(1-3), 724-730. doi: 10.1016/j.jhazmat.2009.06.066

Li, X. H., Niu, J. L., Zhang, J., Li, H. L., & Liu, Z. F. (2003). Labeling the defects of single-walled carbon nanotubes using titanium dioxide nanoparticles. *Journal of Physical Chemistry B, 107*(11), 2453.

Li, Y., & Wasgestian, F. (1998). Photocatalytic reduction of nitrate ions on TiO_2 by oxalic acid. *Journal of Photochemistry and Photobiology A: Chemistry, 112*(2-3), 255-259.

Li, Z. F., Luo, G. H., Zhou, W. P., Wei, F., Xiang, R., & Liu, Y. P. (2006). The quantitative characterization of the concentration and dispersion of multi-walled carbon nanotubes in suspension by spectrophotometry. *Nanotechnology, 17*(15), 3692-3698. doi: 10.1088/0957-4484/17/15/012

Linsebigler, A. L., Lu, G. Q., & Yates, J. T. (1995). Photocatalysis on TiO_2 Surfaces - Principles, Mechanisms, and Selected Results. *Chemical Reviews*, *95*(3), 735.

Liou, Y. H., Lo, S. L., Lin, C. J., Kuan, W. H., & Weng, S. C. (2005). Chemical reduction of an unbuffered nitrate solution using catalyzed and uncatalyzed

nanoscale iron particles. *Journal of Hazardous Materials, 127*(1-3), 102-110. doi: 10.1016/j.jhazmat.2005.06.029

Litter, M. I. (1999). Heterogeneous photocatalysis - Transition metal ions in photocatalytic systems. *Applied Catalysis B-Environmental, 23*(2-3), 89-114.

Liu, B., & Zeng, H. C. (2008). Carbon nanotubes supported mesoporous mesocrystals of anatase TiO_2. *Chemistry of Materials, 20*(8), 2711-2718. doi: 10.1021/cm800040k

Liu, F., Concepcion, J. J., Jurss, J. W., Cardolaccia, T., Templeton, J. L., & Meyer, T. J. (2008). Mechanisms of water oxidation from the blue dimer to photosystem II. *Inorganic Chemistry, 47*(6), 1727-1752. doi: 10.1021/ic701249s

Liu, J. Y., Choe, J. K., Sasnow, Z., Werth, C. J., & Strathmann, T. J. (2013). Application of a Re-Pd bimetallic catalyst for treatment of perchlorate in waste ion-exchange regenerant brine. *Water Research, 47*(1), 91-101. doi: 10.1016/j.watres.2012.09.031

Liu, L., Dong, X., & Yang, F. (2008). *Photocatalytic Removal of Nitrate from Water using Fe^0/TiO_2.* Paper presented at the Bioinformatics and Biomedical Engineering, 2008. ICBBE 2008. The 2nd International Conference on.

Liu, L.-F., Zhang, Y., Yang, F.-L., Chen, G., & Yu, J. C. (2009). Simultaneous photocatalytic removal of ammonium and nitrite in water using Ce_3^+–Ag^+ modified TiO_2. *Separation and Purification Technology, 67*(2), 244.

Liu, L. F., Dong, X. Y., Yang, F. L., & Yu, J. C. (2008). Photocatalytic reduction of nitrate by Ag/TiO_2 catalyst. *Chinese Journal of Inorganic Chemistry, 24*(2), 211-217.

Lozovskii, A. V., Stolyarova, I. V., Prikhod'ko, R. V., & Goncharuk, V. V. (2009). Research of photocatalytic activity of the Ag/TiO_2 catalysts in the reduction reaction of nitrate-ions in aqueous media. *Journal of Water Chemistry and Technology, 31*(6), 360-366. doi: 10.3103/s1063455x09060034

Lu, S. Y., Tang, C. W., Lin, Y. H., Kuo, H. F., Lai, Y. C., Tsai, M. Y., . . . Hsu, W. K. (2010). TiO_2-coated carbon nanotubes: A redshift enhanced photocatalysis at visible light. *Applied Physics Letters, 96*(23), 3.

Luk, G. K., & Au-Yeung, W. C. (2002). Experimental investigation on the chemical reduction of nitrate from groundwater. *Advances in Environmental Research, 6*(4), 441-453. doi: 10.1016/s1093-0191(01)00072-7

Mack, J., & Bolton, J. R. (1999). Photochemistry of nitrite and nitrate in aqueous solution: a review. *Journal of Photochemistry and Photobiology a-Chemistry, 128*(1-3), 1-13.

Maeda, K., Higashi, M., Lu, D. L., Abe, R., & Domen, K. (2010). Efficient Nonsacrificial Water Splitting through Two-Step Photoexcitation by Visible Light using a Modified Oxynitride as a Hydrogen Evolution Photocatalyst. *Journal of the American Chemical Society, 132*(16), 5858-5868. doi: 10.1021/ja1009025

Maeda, K., Teramura, K., Lu, D. L., Takata, T., Saito, N., Inoue, Y., & Domen, K. (2006). Photocatalyst releasing hydrogen from water - Enhancing catalytic performance holds promise for hydrogen production by water splitting in sunlight. *Nature, 440*(7082), 295-295. doi: 10.1038/440295a

Martin, S. T., Herrmann, H., & Hoffmann, M. R. (1994). TIME-RESOLVED MICROWAVE CONDUCTIVITY .2. QUANTUM-SIZED TIO_2 AND THE EFFECT OF ADSORBATES AND LIGHT-INTENSITY ON CHARGE-CARRIER DYNAMICS. *Journal of the Chemical Society-Faraday Transactions, 90*(21), 3323-3330.

Mateju, V., Cizinska, S., Krejci, J., & Janoch, T. (1992). Biological water denitrification - A review. *Enzyme and Microbial Technology, 14*(3), 170-183.

Mattia, D., Rossi, M. P., Kim, B. M., Korneva, G., Bau, H. H., & Gogotsi, Y. (2006). Effect of graphitization on the wettability and electrical conductivity of CVD-carbon nanotubes and films. *Journal of Physical Chemistry B, 110*(20), 9850-9855. doi: 10.1021/jp061138s

Maynard, A. D., Baron, P. A., Foley, M., Shvedova, A. A., Kisin, E. R., & Castranova, V. (2004). Exposure to carbon nanotube material: Aerosol release during the handling of unrefined single-walled carbon nanotube material. *Journal of Toxicology and Environmental Health-Part A, 67*(1), 87-107. doi: 10.1080/15287390490253688

McAdam, E. J., & Judd, S. J. (2006a). A review of membrane bioreactor potential for nitrate removal from drinking water. *Desalination, 196*(1-3), 135-148. doi: 10.1016/j.desal.2006.03.008

McAdam, E. J., & Judd, S. J. (2006b). A review of membrane bioreactor potential for nitrate removal from drinking water. *Desalination, 196*(1-3), 135.

McAdam, E. J., & Judd, S. J. (2008). Biological treatment of ion-exchange brine regenerant for re-use: A review. *Separation and Purification Technology, 62*(2), 264-272. doi: 10.1016/j.seppur.2008.01.007

McAdam, E. J., Pawlett, M., & Judd, S. J. (2010). Fate and impact of organics in an immersed membrane bioreactor applied to brine denitrification and ion exchange regeneration. *Water Research, 44*(1), 69-76. doi: 10.1016/j.watres.2009.08.048

McMurray, T. A., Byrne, J. A., Dunlop, P. S. M., Winkelman, J. G. M., Eggins, B. R., & McAdams, E. T. (2004). Intrinsic kinetics of photocatalytic oxidation of formic and oxalic acid on immobilised TiO2 films. *Applied Catalysis a-General, 262*(1), 105-110. doi: 10.1016/j.apcata.2003.11.013

Milliken, J., Keller, T. M., Baronavski, A. P., McElvany, S. W., Callahan, J. H., & Nelson, H. H. (1991). THERMAL AND OXIDATIVE ANALYSES OF BUCKMINSTERFULLERENE, C60. *Chemistry of Materials, 3*(3), 386-387. doi: 10.1021/cm00015a005

Mills, A., Davies, R. H., & Worsley, D. (1993). WATER-PURIFICATION BY SEMICONDUCTOR PHOTOCATALYSIS. *Chemical Society Reviews, 22*(6), 417-425.

Mirvish, S. S. (1985). GASTRIC-CANCER AND SALIVARY NITRATE AND NITRITE. *Nature, 315*(6019), 461-462. doi: 10.1038/315461c0

Miseki, Y., Kusama, H., Sugihara, H., & Sayama, K. (2010). Cs-Modified WO3 Photocatalyst Showing Efficient Solar Energy Conversion for O-2 Production and Fe (III) Ion Reduction under Visible Light. *Journal of Physical Chemistry Letters, 1*(8), 1196-1200. doi: 10.1021/jz100233w

Molodkina, E. B., Botryakova, I. G., Danilov, A. I., Souza-Garcia, J., & Feliu, J. M. (2012). Mechanism of nitrate electroreduction on Pt(100). *Russian Journal of Electrochemistry, 48*(3), 302-315. doi: 10.1134/s1023193512020115

Mora-Sero, I., Villarreal, T. L., Bisquert, J., Pitarch, A., Gomez, R., & Salvador, P. (2005). Photoelectrochemical behavior of nanostructured TiO_2 thin-film electrodes in contact with aqueous electrolytes containing dissolved pollutants: A model for distinguishing between direct and indirect interfacial hole transfer from photocurrent measurements. *Journal of Physical Chemistry B, 109*(8), 3371-3380. doi: 10.1021/jp045585o

Mori, T., Suzuki, J., Fujimoto, K., Watanabe, M., & Hasegawa, Y. (1999a). Reductive decomposition of nitrate ion to nitrogen in water on a unique hollandite photocatalyst. *Applied Catalysis B-Environmental, 23*(4), 283.

Mori, T., Suzuki, J., Fujimoto, K., Watanabe, M., & Hasegawa, Y. (1999b). Reductive decomposition of nitrate ion to nitrogen in water on a unique hollandite

photocatalyst. *Applied Catalysis B-Environmental*, *23*(4), 283-289. doi: 10.1016/s0926-3373(99)00086-7

Mori, T., Suzuki, J., Fujimoto, K., Watanabe, M., & Hasegawa, Y. (2000). Photocatalytic reduction of nitrate in water on meso-porous hollandite catalyst: A new pathway on removal of nitrate in water. *Journal of Sol-Gel Science and Technology, 19*(1-3), 505.

Mu, S. A., Long, Y. Z., Kang, S. Z., & Mu, J. (2010). Surface modification of TiO_2 nanoparticles with a C-60 derivative and enhanced photocatalytic activity for the reduction of aqueous Cr(VI) ions. *Catalysis Communications, 11*(8), 741-744. doi: 10.1016/j.catcom.2010.02.006

Murphy, A. P. (1991). CHEMICAL REMOVAL OF NITRATE FROM WATER. *Nature, 350*(6315), 223-225.

Myojo, T., Oyabu, T., Nishi, K., Kadoya, C., Tanaka, I., Ono-Ogasawara, M., . . . Shirai, T. (2009). Aerosol generation and measurement of multi-wall carbon nanotubes. *Journal of Nanoparticle Research, 11*(1), 91-99. doi: 10.1007/s11051-008-9450-8

Nakamura, K., Yoshida, Y., Mikami, I., & Okuhara, T. (2006). Selective hydrogenation of nitrate in water over Cu-Pd/mordenite. *Applied Catalysis B-Environmental, 65*(1-2), 31-36. doi: 10.1016/j.apcatb.2005.12.012

National Research Council, C. o. T. (1995). *Nitrate and nitrite in drinking water*. Washington, DC: National Academies Press.

Ng, Y. H., Lightcap, I. V., Goodwin, K., Matsumura, M., & Kamat, P. V. (2010). To What Extent Do Graphene Scaffolds Improve the Photovoltaic and Photocatalytic Response of TiO(2) Nanostructured Films? *Journal of Physical Chemistry Letters, 1*(15), 2222-2227. doi: 10.1021/jz100728z

Nguyen, T. V., & Wu, J. C. S. (2008a). Photoreduction of CO_2 in an optical-fiber photoreactor: Effects of metals addition and catalyst carrier. *Applied Catalysis a-General, 335*(1), 112-120. doi: 10.1016/j.apcata.2007.11.022

Nguyen, T. V., & Wu, J. C. S. (2008b). Photoreduction of CO_2 to fuels under sunlight using optical-fiber reactor. *Solar Energy Materials and Solar Cells, 92*(8), 864-872. doi: 10.1016/j.solmat.2008.02.010

Nguyen, T. V., Wu, J. C. S., & Chiou, C. H. (2008). Photoreduction of CO2 over Ruthenium dye-sensitized TiO_2-based catalysts under concentrated natural sunlight. *Catalysis Communications, 9*(10), 2073-2076. doi: 10.1016/j.catcom.2008.04.004

Nolan, B. (2004). Update on nitrate in water resources of the United States. *Epidemiology, 15*(4), S109-S109.

Nolan, B. T., & Hitt, K. J. (2006). Vulnerability of shallow groundwater and drinking-water wells to nitrate in the United States. *Environmental Science & Technology, 40*(24), 7834-7840. doi: 10.1021/es060911u

Nolan, B. T., Hitt, K. J., & Ruddy, B. C. (2002). Probability of Nitrate Contamination of Recently Recharged Groundwaters in the Conterminous United States. *Environmental science & technology, 36*(10), 2138-2145.

Nolan, B. T., Puckett, L. J., Ma, L. W., Green, C. T., Bayless, E. R., & Malone, R. W. (2010). Predicting Unsaturated Zone Nitrogen Mass Balances in Agricultural Settings of the United States. *Journal of Environmental Quality, 39*(3), 1051-1065. doi: 10.2134/jeq2009.0310

Nolan, B. T., & Stoner, J. D. (2000). Nutrients in groundwaters of the conterminous United States 1992-1995. *Environmental Science & Technology, 34*(7), 1156-1165.

O'Connell, M. J., Bachilo, S. M., Huffman, C. B., Moore, V. C., Strano, M. S., Haroz, E. H., . . . Smalley, R. E. (2002). Band gap fluorescence from individual single-walled carbon nanotubes. *Science, 297*(5581), 593-596.

Oh, W. C., Zhang, F. J., & Chen, M. L. (2009). Preparation of MWCNT/TiO_2 Composites by Using MWCNTs and Titanium(IV) Alkoxide Precursors in Benzene and their Photocatalytic Effect and Bactericidal Activity. *Bulletin of the Korean Chemical Society, 30*(11), 2637-2642.

Ohtani, B. (2008). Preparing articles on photocatalysis - Beyond the illusions, misconceptions, and speculation. *Chemistry Letters, 37*(3), 217-229. doi: 10.1246/cl.2008.216

Ollis, D. F., Pelizzetti, E., & Serpone, N. (1991). PHOTOCATALYZED ... DESTRUCTION ... OF WATER ... CONTAMINANTS. *Environmental Science & Technology, 25*(9), 1522-1529.

Ollis, D. F., & Turchi, C. (1990). HETEROGENEOUS PHOTOCATALYSIS FOR WATER-PURIFICATION - CONTAMINANT MINERALIZATION KINETICS AND ELEMENTARY REACTOR ANALYSIS. *Environmental Progress, 9*(4), 229-234.

Ono-Ogasawara, M., Serita, F., & Takaya, M. (2009). Distinguishing nanomaterial particles from background airborne particulate matter for quantitative exposure

assessment. *Journal of Nanoparticle Research, 11*(7), 1651-1659. doi: 10.1007/s11051-009-9703-1

Oregan, B., & Gratzel, M. (1991). A LOW-COST, HIGH-EFFICIENCY SOLAR-CELL BASED ON DYE-SENSITIZED COLLOIDAL TiO_2 FILMS. *Nature, 353*(6346), 737-740.

Orlanducci, S., Sessa, V., Terranova, M. L., Battiston, G. A., Battiston, S., & Gerbasi, R. (2006). Nanocrystalline TiO2 on single walled carbon nanotube arrays: Towards the assembly of organized C/TiO2 nanosystems. *Carbon, 44*(13), 2839-2843. doi: 10.1016/j.carbon.2006.03.018

Osswald, S., Havel, M., & Gogotsi, Y. (2007). Monitoring oxidation of multiwalled carbon nanotubes by Raman spectroscopy. *Journal of Raman Spectroscopy, 38*(6), 728-736. doi: 10.1002/jrs.1686

Osterloh, F. E. (2008). Inorganic materials as catalysts for photochemical splitting of water. *Chemistry of Materials, 20*(1), 35-54. doi: 10.1021/cm7024203

Ottley, C. J., Davison, W., & Edmunds, W. M. (1997). Chemical catalysis of nitrate reduction by iron(II). *Geochimica Et Cosmochimica Acta, 61*(9), 1819-1828. doi: 10.1016/s0016-7037(97)00058-6

Ou, Y., Lin, J. D., Fang, S. M., & Liao, D. W. (2006). MWNT-TiO2 : Ni composite catalyst: A new class of catalyst for photocatalytic H-2 evolution from water under visible light illumination. *Chemical Physics Letters, 429*(1-3), 199-203. doi: 10.1016/j.cplett.2006.08.024

Ozcan, O., Yukruk, F., Akkaya, E. U., & Uner, D. (2007). Dye sensitized CO2 reduction over pure and platinized TiO_2. *Topics in Catalysis, 44*(4), 523-528. doi: 10.1007/s11244-006-0100-z

Paidar, M., Bouzek, K., Jelinek, L., & Matejka, Z. (2004). A combination of ion exchange and electrochemical reduction for nitrate removal from drinking water Part II: Electrochemical treatment of a spent regenerant solution. *Water Environment Research, 76*(7), 2691-2698.

Palomares, A. E., Franch, C., & Corma, A. (2010). Nitrates removal from polluted aquifers using (Sn or Cu)/Pd catalysts in a continuous reactor. *Catalysis Today, 149*(3-4), 348-351. doi: 10.1016/j.cattod.2009.05.013

Palomares, A. E., Prato, J. G., Marquez, F., & Corma, A. (2003). Denitrification of natural water on supported Pd/Cu catalysts. *Applied Catalysis B-Environmental, 41*(1-2), 3-13. doi: 10.1016/s0926-3373(02)00203-5

Palomares, A. E., Prato, J. G., Rey, F., & Corma, A. (2004). Using the "memory effect" of hydrotalcites for improving the catalytic reduction of nitrates in water. *Journal of Catalysis, 221*(1), 62.

Pan, P. W., & Chen, Y. W. (2007). Photocatalytic reduction of carbon dioxide on NiO/InTaO4 under visible light irradiation. *Catalysis Communications, 8*(10), 1546-1549. doi: 10.1016/j.catcom.2007.01.006

Pang, L. S. K., Saxby, J. D., & Chatfield, S. P. (1993). THERMOGRAVIMETRIC ANALYSIS OF CARBON NANOTUBES AND NANOPARTICLES. *Journal of Physical Chemistry, 97*(27), 6941-6942.

Panyor, L., & Fabiani, C. (1996). Anion rejection in a nitrate highly rejecting reverse osmosis thin-film composite membrane. *Desalination, 104*(3), 165-174. doi: 10.1016/0011-9164(96)00039-2

Park, J. Y., & Lee, Y. N. (1988). SOLUBILITY AND DECOMPOSITION KINETICS OF NITROUS-ACID IN AQUEOUS-SOLUTION. *Journal of Physical Chemistry, 92*(22), 6294-6302. doi: 10.1021/j100333a025

Park, S., Kim, H.-J., Kim, J. S., Yoo, K., Lee, J. C., Anderson, W. A., & Lee, J.-H. (2007). Photocatalytic reduction of nitrate in wastewater using ZnO nanopowder synthesized by solution combustion method. *Journal of Nanoscience and Nanotechnology, 7*(11, Sp. Iss. SI), 4069.

Patterson, A. L. (1939). The Scherrer formula for x-ray particle size determination. *Physical Review, 56*(10), 978-982.

Peng, Y., & Liu, H. W. (2006). Effects of oxidation by hydrogen peroxide on the structures of multiwalled carbon nanotubes. *Industrial & Engineering Chemistry Research, 45*(19), 6483-6488. doi: 10.1021/ie0604627

Penpolcharoen, M., Amal, R., & Brungs, M. (2001). Degradation of sucrose and nitrate over titania coated nano-hematite photocatalysts. *JOURNAL OF NANOPARTICLE RESEARCH, 3*(4), 289-302.

Perissinotti, L. L., Brusa, M. A., & Grela, M. A. (2001). Yield of carboxyl anion radicals in the photocatalytic degradation of formate over TiO_2 particles. *Langmuir, 17*(26), 8422-8427. doi: 10.1021/la0155348

Petersen, E. J., Akkanen, J., Kukkonen, J. V. K., & Weber, W. J. (2009). Biological Uptake and Depuration of Carbon Nano-tubes by Daphnia magna. *Environmental Science & Technology, 43*(8), 2969-2975. doi: 10.1021/es8029363

Petersen, E. J., & Henry, T. B. (2012). Methodological considerations for testing the ecotoxicity of carbon nanotubes and fullerenes: Review. *Environmental Toxicology and Chemistry, 31*(1), 60-72. doi: 10.1002/etc.710

Petersen, E. J., Huang, Q. G., & Weber, W. J. (2008). Bioaccumulation of radio-labeled carbon nanotubes by Eisenia foetida. *Environmental Science & Technology, 42*(8), 3090-3095. doi: 10.1021/es071366f

Pintar, A. (2003). Catalytic processes for the purification of drinking water and industrial effluents. *Catalysis Today, 77*(4), 451-465. doi: 10.1016/s0920-5861(02)00385-1

Pintar, A., Batista, J., & Musevic, I. (2004). Palladium-copper and palladium-tin catalysts in the liquid phase nitrate hydrogenation in a batch-recycle reactor. *Applied Catalysis B-Environmental, 52*(1), 49-60. doi: 10.1016/j.apcatb.2004.02.019

Plata, D. L., Reddy, C. M., & Gschwend, P. M. (Submitted 2011). Thermogravimetry-mass spectrometry for carbon nanotube detection in complex mixtures. *Enviornmental Science & Technology*.

Pletcher, D., & Poorabedi, Z. (1979). REDUCTION OF NITRATE AT A COPPER CATHODE IN AQUEOUS ACID. *Electrochimica Acta, 24*(12), 1253-1256. doi: 10.1016/0013-4686(79)87081-4

Porter, D., Sriram, K., Wolfarth, M., Jefferson, A., Schwegler-Berry, D., Andrew, M., & Castranova, V. (2008). A biocompatible medium for nanoparticle dispersion. *Nanotoxicology, 2*(3), 144-154. doi: 10.1080/17435390802318349

Pourbaix, M., & De Zoubov, N. (1966). Nitrogen *Atlas of Electrochemical Equilibria in Aqueous Solutions* (Vol. First, pp. 493-503). Headington Hill Hall, Oxford: Pergamon Press Ltd.

Power, J. F., & Schepers, J. S. (1989). Nitrate contamination of groundwater in North America. *Effects of Agriculture on Groundwater, 26*(3-4), 165-187.

Prairie, M. R., Evans, L. R., Stange, B. M., & Martinez, S. L. (1993). AN INVESTIGATION OF TiO_2 PHOTOCATALYSIS FOR THE TREATMENT OF WATER CONTAMINATED WITH METALS AND ORGANIC-CHEMICALS. *Environmental Science & Technology, 27*(9), 1776-1782.

Pruden, A. L., & Ollis, D. F. (1983). Photoassisted heterogeneous catalysis: The degradation of trichloroethylene in water. *Journal of Catalysis, 82*(2), 404-417.

Prusse, U., & Vorlop, K. D. (2001). Supported bimetallic palladium catalysts for water-phase nitrate reduction. *Journal of Molecular Catalysis a-Chemical, 173*(1-2), 313-328. doi: 10.1016/s1381-1169(01)00156-x

Prüsse, U., Hähnlein, M., Daum, J., & Vorlop, K.-D. (2000). Improving the catalytic nitrate reduction. *Catalysis Today, 55*(1-2), 79.

Qian, J. M., & Lu, K. (2009). Multiwall Carbon Nanotube and TiO_2 Sol Assembly. *Journal of Nanoscience and Nanotechnology, 9*(10), 5816-5822. doi: 10.1166/jnn.2009.1228

Rabalais, N. N., Turner, R. E., & Scavia, D. (2002). Beyond science into policy: Gulf of Mexico hypoxia and the Mississippi River. *Bioscience, 52*(2), 129-142.

Rabalais, N. N., Turner, R. E., & Wiseman, W. J. (2001). Hypoxia in the Gulf of Mexico. *Journal of Environmental Quality, 30*(2), 320-329.

Rajeshwar, K., Chenthamarakshan, C. R., Ming, Y., & Sun, W. J. (2002). Cathodic photoprocesses on titania films and in aqueous suspensions. *Journal of Electroanalytical Chemistry, 538*, 173-182.

Ramavandi, B., Mortazavi, S. B., Moussavi, G., Khoshgard, A., & Jahangiri, M. (2011). Experimental investigation of the chemical reduction of nitrate ion in aqueous solution by Mg/Cu bimetallic particles. *Reaction Kinetics Mechanisms and Catalysis, 102*(2), 313-329. doi: 10.1007/s11144-010-0274-z

Ranjit, K. T., Krishnamoorthy, R., Varadarajan, T. K., & Viswanathan, B. (1995). Photocatalytic Reduction of Nitrite on CDS. *Journal of Photochemistry and Photobiology a-Chemistry, 86*(1-3), 185-189.

Ranjit, K. T., Krishnamoorthy, R., & Viswanathan, B. (1994a). Photocatalytic reduction of nitrite and nitrate on ZnS. *Journal of Photochemistry and Photobiology A: Chemistry, 81*(1), 55.

Ranjit, K. T., Krishnamoorthy, R., & Viswanathan, B. (1994b). PHOTOCATALYTIC REDUCTION OF NITRITE AND NITRATE ON ZNS. *Journal of Photochemistry and Photobiology a-Chemistry, 81*(1), 55-58.

Ranjit, K. T., Varadarajan, T. K., & Viswanathan, B. (1995). Photocatalytic Reduction of Nitrite and Nitrate Ions to Ammonia on Ru/TiO_2 Catalysts. *Journal of Photochemistry and Photobiology a-Chemistry, 89*(1), 67-68.

Ranjit, K. T., Varadarajan, T. K., & Viswanathan, B. (1996). Photocatalytic reduction of nitrite and nitrate ions over oxide (ZnO, ZrO_2 and Fe_2O_3) semiconductors. *Indian Journal of Chemistry Section a-Inorganic Bio-Inorganic Physical Theoretical & Analytical Chemistry, 35*(3), 177-181.

Ranjit, K. T., & Viswanathan, B. (1997a). Photocatalytic reduction of nitrite and nitrate ions over doped TiO_2 catalysts. *Journal of Photochemistry and Photobiology A: Chemistry, 107*(1-3), 215.

Ranjit, K. T., & Viswanathan, B. (1997b). Photocatalytic reduction of nitrite and nitrate ions over doped TiO_2 catalysts. *Journal of Photochemistry and Photobiology a-Chemistry, 107*(1-3), 215-220.

Ranjit, K. T., & Viswanathan, B. (1997c). Photocatalytic reduction of nitrite and nitrate ions to ammonia on M/TiO2 catalysts. *Journal of Photochemistry and Photobiology a-Chemistry, 108*(1), 73-78. doi: 10.1016/s1010-6030(96)04505-4

Ranjit, K. T., & Viswanathan, B. (1997d). Synthesis, characterization and photocatalytic properties of iron-doped TiO_2 catalysts. *Journal of Photochemistry and Photobiology a-Chemistry, 108*(1), 79-84.

Rao, G. G., & Murty, K. S. (1936). *Photocatalytic reduction of nitrate and the simultaneous oxidation of ammonia to nitrite.* Paper presented at the Proceedings of the National Institute of Sciences, India.

Rautenbach, R., Kopp, W., Vanopbergen, G., & Hellekes, R. (1987). NITRATE REDUCTION OF WELL WATER BY REVERSE-OSMOSIS AND ELECTRODIALYSIS - STUDIES ON PLANT PERFORMANCE AND COSTS. *Desalination, 65*(1-3), 241-258.

Ray, S. C., Pao, C. W., Tsai, H. M., Chen, H. C., Chen, Y. S., Wu, S. L., . . . Tagliaferro, A. (2009). High-Temperature Annealing Effects on Multiwalled Carbon Nanotubes: Electronic Structure, Field Emission and Magnetic Behaviors. *Journal of Nanoscience and Nanotechnology, 9*(12), 6799-6805. doi: 10.1166/jnn.2009.1581

Reisner, E., Powell, D. J., Cavazza, C., Fontecilla-Camps, J. C., & Armstrong, F. A. (2009). Visible Light-Driven H-2 Production by Hydrogenases Attached to Dye-Sensitized TiO2 Nanoparticles. *Journal of the American Chemical Society, 131*(51), 18457-18466. doi: 10.1021/ja907923r

Ren, M. M., & Valsaraj, K. (2009). Inverse Opal Titania on Optical Fiber for the Photoreduction of CO2 to CH3OH. *International Journal of Chemical Reactor Engineering, 7*, 19. doi: A90

Rengaraj, S., & Li, X. Z. (2007b). Enhanced photocatalytic reduction reaction over Bi^{3+}–TiO_2 nanoparticles in presence of formic acid as a hole scavenger. *Chemosphere, 66*(5), 930.

Richard, Y. R. (1989). Operating expenses of full-scale biological and ion-exchange denitrification plants in France. *Journal of the Institution of Water and Environmental Management, 3*(2), 154-167.

Richards, L. A., Vuachere, M., & Schafer, A. I. (2010). Impact of pH on the removal of fluoride, nitrate and boron by nanofiltration/reverse osmosis. *Desalination, 261*(3), 331-337. doi: 10.1016/j.desa1.2010.06.025

Robertson, P. K. J., Bahnemann, D. W., Robertson, J. M. C., & Wood, F. (2005). Photocatalytic detoxification of water and air. In O. Hutzinger (Ed.), *Handbook of Environmental Chemistry* (pp. 367-423): Springer-Verlag Berlin.

Rodriguez-Maroto, J. M., Garcia-Herruzo, F., Garcia-Rubio, A., Gomez-Lahoz, C., & Vereda-Alonso, C. (2009). Kinetics of the chemical reduction of nitrate by zero-valent iron. *Chemosphere, 74*(6), 804-809. doi: 10.1016/j.chemosphere.2008.10.020

Rosca, I. D., Watari, F., Uo, M., & Akaska, T. (2005). Oxidation of multiwalled carbon nanotubes by nitric acid. *Carbon, 43*(15), 3124-3131. doi: 10.1016/j.carbon.2005.06.019

Rosca, V., Duca, M., de Groot, M. T., & Koper, M. T. M. (2009). Nitrogen Cycle Electrocatalysis. *Chemical Reviews, 109*(6), 2209-2244. doi: 10.1021/cr8003696

Rothenberger, G., Moser, J., Gratzel, M., Serpone, N., & Sharma, D. K. (1985). CHARGE CARRIER TRAPPING AND RECOMBINATION DYNAMICS IN SMALL SEMICONDUCTOR PARTICLES. *Journal of the American Chemical Society, 107*(26), 8054-8059. doi: 10.1021/ja00312a043

Roy, S. C., Varghese, O. K., Paulose, M., & Grimes, C. A. (2010). Toward Solar Fuels: Photocatalytic Conversion of Carbon Dioxide to Hydrocarbons. *Acs Nano, 4*(3), 1259-1278. doi: 10.1021/nn9015423

Rupert, M. G. (2008). Decadal-scale changes of nitrate in ground water of the United States, 1988-2004. *JOURNAL OF ENVIRONMENTAL QUALITY, 37*(5, Suppl. S), S240-S248.

Ryu, J., & Choi, W. (2008). Substrate-specific photocatalytic activities of TiO_2 and multiactivity test for water treatment application. *Environmental Science & Technology, 42*(1), 294-300. doi: 10.1021/es071470x

Sa, J., Aguera, C. A., Gross, S., & Anderson, J. A. (2009). Photocatalytic nitrate reduction over metal modified TiO2. *Applied Catalysis B-Environmental, 85*(3-4), 192-200. doi: 10.1016/j.apcatb.2008.07.014

Sa, J., Berger, T., Fottinger, K., Riss, A., Anderson, J. A., & Vinek, H. (2005). Can TiO_2 promote the reduction of nitrates in water? *Journal of Catalysis, 234*(2), 282-291. doi: 10.1016/j.jcat.2005.06.015

Sa, J., Gasparovicova, D., Hayek, K., Halwax, E., Anderson, J. A., & Vinek, H. (2005). Water denitration over a Pd-Sn/Al2O3 catalyst. *Catalysis Letters, 105*(3-4), 209-217. doi: 10.1007/s10562-005-8692-7

Saadi, S., Bouguelia, A., & Trari, M. (2006). Photocatalytic hydrogen evolution over $CuCrO_2$. *Solar Energy, 80*(3), 272-280. doi: 10.1016/j.solener.2005.02.018

Sakamoto, Y., Kanno, M., Okuhara, T., & Kamiya, Y. (2008). Highly selective hydrogenation of nitrate to harmless compounds in water over copper-palladium bimetallic clusters supported on active carbon. *Catalysis Letters, 125*(3-4), 392-395. doi: 10.1007/s10562-008-9574-6

Salzmann, C. G., Chu, B. T. T., Tobias, G., Llewellyn, S. A., & Green, M. L. H. (2007). Quantitative assessment of carbon nanotube dispersions by Raman spectroscopy. *Carbon, 45*(5), 907-912. doi: 10.1016/j.carbon.2007.01.009

Sarkaria, R. S. (1936). Photonitrification of some compounds. *Indian Journal of Agricultural Sciences, 6*, 777-783.

Sasirekha, N., Basha, S. J. S., & Shanthi, K. (2006). Photocatalytic performance of Ru doped anatase mounted on silica for reduction of carbon dioxide. *Applied Catalysis B-Environmental, 62*(1-2), 169-180. doi: 10.1016/j.apcatb.2005.07.009

Sata, T., Yamaguchi, T., & Matsusaki, K. (1995). ANION-EXCHANGE MEMBRANES FOR NITRATE ION REMOVAL FROM GROUNDWATER BY ELECTRODIALYSIS. *Journal of the Chemical Society-Chemical Communications*(11), 1153-1154. doi: 10.1039/c39950001153

Sato, J., Saito, N., Yamada, Y., Maeda, K., Takata, T., Kondo, J. N., . . . Inoue, Y. (2005). RuO_2-loaded beta-Ge3N4 as a non-oxide photocatalyst for overall water splitting. *Journal of the American Chemical Society, 127*(12), 4150-4151.

Sato, T., Sato, K. I., Fujishiro, Y., Yoshioka, T., & Okuwaki, A. (1996). Photochemical reduction of nitrate to ammonia using layered hydrous titanate/cadmium sulphide nanocomposites. *JOURNAL OF CHEMICAL TECHNOLOGY AND BIOTECHNOLOGY, 67*(4), 345-349.

Sayama, K., & Arakawa, H. (1993). PHOTOCATALYTIC DECOMPOSITION OF WATER AND PHOTOCATALYTIC REDUCTION OF CARBON-DIOXIDE OVER ZRO2 CATALYST. *Journal of Physical Chemistry, 97*(3), 531-533.

Sayama, K., & Arakawa, H. (1994). EFFECT OF NA2CO3 ADDITION ON PHOTOCATALYTIC DECOMPOSITION OF LIQUID WATER OVER VARIOUS SEMICONDUCTOR CATALYSTS. *Journal of Photochemistry and Photobiology a-Chemistry, 77*(2-3), 243-247.

Sayama, K., & Arakawa, H. (1996). Effect of carbonate addition on the photocatalytic decomposition of liquid water over a ZrO_2 catalyst. *Journal of Photochemistry and Photobiology a-Chemistry, 94*(1), 67-76.

Scavia, D., & Donnelly, K. A. (2007). Reassessing hypoxia forecasts for the Gulf of Mexico. *Environmental Science & Technology, 41*(23), 8111-8117. doi: 10.1021/es0714235

Schmid, H., Laskus, L., Abraham, H. J., Baltensperger, U., Lavanchy, V., Bizjak, M., . . . Puxbaum, H. (2001). Results of the "carbon conference" international aerosol carbon round robin test stage I. *Atmospheric Environment, 35*(12), 2111-2121. doi: 10.1016/s1352-2310(00)00493-3

Schoeman, J. J. (2009). Nitrate-nitrogen removal with small-scale reverse osmosis, electrodialysis and ion-exchange units in rural areas. *Water Sa, 35*(5), 721-728.

Schoeman, J. J., & Steyn, A. (2003). Nitrate removal with reverse osmosis in a rural area in South Africa. *Desalination, 155*(1), 15-26.

Schonfelder, R., Aviles, F., Bachmatiuk, A., Cauich-Rodriguez, J. V., Knupfer, M., Buchner, B., & Rummeli, M. H. (2012). On the merits of Raman spectroscopy and thermogravimetric analysis to asses carbon nanotube structural modifications. *Applied Physics a-Materials Science & Processing, 106*(4), 843-852. doi: 10.1007/s00339-012-6787-8

Schrauzer, G. N., & Guth, T. D. (1977). PHOTOLYSIS OF WATER AND PHOTOREDUCTION OF NITROGEN ON TITANIUM-DIOXIDE. *Journal of the American Chemical Society, 99*(22), 7189-7193.

Schwab, F., Bucheli, T. D., Lukhele, L. P., Magrez, A., Nowack, B., Sigg, L., & Knauer, K. (2011). Are Carbon Nanotube Effects on Green Algae Caused by Shading and Agglomeration? *Environmental Science & Technology, 45*(14), 6136-6144. doi: 10.1021/es200506b

Schwarz, H. A. (1981). FREE-RADICALS GENERATED BY RADIOLYSIS OF AQUEOUS-SOLUTIONS. *Journal of Chemical Education, 58*(2), 101-105.

Searl, A., & Cullen, R. T. (1997). An enzymatic tissue digestion method for fibre biopersistence studies. *Annals of Occupational Hygiene, 41*(6), 721-727. doi: 10.1093/annhyg/41.6.721

Seidel, C., Gorman, C., Darby, J. L., & Jensen, V. B. (2011). An Assessment of the State of Nitrate Treatment Alternatives: Final Report: American Water Works Association.

Serpone, N. (1997). Relative photonic efficiencies and quantum yields in heterogeneous photocatalysis. *Journal of Photochemistry and Photobiology a-Chemistry, 104*(1-3), 1-12.

Serpone, N., Lawless, D., Khairutdinov, R., & Pelizzetti, E. (1995). SUBNANOSECOND RELAXATION DYNAMICS IN TIO2 COLLOIDAL SOLS (PARTICLE SIZES R(P)=1.0-13.4 NM) - RELEVANCE TO HETEROGENEOUS PHOTOCATALYSIS. *Journal of Physical Chemistry, 99*(45), 16655-16661. doi: 10.1021/j100045a027

Serpone, N., & Salinaro, A. (1999). Terminology, relative photonic efficiencies and quantum yields in heterogeneous photocatalysis. Part I: Suggested protocol (technical report). *Pure and Applied Chemistry, 71*(2), 303-320.

Sharif Zein, S. H., & Boccaccini, A. R. (2008). Synthesis and Characterization of TiO2 Coated Multiwalled Carbon Nanotubes Using a Sol Gel Method. *Industrial & Engineering Chemistry Research, 47*(17), 6598.

Shimazu, K., Goto, R., Piao, S., Kayama, R., Nakata, K., & Yoshinaga, Y. (2007). Reduction of nitrate ions on tin-modified palladium thin film electrodes. *Journal of Electroanalytical Chemistry, 601*(1-2), 161.

Singh, B., & Sekhon, G. S. (1979). NITRATE POLLUTION OF GROUNDWATER FROM FARM USE OF NITROGEN FERTILIZERS - REVIEW. *Agriculture and Environment, 4*(3), 207-225. doi: 10.1016/0304-1131(79)90022-5.

Singh, D. K., Iyer, P. K., & Giri, P. K. (2010). Diameter dependence of oxidative stability in multiwalled carbon nanotubes: Role of defects and effect of vacuum annealing. *Journal of Applied Physics, 108*(8), 10. doi: 08431310.1063/1.3491022

Smith, R. L., Miller, D. N., Brooks, M. H., Widdowson, M. A., & Killingstad, M. W. (2001). In situ stimulation of groundwater denitrification with formate to remediate nitrate contamination. *Environmental Science & Technology, 35*(1), 196-203. doi: 10.1021/es001360p

Soares, M. I. M. (2000). Biological denitrification of groundwater. *Water Air and Soil Pollution, 123*(1-4), 183-193. doi: 10.1023/a:1005242600186

Soares, O., Fan, X. L., Orfao, J. J. M., Lapkin, A. A., & Pereira, M. F. R. (2012). Kinetic Modeling of Nitrate Reduction Catalyzed by Pd-Cu Supported on Carbon Nanotubes. *Industrial & Engineering Chemistry Research, 51*(13), 4854-4860. doi: 10.1021/ie202957v

Soares, O., Orfao, J. J. M., & Pereira, M. F. R. (2008). Activated Carbon Supported Metal Catalysts for Nitrate and Nitrite Reduction in Water. *Catalysis Letters, 126*(3-4), 253-260. doi: 10.1007/s10562-008-9612-4

Soares, O., Orfao, J. J. M., & Pereira, M. F. R. (2010). Pd-Cu and Pt-Cu Catalysts Supported on Carbon Nanotubes for Nitrate Reduction in Water. *Industrial & Engineering Chemistry Research, 49*(16), 7183-7192. doi: 10.1021/ie1001907

Soares, O., Orfao, J. J. M., & Pereira, M. F. R. (2011a). Nitrate reduction in water catalysed by Pd-Cu on different supports. *Desalination, 279*(1-3), 367-374. doi: 10.1016/j.desal.2011.06.037

Soares, O., Orfao, J. J. M., & Pereira, M. F. R. (2011b). Nitrate reduction with hydrogen in the presence of physical mixtures with mono and bimetallic catalysts and ions in solution. *Applied Catalysis B-Environmental, 102*(3-4), 424-432. doi: 10.1016/j.apcatb.2010.12.017

Sobek, A., & Bucheli, T. D. (2009). Testing the resistance of single- and multi-walled carbon nanotubes to chemothermal oxidation used to isolate soots from environmental samples. *Environmental Pollution, 157*(4), 1065-1071. doi: 10.1016/j.envpol.2008.09.004

Somasundaram, S., Ming, Y., Chenthamarakshan, C. R., Schelly, Z. A., & Rajeshwar, K. (2004). Free radical-mediated heterogeneous photocatalytic reduction of metal ions in UV-irradiated titanium dioxide suspensions. *Journal of Physical Chemistry B, 108*(15), 4784-4788. doi: 10.1021/jp036729m

Strebel, O., Duynisveld, W. H. M., & Bottcher, J. (1989). NITRATE POLLUTION OF GROUNDWATER IN WESTERN-EUROPE. *Agriculture Ecosystems & Environment, 26*(3-4), 189-214. doi: 10.1016/0167-8809(89)90013-3

Subramanian, V., Wolf, E., & Kamat, P. V. (2001). Semiconductor-metal composite nanostructures. To what extent do metal nanoparticles improve the photocatalytic activity of TiO_2 films? *Journal of Physical Chemistry B, 105*(46), 11439-11446. doi: 10.1021/jp011118k

Subramanian, V., Wolf, E. E., & Kamat, P. V. (2004). Catalysis with TiO_2/gold nanocomposites. Effect of metal particle size on the Fermi level equilibration. *Journal of the American Chemical Society, 126*(15), 4943-4950. doi: 10.1021/ja0315199

Sun, W. Z., Li, Q., Gao, S. A., & Shang, J. K. (2012). Monometallic Pd/Fe_3O_4 catalyst for denitrification of water. *Applied Catalysis B-Environmental, 125*, 1-9. doi: 10.1016/j.apcatb.2012.05.014

Surdhar, P. S., Mezyk, S. P., & Armstrong, D. A. (1989). REDUCTION POTENTIAL OF THE .CO2- RADICAL-ANION IN AQUEOUS-SOLUTIONS. *Journal of Physical Chemistry, 93*(8), 3360-3363.

Sychev, M., Lozovski, A., Prihod'ko, R., Erdmann, K., & Goncharuk, V. (2008). Photoreduction of Nitrate Ions Over Ag/TiO2 System *Sol-Gel Methods for Materials Processing* (pp. 453-458).

Tachikawa, T., Tojo, S., Fujitsuka, M., & Majima, T. (2004). Direct observation of the one-electron reduction of methyl viologen mediated by the CO_2 radical anion during TiO2 photocatalytic reactions. *Langmuir, 20*(22), 9441-9444. doi: 10.1021/la048100w

Takai, A., & Kamat, P. V. (2011). Capture, Store, and Discharge. Shuttling Photogenerated Electrons across TiO_2-Silver Interface. *Acs Nano, 5*(9), 7369-7376. doi: 10.1021/nn202294b

Tamura, M., Inada, M., Nakazato, T., Yamamoto, K., Endo, S., Uchida, K., . . . Tao, H. (2011). A determination method of pristine multiwall carbon nanotubes in rat lungs after intratracheal instillation exposure by combustive oxidation-nondispersive infrared analysis. *Talanta, 84*(3), 802-808. doi: 10.1016/j.talanta.2011.02.017

Tang, J. W., Durrant, J. R., & Klug, D. R. (2008). Mechanism of photocatalytic water splitting in TiO2. Reaction of water with photoholes, importance of charge carrier dynamics, and evidence for four-hole chemistry. *Journal of the American Chemical Society, 130*(42), 13885-13891. doi: 10.1021/ja8034637

Tawkaew, S., Fujishiro, Y., Yin, S., & Sato, T. (2001). Synthesis of cadmium sulfide pillared layered compounds and photocatalytic reduction of nitrate under visible light irradiation. *Colloids and Surfaces A: Physicochemical and Engineering Aspects, 179*(2-3), 139-144.

Tawkaew, S., Uchida, S., Fujishiro, Y., & Sato, T. (2000). Photoreduction of NO_3- and NO_2- under visible light irradiation with layered $H_4Nb_6O_{17}$/CdS and $H_2Ti_4O_9$/CdS nanocomposites. *Molecular Crystals and Liquid Crystals, 341*, 1041-1046.

Tawkaew, S., Yin, S., & Sato, T. (2001). Photoreduction of nitrate ion and photoevolution of hydrogen on unsupported TiO_2 and TiO2 pillared $H_4Nb_6O_{17}$ nanocomposites. *International Journal of Inorganic Materials, 3*(7), 855-859.

Tchoul, M. N., Ford, W. T., Lolli, G., Resasco, D. E., & Arepalli, S. (2007). Effect of mild nitric acid oxidation on dispersability, size, and structure of single-walled carbon nanotubes. *Chemistry of Materials, 19*(23), 5765-5772. doi: 10.1021/cm0717581

Testa, J. J., Grela, M. A., & Litter, M. I. (2001). Experimental evidence in favor of an initial one-electron-transfer process in the heterogeneous photocatalytic reduction of chromium(VI) over TiO2. *Langmuir, 17*(12), 3515-3517.

Testa, J. J., Grela, M. A., & Litter, M. I. (2004). Heterogeneous photocatalytic reduction of chromium(VI) over TiO2 particles in the presence of oxalate: Involvement of Cr(V) species. *Environmental Science & Technology, 38*(5), 1589-1594. doi: 10.1021/es0346532

Theologides, C. P., Savva, P. G., & Costa, C. N. (2011). Catalytic removal of nitrates from waters in a continuous flow process: The remarkable effect of liquid flow rate and gas feed composition. *Applied Catalysis B-Environmental, 102*(1-2), 54-61. doi: 10.1016/j.apcatb.2010.11.024

Torimoto, T., Liu, B. J., & Yoneyama, H. (1998). Effect of solvents on photocatalytic reduction of carbon dioxide using semiconductor photocatalysts. In T. Inui, M. Anpo, K. Izui, S. Yanagida & T. Yamaguchi (Eds.), *Advances in Chemical Conversions for Mitigating Carbon Dioxide* (Vol. 114, pp. 553-556). Amsterdam: Elsevier Science Publ B V.

Tran, M. Q., Tridech, C., Alfrey, A., Bismarck, A., & Shaffer, M. S. P. (2007). Thermal oxidative cutting of multi-walled carbon nanotubes. *Carbon, 45*(12), 2341-2350. doi: 10.1016/j.carbon.2007.07.012

Tseng, I. H., Chang, W. C., & Wu, J. C. S. (2002). Photoreduction of CO_2 using sol-gel derived titania and titania-supported copper catalysts. *Applied Catalysis B-Environmental, 37*(1), 37-48.

Tseng, I. H., Wu, J. C. S., & Chou, H. Y. (2004). Effects of sol-gel procedures on the photocatalysis of Cu/TiO_2 in CO_2 photoreduction. *Journal of Catalysis, 221*(2), 432-440. doi: 10.1016/j.jcat.2003.09.002

Tseng, Y. H., Yen, C. Y., Yen, M. Y., & Ma, C. C. M. (2010). Effects of the acid pretreated multi-walled carbon nanotubes on the photocatalytic capacity of TiO_2/multi-walled carbon nanotubes nanocomposites. *Micro & Nano Letters, 5*(1), 1-6. doi: 10.1049/mnl.2009.0094

Uo, M., Akasaka, T., Watari, F., Sato, Y., & Tohji, K. (2011). Toxicity evaluations of various carbon nanomaterials. *Dental Materials Journal, 30*(3), 245-263. doi: 10.4012/dmj.2010-039

USEPA. (1995). *SW-846 EPA Method 3050B, Acid digestion of sediments, sludges and soils, in: Test Methods for Evaluating Solid Waste*. Washington DC: US Environmental Protection Agency.

USEPA. (2009). Energy and Water. Retrieved July 14th, 2010, from http://www.epa.gov/waterinfrastructure/bettermanagement_energy.html#basicone

Van Ginkel, S. W., Ahn, C. H., Badruzzaman, M., Roberts, D. J., Lehman, S. G., Adham, S. S., & Rittmann, B. E. (2008). Kinetics of nitrate and perchlorate reduction in ion-exchange brine using the membrane biofilm reactor (MBfR). *Water Research, 42*(15), 4197-4205. doi: 10.1016/j.watres.2008.07.012

Vanderhoek, J. P., Vanderven, P. J. M., & Klapwijk, A. (1988). COMBINED ION-EXCHANGE BIOLOGICAL DENITRIFICATION FOR NITRATE REMOVAL FROM GROUND-WATER UNDER DIFFERENT PROCESS CONDITIONS. *Water Research, 22*(6), 679-684. doi: 10.1016/0043-1354(88)90178-9

Vinu, R., & Madras, G. (2008). Kinetics of simultaneous photocatalytic degradation of phenolic compounds and reduction of metal ions with nano-TiO_2. *Environmental Science & Technology, 42*(3), 913-919. doi: 10.1021/es0720457

Wada, K., Hirata, T., Hosokawa, S., Iwamoto, S., & Inoue, M. (2012). Effect of supports on Pd-Cu bimetallic catalysts for nitrate and nitrite reduction in water. *Catalysis Today, 185*(1), 81-87. doi: 10.1016/j.cattod.2011.07.021

Wakida, F. T., & Lerner, D. N. (2005). Non-agricultural sources of groundwater nitrate: a review and case study. *Water Research, 39*(1), 3-16. doi: 10.1016/j.watres.2004.07.026

Wang, H., Wang, H.-L., Jiang, W.-F., & Li, Z.-Q. (2009). Photocatalytic degradation of 2,4-dinitrophenol (DNP) by multi-walled carbon nanotubes (MWCNTs)/TiO_2 composite in aqueous solution under solar irradiation. *Water research, 43*(1), 204-210.

Wang, N., Zhu, L. H., Deng, K. J., She, Y. B., Yu, Y. M., & Tang, H. Q. (2010). Visible light photocatalytic reduction of Cr(VI) on TiO_2 in situ modified with small molecular weight organic acids. *Applied Catalysis B-Environmental, 95*(3-4), 400-407. doi: 10.1016/j.apcatb.2010.01.019

Wang, R. H., Mikoryak, C., Chen, E., Li, S., Pantano, P., & Draper, R. K. (2009). Gel Electrophoresis Method to Measure the Concentration of Single-Walled Carbon Nanotubes Extracted from Biological Tissue. *Analytical Chemistry, 81*(8), 2944-2952. doi: 10.1021/ac802485n

Wang, R. H., Mikoryak, C., Li, S. Y., Bushdiecker, D., Musselman, I. H., Pantano, P., & Draper, R. K. (2011). Cytotoxicity Screening of Single-Walled Carbon Nanotubes: Detection and Removal of Cytotoxic Contaminants from Carboxylated Carbon Nanotubes. *Molecular Pharmaceutics, 8*(4), 1351-1361. doi: 10.1021/mp2001439

Wang, S., Ji, L., Wu, B., Gong, Q., Zhu, Y., & Liang, J. (2008). Influence of surface treatment on preparing nanosized TiO_2 supported on carbon nanotubes. *Applied Surface Science, 255*(5, Part 2), 3263.

Wang, Y., Westerhoff, P., & Hristovski, K. (2011). Fate and biological effects of silver, titanium dioxide, and C_{60} (fullerene) nanomaterials during simulated wastewater treatment processes. *J. Hazardous Waste (In-press).*

Wang, Y., Wu, J., & Wei, F. (2003). A treatment method to give separated multi-walled carbon nanotubes with high purity, high crystallization and a large aspect ratio. *Carbon, 41*(15), 2939.

Wang, Y. B., Iqbal, Z., & Mitra, S. (2006). Rapidly functionalized, water-dispersed carbon nanotubes at high concentration. *Journal of the American Chemical Society, 128*(1), 95-99. doi: 10.1021/ja053003q

Waterhouse, G. I. N., Bowmaker, G. A., & Metson, J. B. (2001). The thermal decomposition of silver (I, III) oxide: A combined XRD, FT-IR and Raman spectroscopic study. *Physical Chemistry Chemical Physics, 3*(17), 3838-3845.

Watson, J. G., Chow, J. C., & Chen, L.-W. A. (2005). Summary of Organic and Elemental Carbon/Black Carbon Analysis Methods and Intercomparisons. *Aerosol and Air Quality Research, 5*(1), 65-102.

Watts, P. C. P., Hsu, W. K., Kroto, H. W., & Walton, D. R. M. (2003). Are bulk defective carbon nanotubes less electrically conducting? *Nano Letters, 3*(4), 549-553. doi: 10.1021/nl034028v

Wehbe, N., Guilhaume, N., Fiaty, K., Miachon, S., & Dalmon, J. A. (2010). Hydrogenation of nitrates in water using mesoporous membranes operated in a flow-through catalytic contactor. *Catalysis Today, 156*(3-4), 208-215. doi: 10.1016/j.cattod.2010.04.048

Wehbe, N., Jaafar, M., Guillard, C., Herrmann, J. M., Miachon, S., Puzenat, E., & Guilhaume, N. (2009). Comparative study of photocatalytic and non-photocatalytic reduction of nitrates in water. *Applied Catalysis a-General, 368*(1-2), 1-8. doi: 10.1016/j.apcata.2009.07.038

Wei, L. P., Thakkar, M., Chen, Y. H., Ntim, S. A., Mitra, S., & Zhang, X. Y. (2010). Cytotoxicity effects of water dispersible oxidized multiwalled carbon nanotubes on marine alga, Dunaliella tertiolecta. *Aquatic Toxicology, 100*(2), 194-201. doi: 10.1016/j.aquatox.2010.07.001

Wenzler-Rottele, S., Dettenkofer, M., Schmidt-Eisenlohr, E., Gregersen, A., Schulte-Monting, J., & Tvede, M. (2006). Comparison in a laboratory model between the

performance of a urinary closed system bag with double non-return valve and that of a single valve system. *Infection, 34*(4), 214-218. doi: 10.1007/s15010-006-5626-2

Westerhoff, P. (2003). Reduction of nitrate, bromate, and chlorate by zero valent iron (Fe-0). *Journal of Environmental Engineering-Asce, 129*(1), 10-16. doi: 10.1061/(asce)0733-9372(2003)129:1(10)

Westerhoff, P., Crittenden, J. C., Moon, H., & Minakata, D. (2010). Oxidative Destruction of Organics in Membrane Concentrations (pp. 75). Alexandria, VA: WateReuse Foundation.

Westerhoff, P., & James, J. (2003). Nitrate removal in zero-valent iron packed columns. *Water Research, 37*(8), 1818-1830. doi: 10.1016/s0043-1354(02)00539-0

Williams, G., Seger, B., & Kamat, P. V. (2008). TiO_2-graphene nanocomposites. UV-assisted photocatalytic reduction of graphene oxide. *Acs Nano, 2*(7), 1487-1491. doi: 10.1021/nn800251f

Woan, K., Pyrgiotakis, G., & Sigmund, W. (2009). Photocatalytic Carbon-Nanotube-TiO2 Composites. *ADVANCED MATERIALS, 21*(21), 2233-2239.

Woolerton, T. W., Sheard, S., Reisner, E., Pierce, E., Ragsdale, S. W., & Armstrong, F. A. (2010). Efficient and Clean Photoreduction of CO_2 to CO by Enzyme-Modified TiO_2 Nanoparticles Using Visible Light. *Journal of the American Chemical Society, 132*(7), 2132-+. doi: 10.1021/ja910091z

Wu, J. C. S., Wu, T. H., Chu, T. C., Huang, H. J., & Tsai, D. P. (2008). Application of optical-fiber photoreactor for CO_2 photocatalytic reduction. *Topics in Catalysis, 47*(3-4), 131-136. doi: 10.1007/s11244-007-9022-7

Wu, J. M., Yao, J. J., Yang, H. P., Fan, Y. N., & Xu, B. L. (2010). Photocatalytic Properties and the Role of Carbon Nanotubes in TiO_2/Carbon Nanotube Composites. *Acta Chimica Sinica, 68*(14), 1349-1356.

Xia, X. H., Jia, Z. H., Yu, Y., Liang, Y., Wang, Z., & Ma, L. L. (2007). Preparation of multi-walled carbon nanotube supported TiO_2 and its photocatalytic activity in the reduction of CO_2 with H2O. *Carbon, 45*(4), 717-721. doi: 10.1016/j.carbon.2006.11.028

Xiao, H., Zou, H. F., Pan, C. S., Jiang, X. G., Le, X. C., & Yang, L. (2006). Quantitative determination of oxidized carbon nanotube probes in yeast by capillary electrophoresis with laser-induced fluorescence detection. *Analytica Chimica Acta, 580*(2), 194-199. doi: 10.1016/j.aca.2006.07.074

Xie, Y., Heo, S. H., Yoo, S. H., Ali, G., & Cho, S. O. (2010). Synthesis and Photocatalytic Activity of Anatase TiO_2 Nanoparticles-coated Carbon Nanotubes. *Nanoscale Research Letters, 5*(3), 603-607. doi: 10.1007/s11671-009-9513-5

Xie, Y. B., Cao, H. B., Li, Y. P., Zhang, Y., & Crittenden, J. C. (2011). Highly Selective PdCu/Amorphous Silica-Alumina (ASA) Catalysts for Groundwater Denitration. *Environmental Science & Technology, 45*(9), 4066-4072. doi: 10.1021/es104050h

Xiong, Z., Zhao, D. Y., & Pan, G. (2009). Rapid and controlled transformation of nitrate in water and brine by stabilized iron nanoparticles. *Journal of Nanoparticle Research, 11*(4), 807-819. doi: 10.1007/s11051-008-9433-9

Xu, Y., & Schoonen, M. A. A. (2000). The absolute energy positions of conduction and valence bands of selected semiconducting minerals. *American Mineralogist, 85*(3-4), 543-556.

Xu, Y. J., Zhuang, Y. B., & Fu, X. Z. (2010). New Insight for Enhanced Photocatalytic Activity of TiO_2 by Doping Carbon Nanotubes: A Case Study on Degradation of Benzene and Methyl Orange. *Journal of Physical Chemistry C, 114*(6), 2669-2676. doi: 10.1021/jp90855p

Yang, G. C. C., & Lee, H. L. (2005). Chemical reduction of nitrate by nanosized iron: Kinetics and pathways. *Water Research, 39*(5), 884-894. doi: 10.1016/j.watres.2004.11.030

Yang, H. P., Shi, Z. M., Dai, K. J., Duan, Y. P., & Wu, J. M. (2011). Surface Modification of Carbon Nano Tubes for the Photocatalytic Activity Enhancement of Composite TiO2-CNTs. *Acta Chimica Sinica, 69*(5), 536-542.

Yao, N., Lordi, V., Ma, S. X. C., Dujardin, E., Krishnan, A., Treacy, M. M. J., & Ebbesen, T. W. (1998). Structure and oxidation patterns of carbon nanotubes. *Journal of Materials Research, 13*(9), 2432-2437. doi: 10.1557/jmr.1998.0338

Yao, Y., Li, G., Ciston, S., Lueptow, R. M., & Gray, K. A. (2008). Photoreactive TiO2/Carbon Nanotube Composites: Synthesis and Reactivity. *Environmental science & technology, 42*(13), 4952.

Yerga, R. M. N., Galvan, M. C. A., del Valle, F., de la Mano, J. A. V., & Fierro, J. L. G. (2009). Water Splitting on Semiconductor Catalysts under Visible-Light Irradiation. *Chemsuschem, 2*(6), 471-485. doi: 10.1002/cssc.200900018

Yi, W., Sakamoto, Y., & Kamiya, Y. (2009). Remediation of actual groundwater polluted with nitrate by the catalytic reduction over copper-palladium supported on active carbon. *Applied Catalysis a-General, 361*(1-2), 123-129. doi: 10.1016/j.apcata.2009.04.006

Yoneyama, H. (1997). Photoreduction of carbon dioxide on quantized semiconductor nanoparticles in solution. *Catalysis Today, 39*(3), 169-175.

Young, G. K., Bungay, H. R., Brown, L. M., & Parsons, W. A. (1964). CHEMICAL REDUCTION OF NITRATE IN WATER. *Journal Water Pollution Control Federation, 36*(3), 395-398.

Yu, H., Quan, X., Chen, S., & Zhao, H. (2007). TiO_2−Multiwalled Carbon Nanotube Heterojunction Arrays and Their Charge Separation Capability. *The Journal of Physical Chemistry C, 111*(35), 12987.

Yu, H., Quan, X., Chen, S., Zhao, H., & Zhang, Y. (2008). TiO_2–carbon nanotube heterojunction arrays with a controllable thickness of TiO2 layer and their first application in photocatalysis. *Journal of Photochemistry and Photobiology A: Chemistry, 200*(2-3), 301.

Zhang, A. P., & Zhang, J. Z. (2010a). Synthesis and characterization of Ag/$BiVO_4$ composite photocatalyst. *Applied Surface Science, 256*(10), 3224-3227. doi: 10.1016/j.apsusc.2009.12.009

Zhang, A. P., & Zhang, J. Z. (2010b). Visible-light activities of Gd_2O_3/$BiVO_4$ composite photocatalysts. *Journal of Materials Science, 45*(15), 4040-4045. doi: 10.1007/s10853-010-4486-4

Zhang, F. X., Jin, R. C., Chen, J. X., Shao, C. Z., Gao, W. L., Li, L. D., & Guan, N. J. (2005). High photocatalytic activity and selectivity for nitrogen in nitrate reduction on Ag/TiO_2 catalyst with fine silver clusters. *Journal of Catalysis, 232*(2), 424-431. doi: 10.1016/j.jcat.2005.04.014

Zhang, F. X., Miao, S., Yang, Y. L., Zhang, X., Chen, J. X., & Guan, N. J. (2008). Size-dependent hydrogenation selectivity of nitrate on Pd-Cu/TiO_2 catalysts. *Journal of Physical Chemistry C, 112*(20), 7665-7671. doi: 10.1021/jp800060g

Zhang, H., Chen, G., & Bahnemann, D. W. (2009). Photoelectrocatalytic materials for environmental applications. *Journal of Materials Chemistry, 19*(29), 5089.

Zhang, H., Lv, X. J., Li, Y. M., Wang, Y., & Li, J. H. (2010). P25-Graphene Composite as a High Performance Photocatalyst. *Acs Nano, 4*(1), 380-386. doi: 10.1021/nn901221k

Zhang, H., Sun, C. H., Li, F., Li, H. X., & Cheng, H. M. (2006). Purification of multiwalled carbon nanotubes by annealing and extraction based on the difference in van der Waals potential. *Journal of Physical Chemistry B, 110*(19), 9477-9481. doi: 10.1021/jp060271h

Zhang, L. W., Petersen, E. J., & Huang, Q. G. (2011). Phase Distribution of C-14-Labeled Multiwalled Carbon Nanotubes in Aqueous Systems Containing Model Solids: Peat. *Environmental Science & Technology, 45*(4), 1356-1362. doi: 10.1021/es1026097

Zhang, W., Cul, X. L., & Jiang, Z. Y. (2008). Photoelectrochemical properties of multi-walled carbon nanotube/TiO_2 nanocomposite films. *Acta Chimica Sinica, 66*(8), 867-873.

Zhang, W. L., Tian, Z. X., Zhang, N., & Li, X. Q. (1996). Nitrate pollution of groundwater in northern China. *Agriculture Ecosystems & Environment, 59*(3), 223-231. doi: 10.1016/0167-8809(96)01052-3

Zhang, X. Y., Li, H. P., Cui, X. L., & Lin, Y. H. (2010). Graphene/TiO_2 nanocomposites: synthesis, characterization and application in hydrogen evolution from water photocatalytic splitting. *Journal of Materials Chemistry, 20*(14), 2801-2806.

Zhang, Y. H., Tang, Z. R., Fu, X. Z., & Xu, Y. J. (2010). TiO_2-Graphene Nanocomposites for Gas-Phase Photocatalytic Degradation of Volatile Aromatic Pollutant: Is TiO2-Graphene Truly Different from Other TiO2-Carbon Composite Materials? *Acs Nano, 4*(12), 7303-7314. doi: 10.1021/nn1024219

Zhao, D., Chen, C. C., Yu, C. L., Ma, W. H., & Zhao, J. C. (2009). Photoinduced Electron Storage in WO_3/TiO_2 Nanohybrid Material in the Presence of Oxygen and Postirradiated Reduction of Heavy Metal Ions. *Journal of Physical Chemistry C, 113*(30), 13160-13165. doi: 10.1021/jp9002774

Zhao, L. P., & Gao, L. A. (2004). Coating multi-walled carbon nanotubes with zinc sulfide. *Journal of Materials Chemistry, 14*(6), 1001-1004. doi: 10.1039/b315450e

Zhao, X. C., & Liu, R. T. (2012). Recent progress and perspectives on the toxicity of carbon nanotubes at organism, organ, cell, and biomacromolecule levels. *Environment International, 40*, 244-255. doi: 10.1016/j.envint.2011.12.003

Zhao, Z. H., Fan, J. M., Xie, M. M., & Wang, Z. Z. (2009). Photo-catalytic reduction of carbon dioxide with in-situ synthesized CoPc/TiO_2 under visible light irradiation. *Journal of Cleaner Production, 17*(11), 1025-1029. doi: 10.1016/j.jclepro.2009.02.016

Zhou, L., & Zachariah, M. R. (2012). Size resolved particle work function measurement of free nanoparticles: Aggregates vs. spheres. *Chemical Physics Letters, 525-26*, 77-81. doi: 10.1016/j.cplett.2011.11.045

Zhu, Z. P., Zhou, Y., Yu, H. W., Nomura, T., & Fugetsu, B. (2006). Photodegradation of humic substances on MWCNT/nanotubular-TiO_2 composites. *Chemistry Letters, 35*(8), 890-891. doi: 10.1246/cl.2006.890